APPENDICES 1, 2, AND 3

BIOSENSOR-BASED DETECTION AND VERIFICATION SYSTEM FOR BIO-CHEMICAL WARFARE AGENTS

FINAL REPORT

MOLECULAR DEVICES CORPORATION

8 JULY 1996

Sponsored by
ADVANCED RESEARCH PROJECTS AGENCY,
DEPARTMENT OF DEFENSE

DEFENSE SCIENCE OFFICE

ARPA ORDER NO. 8143

ISSUED BY DARPA/CMO UNDER CONTRACT
#MDA972-92-C-0005

DISCLAIMER NOTICE

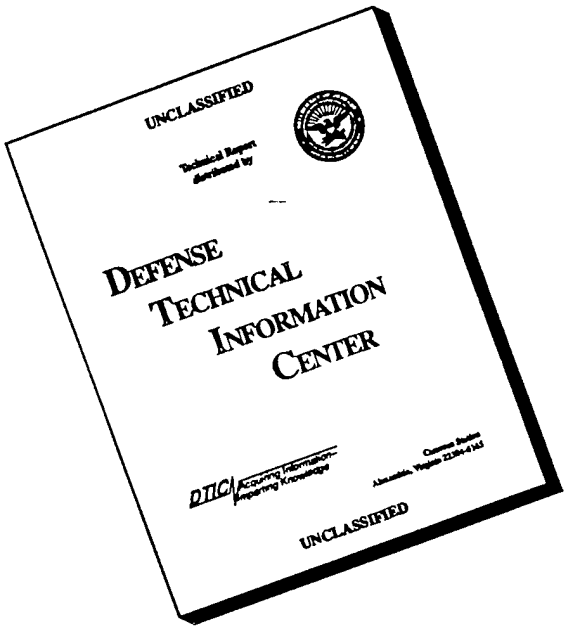

THIS DOCUMENT IS BEST QUALITY AVAILABLE. THE COPY FURNISHED TO DTIC CONTAINED A SIGNIFICANT NUMBER OF PAGES WHICH DO NOT REPRODUCE LEGIBLY.

REPORT DOCUMENTATION PAGE

Form Approved
OMB No. 0704-0188

1. AGENCY USE ONLY (Leave blank)	2. REPORT DATE	3. REPORT TYPE AND DATES COVERED
	8 July 1996	Final Report (9 Jun 91 - 9 Jun 96)

4. TITLE AND SUBTITLE
Biosensor-Based Detection and Verification System for Bio-Chemical Warfare Agents, Appendices 1, 2 and 3 Final Report

5. FUNDING NUMBERS
MDA972-92-C-0005

6. AUTHOR(S)
John C. Owicki

7. PERFORMING ORGANIZATION NAME(S) AND ADDRESS(ES)
Molecular Devices Corporation
1311 Orleans Drive
Sunnyvale, CA 94089

8. PERFORMING ORGANIZATION REPORT NUMBER
DA9196

9. SPONSORING / MONITORING AGENCY NAME(S) AND ADDRESS(ES)
ARPA / DSO
3701 N. Fairfax Dr.
Arlington, VA 22203-1714

10. SPONSORING / MONITORING AGENCY REPORT NUMBER

11. SUPPLEMENTARY NOTES
The view, opinions and/or findings contained in this report are those of the author(s) and should not be construed as an official ARPA position, policy, or decision, unless so designated by other documentation.

12a. DISTRIBUTION / AVAILABILITY STATEMENT
Approved for public release; distribution unlimited.

12b. DISTRIBUTION CODE

13. ABSTRACT *(Maximum 200 words)*

The purpose of this contract was to explore and demonstrate the application of technology based on the Light Addressable Potentiometric Sensor (LAPS) to detection and verification problems for bio-chemical warfare agents. The principal analytical method employed was microphysiometry, by which perturbations of cell physiology are detected using the LAPS. The work was done in three principal segments. First, silicon microtechnology was used to design and fabricate sensor chips and microfluidic components suitable for the project. Second, a systems-engineering effort designed and assembled a prototype high-performance microphysiometer. Third, a biological effort employed a wide variety of cellular and ligand-receptor model systems to validate the generality of the method and the performance of the prototype instrument.

14. SUBJECT TERMS	15. NUMBER OF PAGES
Biosensor, CBW agent detection, microphysiometer, microfluidics	207
	16. PRICE CODE

17. SECURITY CLASSIFICATION OF REPORT	18. SECURITY CLASSIFICATION OF THIS PAGE	19. SECURITY CLASSIFICATION OF ABSTRACT	20. LIMITATION OF ABSTRACT
UNCLASSIFIED	UNCLASSIFIED	UNCLASSIFIED	UL

NSN 7540-01-280-5500

Standard Form 298 (Rev. 2-89)
Prescribed by ANSI Std. Z39-18
298-102

APPENDIX 1

DRAFT OF SOFTWARE MANUALS FOR HIGH-PERFORMANCE MICROPHYSIOMETER INSTRUMENT

USER'S MANUAL

High Throughput MicroPhysiometer (HTuP)

Display side

Version 1.5

By

Dana Redington, Ph.D.

Contents

Background	2
Systems Requirements	3
The Gertrude side of things.	4
Running Gertrude.	6
Quaddisplay.ad.vi	7
Set.sys.params.vi	12
Detail Display	15
Detail Rate Display	18
Training Data	20
Calibrating Nernst Coefficients	21
Using Nernst Coefficients	22
General suggestions	23
Comments and "bug" reports.	24

Background.

The High Throughput MicroPhysiometer (HTuP) system is a set of two programs. There is the **acquire side** program, Master.Acquire.1.5.vi., and the **display side** program, Master.Display.vi. The computers that use these two programs are referred to as the "Allen" and "Gertrude" sides, respectively. Both programs are written in National Instruments LabVIEW (Version 3.1.x). These programs require a large amount of memory, on the order of 50 + MBytes for about three hours of data: they store and process all data in random access memory.

This document describes the general requirements and usage of the Gertrude side of the HTuP system.

System Requirements

Allen side computer

Macintosh Quadra 800 with system 7.1 or higher
~72 MB RAM
1 GB hard disk
NuLogic Board
National Instruments GPIB Board
National Instruments DIO board
LabVIEW 3.1; set to~ 60MB
1 Sony 17se monitor

Gertrude side computer.

Macintosh Quadra 840 with system 7.1 or higher
~72 MB RAM
1 GB Hard disk
National Instruments GPIB Board
LabVIEW 3.1; set to~ 60MB
Radius 8xJ Video Card or equivalent
2 Sony 17se monitors

The two computer systems are interconnected via the serial (Modem) ports, GPIB, and Ethernet connections. During the running of an experiment timely communications are aperiodically exercised via serial and GPIB transactions on both computers.

The Gertrude side of things.

The Gertrude side of the HTuP system is loaded into memory by double clicking the Master.Display.vi in the GertrudeSide*f* folder.

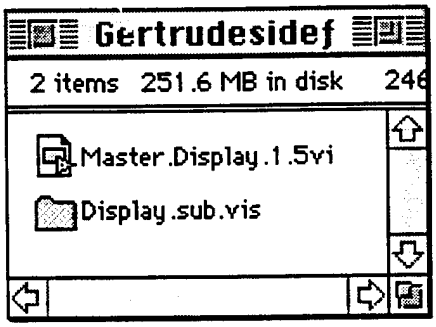

Figure: The GertrudeSide*f* folder.

The process of loading LabVIEW and all the virtual instruments, approximately 125 VIs, that make up the HTuP system will take a few minutes. After the system is loaded the following VI should appear in the left hand region of the desktop.

The Master.Display.1.5.vi has three important areas of controls (see figure below). These are the menu bar at the top of the VI, a set of button controls on the left side of the VI, and a set of four digital controls on the upper right side of the VI. In the menu bar, the application is run by depressing the "right arrow." When the program is running, there are three relevant button controls that provide functions for acquiring data, reviewing data, and quitting the application. These buttons are the ACQUIRE DATA button, the Review Acquired Data button, and the QUIT button, respectively. Finally, of the four digital controls, the MAXDATA control provides a means for setting the maximum number of data samples. A sample is equivalent to one-seconds worth of data, i.e., a record of 40 points for each of 32 channels. (This system is capable of varying the number of sample points, i.e., pts/swp, between 40-50. It is also capable of changing the number of packets per srq to 2. And the number of channels can also be increased. However, these variables are for future versions of the system.). So, the controls should be set as in the figure below, i.e., to 32, 40, and 1 for #chans, pts/swp, and pkts/srq, respectively.

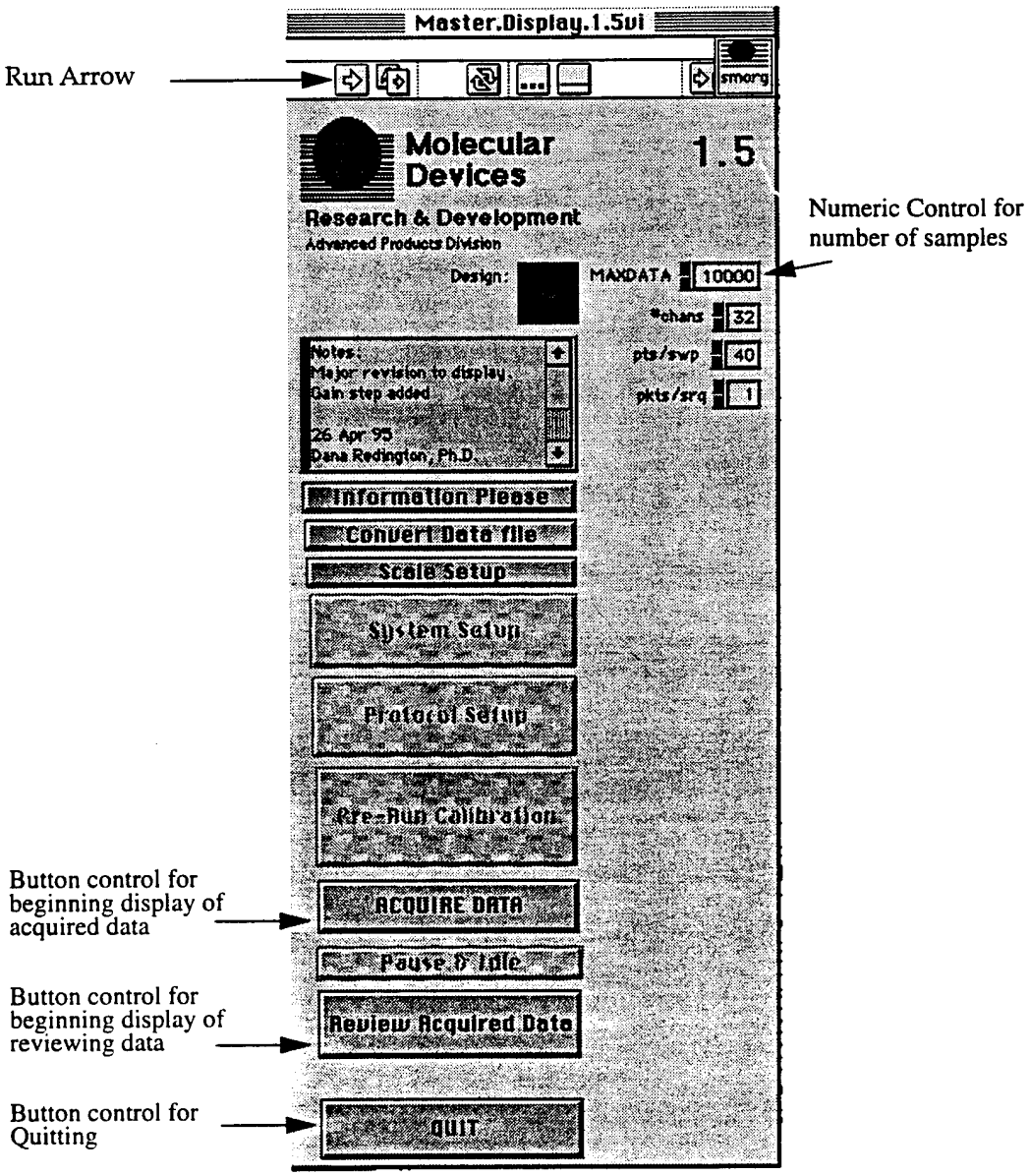

Figure: Master.Acquire.1.5.vi

Running Gertrude.

Running Gertrude is accomplished by performing the following steps:

1. **Confirm/Set the number of samples.** A default value appears in the digital control. This number should be the same number used on the Allen side.

   Note: Typically, the other three digital controls, #chans, pts/swp, and pkts/srq, should NOT be changed. Also these numbers must be identical to those on the Allen side of things.

2. **Depress the run arrow** on the front panel of the Master.Display.1.5.vi.

3. **Press ACQUIRE DATA** button.

A few moments will pass and a new window will appear on the desktop. This window is quaddisplay.ad.vi. It is shown in the figure below.

Quaddisplay.ad.vi

The quaddisplay.ad.vi is the main window for viewing data. It is shown in the figure below.

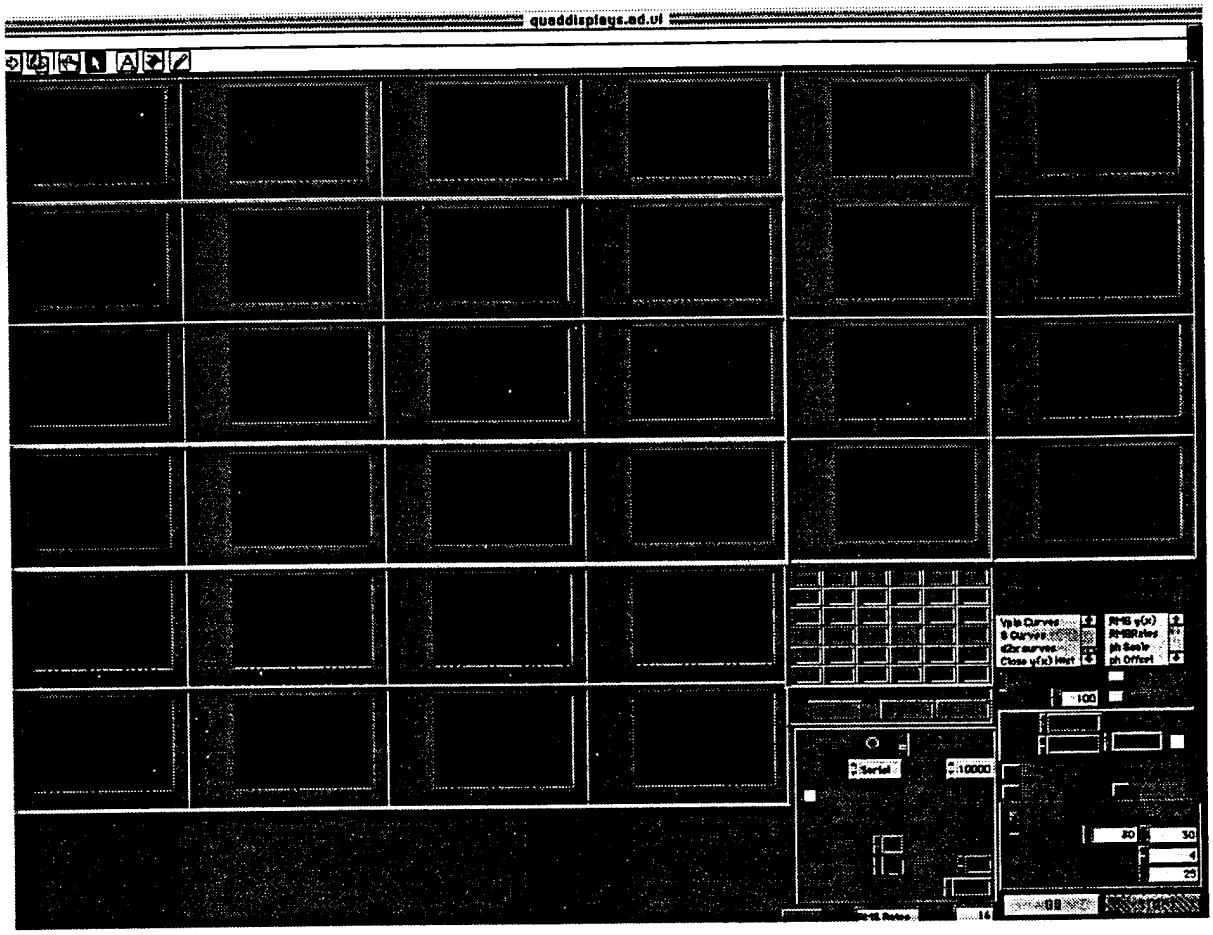

Figure: Quaddisplay.ad.vi

The VI Quaddisplay.ad shows 32 graphs and a number of controls on the lower right hand corner of the window. The 32 graphs are arranged in groups of four corresponding to the eight flow channels of the LAPS. The arrangement of the flow channels is shown in the figure below.

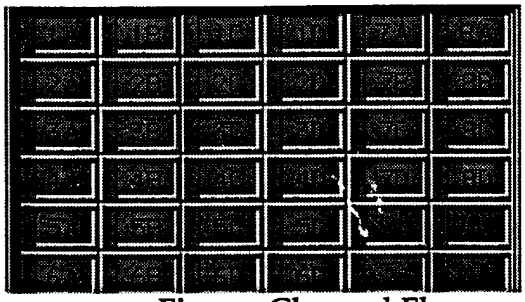

Figure: Channel Flow.

A close up of the controls for this VI are shown in the following figure.

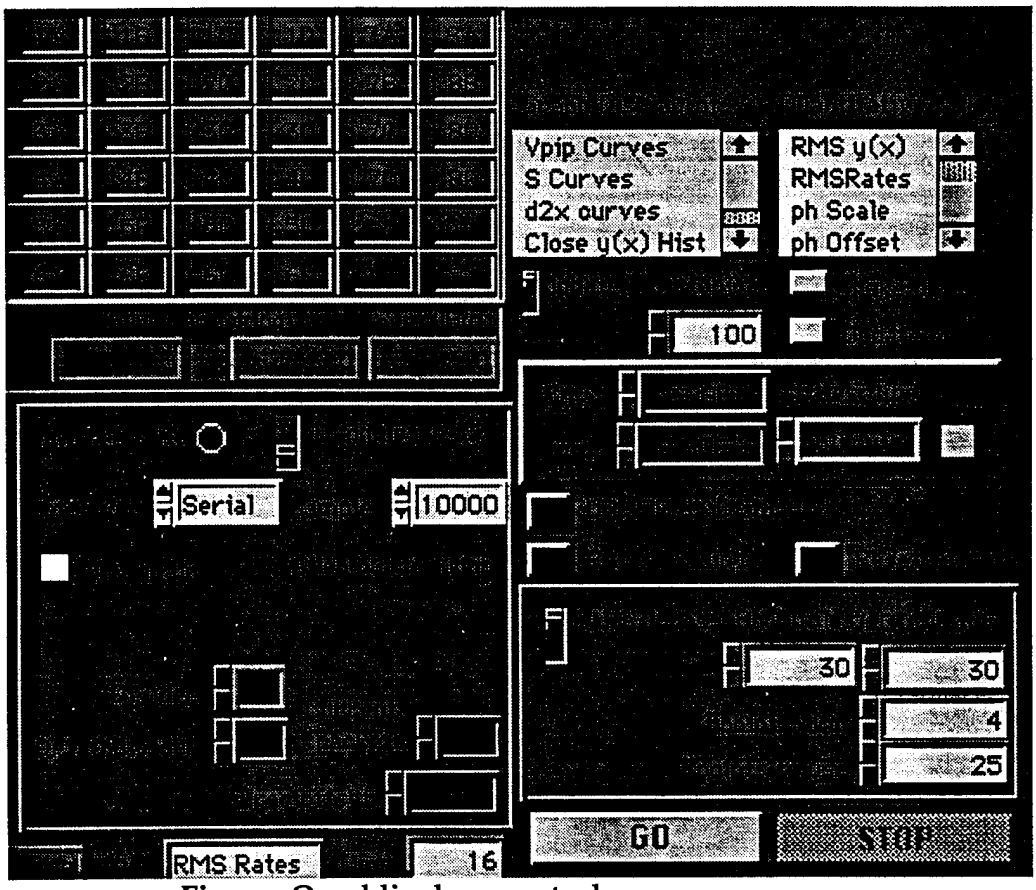

Figure: Quaddisplays controls.

The following table describes the main controls of this window.

Table 1: Description of Quaddisplays controls.

Name	Description	Comment
Index	indicates current sample number	
Backlog	indicates number of bytes to be processed	
SerialBuff	indicates number of bytes in buffer	
Adaptive fit	indicates whether training of nearest x is in process	
Train nearest	control to turn on or off the process of averaging x values.	can be activated any time while running.
Data From	control for source of data. Typically either Serial or from disk	this should be checked/set before pressing GO.
Samples	indicates the number of maximum samples	this number is pulled from the Master.Display.vi.
Try again	a control to attempt re-establishing communications with Allen.	this should be used when Allen has stopped responding to Gertrude.
Allen.out.to.lunch	indicates if communications with Allen have been stopped.	If communications have been stopped then Allen is ignored until the "Try again" button is pressed.
Divider	a control counter for determining when graph updates should occur	This number can be 1. If "Divider" is set to 10 then updates will occur every 10 seconds.
Detail.divider	a control counter for determining when the detail display is updated when open.	This number can be 0 resulting in continuous updates of the detail display. If the number is greater than 1 then updates will occur at intervals of "Detail.divider" in seconds.
Current #packets	a control for setting the number of packets per transfer.	This number should be between 4 and 8. 4 for regular transfers and 8 for catching up.

Table 1: Description of Quaddisplays controls.

Name	Description	Comment
rec offset	a control for setting the offset into the current data	This number should be 0 for keeping the data on the display side identical to that on the acquire side.
Graph Display of	a control for selecting the type of graph: Vpip, S curves, algorithm curves, closest x, or rate	Any of the five graphs can be selected. It will take a few moments to update all 32 sites to the selected graph type.
Quantitative calcs	a control for selecting the type of tabled calculations	Normally set to None. It is used for viewing numerical noise analyses of all 32 sites.
update	a control to set updating on or off. On will update graphs. Off will not.	Normally this is on for displaying data. It can be turned off momentarily to enable expediting the process of catching up to Allen.
#ptstoplot	a control to set the maximum number of points per graph (except for S curves and algorithm curves).	The minimum is 1 and the maximum is 1500. However the number should be reasonable. The more points per plot the longer it takes to update the graphs.
Make default now	a button used to reset the window width that algorithm uses to calculate the peak in the d2 curve.	This is used when initial characterization of the curves fails as a result of faulty data at the beginning of data collection.
Update.now2	a button used to reset the window width around the currently trained "center" of the d2-S curve.	This is used following the "Make default now" control in order to retrain the algorithm for optimal processing of S curves.
Ymax	a control to set the maximum y value of the 32 graphs when the control "Now" is set.	This is extremely useful for setting the upper limit of all graphs to the same level, e.g., when viewing Vpip' or Rate graphs.
Ymin	a control to set the minimum y value of the 32 graphs when the control "Now" is set.	This is extremely useful for setting the lower limit of all graphs to the same level, e.g., when viewing Vpip' or Rate graphs.
scales type	a control to select the type of scaling: manual, auto now, auto	The "auto" mode is for general use. The "manual" mode is for fixing the graphs according to Ymax and Ymin controls.

Table 1: Description of Quaddisplays controls.

Name	Description	Comment
now	a button to enable the scaling function.	This requires "cpu" cycles and is typically used momentarily to apply the Ymax and Ymin scales to all 32 graphs.
DetailRate Display	a button to turn on the Detail Rate Display.	see the section on the Detail Rate Display.
Reset Scaling	a button to examine Nernst values.	see the section on Set.sys.params.
Reset Offsets	a button to reset the offset values of the Vpips' graphs	see the section on training the data.
Calc Slopes	a control to turn on the calculation of slopes	left over from an version 1.0; should always be on.
On(Cycles)	a numeric control to set the number of on cycles	This must be set before GO is pressed and should be the same as the Allen side.
Off(cycles)	a numeric control to set the number of off cycles	This must be set before GO is pressed and should be the same as the Allen side.
#points.skip	a numeric control to set the number of points to skip for slope calculations	this number should be > 4. It also must be set before pressing GO
#points to use	a numeric control to set the number of points used for slope calculations.	This number must be set correctly before pressing GO.
GO	a button used to begin the displaying of data	This button should only be used after all other controls have been checked for appropriate values.
32 channel button array	A button array for choosing a channel for the detail display.	Selecting a channel will open the Detail Display window.

Several additional windows can be opened from this main window. The additional windows are Set.sys.params, Detail Display, and Detail Rates. These are described in the following three sections.

Set.sys.params

Set.sys.params is opened by depressing the Reset Scaling button. This window is used for examining various variables associated with graphing data and in calculating rates. The Nernst constants are also displayed in this window. Set.sys.params is shown in the figure below.

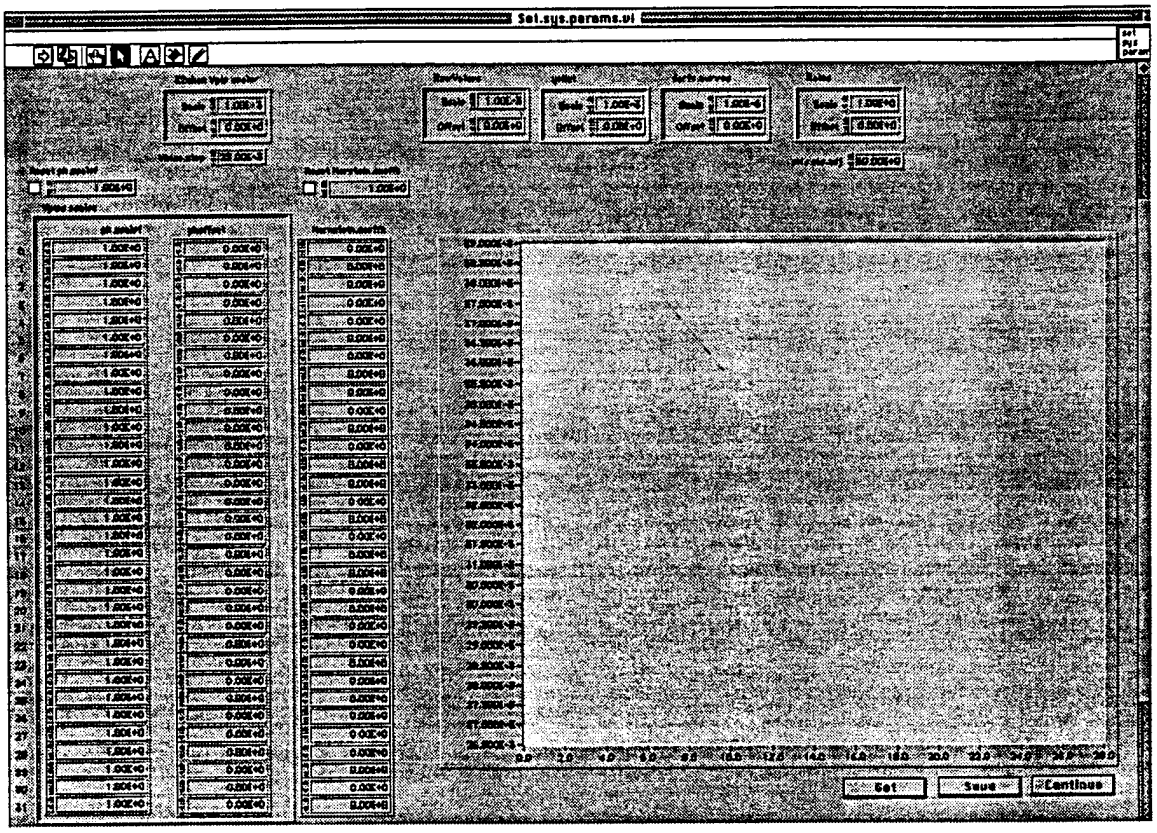

Figure: Set.sys.params.vi

The Set.sys.params.vi is used for reviewing and setting the variables associated with processing the data and displaying of graphs. This is particularly important for either viewing the calibrated Nernst coefficients taken from a known pH shift or by "getting" a previous calibration file. Each of the controls and indicators are described in the following table.

Table 2: Description of Set.sys.params controls.

Name	Description	Comment
32chan Vpip scaler	two numeric controls for setting the scale factor and y offset when displaying a Vpip graph.	typically this is not modified here, rather automatically set for common baselines using the "reset offsets button" on the main control panel
RawValues	two numeric controls for setting the scale factor and offset when displaying a raw value graph.	The graph will be scaled in mpH if calibrated Nernst coefficients are used. The default values should be used and not modified.
yHist	two numeric controls for setting the scale factor and y offset when displaying a Vpip graph.	the graph will be in scaled dac counts.The default values should be used and not modified.
deriv.curves	two numeric controls for setting the scale factor and y offset when displaying a derivative graph.	The default values should be used and not modified.
Rates	two numeric controls for setting the scale factor and y offset when displaying a Rate graph.	The default values should be used and not modified.
Vbias.step	a numeric control for setting the bias step.	Typically 25 mV.
Reset	a button used to force the pH scale function into the 32 channel array of ph.scale factors	
ph scalef	a numeric control for setting the ph scale factor.	
Vpips.scales	a cluster of two arrays for setting the ph scale factor and offset.	
Reset - Nernst.coeffs	a button used to force the default Nernst value (in the box to the right) into the 32 channel array of Nernst coefficients	

Table 2: Description of Set.sys.params controls.

Name	Description	Comment
Nernst.coeffs	a numeric array of Nernst coefficients for each of the 32 channels of the LAPS.	
pH.rate.adj	a numeric control for setting the number of millivolts per pH unit when calculating rates.	Typically 60.0
Multi channel graph.	an indicator that displays a plot of the nernst values for all 32 channels	This is used to evaluate the calculated coefficients across the 32 sites.
Get	a button to retrieve a previously saved Nernst coefficient data file.	This should be used to retrieve a Nernst data file at the beginning of an experiment.
Save	a button to save the current Nernst coefficients as a datafile.	This should be used after a pH shift calibration sequence has been performed. The saved data file will accurate reflect the current state of the 32 LAPS sites.
Continue	a button to return to the main display.	This function must be used in order to leave this control panel and return to the main window.

Detail display

The Detail display is opened automatically when a channel is selected from the 32 channel button array on the main window. A figure of the window is shown below.

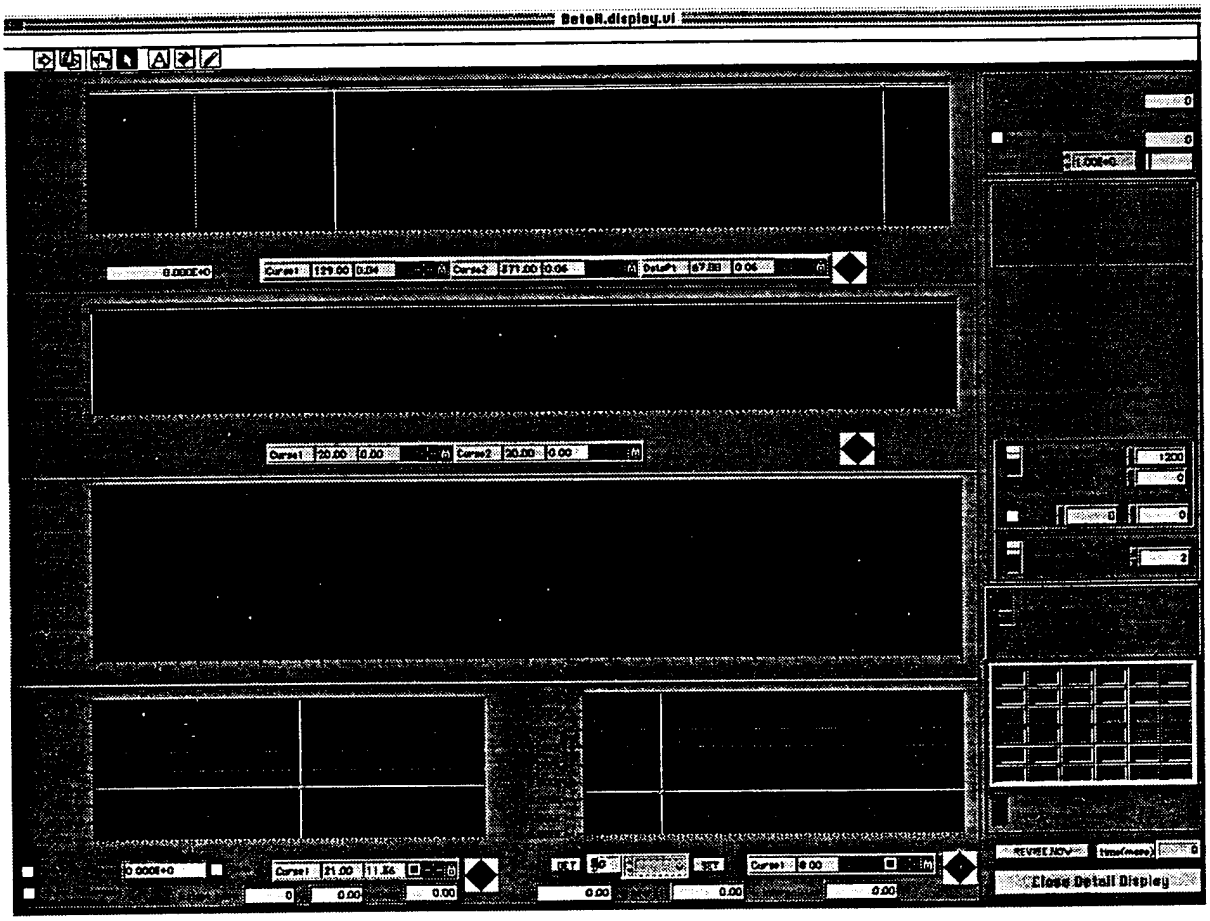

Figure Detail Display.vi

The detail display is composed of five graphs on the left-center of the window and a number of controls on the right of the window. These are described in the table below.

Table 3: Detail Display controls.

Name	Description	Comment
Top graph	displays Vpips' (actually calculated pH values) for the data collected	Cursor 1, 2, and 3 are used for several important functions.

Table 3: Detail Display controls.

Name	Description	Comment
Middle graph	displays y(x)History;	
Rate graph	The graph, third from the top, displays the rate points for an experiment.	
Lower Left graph	displays S curves, that is fundamental data, and difference in S curves.	This graph is used for examining the signal integrity, and in evaluating the noise present in the S curves.
Lower Right graph	displays the result of convolving 2 s curves.	the left and right vertical bars denote the window within which the maximum peak in the curve is search for.
Current index	indicates the current data sample	
Current Channel	indicates which of the 32 sites is currently being displayed	
Make Same Now	control to calculate Nernst values	This uses Cursor 1, Cursor 2, and the with pH shift to perform a calibration.
with pH shift	a known pH shift (used with the above).	
Limit Graphs	a switch to turn on graph maximum points	used with the top two graphs of this window to restrict the number of points plotted. Fewer points plotted results in faster plotting speed.
graph pts	a control for setting the maximum width of Vpip and yxHist plots	This is only used when the "Limit Graphs" button is set.
Offset	a control for setting the offset in samples into the data, i.e, ignoring the first n points.	This is used in the top two graphs and can restrict the amount of data plotted.
Absolute	a switch to set use of absolute indexing versus relative to the last point collected.	This is used with the top two graphs and restricts how much of the data is plotted.
Abs.start	a control for setting the start point for plotting.	This value sets the left hand side of the data window that is plotted.
Abs end	a control for setting the ending point for plotting.	This value sets the right hand side of the data window plotted.

Table 3: Detail Display controls.

Name	Description	Comment
Strip n points	a switch for stripping a number of points from the RATE graph	this is used to ignore n points from the Rate graph.
points	a control for setting the number of points to "strip" from the data.	This is typically set to 2 to eliminate aberrant rate data.
Cursor Select of point	a switch indicating which point, as referenced by cursor 3, is to be plotted in the lower two graphs	If this is set, then the location of cursor 3 will be used to index which S and algorithm curves are plotted.
32 channel array	a 32 button control to select which channel of data is to be displayed.	
Manual Channel	a switch to turn on manual channel indexing.	
Revise.Now	a button to update the graphs	only works if "update" is on quaddisplays.vi.
time(msec)	an indicator showing the time to update graphs.	
Close Detail Display	a button used to close this window.	This must be used to close the current display and return to the main window control window.

Detail Rate Display

The detail display is activated by depressing the DetailRate Display button on the quaddisplays.ad.vi. This window is used for examining rate data across all 32 channels. The window is composed of a multichannel graph on the left of the window and several controls on the right of the window. The window is shown below followed by a description of the controls.

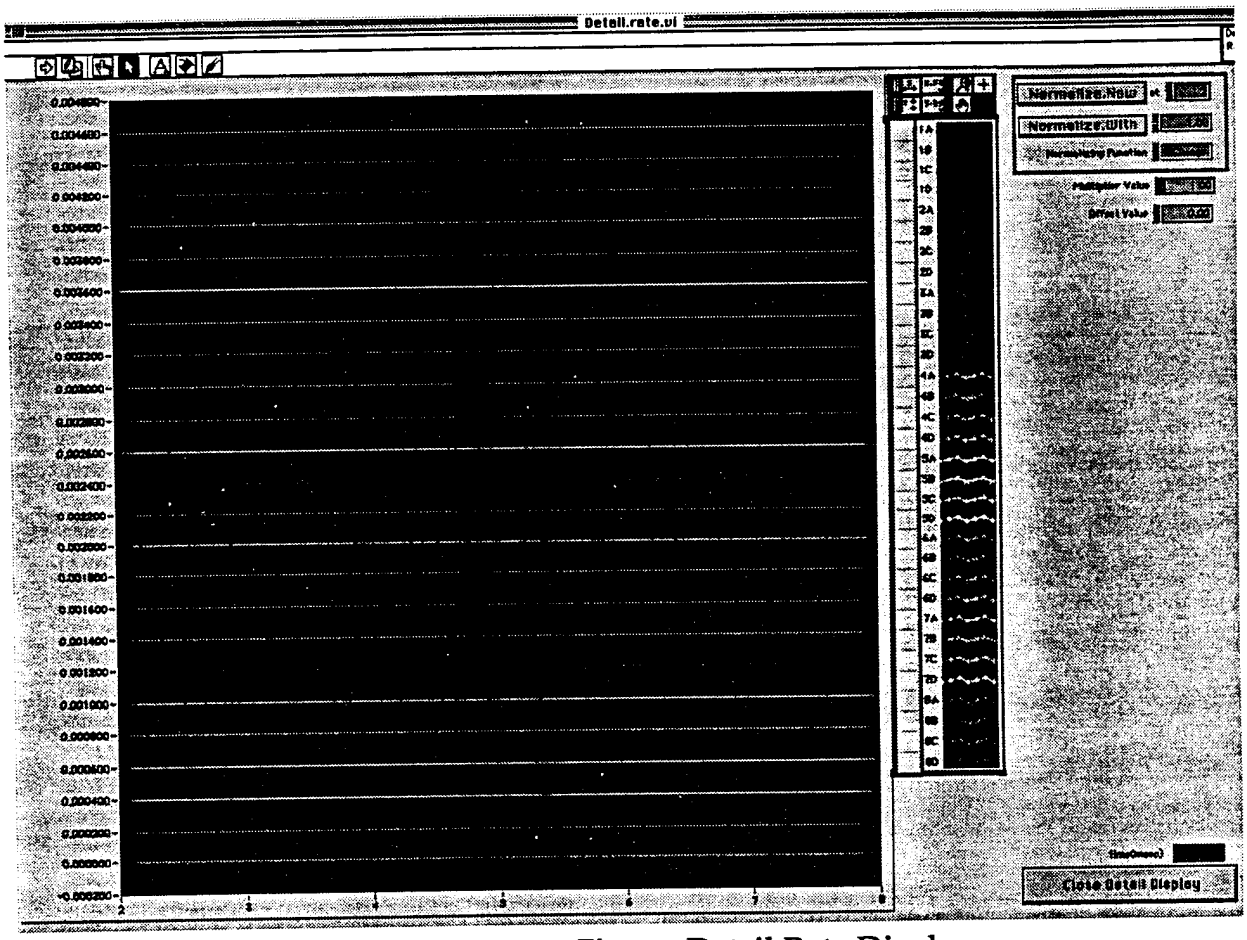

Figure: Detail Rate Display.

Table 4: Detail.rate controls

Name	Description	Comment
Multichannel graph	a display of rate data for selected channels	This is used to plot the rate data of various channels on a single graph for comparison purposes.
32 button array	an array of 32 buttons used to select which sites are displayed.	Pressing any of the 32 buttons turns on the graph for that site. More than one site can be turned on at the same time.
Normalize.Now	a button used to normalize all data within a channel to a certain "at" point.	This enables setting the display of rate data to the same relative level.
at	a numeric control to select a point to normalize at.	This is used with the "Normalize.Now" button.
Normalize with	a button to normalize a particular value	This is used to set
with	a particular value used in normalizing rate data.	
Multiplier Value	a numeric control for determining scaling of the% of change.	This is similar to a zoom function.
Offset value	a numeric control for determining the minimum display.	This is used to set the lower threshold of plotting data.
time(msec)	an indicator displaying the duration in msec for plotting the last multiplot graph.	
Close Detail Display	a button used to close the detail display.	This must be used to close this window.

Training on the Data.

Training on the data is an important pre-requisite for conducting a good experiment that yields meaningful data. Training is required to tune the algorithm used in rate calculations and involves a several step process. this is done automatically at the beginning of each experiment. However, if the initial data is unstable then the automatic calibration will fail to yield useful results: it must be redone manually. the following training steps can be followed:

Make sure that the Detail display is open and that the quaddisplay.vi "Graph Display of" is set for d2x curves. The update button should also be asserted.

1. Depress Make.default now. This will reset the algorithm window to full width. As a result of this the "peak point" should be correctly indicated for all 32 channels.

2. Wait for a stable flow ON period.

3. Set # ptstoplot on Quaddisplays to a reasonable number. A number of between 12-20 is reasonable. This number represents the number of values to train on.

4. Assert Train nearestx. This will average out the best yxHist value. This should be left on for a number of samples, about 12.

5. Deassert Train nearestx. This will stop the averaging process.

6. Depress Update.now2. This will apply the averaged values to determine the optimal window for each of the 32 channels.

Part 2: Training on y(x) History.

7. Choose the y of x history plot.

8. wait for a period of stable period of activity lasting at least 12 samples (seconds).

9. Depress the Reset Offsets button on the main display. This will result in setting the appropriate levels across all 32 sites.

Calibrating Nernst coefficients.

Calibrating the Nernst coefficients is also important pre-requisite for obtaining good data from an experiment. This is a multi-step process and involves conducting a pH switch between two known buffers. Typically the pH shift is performed by "sipping" from two well columns. The difference in pH between the two wells is on the order of.1M. The process of calibration can also be performed on previously recorded data, i.e., from a data file.
The steps for calibrating the Nernst coefficients are:

Step 0. The Detail display should be open with updates asserted. An appropriate channel should also be chosen.

Step 1. Collect the data from an experiment.

Step 2. Enter the known pH shift. This is accomplished by setting the "with pH shift" control with the difference in pH between the two buffers.

Step 3. Position Cursor 1. Cursor 1 should be moved to a stable baseline region before the pH shift; the cursor should be in a yellow "flow off" region.

Step 4. Position Cursor 2. Cursor 2 should be moved to a stable region immediately after the pH shift; the cursor should be in a yellow "flow off" region with at least 12 points to its left.

Step 5. Set the Make Same Now button. Set it only once. A moment will pass and the application will update the Nernst coefficients and use them to correctly display Vpips'. Note that the difference between the two cursors will be reflected in the indicator labeled "Cursor1-cursor2": this value should be close to the known pH shift.

Suggestions: Viewing the coefficients. The Nernst coefficients can be examined immediately after they are calibrated. this can be accomplished by depressing the Reset Scaling button on the quaddisplays control panel.

Saving the coefficients. After the Nernst coefficients are examined they can be saved to a disk file for later use by depressing the SAVE button on the Set.sys.params control panel.

Using Nernst Coefficients

Nernst Coefficients can be applied to data by retrieving them from a previously stored data file. The steps for this process are:

Step 0. Quaddisplays.ad.vi running after being properly set up.

Step 1. Depress Reset Scaling. This should open the Set.sys.params.vi.

Step 2. Depress "Get". This will open a dialog box to perform retrieval of a previously saved nernst file.

Step 3. Examine the value. The Nernst values will be plotted on the main graph and numerically display in the array "Nernst.coeffs."

Note: The values for a particular channel can be "edited" or adjusted by changing the value in the Nernst.coeffs array.

Step 4. Depress "Continue." This will close the current window and return control to the main display window.

General Suggestions

The successful use of Allen and Gertrude should take into considerations the following:

- For the time being, the Master.Acquire.1.5.vi should be run, fresh, for each experiment. This will also mean that Gertrude will need to be stopped and the run again.

- Some data should be collected on the Allen side before Gertrude requests data. Gertrude will automatically stop communicating with Allen. In order to attempt to resume communications the Try again button must be pressed on quaddisplays.vi.

- Gertrude should be stopped before data collection is halted on the Allen side.

- Data can be reviewed and exported at the end of an experiment.

Comments and "bug" reports.

The development of the HTuP system is an ongoing effort. As such we would appreciate any and all comments and suggestions about improvements of the system.

In those rare instances when an error occurs, we would also appreciate any "bugg reports." These reports should elucidate the conditions that led up to the error and suggest a desired outcome.

	1	2	3	4	5	6	7	8
A	cell type	cell type	cell type	cell type	cell type	cell type	cell type	cell type
B	cell type	cell type	cell type	cell type	cell type	cell type	cell type	cell type
X	cell type	cell type	cell type	cell type	cell type	cell type	cell type	cell type
Δ	cell type	cell type	cell type	cell type	cell type	cell type	cell type	cell type

	1	2	3	4	5	6	7	8	9	10	11	12	13
1		1	2	3	4	5	6	7	8	9	10	11	12
2	A	analyte'	analyte'	analyte'	analyte'	analyte'	analyte'	analyte'	analyte'	analyte'	analyte'	analyte'	analyte'
3	B	analyte'	analyte'	analyte'	analyte'	analyte'	analyte'	analyte'	analyte'	analyte'	analyte'	analyte'	analyte'
4	C	analyte'	analyte'	analyte'	analyte'	analyte'	analyte'	analyte'	analyte'	analyte'	analyte'	analyte'	analyte'
5	D	analyte'	analyte'	analyte'	analyte'	analyte'	analyte'	analyte'	analyte'	analyte'	analyte'	analyte'	analyte'
6	E	analyte'	analyte'	analyte'	analyte'	analyte'	analyte'	analyte'	analyte'	analyte'	analyte'	analyte'	analyte'
7	F	analyte'	analyte'	analyte'	analyte'	analyte'	analyte'	analyte'	analyte'	analyte'	analyte'	analyte'	analyte'
8	G	analyte'	analyte'	analyte'	analyte'	analyte'	analyte'	analyte'	analyte'	analyte'	analyte'	analyte'	analyte'
9	H	analyte'	analyte'	analyte'	analyte'	analyte'	analyte'	analyte'	analyte'	analyte'	analyte'	analyte'	analyte'

Column

	1	2	3	4	5	6	7	8	9	10
1	Step Number	~~Well Row~~	On Cycles	Off Cycles	Flow Rate	Dwell Periods	Pts to skip	Pts to use	...	Comment
2	1	1	*	*	*	20	*	*	...	baseline
3	2	2	*	*	*	20	*	*	...	condition...
4	3	3	*	*	*	20	*	*	...	condition...
5	4	4	*	*	*	20	*	*	...	condition...
6	5	5	*	*	*	20	*	*	...	condition...
7	6	6	*	*	*	20	*	*	...	condition...
8	7	7	*	*	*	20	*	*	...	condition...
9	8	8	*	*	*	20	*	*	...	condition...
10	9	9	*	*	*	20	*	*	...	condition...
11	10	10	*	*	*	20	*	*	...	condition...
12	11	11	*	*	*	20	*	*	...	condition...
13	12	12	*	*	*	20	*	*	...	condition...
14										
15										
16	Note:	* -- indicates that these are filled in automatically as a result of pre-run calibration								
17		For bug-off, idle, or other protocols an explicit number can be used to manually define the value								
18										
19										
20										
21										
22										
23										
24										
25										
26										
27										
28										
29										
30										
31										
32										
33										
34										
35										
36										
37										

AnalyteWellSummary.03.2vi
1/16/95 8:28 AM

Front Panel

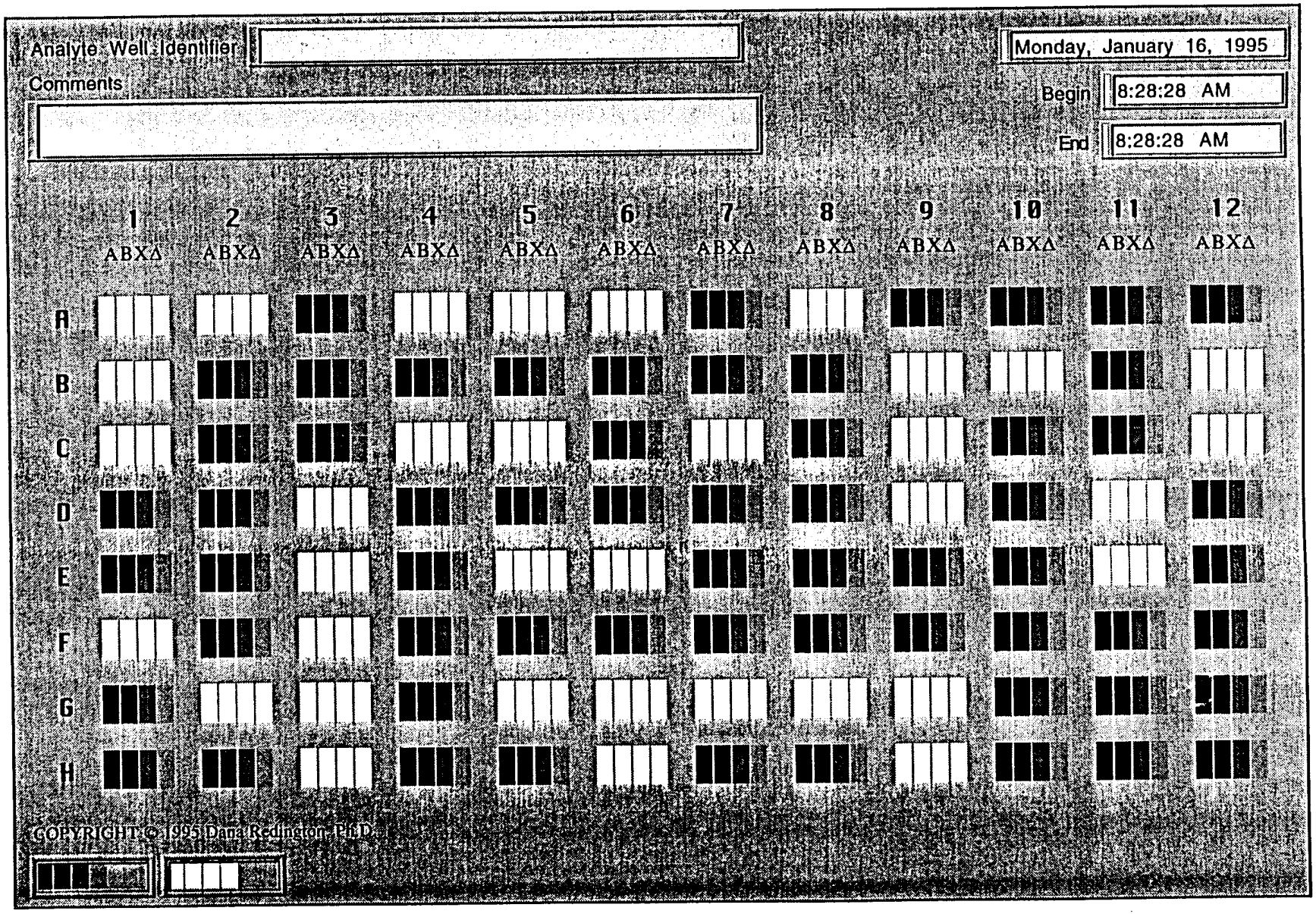

HTuP.graph.03vi
1/16/95 2:49 AM

Front Panel

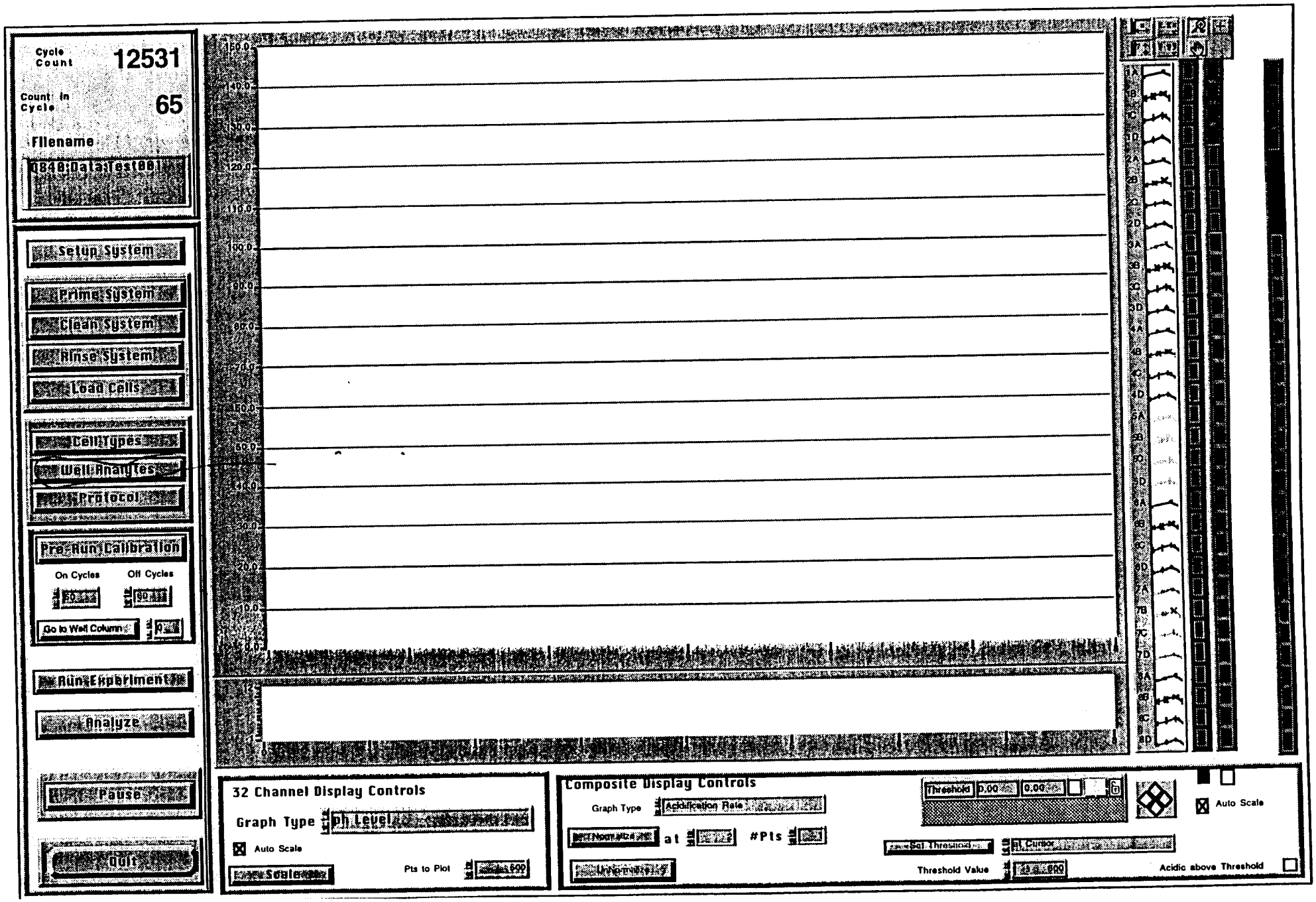
Cycle Count
12531
Count In Cycle
65
Filename
0848:Data:Test00.1
Setup System
Prime System
Clean System
Rinse System
Load Cells
Cell Types
Well Analytes
Protocol
Pre-Run Calibration
On Cycles
Off Cycles
Go to Well Column
Run Experiment
Analyze
Pause
Quit
32 Channel Display Controls
Graph Type
pH Level
Auto Scale
Scales
Pts to Plot
Composite Display Controls
Graph Type
Acidification Rate
Normalize
at
#Pts
Threshold
Set Threshold
at Cursor
Threshold Value
Auto Scale
Acidic above Threshold

USER'S MANUAL

High Throughput MicroPhysiometer (HTuP)

Acquire side

Version 1.5

By

Dana Redington, Ph.D.

Contents

Background	2
Systems Requirements	2
The Allen side of things.	3
Running Allen.	4
Synchronized.occur.dataCom.vi	4
Smorg.peripherals.vi	4
SMORGDASfootBoard.vi	5
HTuP User Interface 1.5	6
User Interface control buttons	7
User Interface Experiment Protocol Variables	11
General Suggestions	13
Comments and "bug" reports.	14
Timing Diagrams	15

Background.

The High Throughput MicroPhysiometer (HTuP) system is a set of two programs. There is the acquire side program, Master.Acquire.1.5.vi., and the display side program, Master.Display.vi. The computers that use these two programs are referred to as the "Allen" and "Gertrude" sides, respectively. Both programs are written in National Instruments LabVIEW (Version 3.1). These programs require a large amount of memory, on the order of 50 MBytes for about three hours of data: they store and process all data in random access memory.

This document describes the general requirements and usage of the Allen side of the HTuP system. It also includes timing diagrams of various processes and events associated with the HTuP system.

System Requirements

Allen side computer
- Macintosh Quadra 800
- ~72 MB RAM
- 1 GB hard disk
- NuLogic Board
- National Instruments GPIB Board
- National Instruments DIO board
- LabVIEW 3.1; set to~ 60MB

Gertrude side computer.
- Macintosh Quadra 840
- ~72 MB RAM
- 1 GB Hard disk
- National Instruments GPIB Board
- LabVIEW 3.1; set to~ 60MB

The two computer systems are interconnected via the serial (Modem) ports, GPIB, and Ethernet connections. During the running of an experiment timely communications are aperiodically exercised via serial and GPIB transactions on both computers.

The Allen side of things.

The Allen side of the HTuP system is run by double clicking the Master.Acquire.vi in the AllenSide*f* folder.

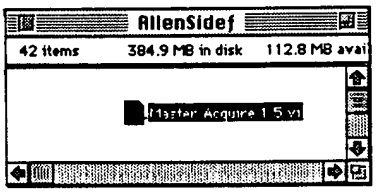

Figure: The AllenSide*f* folder.

The process of loading LabVIEW and all the virtual instruments, approximately 200 vis, that make up the HTuP system will take a few minutes. After the system is loaded the following VI should appear in the upper left hand region of the desktop.

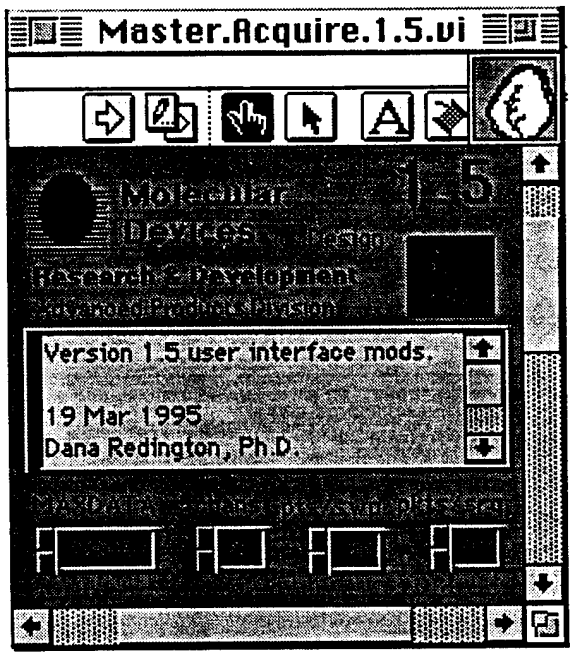

Figure: Master.Acquire.1.5.vi

The Master.Acquire.1.5.vi has four important variable controls. These are MAXDATA, #chans, pts/swp, and pkts/srq. Only the MAXDATA control should be modified. It represents the number of data packets to collect. With a one second per data packet rate, this number also represent the number of seconds of fundamental data.

Running Allen.

Running Allen is accomplished by depressing the run arrow on the front panel of the Master.Acquire.1.5.vi. A few moments will pass and four additional windows will appear on the desktop. These windows are: Synchronized.occur.dataCom.vi, Smorg.peripherals.vi, Smorgdasboard.foot.vi, and the User.Interface.1.5.vi. Each of these are described below.

Synchronized.occur.dataCom.vi

This window displays the status of communications between Allen and Gertrude, hence the ear icon. The numeric indicator on the top left displays the difference between the current data sample and the last sent to Gertrude. The number below it is the data sample number last requested by Gertrude.

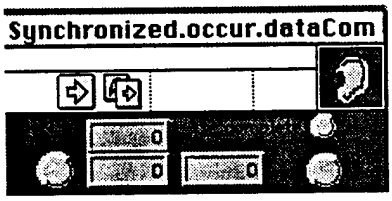

Figure: Synchronized.occur.dataCom

Smorg.peripherals.vi

The Smorg.peripherals.vi displays the status of that part of the program involved with controlling and sensing the microplate and syringe pump.

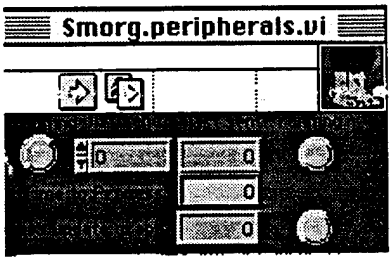

Figure: Smorg.peripherals.vi

SMORGDASfootBoard.vi

the SMORGDASfootBoard.vi display the status of that part of the program involved with regulating the on/off flow of solution through the LAPS. The important indicators are described in the following table.

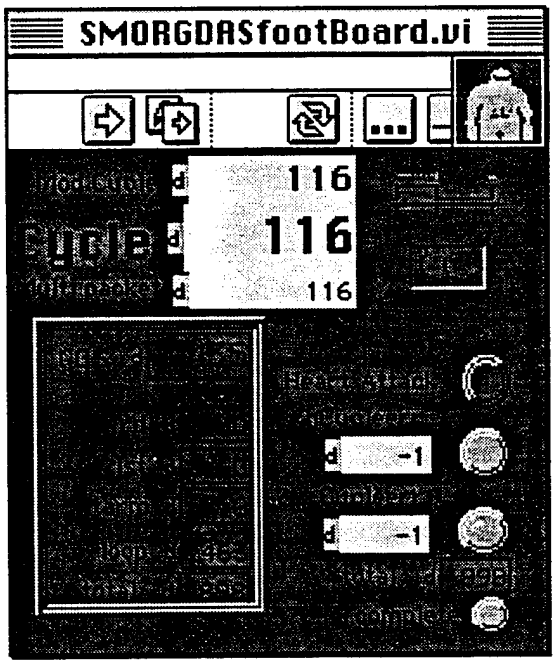

Figure: SMORGDASfootBoard.vi

Table 1: SMORGDASfootBoard indicators

Indicator	Brief Description
Mod Cycle	indicates the current number within an on/off protocol. It is a decrementing counter.
Cycle	indicates the data sample number
Multi.packet	indicates the cycle number since initialization.
Heart Attack	indicates an error in on/off flow control.
hCycleerr	indicates the cycle number when a hardware overrun occurred.
Cycleerr	indicates the cycle number when a software overrun occurred.
Waste/Laps indicator	Indicates the state of the shear valve: that is at waste a loose "W" or at LAPS (lips). 

HTuP User Interface 1.5.

The User Interface of the HTuP system provides the necessary controls and displays for commanding the system to perform different microphysiometry functions. The user interface, shown below, is divided into three main areas. The upper left side displays various indicators of the system state. The lower left side provides a set of controls for initiating different processes and functions. The right side of the display lists the current set of protocols.

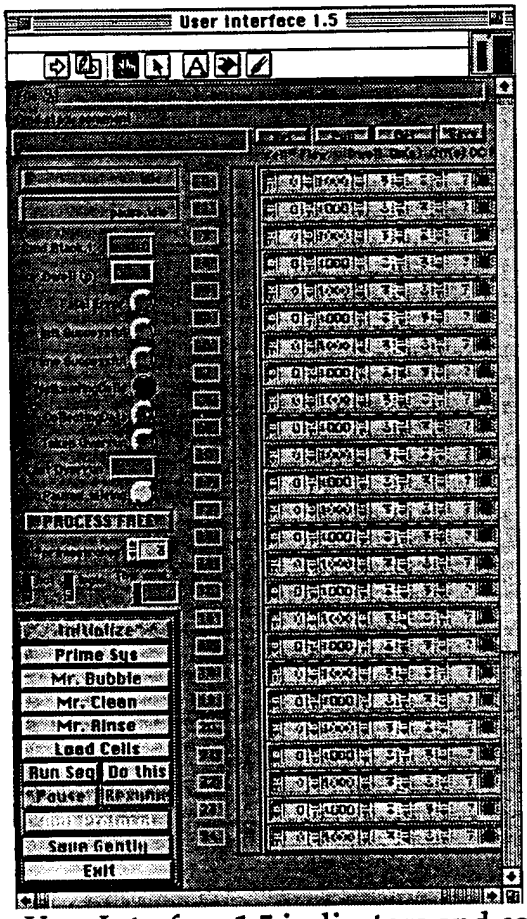

Figure: User Interface 1.5 indicators and controls.

Table 2: User Interface Indicators

Indication	Brief description
File	name of the experiment file used
Cmd.stack comment	a comment associated with the current experiment
idle	a label for Step 0 in the experiment stack.
pause.idle	a label for Step 1 in the experiment stack
Cmd.Stack	the current step in the experiment
cur.Dwell(p)	indicates the current dwell number within a protocol. It is a decrementing counter.
Fatal Error	indicates a very bad condition.
Init Successful	indicates proper initialization of the system
Prime Successful	indicates proper priming of the system.
NotLoadingCells	indicates whether or not a cell loading sequence is in progress
CollectData	indicates whether or not fundamental data is being collected.
Token Overrun	indicates if too many tokens are in the machine.
Last Overrun	indicates the cycle when the last overrun occurred.
Paused, idling	indicates if the system is paused.
PROCESS FREE	indicates when the system is not processing a command.

User Interface control buttons.

The User Interface control buttons are shown below and described in the following table.

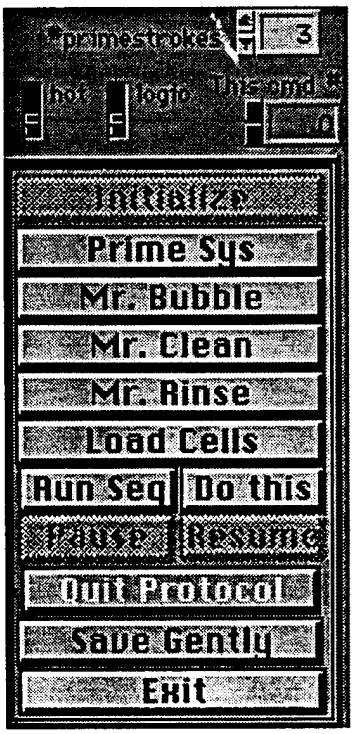

Figure: User Interface control buttons

Table 3: User Interface Controls

Control	Brief description	
#prime strokes	the number of priming strokes for filling fluid into the system.	used with Prime
hot	a flag, when up indicates that a warm or hot start (i.e., the system already has fluid in it).	normally off, but when used must be set before initializing.
logic	a flag, when up indicates that diagnostic information is to be acquired in the "logic analyzer."	normally off.
This cmd#	a numeric variable that indicates the step in the experiment to be run.	used with Do this

Table 3: User Interface Controls

Control	Brief description	
Initialize	a button that activates an initialization sequence. All peripherals and hardware are set up.	used once at the beginning, or with the "hot" flag to perform a warm start.
Prime Sys	a button that activates a priming sequence. This fills the system with fluid.	uses "#prime strokes"
Mr. Bubble	a button that activates a default de-bubbling protocol.	
Mr.Clean	a button that activates a default cleaning, aka "bugg-off" protocol.	
Mr. Rinse	a button that activates a default de-bubbling protocol.	
Load Cells	a button that activates a cell loading sequence.	prompts provided at each step.
Run Seq	a button that initiates an experimental set of protocols.	
Do this	a button that initiates a one step protocol	uses "This cmd#"
Pause	a button that provides a pause when running a sequence.	Step 1 in the experiment is used.
Resume	a button that provides re-entering the running sequence	prompts are provided.
Quit Protocol	a button that enables leaving an experimental protocol.	Step 0 in the experiment is used
Save Gently	a button that enables saving data to a file.	should be used after an experiment when sipping from the trough
Exit	a button that enables leaving the HTuP program.	The program stops when this button is used.

User Interface Experiment Protocol Variables.

The experiment is defined by the editable control on the right side of User Interface window, see figure below. There are four buttons and an array of 24 steps. These are described in the following two tables.

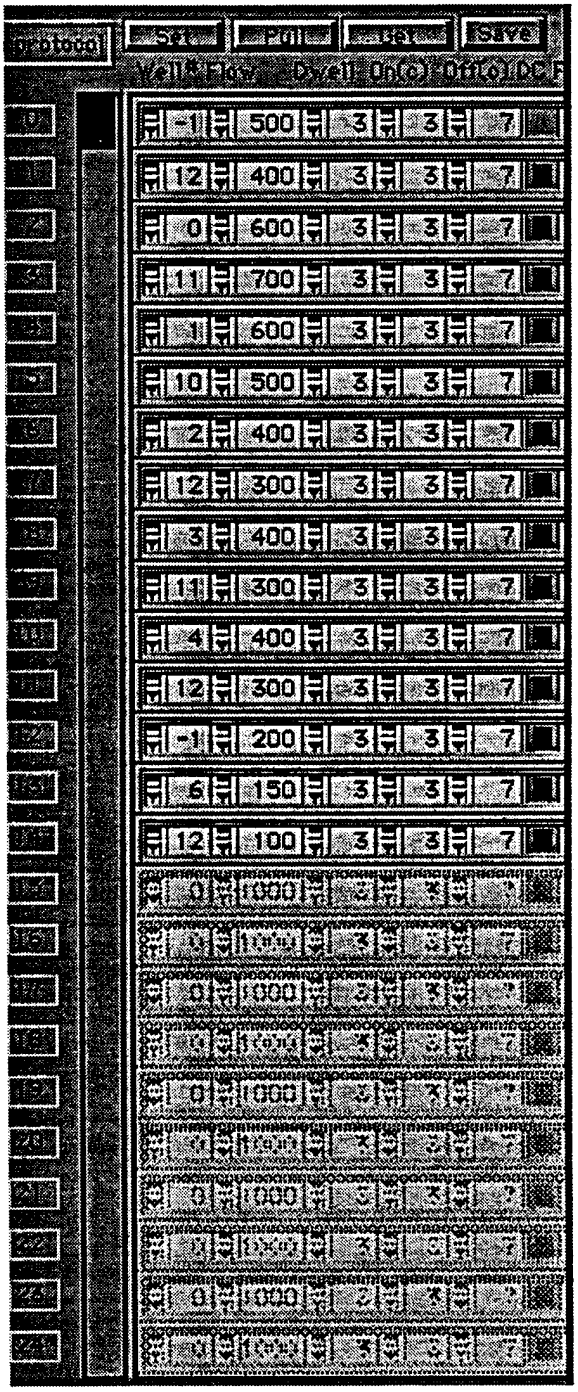

Figure: User Interface 1.5

Table 4: command buttons

Control	Brief Description	Comment
Set	places the current experiment into the "gear box--under the hood"	can be done at any time after initialization. Any changes done to the experiment variables are used by the gear box.
Pull	retrieves a copy of the current experiment from under the hood.	can be done at any time.
Get	retrieves an experiment from a disk file.	should be done before data collection
Save	stores the current experiment to a disk file.	should be done before or after data collection.

Table 5: Protocol Variables

Column	Brief Description.
Step Number	the number of the step in the experiment
Well Numbert	the well column number of the microplate to sip from
Flow Rate *	the rate of flow
Dwell	the number of periods, i.e., on/off cycles used
On Time*	the number of pump cycles for flow on at the current column location.
Off Time *	the number of pump cycles for stopped flow at the current column location.
DC	When set enables collection of fundamental data.

Note: On Time, Off Time, Flow Rate, and Dwell determine the amount of fluid sipped from the trough or a well.

General Suggestions

The successful use of Allen and Gertrude should take into considerations the following:

• For the time being, the Master.Acquire.1.5.vi should be run, fresh, for each experiment. This will also mean that Gertrude will need to be stopped and the run again.

• Data must be collected on the Allen side before Gertrude requests data.

• Gertrude should be stopped before data collection is halted on the Allen side.

•Warm start can be accomplished by exiting Allen, re-running Allen, then setting the "hot" button followed by depressing initialize. After this a protocol can be run, immediately.

•Data should only be saved at the end of an experiment.

Comments and "bug" reports.

The development of the HTuP system is an ongoing effort. As such we would appreciate any and all comments and suggestions about improvements of the system.

In those rare instances when an error occurs, we would also appreciate any "bugg reports." These reports should elucidate the conditions that led up to the error and suggest a desired outcome.

Timing Diagrams.

The timing of various events in the HTuP system are shown in three diagrams. Diagram 1, HTuP DAQ-XFR cycle, shows the relationship between VPIP' data points and the data acquisition and transfer cycle. diagram 2, HTuP VI timings, shows the relationship between the DAQ-XFR cycle and the key VIs on the Allen side. Diagram 3, HTuP Timing of Events, shows the relationship between the DAQ-XFR cycle and the various peripherals as well as key variables used in the Master Acquire.vi.

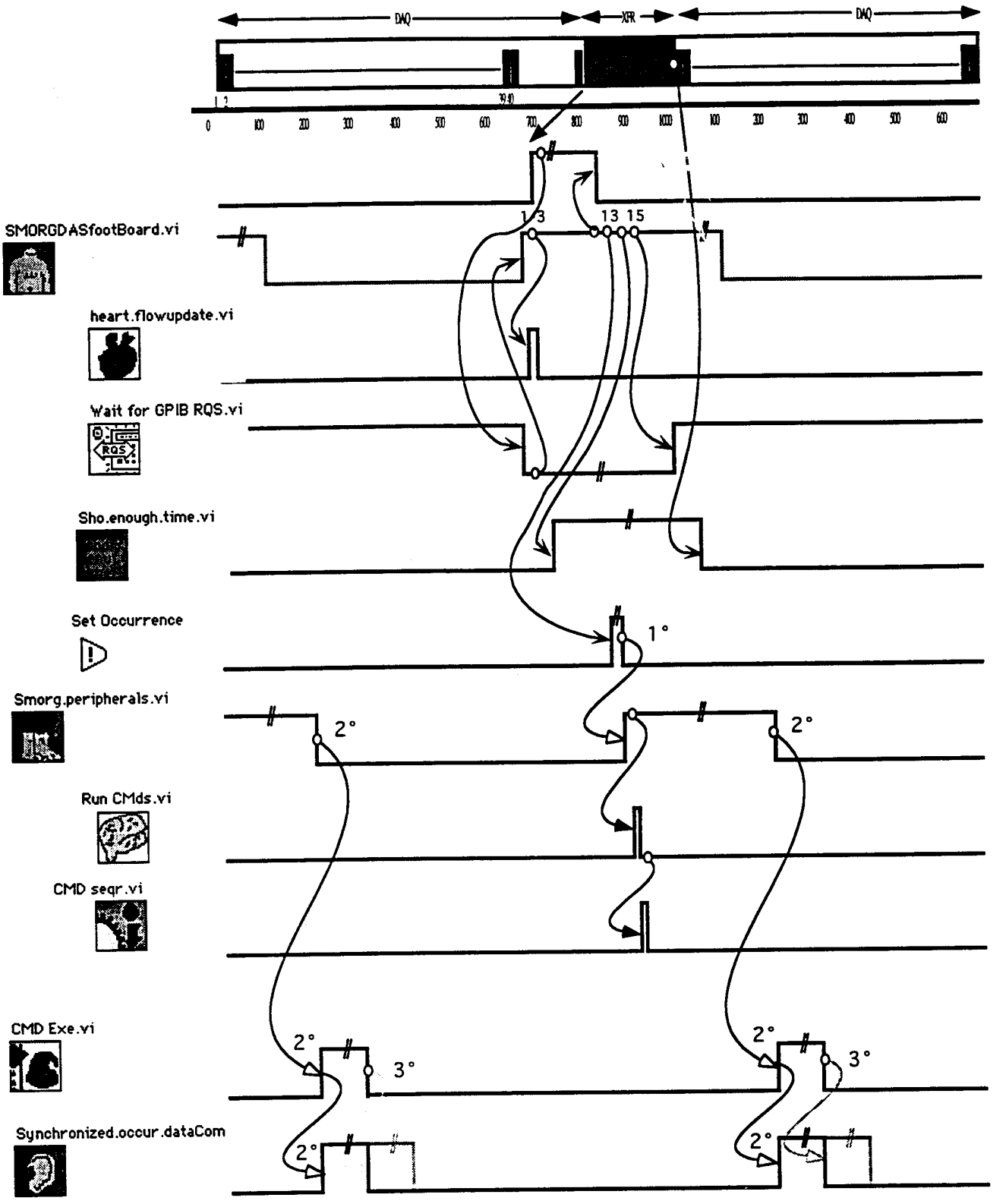

1° Primary Occurence
2° Secondary Occurence
3° Tertiary Occurence

Occurrence Chaining
Code Chaining

HTuP VI timings
Dana Redington, Ph.D.
3/24/95; rev'd 4/26/95

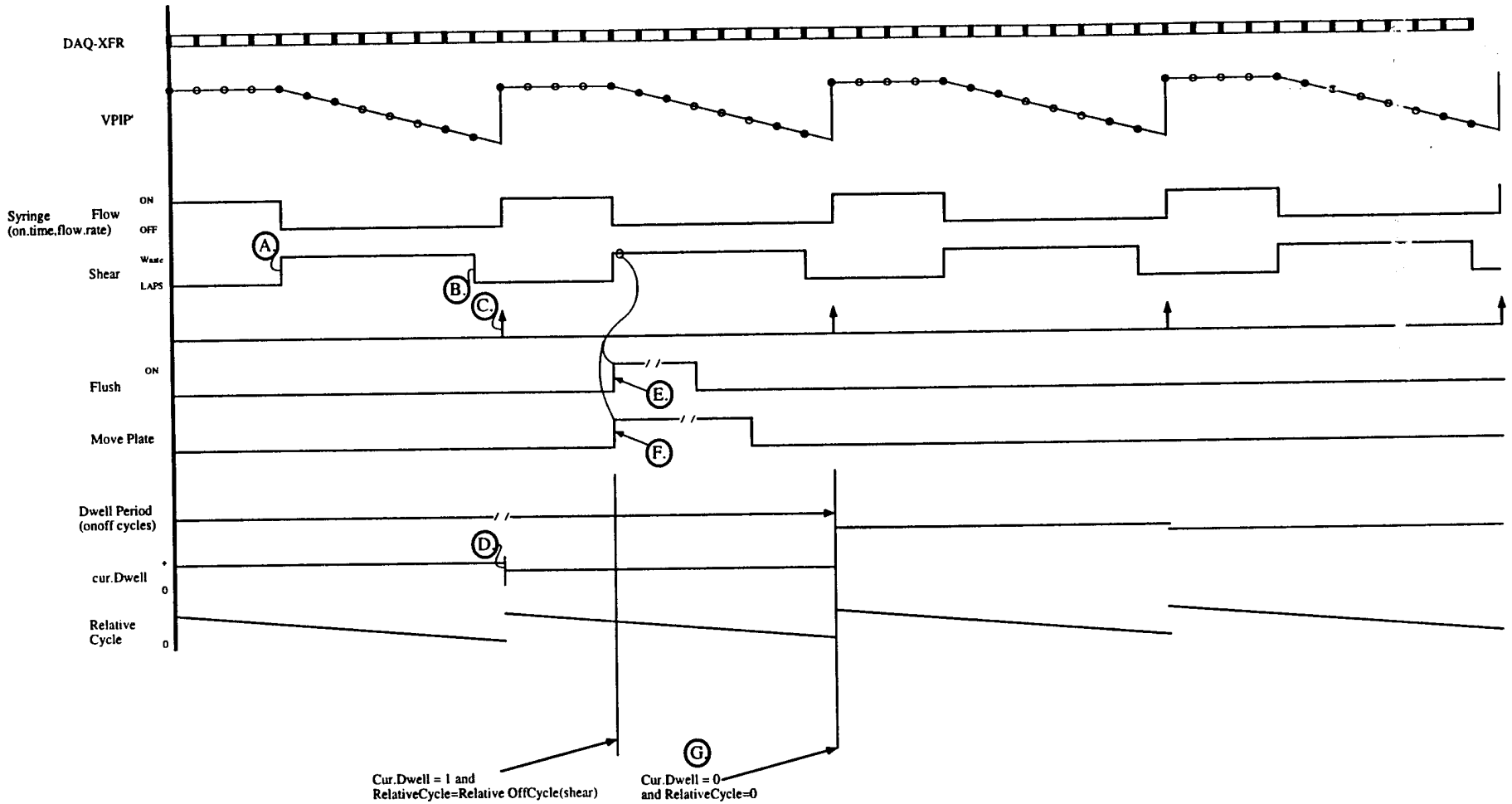

In Heartflowupdate.VI

(A) RelativeCycle = Relative OffCycle(shear)

(B) RelativeCycle = Relative OffCycle(laps)

(C) RelativeCycle = Relative OffCycle(flow)

(D) Cur.Dwell = 1

E. Time to Flush System

HTuP Timing of Events
Dana Redington, Ph.D.
1/12/94; rev'd 2/27/95; 3/23/95; 4/26/95

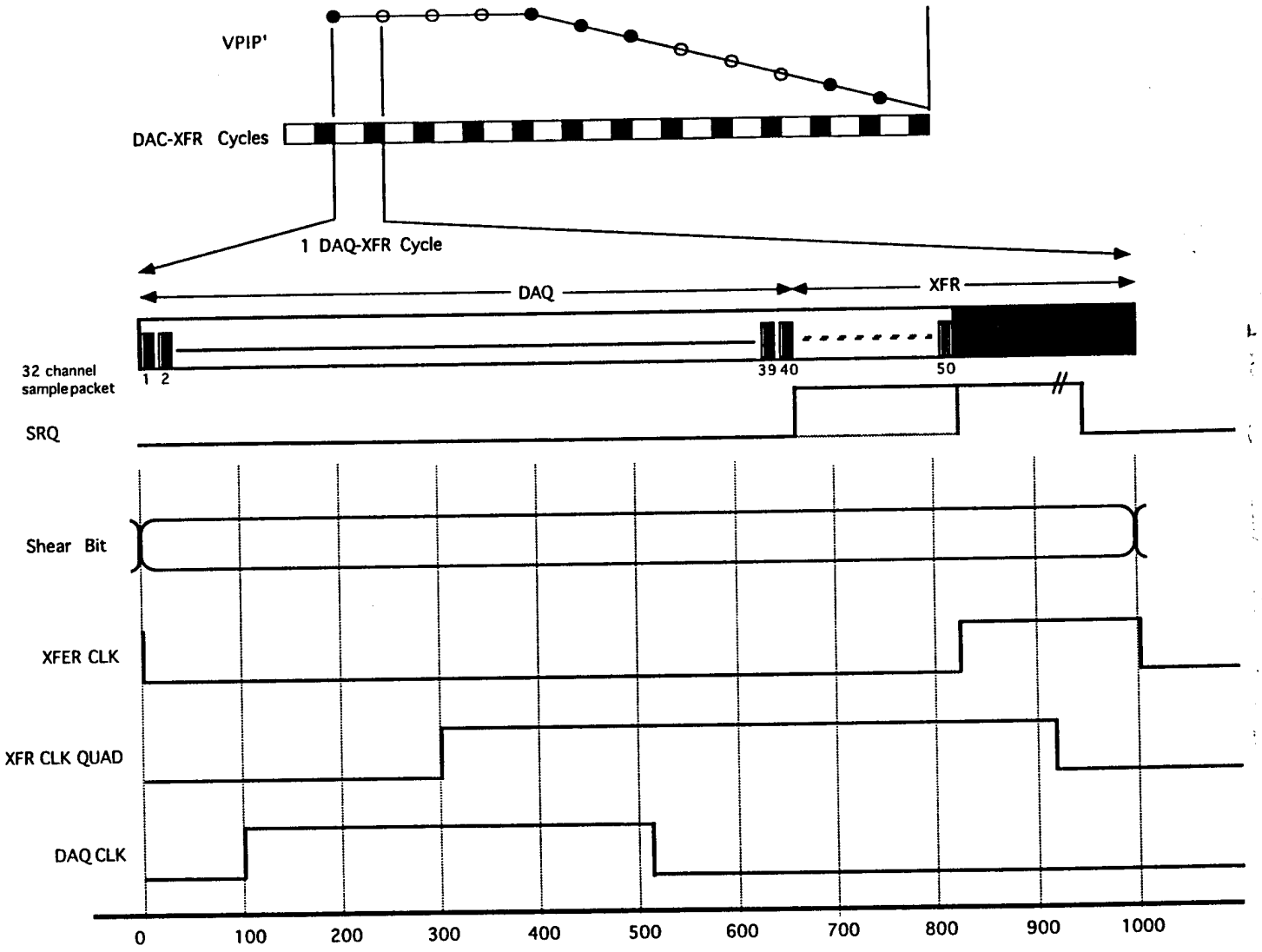

HTuP DAQ-XFR cycle
Dana Redington, Ph.D.
3/24/95; mod'd 3/26/95; 4/25/95

APPENDIX 2

BIBLIOGRAPHY OF PUBLICATIONS
PRODUCED WITH SUPPORT FROM THIS CONTRACT

(Copies of those preceded by a bullet, •, are included in Appendix 3)

•Baxter, G. T. et al. (1992). "PKCε is Involved in GM-CSF Signal Transduction. Evidence from Microphysiometry and Antisense Oligonucleotide Experiments." Biochemistry 31: 10950-10954.

Baxter, G. T. et al. (1993). "The Muscarinic Acetylcholine Receptor Subtypes m1 and m3 Mediate the Activation of the Na/H Antiporter via PKC when Expressed in CHO-K1 Cells." Mol. Biol. Cell 4: 123a.

Baxter, G. T. and Owicki, J. C. (1993). Real-Time Detection of the Inhibition of Glycolysis by Antisense Oligonucleotides against Phosphofructokinase Isoforms using the Microphysiometer. International Conference on Nucleic Acid Medical Applications, Cancun, Mexico.

•Baxter, G. T. et al. (1994). "Microfabrication in Silicon Microphysiometry." Clin. Chem. 40: 1800-1804.

•Baxter, G. T. et al. (1994). "Using Microphysiometry to Study the Pharmacology of Exogenously Expressed m1 and m3 Muscarinic Receptors." Life Sci. 55: 573-583.

Bousse, L. et al. (1993). Micromachined Multichannel Systems for the Measurement of Cellular Metabolism. Proceedings of Transducers 93, the 7th International Conference on Solid-State Sensors and Actuators, Yokohama, Japan.

Bousse, L. and Mostarshed, S. (1991). "The Zeta Potential of Silicon Nitride Thin Films." J. Electroanal. Chem. 302: 269–274.

Bousse, L. et al. (1992). "Combined Measurement of Surface Potential and Zeta Potential at Insulator/Electrolyte Interfaces." Sensors and Actuators B 10: 67–71.

Bousse, L. et al. (1991). "Zeta Potential Measurements of Ta2O5 and SiO2 Thin Films." J. Colloid Interface Sci. 147: 22-32.

Bousse, L. et al. (1992). Biosensors with Microvolume Reaction Chambers. Chemical Sensor Technology. S. Yamauchi. Amsterdam: Elsevier, Kodansha: Tokyo. 4: 145-166.

Bousse, L. J. et al. (1993). Integrated Fluidics for Biosensors Used to Measure Cellular Metabolism. Proceedings of the Symposium on Chemical Sensors II, Proceedings of the Electrochemical Society, Hawaii.

Bousse, L. J. et al. (1991). "Rapid Determination of Cellular Metabolic Rates with a Silicon Microphysiometer." Technical Digest Transducers '91, 74–77, San Francisco.

Bruner, L. H. et al. (1991). "Testing Ocular Irritancy In Vitro with the Silicon Microphysiometer." Toxicol. In Vitro 5: 277–284.

•Cao, V., et al. (1991). "Effects of Cholinergic Agents on Cellular Metabolism in Cultured Suprachiasmatic Nucleus." Soc. Neurosci. Abstr. 17:672.

Chan, S.D., et al. (1995). "Heregulin Activation of Extracellular Acidification in Mammary Carcinoma Cells is Associated with Expression of HER2 and HER3." J. Biol. Chem. 270:22608-22613.

Davis, A.S., et al. (1994). "Sodium/Proton Exchanger (NHE) Activity in Chinese-Hamster Lung (CHL) Fibroblasts: Real-time Detection using Microphysiometry." FASEB J. 8:AA21.

Davis, A.S., et al. (1994). "Differentiated TF-1 Cells Are Insensitive to TNF-Alpha-Induced Apoptosis." FASEB J. 9:A832.

Fok, K.S., et al. (1994). "Use of the Cytosensor for Detection of an EGF Receptor Ligand in Ovarian Carcinoma Conditioned Media." Mol. Biol. Cell. 5:140a.

Hahnenberger, K., et al. (1993). "Rapid Analysis of Metabolism and Signal Transduction with a Microphysiometer: Application of Silicon Technology to Yeast Cell Biology." Cold Spring Harbor Yeast Cell Biology Meeting, p. 159.

•Hahnenberger, K., et al. (1995). "Monitoring Changes in Proton Metabolism Enables a Functional Analysis of Inwardly Rectifying Potassium Channels Expressed in Yeast." Soc. Neurosci. Abstr. 21:1324.

Hahnenberger, K., et al. (1996). "Functional Expression of the *Schizosaccharomyces pombe* Na+/H+ Antiporter Gene, *sod2*, in *Saccharomyces cerevisiae*." Proc. Natl. Acad. Sci. USA 93:5031-5036.

•Kuo, R. C. et al. (1993). "A Metabolic View of Receptor Activation in Cultured Cells Following Cryopreservation." Cryobiology 30: 386-395.

Kuo, R.C., et al. (1994). "Cell Cycle Dependency of the TNF-alpha Effects on TF-1 Cells: A Role for the TNFR-II in Mediating Apoptosis." Mol. Biol. Cell 5:26a.

•Kurtz, S., et al. (1995) "Growth Impairment Resulting from Expression of Influenza Virus M2 Protein I Yeast: Identification of a Novel Inhibitor of Influenza Virus." Antimicrobial Agents Chemotherapy 39:2204-2209.

•McConnell, H. M. et al. (1991). "The Microphysiometer Biosensor." Current Opinion in Structural Biology 1: 647–652.

•McConnell, H. M. et al. (1992). "The Cytosensor Microphysiometer: Biological Applications of Silicon Technology." Science 257: 1906-1912.

•McConnell, H.M., et al. (1995). "Stimulation of T Cells by Antigen-Presenting Cells is Kinetically Controlled by Antigenic Peptide Binding to Major Histocompatibility Complex Class II Molecules." Proc. Natl. Acad. Sci., USA 92:2750-2754.

•Miller, D. L. et al. (1993). "Cholinergic Stimulation of the Na+/K+ ATPase as Revealed by Microphysiometry." Biophys. J. 64: 813-823.

Miller, D.L., et al. (in preparation). "A Ryanodine-Receptor Activated Pool of Calcium is Expressed upon Phorbol 12-Myristate 13-Acetate -Induced Differentiation of TE671/RD Cells.

•Nag, B. et al. (1993). "Stimulation of T Cells by Antigenic Peptide Complexed with Isolated Chains of Major Histocompatibility Complex Class II Molecules." Proc. Natl. Acad. Sci. U.S. 90: 1604-1608.

Nag, B. et al. (1992). "Antigen-Specific Stimulation of T Cell Extracellular Acidification by MHC Class II-Peptide Complexes." J. Immunol. 148: 2040-2044.

Nag, B. et al. (1993). "Purified Beta Chain of Major Histocompatibility Complex Class II Binds to CD4 Molecules on Transfected HeLa Cells." J. Immunol. 150: 1358-1364.

•Owicki, J. C. et al. (1994). "The Light-Addressable Potentiometric Sensor: Principles and Biological Applications." Ann. Rev. Biophys. Biomol. Struct. 23: 87-113.

Owicki, J. C. and Parce, J. W. (1992). "Biosensors Based on the Energy Metabolism of Living Cells: The Physical Chemistry and Cell Biology of Extracellular Acidification." Biosensors and Bioelectronics 7: 255-272.

Parce, J. W. and Kirk, G. L. (1989). High Sensitivity Silicon Biosensors Designed for Continuous Environmental Monitoring. International Chemical Congress of the Pacific Basin Societies, Honolulu, Hawaii.

•Radke, M.J., et al. (1994). "Signal Transduction by the Truncated trkB Isoform, trkB.T1." Soc. Neurosci. Abstr. 20:37.

•Raley-Susman, K. M. et al. (1992). "Effects of Excitotoxin Exposure on Metabolic Rate of Primary Hippocampal Cultures: Application of Silicon Microphysiometry to Neurobiology." J. Neuroscience 12: 773-780.

Renschler, M.F., et al. (1995). "B-Lymphoma Cells Are Activated by Peptide Ligands of the Antigen Binding Receptor or by Anti-Idiotypic Antibody to Induce Extracellular Acidification." Cancer Res. 55:5642-5647.

Salon, J. A. and Owicki, J. C. (1994). Real-Time Measurements of Receptor Activity; Applications of Microphysiometric Techniques to Receptor Biology. Receptor Molecular Biology. S. C. Sealfon. Orlando, FL, Academic.

Sartore, M. et al. (1992). "Minority Carrier Diffusion Length Effects on Light-Addressable Potentiometric Sensor (LAPS) Devices." Sensors and Actuators A 32: 431-436.

Thibodeau, A. et al. (1994). "Direct Measurement of Extracellular Proton Flux from Isolated Gastric Glands." Am. J. Physiol. 267:C1473-C1482.

•Wada, H. G. et al. (1992). "Measurement of Cellular Responses to Toxic Agents using a Silicon Microphysiometer." Alternatives to Animal Testing and Experiments 1: 154-164.

Wada, H. G. et al. (1993). "Functional Analysis of Transiently Transfected Receptors using the Cytosensor Microphysiometer." Mol. Biol. Cell 4 (Supplement): 89a (abstract).

•Wada, H. G. et al. (1993). "GM-CSF Triggers a Rapid Glucose Dependent Extracellular Acidification by TF-1 Cells. Evidence for Sodium/Proton Antiporter and PKC Mediated Activation of Acid Production." J. Cell. Physiol. 154: 129-138.

•Wada, H.G., et al. (1994). "Activation of the TNF-R1 Receptor in the Presence of Copper Kills TNF Resistant CEM Leukemic T Cells." J. Cell. Physiol. 161:597-605.

Wada, H.G., et al. (1995). "The Extracellular Acidification Response of trkA Expressing Cells to NGF is Down-Regulated by Co-Expression of p75 in PC12 Cells and Transfected L Cells." Soc. Neurosci. Abstr. 21:1989.

APPENDIX 3

COPIES OF SELECTED PUBLICATIONS PRODUCED WITH SUPPORT FROM THIS CONTRACT

Reprinted from Biochemistry, 1992, 31.

PKCε Is Involved in Granulocyte–Macrophage Colony-Stimulating Factor Signal Transduction: Evidence from Microphysiometry and Antisense Oligonucleotide Experiments†

Gregory T. Baxter, Donald L. Miller, Richard C. Kuo, H. Garrett Wada, and John C. Owicki*

Molecular Devices Corporation, 4700 Bohannon Drive, Menlo Park, California 94025

Received April 28, 1992; Revised Manuscript Received September 4, 1992

ABSTRACT: We have used microphysiometry and antisense methodology to show that the ε isoenzyme of protein kinase C (PKC) is involved in the signal transduction pathway of granulocyte–macrophage colony-stimulating factor (GM-CSF) in a human bone marrow cell line, TF-1. These cells require GM-CSF or a related cytokine for proliferation. When the cells are appropriately exposed to GM-CSF, they exhibit a burst of metabolic activity that can be detected on the time scale of minutes in the microphysiometer, a biosensor-based instrument that measures the rate at which cells excrete protons. These cells express PKCα and -ε, as determined by Western blot analysis. Treatment with isoenzyme-specific antisense oligonucleotides inhibits expression appropriately, but only inhibition of PKCε appreciably diminishes the burst of metabolic activity induced by GM-CSF. Consistent with the involvement of PKCε, GM-CSF appears to activate phospholipase D and does not cause a detectable increase in cytosolic [Ca^{2+}].

Since being established from the bone marrow of a human erythroleukemia patient by Kitamura et al. (1979), the TF-1 cell line has proven to be useful model system with which to study signal transduction by hemopoietic growth factors (Kitamura et al., 1991).

We[1] (Wada et al., 1992) have used a novel biosensor-based instrument, the microphysiometer (Parce et al., 1989; McConnell et al., 1992), to detect integrative physiological responses of these cells to cytokines. For example, GM-CSF[2] induces a burst of metabolic activity that occurs at physiologically relevant concentrations and is inhibitable by antibodies to GM-CSF. The abilities of GM-CSF and five other cytokines to elicit such responses correlate very well with their abilities to cause the proliferation of these cells.

The microphysiometer has been shown to detect the activation of a wide variety of cellular receptors in a pharmacologically relevant manner, for example, the T-cell (Nag et al., 1992), kainate glutamate (Rayley-Susman et al., 1992), epidermal growth factor (Owicki et al., 1989), m_1-muscarinic receptor (Owicki et al., 1989), and β_2-adrenergic receptor (Owicki et al., 1989). It does so by detecting changes, sometimes weak and transient, in the rates at which cells excrete protons. Extracellular acidification reflects the rate of production of the acidic products of energy metabolism (principally lactic acid and CO_2) and the regulation of intracellular pH (Owicki & Parce, 1992). Changes in extracellular acidification caused by receptor activation therefore reflect changes in these processes.

Our earlier work (Wada et al., 1992) suggested that PKC was involved in the GM-CSF signal transduction in these cells: pretreatment with a phorbol ester inhibited the GM-CSF acidification response. The response was also suppressed by calphostin C, an inhibitor of PKC.

PKC is a family of multiple isoforms having closely related but different structures (Ono et al., 1988; Nishizuka, 1988; Parker et al., 1989). Some cells express only one of the isoforms identified to date (Pelosin et al., 1987; Rose-John et al., 1988; Heidenreich et al., 1990) while the majority coexpress multiple isoforms (Strulovici et al., 1989, 1991; Kiley et al., 1990; Pfeffer et al., 1990). It is anticipated that each of these isoforms mediates distinct cellular responses. Biochemically, PKCα, -$\beta_{I/II}$, and -γ exhibit subtle differences and are known as Ca^{2+}- and phospholipid-dependent kinases (Jaken & Kiley, 1987) whereas PKCδ, -ε, and -η are phospholipid-dependent yet Ca^{2+}-independent kinases (Kiley et al., 1990; Leibersperger et al., 1990; Bacher et al., 1991).

The present paper strengthens the conclusion that PKC is involved in the response of TF-1 cells to GM-CSF by demonstrating that staurosporine, another PKC inhibitor, also inhibits the acidification response. More importantly, this work identifies an isoenzyme of PKC that is involved in GM-CSF signal transduction by showing that the response can be inhibited by treatment with antisense oligonucleotide. Evidence is also provided that the activation of phospholipase D is involved in the process.

MATERIALS AND METHODS

Chemicals. Unless otherwise noted, chemicals were purchased from Sigma (St. Louis, MO). Antisense 15-mer oligodeoxynucleotides to the PKC isoenzymes were synthesized by Operon Technologies (Alameda, CA) on the basis of sequences obtained from the GenBank database. No human PKCε sequence was available, but a partial human PKCα sequence permitted construction of an antisense oligonucleotide beginning at nucleotide 41. Oligonucleotides based on rat PKCα and -ε sequences began at the start codon. Following are the antisense sequences used (5′ → 3′): human PKCα,

† This work was supported in part by DARPA, Contract MDA972-92-C-0005.

* To whom correspondence should be addressed. Phone (415) 322-4700; FAX (415) 322-2069.

[1] DeVries et al., Abstract, International Cytokine Workshop, Stresa, Italy, Nov 1991; Indelicato et al., submitted for publication.

[2] Abbreviations: AM, acetoxymethyl ester; $[Ca^{2+}]_i$, intracellular (cytosolic) free calcium ion concentration; FBS, fetal bovine serum; GM-CSF, granulocyte–macrophage colony-stimulating factor; HSA, human serum albumin; PAF, platelet-activating factor; pH_i, intracellular (cytosolic) pH; PKC, protein kinase C; SDS/PAGE, sodium dodecyl sulfate/polyacrylamide gel electrophoresis.

CGGTTGGCCACGTCC; rat PKCα, GTAAACGTCAGCCAT; rat PKCε, ATTGAACACTACCAT.

Cells. TF-1 cells were a gift from S. Indelicato (Schering-Plough, Bloomfield, NJ) and were cultured in RPMI 1640 medium (Irvine Scientific, Irvine, CA) supplemented with 10% FBS, 2 mM sodium pyruvate, and 1 ng/mL recombinant human GM-CSF (Sandoz/Schering-Plough Corp., Bloomfield, NJ).

Treatment of Cells with Antisense Oligonucleotides. Cells were seeded at 1×10^6/mL in 2 mL of medium and grown in the presence or absence of 15 μM oligonucleotide, replaced with fresh medium and oligonucleotide every 24 h. Twenty-four hours prior to an experiment in the microphysiometer the cells were transferred to medium that was identified except that it lacked GM-CSF; such cytokine deprivation has been shown to potentiate GM-CSF responses in the microphysiometer. Control cells were not exposed to oligonucleotide but otherwise were treated similarly (including daily change of medium).

Western Blot Analysis. Sodium dodecyl sulfate/polyacrylamide gel electrophoresis and immunoblot analysis were performed exactly as described before (Strulovici et al., 1989). Antisera to PKCα and -ε were a generous gift from Dr. Berta Strulovici (Syntex Research, Palo Alto, CA).

Microphysiometry. The microphysiometer is based on a pH-sensitive silicon sensor, the light-addressable potentiometric sensor (Hafeman et al., 1988), which forms one surface of a flow chamber (volume of several microliters) in which cultured cells are immobilized. Culture medium is supplied by a pump to maintain cell viability. Periodically the pump is stopped, and the pH in the chamber decreases, typically by 0.05–0.1 pH unit in a minute. This rate of acidification is recorded by a computer that controls the instrument, and flow is resumed, restoring the original pH. For more instrumental details, see Parce et al. (1989) or McConnell et al. (1991).

The microphysiometer was loaded with low-buffered RPMI 1640 medium (Molecular Devices Corp., Menlo Park, CA) containing 1 mg/mL endotoxin-free HSA (Miles, Elkhart, IN), and each flow chamber of the instrument was assembled with 10^6 TF-1 cells embedded in a fibrin clot (Parce et al., 1989; McConnell et al., 1991). The acidification rate was measured every 135 s (flow on at 100 μL/min for 90 s, flow off for 15 s, flow off with acidification rate measured for 30 s). The chamber temperature was 37 °C.

Acidification rate was monitored until steady (typically 30 min), at which time a sham treatment (culture medium without GM-CSF) was performed for 10 min. Then, GM-CSF was added at 5 ng/mL for 10 min.

Absolute acidification rates can vary from chamber to chamber, for example, by about ±20% due to fluctuations in the number of cells in the ~300-nL part of the cell chamber near the active site of the sensor. To correct for this, data are normalized within a chamber by expression as percent of basal (unstimulated) acidification rate. For identically prepared chambers from the same flask of cells on the same day, we have found the standard deviation of the peak stimulation of acidification by GM-CSF to be 3.5% of the basal acidification rate (Wada et al., 1992). To compare cells with differing culture history prior to use in the microphysiometer, as in Figure 3B, we have previously found (Wada et al., 1992) that statistical consistency is improved if the peak response to GM-CSF is instead normalized to the peak of an unrelated response, the acidification increase that occurs when cells are exposed to 1 μg/mL calcium ionophore ionomycin administered 90 min after removal of GM-CSF.

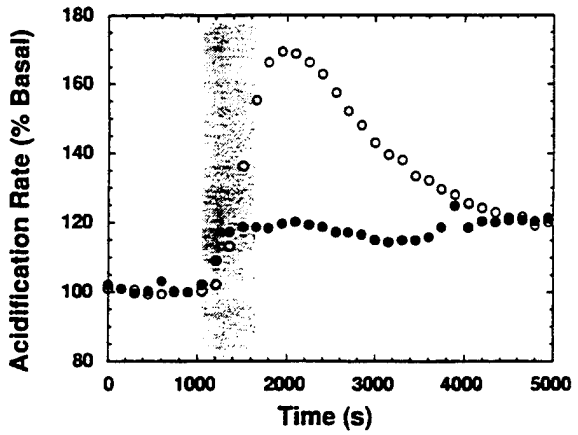

FIGURE 1: Metabolic response of TF-1 cells to GM-CSF and inhibition by staurosporine. TF-1 cells were treated with 5 ng/mL GM-CSF for 10 min (shaded period in figure) in the absence (open symbols) and presence (closed symbols) of 100 nM staurosporine (5-min preincubation and present with GM-CSF), and the acidification rate was measured as described under Materials and Methods. The experiment was repeated four times, each time yielding an inhibition at least as great as that shown.

Measurement of Intracellular $[Ca^{2+}]$. TF-1 cells that had been GM-CSF-starved overnight were centrifuged and resuspended in low-buffered RPMI 1640 medium supplemented with 10 mM HEPES and then incubated at room temperature for 45 min with 5 μM fura-2, AM (1 mM in DMSO). The cells were then centrifuged and resuspended in a balanced salt solution (NaCl, 138 mM; KCl, 5 mM; KH_2PO_4, 0.11 mM; Na_2HPO_4, 0.81 mM; $MgCl_2$, 0.05 mM; $CaCl_2$, 1.3 mM; glucose, 10 mM; HEPES, 10 mM; pH 7.4) and transferred to a stirred cuvette kept at 37 °C in the sample compartment of a PTI Model 4000 ratiometric fluorometer (South Brunswick, NJ). $[Ca^{2+}]_i$ was monitored ratiometrically using 340 and 380 nm as the excitation wavelengths and 510 nm as the emission wavelength. $[Ca^{2+}]_i$ was calibrated with the equation of Grynkiewicz et al. (1985) with R_{min}, R_{max}, S_{f2}, and S_{b2} determined empirically for each experiment using ionomycin and EGTA in the salt solution.

Choline Assay. Briefly, cells were incubated in suspension with 10 ng/mL GM-CSF. After various reaction times the cells were added to excess phosphate-buffered saline at 0 °C and rapidly collected by centrifugation. Cells were lysed in hypotonic lysis buffer; cytosolic fractions were collected, and cytosolic choline levels were determined by using choline kinase to synthesize radiolabeled choline phosphate from choline and [γ-^{32}P]ATP (2–10 Ci/mmol, from Du Pont/NEN Research Products, Boston, MA) according to the method of Wang and Haubrich (1975) as modified by Thompson et al. (1990).

RESULTS AND DISCUSSION

Response of TF-1 Cells to GM-CSF and Inhibition by Staurosporine. Exposure to 5 ng/mL GM-CSF for 10 min causes the extracellular acidification rate of TF-1 cells to approximately double within 5–10 min (Figure 1). Thereafter, the acidification rate gradually falls, remaining significantly above basal levels 45–60 min after the initial exposure to GM-CSF.

These results are consistent with our earlier observations (Wada et al., 1992). There we kinetically resolved the response into low-amplitude short-lived and higher-amplitude long-lived components. The former is associated with the activation of the Na^+/H^+ antiporter. The latter requires the presence

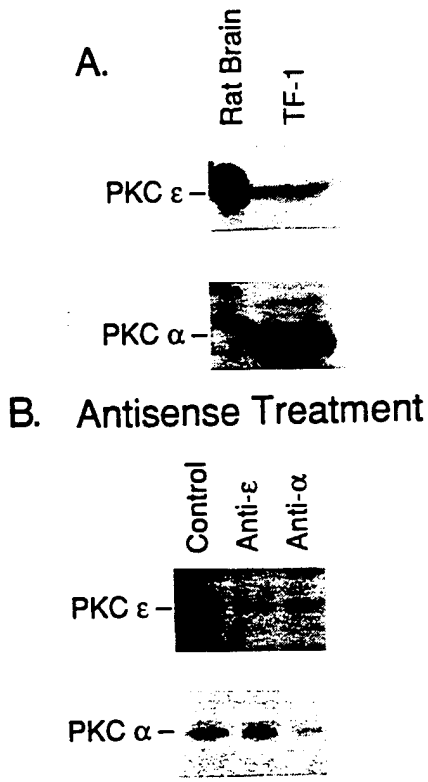

FIGURE 2: Expression of PKC isoenzymes in TF-1 cells. (A) Total cell homogenates (200 μg of protein per lane for TF-1 cells and 20 μg per lane for rat brain) were subjected to SDS/PAGE, transferred to nitrocellulose membranes, and immunoblotted with antibodies specific for PKCα and PKCε as described under Material and Methods. Immunoblots were labeled with ^{125}I protein A and exposed to Kodak XAR film for 7 days at −70 °C. Rat brain was loaded as a control. PKC isoforms are indicated. (B) TF-1 cells were treated with or without PKC–antisense oligonucleotides for 5 days as described under Materials and Methods, and immunoblot analysis was performed as described above. Cell treatments are indicated in the figure, and PKC isoforms are identified. The experiment was repeated twice with similar results, and representative Western blots are shown.

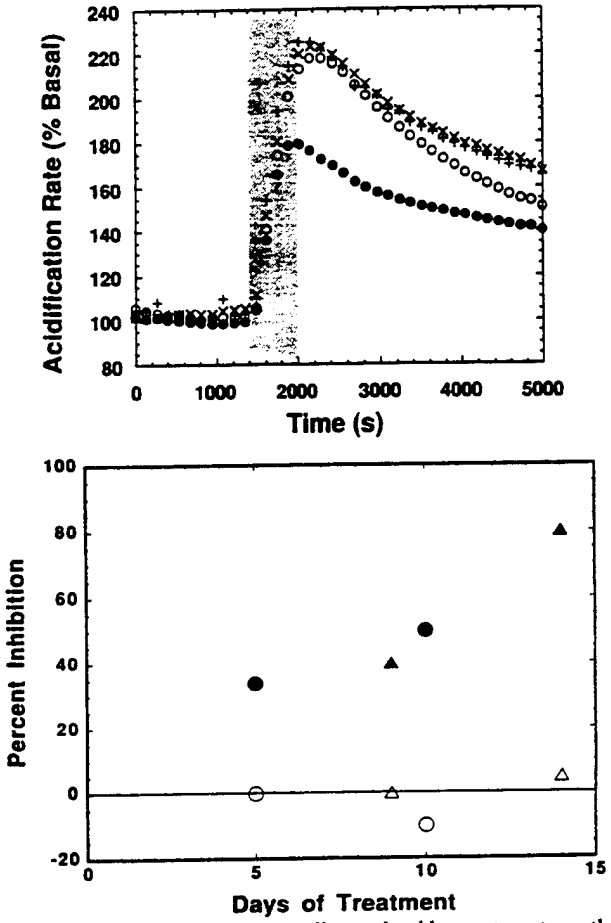

FIGURE 3: Effect of antisense oligonucleotide treatment on the acidification response of TF-1 cells to GM-CSF. (A, top) TF-1 cells were treated in the presence or absence of antisense oligonucleotide to PKCα or PKCε for varying periods (5 days shown here) as described under Materials and Methods. Cells were then challenged with GM-CSF (5 ng/mL for 10 min; shaded period in figure), and the acidification rate was measured as described under Materials and Methods. Antisense treatment: control, open circles; human α, crosses; rat α, ×'s; rat ε, filled circles. (B, bottom) Time course of the inhibitory effects of antisense treatment on the GM-CSF response of TF-1 cells, represented in percent inhibition compared to control cells. TF-1 cells were treated in the presence or absence of antisense oligonucleotides to PKCα or -ε for up to 14 days. For each time point, cells were treated with 5 ng/mL GM-CSF for 10 min, and the acidification rate was measured as described above. Percent inhibition was determined by first normalizing GM-CSF responses to ionomycin responses within each chamber as described under Materials and Methods and then comparing the maximum normalized GM-CSF-mediated acidification response of antisense-treated cells to that of control cells for each time point. Simply normalizing responses to basal rates rather than using this procedure would have made a significant difference at only one data point, substantially decreasing the apparent inhibition for the 14-day incubation with anti-PKCε. Four experiments were performed for each antisense treatment, one for each of four durations of exposure. There were two independent series of experiments (two durations each), indicated by the circular and triangular symbols. The open symbols show the (lack of) inhibition of PKCα and the filled symbols the progressive inhibition for PKCε.

of a carbon source in the medium (glucose, but not glutamine, is sufficient) and presumably reflects an increased rate of glycolysis.

Several PKC inhibitors have been described (Tamaoki et al., 1986; Hannun & Bell, 1987; Davis et al., 1989); of these, staurosporine has been shown to be the most potent (Davis, et al., 1989). To determine whether PKC is involved in mediating the GM-CSF acidification response, we treated TF-1 cells in the microphysiometer with 5 ng/mL GM-CSF, with or without 100 nM staurosporine, and monitored extracellular acidification as described under Materials and Methods. As shown in Figure 1, staurosporine strongly inhibited the acidification increase mediated by GM-CSF. This concentration of staurosporine was determined not to be cytotoxic to these cells, as indicated by the constant acidification rate (Figure 1).

Expression of PKC Isoenzymes and Inhibition with Antisense Oligonucleotides. Whole-cell extracts from TF-1 cells were analyzed by immunoblot analysis using affinity-purified antibodies directed against synthetic peptides unique to the PKCα and -ε isoforms (Strulovici et al., 1991). As shown in Figure 2A, TF-1 cells express both PKCα and -ε. To determine which PKC isoforms are involved in GM-CSF signaling, we attempted specifically to reduce or inhibit the expression of PKCα and -ε by treating the TF-1 cells with antisense oligonucleotides specific for each of these isoforms. TF-1 cells were grown with or without antisense oligonucleotides for 5 days. Western blot analysis was performed on these cells to determine the amount of immunoreactive PKC remaining after treatment. As seen in Figure 2B, the amount of immunoreactive PKCα is significantly reduced in the human PKCα–antisense-treated cells when compared with either control cells or the PKCε–antisense-treated cells. Similarly, the amount of PKCε is significantly reduced in the PKCε–antisense-treated cells when compared with either control cells or human PKCα–antisense-treated cells. The rat

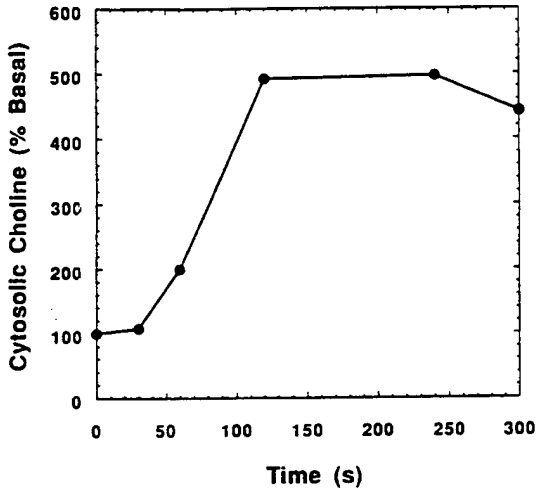

FIGURE 4: Effect of GM-CSF on cytosolic choline concentrations in TF-1 cells. TF-1 cells were treated with 10 ng/mL GM-CSF for the indicated time periods, and the cytosolic fractions were measured for free choline concentration as described under Materials and Methods. The experiment was repeated three times, each displaying identical kinetics (peak choline levels were reached at 2 min) and similar basal choline levels; the maximum level of cytosolic choline varied between 500 and 800 pmol/10^7 cells. A representative experiment is shown.

PKCα–antisense-treated cells showed comparable levels of inhibition (data not shown). Therefore, this treatment was successful in reducing the levels of the targeted PKC isoforms.

Inhibition of Acidification Responses to GM-CSF by Antisense Oligonucleotides to PKCϵ but Not PKCα. TF-1 cells were treated with the PKC–antisense oligonucleotides in two series of experiments, each lasting up to 14 days. As seen in Figure 3A, the burst of acidification caused by 5 ng/mL GM-CSF is significantly diminished by treatment with antisense oligonucleotide to PKCϵ but not to PKCα–antisense. The PKCϵ–antisense treatments showed a consistent and progressive inhibition of the GM-CSF response corresponding to length of antisense treatment, up to 80% after 14 days (Figure 3B). These data suggest that PKCϵ may be involved in the signal transduction pathway associated with GM-CSF-mediated increase in the metabolic response observed with the microphysiometer.

The stimulation of acidification by GM-CSF has been shown to comprise at least two processes: a brief (<10 min) activation of the Na^+/H^+ antiporter and a larger and longer-lasting stimulation that involves the activity of glycolysis (Wada et al., 1992). On the basis of the amplitudes and shapes of the inhibited responses, the PKCϵ–antisense treatment inhibits the glycolytic component. The absence of initial broadening in the inhibited response suggests that the smaller antiporter component is also inhibited, but additional experiments need to be done to show this conclusively.

Increased Intracellular Choline after Exposure to GM-CSF but No Increase in Cytosolic [Ca^{2+}]. It has been suggested that the activation of PKCϵ may be associated with the hydrolysis of phosphatidylcholine, possibly by a phospholipase D, which contrasts with the well-described hydrolysis of phosphatidylinositol by a phospholipase C (Koide et al., 1992). If this is true for the present case, then it should be possible to detect increased levels of choline in the GM-CSF-activated cells. We detected an approximately 5-fold increase in free cytosolic choline within 2 min after exposure to 10 ng/mL GM-CSF (Figure 4). The amplitude and kinetics are similar to those observed for agonist-induced phosphatidylcholine hydrolysis in other human cells (Duronio et al., 1989; Thompson et al., 1990). GM-CSF fails to alter [Ca^{2+}] significantly under conditions where it elicits strong acidification and proliferative responses (Figure 5). The positive response to PAF (Figure 5) shows that the cells are capable of an agonist-induced increase in cytosolic [Ca^{2+}]. That GM-CSF increases cytosolic choline without increasing $[Ca^{2+}]_i$ strongly implicates phospholipase D in the transduction of the GM-CSF signal in TF-1 cells.

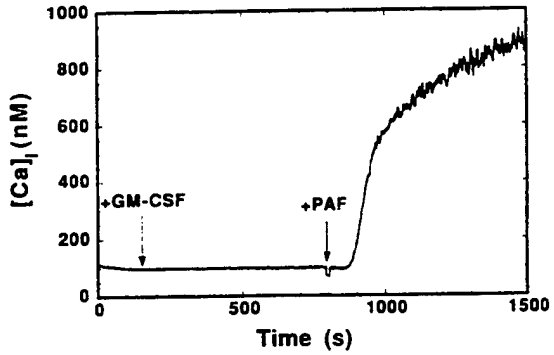

FIGURE 5: Effect of GM-CSF on cytoplasmic [Ca^{2+}] in TF-1 cells. GM-CSF (10 ng/mL) had no effect on cytoplasmic [Ca^{2+}] of cells suspended in a cuvette. Subsequent exposure to 5 μM PAF did elicit an increase in cytoplasmic [Ca^{2+}]. This experiment was repeated five times with similar results; a representative experiment is shown.

Conclusion. We have combined antisense methodology with microphysiometry, a novel biosensor-based means of detecting alterations of cellular physiology, to provide evidence that the ϵ isoenzyme of protein kinase C is involved in GM-CSF signal transduction in TF-1 cells. We have found that the signal transduction does not cause an increase in cytosolic [Ca^{2+}] but does involve an increase in intracellular choline, both of which are consistent with the involvement of phospholipase D, as might be expected for the activation of PKCϵ. The failure of antisense oligonucleotides against PKCα to inhibit cellular response to GM-CSF in the microphysiometer, together with the failure of GM-CSF to increase cytosolic [Ca^{2+}], suggests that this isoenzyme is not involved in GM-CSF signal transduction in these cells. Further studies on the effects of antisense of oligonucleotides on GM-CSF-driven proliferation, acidification responses, and the relationship between the two in TF-1 cells are in progress.

ACKNOWLEDGMENT

We gratefully acknowledge help with the immunoblot analysis from B. Strulovici.

REFERENCES

Bacher, N., Zisman, Y., Berent, E., & Livneh, E. (1991) *Mol. Cell. Biol. 11*, 126–133.

Davis, P., Hill, C., Keech, E., Lawton, G., Nixon, J., Sedgwick, A., Wadsworth, J., Westmacott, D., & Wilkinson, S. (1989) *FEBS Lett. 259*, 61–63.

Duronio, V., Nip, L., & Pelech, S. L. (1989) *Biochem. Biophys. Res. Commun. 164*, 804–808.

Grynkiewicz, G., Poenie, M., & Tsien, R. Y. (1985) *J. Biol. Chem. 260*, 3440–3448.

Hafeman, D., Parce, J., & McConnell, H. (1988) *Science 240*, 1182–1185.

Hannun, Y., & Bell, R. (1987) *Science 235*, 670–674.

Heidenreich, K. A., Toledo, S. P., Brunton, L. L., Watson, M. J., Daniel-Issakani, S., & Strulovici, B. (1990) *J. Biol. Chem. 265*, 15076–15082.

Jaken, S., & Kiley, S. (1987) *Proc. Natl. Acad. Sci. U.S.A. 84*, 4418–4422.

Kiley, S., Schaap, D., Parker, P., Hsieh, L., & Jaken, S. (1990) *J. Biol. Chem. 265*, 15704–15712.
Kitamura, T., Tange, T., Terasawa, T., Chiba, S., Kuwaki, T., Miyagawa, K., Piao, Y.-F., Miyazono, K., Urabe, A., & Takaku, F. (1979) *J. Cell. Physiol. 140*, 323–334.
Kitamura, T., Kakaku, F., & Miyajima, A. (1991) *Int. Immunol. 3*, 571–577.
Koide, H., Kouji, O., Kikkawa, U., & Nishizuka, Y. (1992) *Proc. Natl. Acad. Sci. U.S.A. 89*, 1149–1153.
Leibersperger, H., Gschwendt, M., & Marks, F. (1990) *J. Biol. Chem. 265*, 16108–16115.
McConnell, H., Rice, P., Wada, H., Owicki, J., & Parce, J. (1991) *Curr. Opin. Struct. Biol. 1*, 647–652.
McConnell, H. M., Owicki, J. C., Parce, J. W., Miller, D. L., Baxter, G. T., Wada, H. G., & Pitchford, S. (1992) *Science 257*, 1906–1912.
Nag, J., Wada, H., Fok, K., Green, D., Sharma, S., Clark, B., Parce, J., & McConnell, H. (1992) *J. Immunol. 148*, 2040–2044.
Nishizuka, Y. (1988) *Nature 334*, 661–668.
Ono, Y., Fujii, T., Ogita, K., Kikkawa, U., Igarashi, K., & Nishizuka, Y. (1988) *J. Biol. Chem. 263*, 6927–6932.
Owicki, J., & Parce, J. (1992) *Biosens. Bioelectron. 7*, 255–272.
Owicki, J., Parce, J., Kercso, K., Sigal, G., Muir, V., Venter, J., Fraser, C., & McConnell, H. (1990) *Proc. Natl. Acad. Sci. U.S.A. 87*, 4007–4011.
Parce, J., Owicki, J., Kercso, K., Sigal, G., Wada, H., Muir, V., Bousse, L., Ross, K., Sikic, B. & McConnell, H. (1989) *Science 246*, 243–247.
Parker, P., Kour, G., Marais, R., Mitchell, F., Pears, C., Schaap, D., Stabel, S., & Webster, C. (1989) *Mol. Cell. Endocrinol. 65*, 1–11.
Pelosin, J.-M., Vilgrain, I., & Chambaz, E. M. (1987) *Biochem. Biophys. Res. Commun. 147*, 382–391.
Pfeffer, L., Strulovici, B., & Saltiel, A. (1990) *Proc. Natl. Acad. Sci. U.S.A. 87*, 6537–6541.
Rayley-Susman, K., Miller, K., Owicki, J., & Sapolsky, R. (1992) *J. Neurosci. 12*, 773–780.
Rose-John, S., Dietrich, A., & Marks, F. (1988) *Gene 74*, 465–471.
Strulovici, B., Daniel-Isaakani, S., Oto, E., Nestor, J., Chan, H., & Tsou, A.-P. (1989) *Biochemistry 28*, 3569–3576.
Strulovici, B., Daniel-Issakani, S., Baxter, G., Knopf, J., Sultzman, L., Cherwinski, H., Nestor, J., Webb, D., & Ransom, J. (1991) *J. Biol. Chem. 266*, 168–173.
Tamaoki, T., Nomoto, H., Takahashi, I., Kato, Y., Morimoto, M., & Tomita, F. (1986) *Biochem. Biophys. Res. Commun. 135*, 397–402.
Thompson, N., Tateson, J., Randall, R., Spacey, G., Bonser, R., & Garland, L. (1990) *Biochem. J. 271*, 209–213.
Wada, H. G., Indelicato, S. R., Meyer, L., Kitamura, T., Miyajima, A., Kirk, G., Muir, V. C., & Parce, J. W. (1992) *J. Cell. Physiol.* (in press).
Wang, F., & Haubrich, D. (1975) *Anal. Biochem. 63*, 195–201.

Registry No. GM-CSF, 83869-56-1; PKC, 141436-78-4; phospholipase D, 9001-87-0.

CLIN. CHEM. 40/9, 1800-1804 (1994) • Oak Ridge Conference

Microfabrication in Silicon Microphysiometry

Gregory T. Baxter, Luc J. Bousse, Timothy D. Dawes, Jeffrey M. Libby, Douglas N. Modlin, John C. Owicki,[1] and J. Wallace Parce

Over the past 5 years, microphysiometry has proved an effective means for detecting physiological changes in cultured cells, particularly as a functional assay for the activation of many cellular receptors. To demonstrate the clinical relevance of this method, we have used it to detect bacterial antibiotic sensitivity and to discriminate between bacteriostatic and bacteriocidal concentrations. The light-addressable potentiometric sensor, upon which microphysiometry is based, is well suited for structural manipulations based on photolithography and micromachining, and we have begun to take advantage of this capability. We present results from a research instrument with eight separate assay channels on a 5-cm^2 chip. We discuss the planned evolution of the technology toward high-throughput instruments and instruments capable of performing single-cell measurements.

Indexing Terms: *potentiometry/cell physiology/biosensor/microbiology/bacteria/antibiotics, sensitivity to*

Cellular energy metabolism is coupled to so many biochemical processes that physiologically significant events generally affect the rate of (free) energy flux through the cell (*1*). The silicon microphysiometer takes advantage of this coupling to detect physiological changes in cultured cells by sensing changes in cellular metabolic activity (*2, 3*). Metabolic activity can be measured by, e.g., oxygen consumption or microcalorimetry. We have chosen to monitor the rate of extracellular acidification, reflecting the rate of production of acidic products of energy metabolism such as lactic acid and CO_2. This choice was motivated by the availability of a particularly suitable semiconductor-based sensor, the light-addressable potentiometric sensor (LAPS), which is configured to detect pH (*4, 5*).[2]

Here we present a brief survey of microphysiometer technology, organized around the theme of microfabrication. Being derived from a silicon chip, the LAPS is amenable to micromachining. Importantly, the processes by which micromachining is accomplished do not conflict with the requirements for sensor function; it is possible to produce functional sensors that are integrated with useful structural features.

Cytosensor Microphysiometer

The heart of a microphysiometer is a microvolume flow chamber in which living cells are held in diffusive contact with the LAPS pH sensor. The flow of culture medium provides nutrients and flushes away waste products, so that the cells can be maintained for relatively long periods (days, if necessary). Periodically, the flow of medium is halted, causing the extracellular pH to decrease as acidic metabolites build up until flow is restored. Typically the rate of decrease is ~0.1 pH unit/min during a halt of ~1 min. This acidification rate is the primary datum for microphysiometry.

The Cytosensor® system (Molecular Devices Corp., Sunnyvale, CA) is a bench-top microphysiometer that contains eight such flow chambers operating in parallel and controlled by a microcomputer (see Fig. 1). Each chamber contains a disk-shaped cavity ~100 μm thick and 6 mm in diameter in which cells are immobilized between two microporous polycarbonate membranes. A cavity usually contains 10^4–10^5 mammalian cells, depending on cell type; the cells may be adherent or nonadherent. Medium is pumped tangentially across the membranes at a flow rate of 50–100 μL/min. A programmable valve upstream of the chamber determines which of two fluid streams, typically sample and control, enters the chamber. For a more detailed description of the instrument, see refs. *3* and *6*.

To date, the Cytosensor microphysiometer and its prototypes have been used mainly for two purposes: to detect receptor activation and to perform in vitro toxicological studies. Activation of plasma membrane receptors belonging to all the major superfamilies causes detectable changes in extracellular acidification rate under appropriate conditions (*3*). This typically is manifest as a 10–100% increase in acidification rate within a few minutes of exposure to agonist. Regarding toxicology, the ability of ocular irritants to inhibit extracellular acidification rate has been shown to correlate well with in vivo measures of irritancy (*7*).

Clinical applications have not yet been explored in depth, but three areas hold promise. First, on the basis of pilot studies with human tumor cell lines (*2*), microphysiometry may provide a rapid assay for resistance of patients' tumors to chemotherapeutic agents. Second, T-cell activation has been detected via microphysiometry (*8*), indicating that some aspects of patients' immune status may be monitored by this method. Third, the ability to use microbes in the microphysiometer instead of mammalian cells suggests applications in clinical microbiology.

Use of the microphysiometer to determine the suscep-

Molecular Devices Corp., 1311 Orleans Dr., Sunnyvale, CA 94089.

[1] Author for correspondence. Fax 408-747-3601; E-mail jack_owicki@moldev.com.

[2] Nonstandard abbreviations: LAPS, light-addressable potentiometric sensor; MBC, minimum bactericidal concentration; and S/N, signal-to-noise ratio.

Received April 19, 1994; accepted June 20, 1994.

Fig. 1. The Cytosensor microphysiometer: two four-channel subunits shown with controlling computer.

The flow chambers are concealed beneath the closed covers of the instrument, but the tubes that supply the two fluidics lines of each channel are visible on the front.

tibility of bacteria to an antibiotic is shown in Fig. 2. For some patients, including those with endocarditis or who are immunocompromised and infected with a pathogenic bacterium, an assay for minimum bactericidal concentration (MBC) may be required since merely inhibitory concentrations of an antimicrobial agent may be insufficient to treat such an infection. MBC assays are generally performed by diluting and plating culture broths that show no growth in an antimicrobial inhibition assay, and then determining whether the bacteria were actually killed or whether they survived exposure to the antibiotic at the tested concentration. An MBC is often considered to be that which kills 99.9% of an inoculum of 10^8 to 10^9 cells/L within 12–24 h. At present, no automated assay exists for determining MBCs. As shown in Fig. 2, however, the Cytosensor microphysiometer may be used to determine whether exposure to an antimicrobial agent has killed a significant proportion of a microbial population without the diluting, plating, and colony-counting steps required in the standard assay.

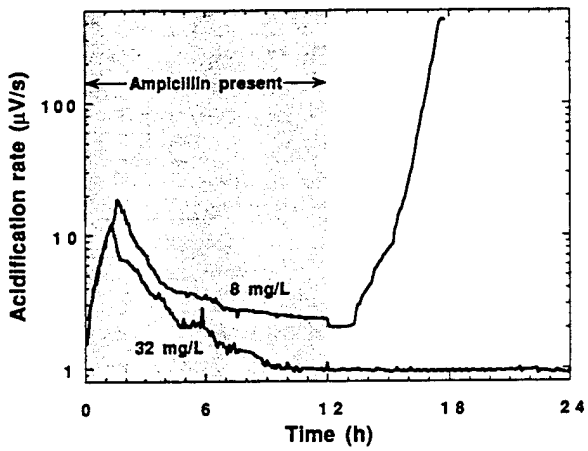

Fig. 2. Effects of lethal and sublethal concentrations of ampicillin on *Escherichia coli* metabolism.

E. coli (ATCC 25922) was grown in a Cytosensor microphysiometer at 35°C in Mueller–Hinton broth and exposed to ampicillin for 12 h at 32 mg/L; bacterial metabolic activity in the chamber increased briefly until the effects of the antibiotic appeared, and then declined and remained near zero even after the antibiotic was removed. A sublethal concentration of the antibiotic (8 mg/L) likewise inhibited bacterial metabolism, though not as completely; removal of the antibiotic after a 12-h exposure allowed this population to recover its metabolic activity. A standard minimum bactericidal assay performed with broth and plate cultures confirmed that ampicillin at 8 mg/L was the minimum concentration necessary to inhibit this *E. coli* strain, and a concentration of 32 mg/L was the minimum required to kill the bacteria after a 12-h exposure.

Micromachined Multichannel Sensor Chips

In applications such as screening for drug discovery, it would be useful to have higher sample throughput and lower minimum sample volume than the Cytosensor system offers ($\sim 10^4$ samples/year and ~ 1 mL/sample, respectively). Through silicon fabrication technology, the parallelism of the instrument can be increased and its size can be decreased, changes that bear directly on throughput and sample size. One can reasonably expect to see a 10–100 times improvement in throughput and a concomitant decrease in sample volume with a micromachined technology.

In the Cytosensor microphysiometer, each channel has an individual silicon sensor chip in every flow chamber. To achieve higher density and throughput, a logical next step would be to place several flow channels on a single chip, each with its own sensor spot. The LAPS is intrinsically a multisensor and is compatible with silicon micromachining, a technology that has been applied previously to biological problems (*9, 10*). Since Petersen reviewed silicon micromachining in 1982 (*11*), the field has expanded greatly, with many new methods of creating complex and accurately defined shapes. What we need can actually be accomplished with the most well-established method: anisotropic etching.

Flow channels in a chip are easily created with an anisotropic etch from the front. This enables one to control the depth (typically 100 μm) very accurately and produces a smooth surface at the bottom, where the active area of the LAPS device will be located. Adherent cells are introduced to all channels at once by coating a glass cover slip with cells and placing it over the silicon chip. Because the coverslip is placed on the front side of the chip, the solution must flow from the back side. This means that fluid port openings must be made through the chip.

The fabrication process is started by making all the channels and openings needed in the silicon wafer. The chip size currently used is 23-mm square. The starting material consists of double-sized polished 100-mm-diameter n-type silicon wafers, at their standard thickness of ~ 525 μm. An oxide is grown and patterned to form a mask for the first silicon anisotropic etch, which creates the flow channels on the front side of the chip. This oxide is then stripped, and a second masking oxide is grown and patterned to place openings at the location of the flow-through holes. In contrast to our first description of this process (*12, 13*), we now etch this opening from both sides at once. This requires that the photolithography of the etch mask be accurately aligned from front to back. After the holes are etched through the wafer, the masking oxide is again removed, leaving a bare silicon wafer, but with all necessary fluidics features.

This bare micromachined wafer is then the starting point of the process to make LAPS multisensors (*14*). The LAPS process entails field oxidation (to 1-μm-thick oxide); patterning to remove the field oxide in the active device areas; growth of a thin (30-nm) gate oxide; and

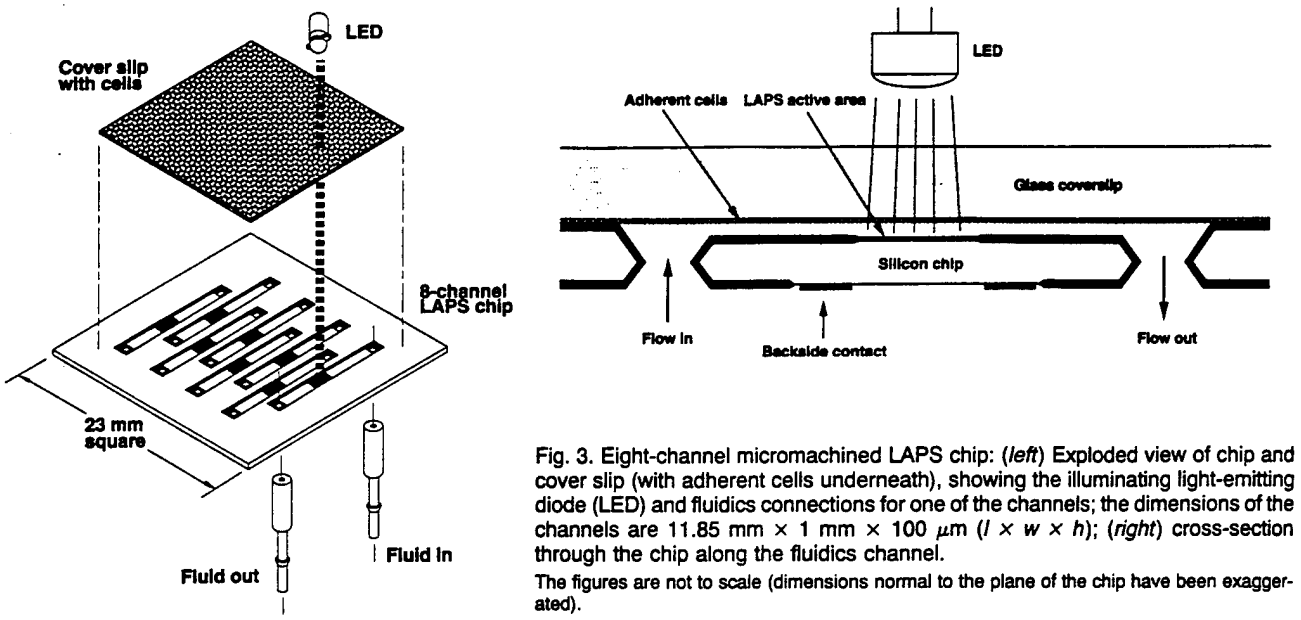

Fig. 3. Eight-channel micromachined LAPS chip: (*left*) Exploded view of chip and cover slip (with adherent cells underneath), showing the illuminating light-emitting diode (LED) and fluidics connections for one of the channels; the dimensions of the channels are 11.85 mm × 1 mm × 100 μm ($l \times w \times h$); (*right*) cross-section through the chip along the fluidics channel.

The figures are not to scale (dimensions normal to the plane of the chip have been exaggerated).

deposition of 100 nm of low-pressure chemical vapor-deposited silicon nitride. On the back of the chip a gold layer is deposited and patterned; this layer is used as the bulk silicon contact.

This micromachining involves photolithography of wafers into which deep channels and holes have been etched. We have been able to overcome the serious difficulties this creates by using very thick layers of photoresist, while still maintaining a reasonable precision of the patterning. Etching the openings from both sides of the wafer has several advantages. First, for a given size of the minimum opening, the extra space needed because of the angle of the anisotropic etch [55° between the (111) and the (100) planes] is only half as large as for the single-sided etch. Second, the etch time is only half as long. Finally, the chip is less vulnerable to mechanical damage than when processed with a single-sided etch, which creates a sharp angle (35°) at the opening on the front of the chip.

The eight-channel chip (see Fig. 3) has been integrated into a breadboard microphysiometer with manual sample-switching valves and pneumatically actuated flow of culture medium. The chamber volume is ~1 μL, and the system is capable of operating routinely at flow rates as low as ~10 μL/min.

Results of a mock drug-discovery experiment performed on this instrument are shown in Fig. 4. A pharmacologically active compound was successfully identified from a mixture of 16 components in eight acidification-rate measurements. The optimum algorithm for analyzing mixtures of compounds depends on several factors, including the costs of sample preparation, the frequency of positive responses, and the range of sample concentrations that are high enough to elicit specific responses, yet low enough to avoid nonspecific responses (*16*).

These results demonstrate the feasibility of microphysiometry based on micromachined LAPS chips. We are producing chips with multiple sensing spots per fluidics channel so that, e.g., several types of cells could be tested with a single sample. Given a fixed number of sensing spots per chip, some applications may be optimized with few fluidics channels and many spots per channel, others with many channels containing few spots.

Additional improvements may be made in components of the microphysiometer system other than the LAPS chip. Optimization of the electronics for this chip configuration would increase both the signal-to-noise ratio (S/N) and the time resolution. It would also be desirable to microfabricate some of the fluidics components of the system. In particular, a microvalve array placed close to the flow-through chip would minimize the volume between the valves and the sensor and thus the time needed for a new compound to reach the sensing area. Reducing the fluid volume of the system upstream of the cell chamber would decrease the minimum sample volume.

Single-Cell Microphysiometry

In the microphysiometers discussed above, acidification rates are determined from those cells that are directly above the sensing spot on the LAPS chip, an area of 1–3 mm^2. Such a measurement is a mean property of a population of a few thousand cells (~10^3 cells/mm^2 in a confluent monolayer). This mean may mask substantial heterogeneity that would be revealed if a histogram of the properties of individual cells were obtained. The issue of mean vs distribution is best known in the use of fluorescence to analyze a population of cells: The data obtained from flow cytometry are far richer than those obtained from a cuvette of cells in a standard spectrofluorometer. Here we describe the prospects for a microphysiometer that could be used to determine histograms of single-cell acidification rates, focusing on issues relating to LAPS technology rather than the hurdles posed by fluidics and cell handling.

A single cell on a sensing site in any of the microphys-

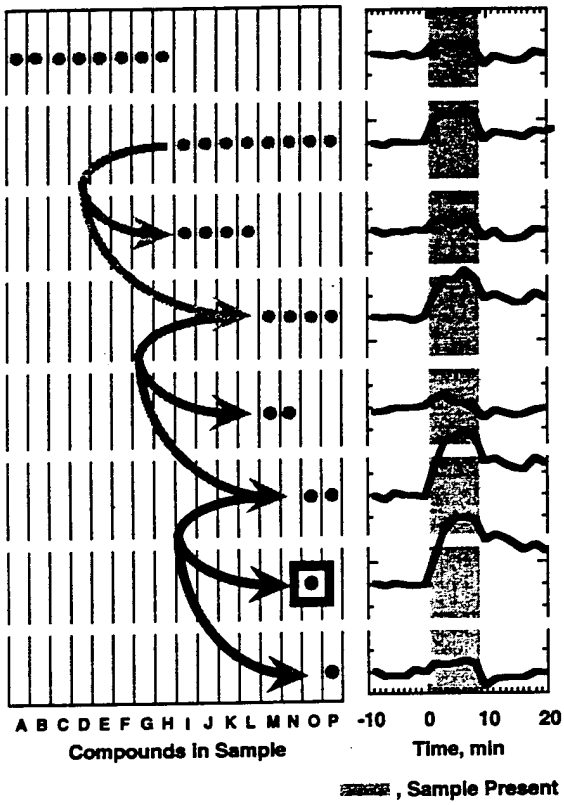

Fig. 4. Mock drug discovery by a microphysiometer based on an eight-channel micromachined LAPS chip.

A common strategy to increase throughput when screening chemical libraries for pharmacological activity is to combine many different chemicals into a single sample and, if that sample shows activity, to screen its components. We have assumed that before the start of the experiment shown here, a mixture of 16 compounds has been shown to contain at least one compound with muscarinic activity: The sample has elicited a microphysiometric response from CHO-K1 cells exogenously expressing the rat m_1 muscarinic receptor but not from the parental cells without the receptor. (For a description of the cells, see ref. *15*.) To identify the active compound, one prepares two samples containing the 16 compounds as disjoint sets of eight. As shown in the *top two lines*, only the sample containing compounds *I–P* elicits a response. The components of this sample are then tested as two four-component samples in the *third* and *fourth lines*, and this binary-search strategy is repeated twice more to identify chemical *O* as the active one. Chemical *O* was indeed the muscarinic agonist carbachol; the other 15 were taken from a study on the microphysiometric effects on CHO-K1 cells of chemicals randomly selected from the Aldrich Chemicals catalog; they were known to elicit no response in the parental CHO-K1 cells but had not previously been tested for muscarinic activity (*16*). In the experiment shown here, the sum of the concentrations of chemicals in a sample was 100 μmol/L for all samples. Had this experiment not been for demonstration purposes, it would have been performed as four successive experiments by using two channels at a time, rather than eight channels simultaneously.

iometers described above would produce an acidification rate that is undetectably small when averaged over the site of ~1 mm^2. Simply reducing the sensing site to cell size is not sufficient, for two reasons. First, protons diffuse several hundred micrometers during 1 min, the time of a typical measurement; by dilution, this would greatly attenuate pH changes in the cell-sized sensing region. This is not an issue in the existing microphysiometer systems, in which the layer of cells extends uniformly throughout the chamber so that there is no net lateral diffusion of protons into or out of the sensitive site. Second, the electronic S/N would be unacceptably low with the present detection scheme, in which the excitation light is directed to the back of the chip.

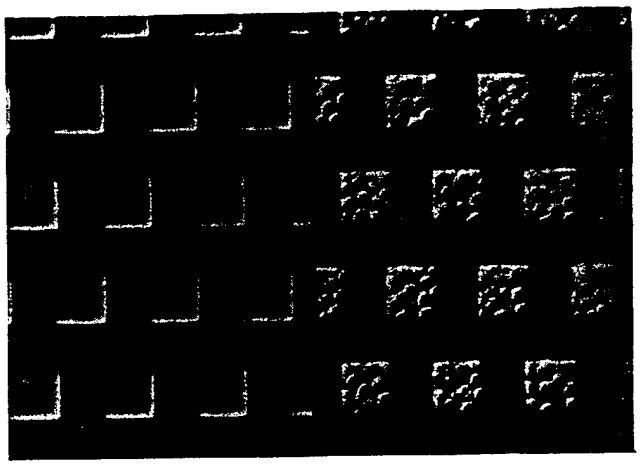

Fig. 5. Cells in micromachined wells in a LAPS chip: (*left panel*) photomicrograph of cubic wells, 50 μm on a side, micromachined into the surface of a LAPS chip in a square array with 75-μm separation between neighbors (center-to-center); (*right panel*) nonadherent P388D1 macrophage-like cells trapped within the wells by sedimentation.

Microphysiometric data from an entire array of such wells have been reported elsewhere (*2*).

The first problem can be reduced by confining the cells within a structure that retards long-distance diffusion of protons. For example, a cell at the bottom of a cubic 50-μm well in the surface of the LAPS chip would induce higher pH changes in the well than would a cell on a planar surface in its neighborhood. Transiently blocking proton transport across the mouth of the well by some means would increase the pH changes still more. Earlier in the development of microphysiometry, arrays of such wells were micromachined in LAPS chips under conditions in which the five faces of each cube were the sensitive sites on the sensor (*2*); an example is shown in Fig. 5. In that case, however, each well contained more than one cell, and a single acidification rate was determined by directing a 1-mm^2 laser beam onto an array of ~180 wells.

Confining cells to wells somewhat ameliorates the second problem, i.e., low S/N for small sensing spots: Compared with a planar arrangement, the five faces of the cube do increase the amount of sensitive surface near the cell. In addition, our calculations indicate that an electronic S/N comparable with that of the Cytosensor microphysiometer can be achieved by directing the light-emitting diode excitation to the top side of the chip and by making improvements in the detection circuitry.

In conclusion, microfabrication can substantially increase the capabilities of microphysiometry. The combination of multichannel micromachined chips with microfluidics should increase throughput and decrease sample size, which are of particular benefit to drug-screening applications. The microfabrication of enclosures on the cellular size scale, together with foreseeable improvements in LAPS optical and electronics technology, suggests not only that single-cell microphysiometry is feasible, but also that such measurements can be made on arrays of single cells.

We acknowledge partial support from the Advanced Research Projects Agency, contract MDA972-92-C-0005.

References

1. Owicki JC, Parce JW. Biosensors based on the energy metabolism of living cells: the physical chemistry and cell biology of extracellular acidification. Biosens Bioelectron 1992;7:255–72.
2. Parce JW, Owicki JC, Kercso KM, Sigal GB, Wada HG, Muir VC, et al. Detection of cell affecting agents with a silicon biosensor. Science 1989;246:243–7.
3. McConnell HM, Owicki JC, Parce JW, Miller DL, Baxter GT, Wada HG, Pitchford S. The Cytosensor microphysiometer: biological applications of silicon technology. Science 1992;257:1906–12.
4. Hafeman DG, Parce JW, McConnell HM. Light-addressable potentiometric sensor for biochemical systems. Science 1988;240: 1182–5.
5. Owicki JC, Bousse LJ, Hafeman DG, Kirk GL, Olson JD, Wada HG, Parce JW. The light-addressable potentiometric sensor: principles and biological applications. Annu Rev Biophys Biomol Struct 1994;23:87–113.
6. Salon JA, Owicki JC. Real-time measurements of receptor activity; applications of microphysiometric techniques to receptor biology. In: Sealfon SC, ed. Receptor molecular biology. Orlando, FL: Academic Press, 1994 (in press).
7. Bruner LH, Miller KR, Owicki JC, Parce JW, Muir VC. Testing ocular irritancy in vitro with the silicon microphysiometer. Toxicol In Vitro 1991;5:277–84.
8. Nag B, Wada HG, Deshpande SV, Passmore D, Kendrick T, Sharma SD, et al. Stimulation of T cells by antigenic peptide complexed with isolated chains of major histocompatibility complex class II molecules. Proc Natl Acad Sci USA 1993;90:1604–8.
9. Wilding P, Pfahler J, Bau HH, Zemel JN, Kricka LJ. Manipulation and flow of biological fluids in straight channels micromachined in silicon. Clin Chem 1994;40:43–7.
10. Kricka LJ, Nozaki N, Heyner S, Garside WT, Wilding P. Applications of a microfabricated device for evaluating sperm function. Clin Chem 1993;39:1944–7.
11. Petersen KE. Silicon as a mechanical material. Proc IEEE 1982;70:420–57.
12. Bousse LJ, McReynolds RJ, Kirk G, Lam P, Parce JW. Integrated fluidics for biosensors used to measure cellular metabolism. In: Proc. symposium on chemical sensors II, Proc., Electrochemical Society, Honolulu, Hawaii. Pennington, NJ: Electrochemical Society, 1993:742–5.
13. Bousse L, McReynolds RJ, Kirk G, Dawes T, Lam P, Bemiss WR, Parce JW. Micromachined multichannel systems for the measurement of cellular metabolism. In: Proc. Int. Conf. on Solid State Sensors and Actuators, Yokohama, Japan. Tokyo: Inst. Electrical Engineers, 1993:916–20.
14. Bousse L, Hafeman D, Tran N. Time dependence of the chemical response of silicon nitride surfaces. Sens Actuat 1990;B1: 361–7.
15. Owicki JC, Parce JW, Kercso KM, Sigal GB, Muir VC, Venter JC, et al. Continuous monitoring of receptor-mediated changes in the metabolic rates of living cells. Proc Natl Acad Sci USA 1990;87:4007–11.
16. Parce JW, Wada HG, Baxter GT, Kuo RC, Alajoki ML, Fok KS, Owicki JC. The microphysiometer in drug discovery: screening for functional activity. Biochemie 1994, in press.

Pergamon

Life Sciences, Vol. 55, No. 8, pp. 573-583, 1994

0024-3205/94 $6.00 + .00

0024-3205(94)00164-2

USING MICROPHYSIOMETRY TO STUDY THE PHARMACOLOGY OF EXOGENOUSLY EXPRESSED m_1 AND m_3 MUSCARINIC RECEPTORS

Gregory T. Baxter, Mary-Louise Young, Donald L. Miller, and John C. Owicki

Molecular Devices Corp., 4700 Bohannon Drive, Menlo Park, CA 94025

(Received in final form June 6, 1994)

Summary

The microphysiometer, an instrument that uses a semiconductor-based sensor to monitor cellular metabolic activity, has been shown to detect the activation of a variety of receptors in living cells, largely irrespective of the signal-transduction mechanism. Using the Cytosensor® Microphysiometer, we have studied agonist concentration responses for the activation of CHO-K1 cell lines exogenously expressing rat m_1 or m_3 receptors. Three levels of receptor expression were investigated for each subtype. Carbachol is more potent for m_3 than m_1 receptors (0.5 to 1.0 log unit lower EC_{50}); for both, potency correlates positively with receptor density. The results agree well with those obtained by measuring phosphoinositide hydrolysis and intracellular [Ca^{++}] in the same cells. We also determined that two subtype-selective antagonists, pirenzepine (for m_1) and p-fluoro-hexahydro-sila-difenidol (for m_3) displayed appropriate differential ability to shift carbachol concentration-response curves in the microphysiometer. This study provides additional evidence that pharmacological results obtained by microphysiometry are consistent with those obtained by more conventional functional assays.

Key Words: biosensor, microphysiometer, muscarinic receptors

The activation of a receptor in a living cell or tissue is most commonly observed by monitoring products of a second-messenger pathway, such as cAMP or protein phosphorylation, or else a physiological process, such as proliferation or muscular contraction. Each particular receptor activates only a small proportion of the large number of signal-transduction pathways and functional effects that are known to be associated with receptor activation. In consequence, a wide spectrum of functional assays are in use, each appropriate for a small subset of known receptors. This contrasts with assays for ligand binding, where one type of assay, radio-ligand binding, is nearly universally used.

We have developed a functional assay for receptor activation that approaches the generality of radio-ligand binding. It is based on an instrument, the microphysiometer, that measures the rates at which cultured cells acidify their environment in a flow

Corresponding Author: John C. Owicki, Molecular Devices Corp., 4700 Bohannon Drive, Menlo Park, CA 94025 USA. Fax: (415) 322-2069. E-mail: jack@moldev.com

chamber (1, 2). This extracellular acidification rate is a measure of metabolic activity, because it reflects the rate of production of the acidic products of catabolism, typically lactic acid and CO_2. It can also reflect changes in intracellular pH (pH_i) caused purely by the regulation of proton transport across the plasma membrane (3).

These sources of extracellular acidification, catabolism and the regulation of pH_i, are altered by the activation of most cell-membrane receptors in ways that can be detected by the microphysiometer. Typically, the activation of a receptor increases the acidification rate by 10-100% within a few minutes. Depending on the biological system, the response may be short lived or sustained.

One may then ask how receptor activation is coupled to changes in extracellular acidification rate. A general answer is that energy metabolism and the proton economy of a cell are involved in so many cellular biochemical processes that changes in cell physiology usually cause changes in acidification rate. Specific answers depend on the system being studied; for example, the regulation of glycolysis and the activity of the amiloride-sensitive sodium-proton exchanger (NHE-1) are frequently involved (4, 5).

In other work we are attempting to elucidate these mechanisms further. In this paper we pose a different question: How does the pharmacology of receptor activation that is observed by microphysiometry compare with that observed by more conventional means? To answer this, at least in part, we have studied a model system in which muscarinic receptors are exogenously expressed in a mammalian cell line.

Since 1986, when Numa's group (6) cloned the first of the five muscarinic acetylcholine receptors subtypes known to date, this family of G-protein linked receptors has been studied extensively by heterologous expression in a variety of mammalian cells (7-10). Of particular interest here is a study by Buck and Fraser (11) in which rat m_1 and m_3 muscarinic receptors (m_1R and m_3R) were expressed in CHO-K1 cells at three different expression levels for each subtype. Concentration-response curves were obtained by those authors for the carbachol-induced accumulation of inositol phosphates.

Using these same six cell lines, we have also observed responses of intracellular calcium-ion concentration, $[Ca^{++}]_i$, to carbachol, and we have compared both to the concentration-response characteristics for extracellular acidification rate. In addition, we have explored the effects of two antagonists, one m_1R-selective and one m_3R-selective, on the stimulation of acidification rate evoked by carbachol in single examples of both the m_1R and m_3R lines.

This work expands on brief previous studies in which we reported a concentration-response curve for carbachol stimulation of extracellular acidification by activating an m_1R (2) and showed that atropine, a muscarinic antagonist, inhibited this stimulation (12).

Methods

Chemicals and cell lines. Unless otherwise noted, chemicals were obtained from Sigma (St. Louis, MO). Pirenzepine (PZP) and p-fluoro-hexahydro-sila-difenidol (pFHHS) were obtained from RBI (Natick, MA). L-[benzilic-4,4'-^{3}H(N)]-quinuclidinyl benzilate ([^{3}H]QNB, 38.8 Ci/mmol), was purchased from NEN Research Products (Buster, NH). The three m_1R/CHO and three m_3R/CHO cell lines studied by Buck and Fraser (11) were obtained from ATCC. The ATCC designations are listed in Table I, along with the designations that we have used in this paper: m1Low, m1Mid, m1High, m3Low, m3Mid, and m3High, to indicate the subtype of the muscarinic receptor and the rank order of expression level. Cells were maintained in Ham's F-12 culture medium supplemented with 50 µg/mL G-418

and 10% fetal bovine serum in a humidified atmosphere (5% CO_2) at 37 C. Cells were serum starved for 18 hours prior to experiments.

Radioligand binding assays. Cells were removed from flasks using EDTA and centrifuged for 5 min at 500 x g. The cell pellets were suspended in ice-cold hypotonic lysis buffer (5 mM $NaPO_4$, pH 7.4, 2 mM $MgSO_4$) and homogenized using a glass Dounce homogenizer. Cell homogenates were centrifuged at 1000 x g for 5 min, and the supernatant was collected. Supernatants were centrifuged at 100,000 x g for 15 min, and the pellet was resuspended in binding buffer containing 20 mM $NaPO_4$, pH 7.4, 2 mM $MgSO_4$. Protein concentrations were determined using BioRad protein-concentration determination reagent and bovine serum albumin as a standard. [^{3}H]-QNB binding reactions were performed in triplicate at concentrations from 25 pM to 5 nM. Binding was initiated by the addition of membranes (~10 µg membrane protein per assay) for a final volume of 0.5 mL. After 60 min at 37 C, the reaction was terminated by filtration over Whatman GF/C filters. Filters were washed with 2 x 5 mL ice-cold binding buffer and placed in glass vials. Radioactivity was determined by counting in a liquid scintillation counter. Data were analyzed in terms of a single population of receptors using the nonlinear curve-fitting routine on KaleidaGraph®.

Microphysiometry. Microphysiometry was performed in a Cytosensor Microphysiometer (Molecular Devices, Menlo Park, CA). Each flow chamber of the instrument was assembled with $2.5 \cdot 10^5$ cells grown on the 3 µm microporous polycarbonate membrane of a capsule cup (Molecular Devices). Cells were perfused with a low buffered RPMI-1640 culture medium (Irvine Scientific, Santa Ana, CA) at 37 C. The acidification rate was measured every 90 s (flow on at 100 µL/min for 60 s, flow off for 30 s, with acidification rate measured during seconds 5 to 25 of the flow-off period). Agonist was introduced just prior to a flow-off period and flushed out when flow resumed. The total time of exposure to agonist was about 1 min.

Concentration-response curves were obtained by exposing the cells sequentially to increasing concentrations of agonist for durations of 1 min at intervals of 30 min, a protocol designed to limit desensitization. The response was taken as the increase in acidification rate upon addition of agonist (difference in rates for the data points immediately before and after exposure to agonist), normalized by the basal acidification rate prior to the lowest concentration of agonist. Agonist potency was calculated by determining the concentration of agonist that produced half-maximal stimulation (EC_{50}) by interpolation on a plot of response vs. log[agonist], and is reported as $pEC_{50} \equiv -\log(EC_{50})$.

$[Ca^{++}]_i$ measurements. Cells grown on 25 mm cover slips were incubated for 10 min at room temperature in medium augmented with 10 mM N-2-hydroxyethylpiperazine-N'-2-ethanesulfonic acid (HEPES), containing 12 µM fura-2 AM (Molecular Probes, Eugene, OR). The cover slip was then transferred to a petri dish containing fresh medium and incubated for another 10 min to allow complete de-esterification of the dye. It was then placed in an open chamber atop the stage of an inverted microscope (Nikon Diaphot). Solutions were changed by rapidly drawing off medium in the chamber and pipetting in fresh medium. In this manner solutions could be changed in about 1 second. Fluorescence was measured in a PTI (Deltascan, Model 4000, South Brunswick, NJ) dual-excitation spectrofluorometer. The excitation monochromators were set at 345 and 380 nm (bandwidth of 3 nm), and the fluorescence was measured at 510 nm (bandwidth 20 nm) as the ratio of the intensities resulting from excitation at 345 and 380 nm. This ratio was approximately a linear function of $[Ca^{++}]_i$ throughout the range of changes in $[Ca^{++}]_i$ evoked by the agonist. EC_{50} was determined by interpolation on a plot of ratio vs. log[agonist].

Statistical analysis. Uncertainties are reported as ± standard error of the mean (SEM). A two-tailed unpaired t test with $p<0.05$ was used as the test of statistical significance.

Results and Discussion

Ligand binding. Radio-ligand binding experiments were performed on plasma-membrane preparations to confirm the values of receptor density reported by Buck and Fraser (11) for these same cell lines. The resulting estimates of the receptor densities are shown in Table I. Agreement with the previously published values is close at low densities and within about a factor of two at high densities; the rankings of densities within a receptor subtype are identical. We did not attempt to obtain reliable estimates of affinities, instead referring the reader to Buck and Fraser (11).

Kinetics of agonist-induced changes in extracellular acidification rate. Agonist-induced changes in acidification rate were detectable for all cell lines except the lowest-density m_1R construct, m1Low. The kinetic profile of the response depended on the receptor, the level of expression, the concentration of agonist, and the length of time that the cells were exposed to the agonist.

For sustained exposure to agonist (>1 min), under most circumstances the response began with a peak at the first data point after the beginning of exposure to agonist (~1 min) and thereafter fell to a lower, slower response that was sustained even after the withdrawal of agonist; see Fig. 1. Exceptions were when agonist concentration was low ($<<EC_{50}$) or the expression level of receptor was low. In these cases, instead of an initial peak, the maximum response appeared after several minutes. Thus, muscarinic stimulation of acidification rate in this system was characterized by fast and slow phases, and the fast phase was not observed when the number of occupied receptors was low. Qualitatively the same two-component behavior was shown by $[Ca^{++}]_i$ (data not shown). The existence of these two components of the response is consistent with the work of Lambert et al. (13) on m_1R/CHO and m_3R/CHO and of Tobin et al. (14) on m_3R/CHO cells; in these studies, inositol trisphosphate concentrations peaked less than one minute after the addition of agonist and then fell to lower, but still elevated, levels that were sustained for tens of minutes.

When exposure to agonist was brief (≤1 min), the slow, sustained phase was diminished (Fig. 1). This was more pronounced for the m_1R than the m_3R cells. Whether this difference was due to the higher affinity of the m_3R for carbachol (11) or to differences in signal transduction intracellularly is not clear.

Desensitization and assay protocol. Receptor desensitization is worth studying because of its regulatory significance (15), and in our study it has additional practical importance. Our assays were based on repeated applications of increasing concentrations of agonist to a population of cells; desensitization would decrease the later, high-concentration responses. It was therefore necessary to design the protocol to minimize the effects of receptor desensitization. One part of the strategy was to limit the exposure of the cells to agonist to ~1 min for each application.

The second part was to wait long enough between challenges with agonist for substantial recovery of the cells. As is shown in Fig. 2, when cells were re-exposed to a high concentration of agonist within 10 min of an initial stimulation, the second response was greatly diminished. When 20 min elapsed between exposures, the second response was decreased by 10-15%. The cellular response did not recover completely within 30 min, the longest time tested. The kinetics of desensitization were similar to those observed

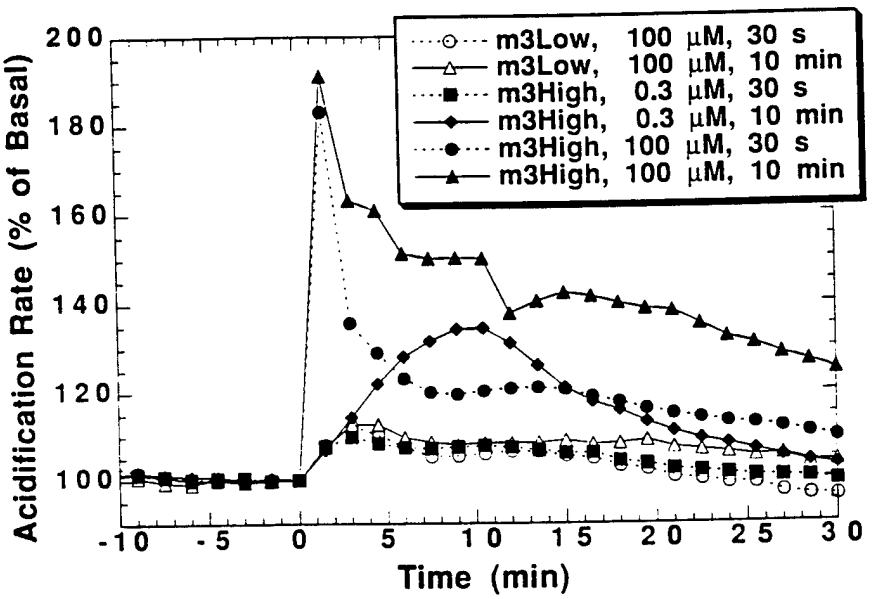

Fig. 1

Response to cholinergic stimulation in the microphysiometer. As indicated in the legend, cells expressing low or high levels of the m_3R were exposed to 0.3 µM or 100 µM carbachol for 1 or 10 min. Representative data are shown (n=3 or 4).

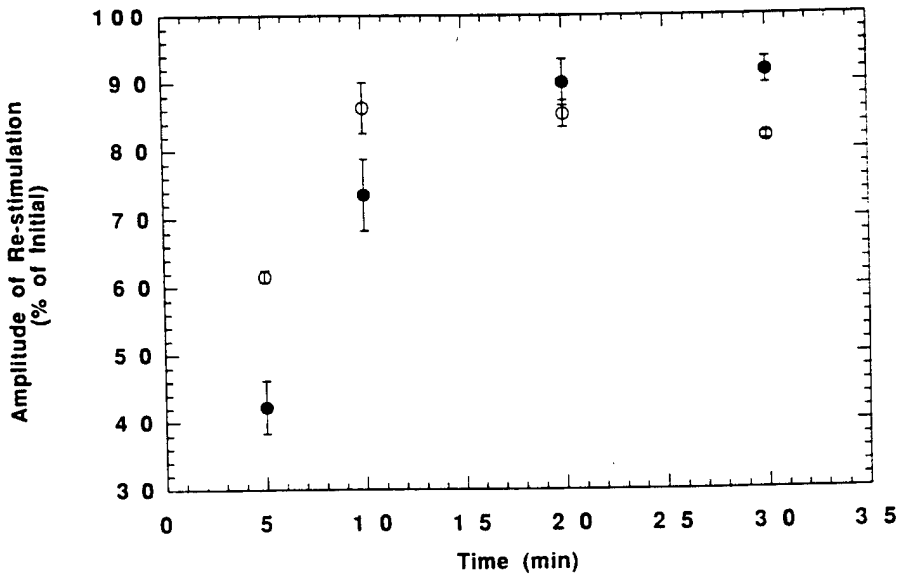

Fig. 2

Time course of recovery from desensitization. Each chamber was exposed to 100 µM carbachol for 1 min twice: once at t=0 and subsequently at t=5 to 30 min. The peak height of the second response in the microphysiometer was plotted as a percent of the initial response. m1High is indicated by filled circles, m3High by open circles. Error bars represent SEM (n=2).

by Tobin et al. (14) for the agonist-induced desensitization of phosphoinositide hydrolysis in m_3R/CHO cells, which itself may be linked to phosphorylation of the receptor (16).

Designing a functional assay is facilitated by the fact that the microphysiometer is based on a flow chamber; one can control the time that cells are exposed to effector agents with a resolution of <1 min. Nevertheless, some effects of desensitization can be seen in the diminished responses at the highest agonist concentrations for the cells expressing the highest density of receptors (Fig. 3). Based on comparisons with other functional assays in the same system (see below), it appears that desensitization had no major impact on the estimates of agonist potency that we obtained. The effects of desensitization on acidification rate vary with receptor/cell system, so our results do not necessarily shed light on the behavior of other systems.

Concentration-response results. Typical concentration-response curves are shown in Fig. 3, and the derived pEC_{50} values are presented in Fig. 4 and Table I. For both the m_1R and m_3R constructs, increasing receptor density increased the potency of carbachol (decreased EC_{50}) throughout the range of expression levels studied. The effect of receptor density on response was greater for the m_1R system, which showed the greater range of receptor densities. There, no carbachol-induced change in acidification rate was detectable for the lowest-density cell line, and the potencies of carbachol differed by almost an order of magnitude between the higher-density cell lines ($\Delta pEC_{50}=0.86\pm0.21$).

Controlling for receptor density, carbachol was more potent on the m_3R than the m_1R cells. A response could be detected for m3Low, but not m1Low. At higher receptor density, the pEC_{50} for the m_3 cells was the higher by ≈0.8 (from Fig. 4).

The maximum amplitude of the agonist-induced increase in acidification rates was not as reproducible as the EC_{50}, and it varied primarily between experiments rather than within an experiment. The four cell lines expressing medium and high levels of receptor were statistically indistinguishable from one another based on n=3 to 7 determinations of maximum amplitude per cell line. Lumped together, they had a mean maximum increase of 47±5% (standard deviation 22%, n=18). The maximum amplitude of the response of m3Low was 9±3% (n=3), which was significantly lower than that of the other responding

TABLE I.

The potency of carbachol in the six muscarinic/CHO cell lines, determined by three methods.

Cell line	ATCC designation	Receptor	Density fmol/mg protein	pEC_{50}		
				Microphys.	$[Ca^{++}]_i$	PI Hydrolysis[a]
m1Low	CRL1986	m_1	100 (70)[b]	NR	NR	NR[c]
m1Mid	CRL1984	m_1	360 (370)	4.69±0.08	4.91±0.11	5.20±0.14
m1High	CRL1985	m_1	1900 (800)	5.55±0.19	5.36±0.04	5.46±0.16
m3Low	CRL1983	m_3	110 (75)	4.77±0.06	4.86±0.08	NR
m3Mid	CRL1981	m_3	750 (450)	5.99±0.07	5.98±0.32	5.66±0.19
m3High	CRL1982	m_3	1400 (690)	6.33±0.13	6.07±0.17	5.87±0.30

[a] Estimated from Fig. 2 of Buck and Fraser (11).
[b] Numbers in parentheses are determinations by Buck and Fraser (11).
[c] No response detected

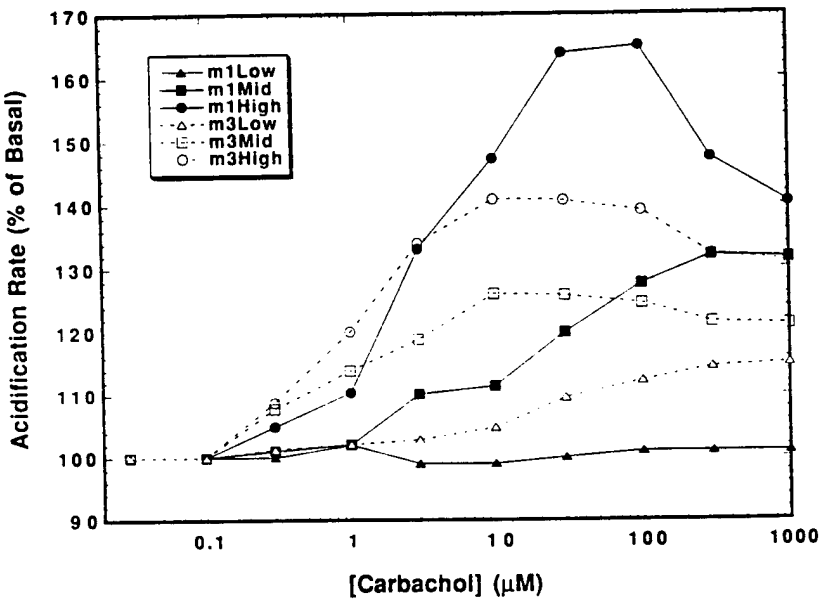

Fig. 3

Concentration responses of the six cell lines to carbachol. Representative data are shown (n=3 to 5).

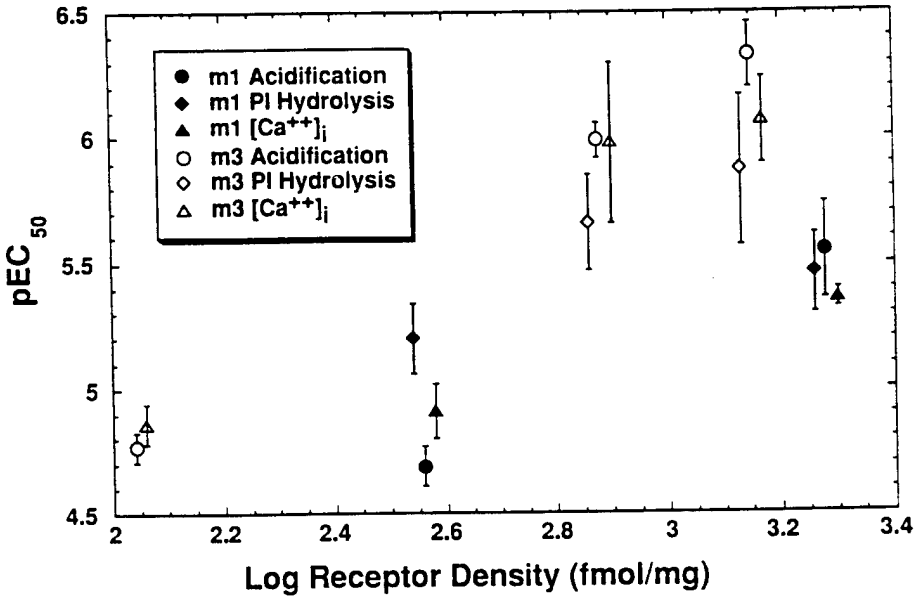

Fig. 4

Potency of carbachol as a function of receptor density for the m_1R and m_3R cell lines, as determined by three functional assays: microphysiometry, intracellular Ca^{++}, and PI hydrolysis. Error bars represent SEM (n=3 to 5). The PI hydrolysis data were taken from Buck and Fraser (11), with error bars estimated from their Fig. 2. Data are slightly offset horizontally for clarity of presentation.

cells. It is well established that, in m_1R/CHO and m_3R/CHO cells, the former show a substantially greater maximal stimulated hydrolysis of phosphoinositides (11, 17, 18). There is no evidence that similar differences exist in the maximum amplitudes of agonist-induced increases in acidification rates.

Intracellular [Ca^{++}]. Increases of $[Ca^{++}]_i$ evoked by carbachol showed a pattern similar to that for the stimulation of acidification rates. No response was observed for m1Low, and the pEC_{50} values for the remaining cell lines are shown in Table I and Fig. 4. The dependence of pEC_{50} on receptor density was statistically significant comparing m1Mid and m1High, and comparing m3Low to either m3Mid or m3High, but not comparing m3Mid and m3High.

Comparison of microphysiometry to second-messenger assays. Examination of the results in Fig. 4 and Table I shows that functional assays based on microphysiometry, phosphoinositide hydrolysis, and $[Ca^{++}]_i$ give a broadly consistent picture of the potency of carbachol for activating m_1R and m_3R in CHO-K1 cells, for expression levels ranging from 100 fmol/mg protein to nearly 2000 fmol/mg protein. By all three assays, the potency of carbachol for activating the m_3R was 0.5-1 log unit higher than that for the m_1R.

The lowest expression levels studied, ~100 fmol/mg protein, induced responses that were near or below the limits of detection of the assays. None of the three methods detected a response in the m1Low cells. No change in phosphoinositide hydrolysis was observed in m3Low. This might reflect a lower sensitivity of the phosphoinositide assay (see, e.g., (19) or perhaps some difference between the cells used by Buck and Fraser (11) and those used in our study.

At higher densities, >300 fmol/mg protein, microphysiometry clearly indicated that potency increased with receptor density. The two second-messenger assays displayed the same trend, but statistical significance was only present for $[Ca^{++}]_i$ measurements on the m_1R system. The relationship between potency and receptor density is not necessarily straightforward. For example, Mei et al. (20) examined a series of eight B82 fibroblast cell lines into which the rat m_1R had been expressed at levels ranging from 60 to 1300 fmol/mg protein. They found an eight-fold range of EC_{50} for carbachol, but only a weak positive correlation with receptor density.

Subtype-selective antagonists. Buckley et al. (21) have described the binding properties of nine muscarinic antagonists for the rat m_1R and human m_2R through m_5R expressed in CHO-K1 cells. Considering the m_1R and m_3R, the greatest m_1R selectivity was 11-fold, shown by PZP. No antagonist showed comparable selectivity for the m_3R. Another antagonist, pFHHS, was reported to have 14-fold selectivity for m_3R vs. the m_1R in a binding study on tissues (22), though a later study using the receptors expressed in CHO-K1 cells found a selectivity of only 5-fold (23).

We studied the effects of PZP and pFHHS on the carbachol concentration-response relationship for the cells expressing the highest densities of each receptor subtype. As is shown in Fig. 5, the antagonists shifted the carbachol concentration-response curves to the right in a concentration-dependent fashion. Fig. 6 summarizes the shifts in carbachol pEC_{50} induced by the two antagonists. In all cases, increasing the concentration of antagonist progressively shifted the carbachol curve to the right, except that for 100 nM pFHHS on the m_1R cells the shift was not statistically different from zero. We do not present a Schild analysis, which assumes agonist-antagonist binding equilibrium; under our rapid data-collection protocol the agonist had not fully equilibrated with the slowly dissociating antagonist (24, 25).

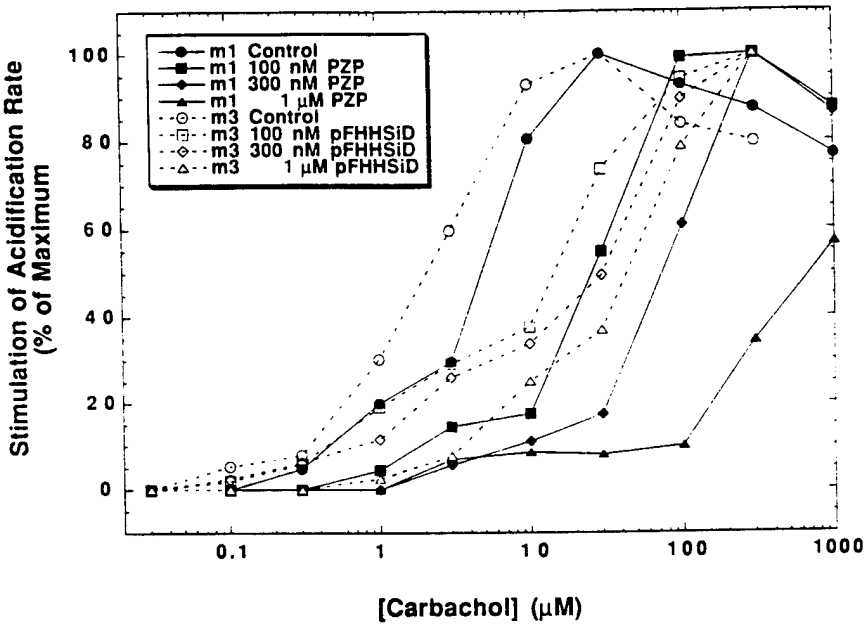

Fig. 5

Shifting the concentration-response curves for carbachol with competitive antagonists. Results are shown for PZP with m1High and pFHHS with m3High. The two other combinations (PZP with m3High and pFHHS with m1High) are not shown. Representative data are shown (n=3).

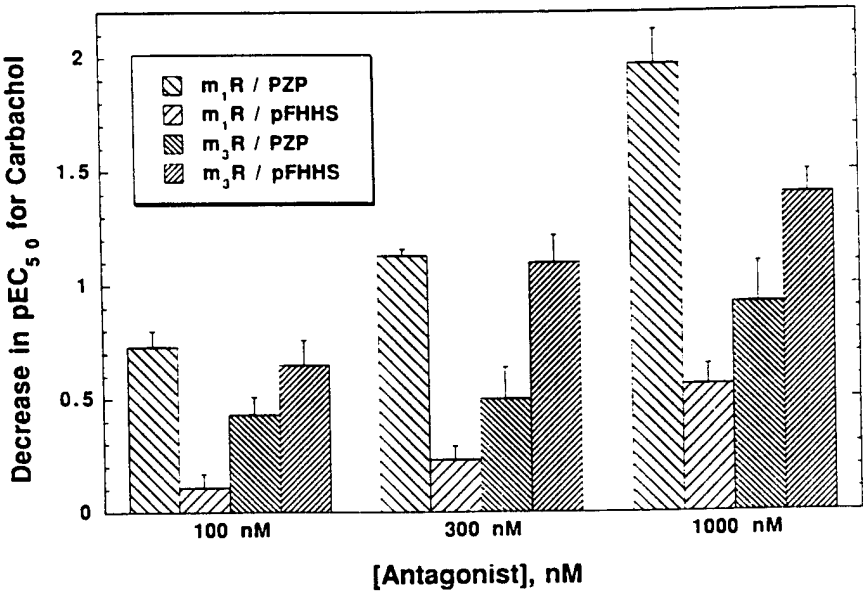

Fig. 6

Summary of studies with subtype-selective antagonists. PZP and pFHHS show the expected subtype selectivity in shifting the agonist concentration-response curves for m1High and m3High. Error bars represent SEM (n=3).

7. M.H. RICHARDS, Biochem. Pharmacol. 9 1645-1653 (1991).
8. T.I. BONNER, Trends Neurosci. 12 148-151 (1989).
9. M.M. HOSEY, FASEB J. 6 845-852 (1992).
10. R.D. SCHWARZ, R.E. DAVIS, J.C. JAEN, C.J. SPENCER, H. TECLE, and A.J. THOMAS, Life Sci. 52 465-472 (1993).
11. M.A. BUCK and C.M. FRASER, Biochem. Biophys. Res. Commun. 173 666-672 (1990).
12. J.C. OWICKI, J.W. PARCE, K.M. KERCSO, G.B. SIGAL, V.C. MUIR, J.C. VENTER, C.M. FRASER, and H.M. McCONNELL, Proc. Natl. Acad. Sci. U.S.A. 87 4007–4011 (1990).
13. D.G. LAMBERT, N.T. BURFORD, and S.R. NAHORSKI, Biochem. Soc. Trans. 20 130-135 (1992).
14. A.B. TOBIN, D.G. LAMBERT, and S.R. NAHORSKI, Mol. Pharmacol. 42 1042-1048 (1993).
15. R.J. LEFKOWITZ, Cell 74 409-412 (1993).
16. A.B. TOBIN and S.R. NAHORSKI, J. Biol. Chem. 268 9817-9823 (1993).
17. J. HU and E.E. EL-FAKAHANY, Mol. Pharmacol. 38 895-903 (1990).
18. E.G. PERALTA, A. ASHKENAZI, J.W. WINSLOW, J. RAMACHANDRAN, and D.J. CAPON, Nature 334 434-437 (1988).
19. A.K. THOMPSON and S.K. FISHER, J. Pharmacol. Exp. Ther. 252 744-752 (1990).
20. L. MEI, J. LAI, H.I. YAMAMURA, and W.R. ROESKE, J. Pharmacol. Exp. Ther. 251 90-97 (1989).
21. N.J. BUCKLEY, T.I. BONNER, C.M. BUCKLEY, and M.R. BRANN, Mol. Pharmacol. 35 469-476 (1989).
22. G. LAMBRECHT, R. FEIFEL, M. WAGNER-RODER, C. STROHMANN, H. ZILCH, R. TACKE, M. WAELBROECK, J. CHRISTOPHE, H. BODDEKE, and E. MUTSCHLER, Eur. J. Pharmacol. 168 71-80 (1989).
23. Y. MENG, J. HU, and E.E. EL-FAKAHANY, Membr. Biochem. 9 293-300 (1990).
24. T. KENAKIN, Pharmacologic Analysis of Drug-Receptor Interaction, 2nd. Ed., 423-427 (1993).
25. C. SCHUDT, C. AURIGA, N. BIRDSALL, and R. BOER, Pharmacology 37(Suppl 1) 32-39 (1988).
26. R.E. DAVIS, P.D. DOYLE, J.C. JAEN, D.J. LAUFFER, C. RABY, R. SCHWARZ, H. TECLE, and A.J. THOMAS, Soc. Neurosci. Abst. 19 1040 (1993).
27. M.A. HIRST and S. PITCHFORD, J. NIH Res. 5 69 (1993).
28. J.C. DENYER, P. THORN, C. BOUNTRA, and C.C.JORDAN, J. Physiol. (London) 459 390P (1993).
29. J.C. DENYER, J. GRAY, M. WONG, M. STOLZ, and S. TATE, Eur. J. Pharmacol., in press (1994)
30. S. SKWISH and K.E.J. DICKINSON, FASEB J. 8 A650 (1994).

Effects of Cholinergic Agents on Cellular Metabolism in Cultured Suprachiasmatic Nucleus

V. Cao, J. Owicki, D. Edgar, and J.D. Miller, Departments of Psychiatry and Biology, Stanford University, Stanford, CA and Molecular Devices Corporation, Menlo Park, CA

Soc. Neurosci. Abstr. 17: 672 (1991)

Introduction

Cholinergic agents phase shift the circadian clock *in vivo*, presumably through a nicotinic receptor. Since high affinity nicotinic binding site in the suprachiasmatic nucleus (SCN) have not been demonstrated autoradiographically, it has been suggested that phase shifting effects of cholinergic agents are mediated by a receptor remote from the SCN. However, more recent electrophysiological and immunohistochemical data indicate the existence of both nicotinic and muscarinic receptors in the SCN.

The present investigation examined the nature of cholinergic receptors in cultured SCN cells from two day old rats. Extracellular acidification, following a one minute pause in the perfusion of oxygenated medium, was used as an index of cellular metabolism in a microphysiometer. Sister cultures were immunohistochemically labelled for neurons (MAP2) and astrocytes (GFAP). The effects of carbachol (a non-specific cholinergic agonist) and nicotine on SCN metabolism were directly compared and a dose response curve was constructed for nicotine. Finally, we examined whether the effects of nicotine could be blocked by the classical nicotinic antagonist, mecamylamine.

Methods

Pregnant Sprague Dawley rats were housed on a 12:12 light dark cycle for two weeks prior to giving birth. On the day of tissue harvest, two day old rats were sacrificed and their brains removed into Hank's Balanced Salts Solution (HBSS) containing 0.1% Bovine Serum Albumin (BSA) and 1 mM Hepes. The SCN were extracted under a dissecting scope, with the optic nerve as the major landmark. A cubic millimeter of tissue surrounding the optic nerve was dissected out. After all the SCNs were harvested, they were washed three times in sterile HBSS with 0.1% BSA and 1 mM Hepes. The tissues were then transferred to a tube containing HBSS with 0.1% BSA, 1 mM Hepes and 10% trypsin. The tissues were digested in trypsin at 37° C for 20 minutes, at which point they were triturated using a firepolished Pasteur pipette, pretreated with 1% prosil, until the cells were fully dispersed. The cell suspensions were then centrifuged at 1100g for 8 minutes at room temperature. The cell pellets were then resuspended in 5 ml HBSS with 0.1% BSA and 1 mM Hepes, overlaid on the surface of a 4% BSA solution and spun down for 5 minutes. Cells were washed three times in plating media (Dulbecco's Modified Eagle Medium with 5% Fetal Bovine Serum and 1% Penicillin-Streptomycin), each wash consisting of resuspending the cells in plating media and centrifuging at 1100g for 5 minutes. Cells were plated onto a transwell cup (3 μ pore) polycarbonate membrane which had been pretreated with poly-d-lysine overnight.

Experiments were performed from CT 4-CT 8 (day 5 or 6 in culture) on a given day. A 50 μ spacer and a transwell insert were added to the transwell cup, forming a kind of cellular sandwich (Figure 1). The assembly was then loaded into the flow chamber of a microphysiometer provided by the Molecular Devices Corporation; Figure 2 shows the schematic diagram of a microphysiometer system. The cells were perfused at 100 μl/min with Dulbecco's Modified Eagle Medium (DMEM) without sodium bicarbonate or pyruvate, pHed to 7.4 ± .01 and allowed to equilibrate for one hour. Various concentrations of nicotine, carbachol and mecamylamine were dissolved in DMEM and pHed to 7.4 ± .01. For the nicotine dose response experiments 1 μM, 3 μM, 10 μM, and 30 μM nicotine concentrations were employed. Each chamber was pulsed with a single concentration of nicotine for 20 minutes followed by a 20 minute recovery period; this protocol was repeated twice for each chamber. In a second experimental series, the non-specific cholinergic agonist carbachol (10 μM) was administered three times for 5 minutes with 10 minute recovery periods between pulses. Three pulses of 10 μM nicotine for 5 minutes, each followed by 10 minute recovery periods, were then applied to the chambers which had previously received the pulses of carbachol. Other cultures received the two drugs in counterbalanced order (nicotine, then carbachol). In the third study, 10 μM nicotine was applied twice for 20 minutes with 20 minute recovery periods between each pulse. After the pulses of nicotine, 10 μM nicotine and 10 μM mecamylamine (a nicotinic antagonist) were coadministered for 20 minutes in two consecutive trials to the same chambers which had received the pulses of 10 μM nicotine; each pulse was followed by a 20 minute recovery period.

Cellular metabolic rate was indexed by taking the slope of the best fit line of the acidification rate during a one minute pause in tissue perfusion. Mean acidification rates were then calculated over each drug or baseline period. Percent change from baseline scores were then calculated for the various drug treatments for the individual cultures.

Microphysiometer Cell Capsule and Plunger

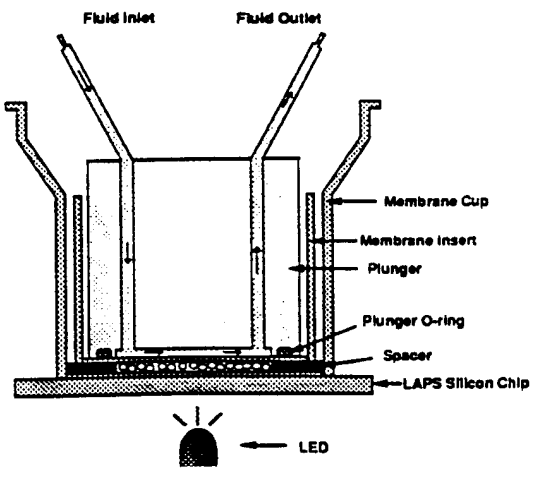

Schematic Diagram of Microphysiometer System

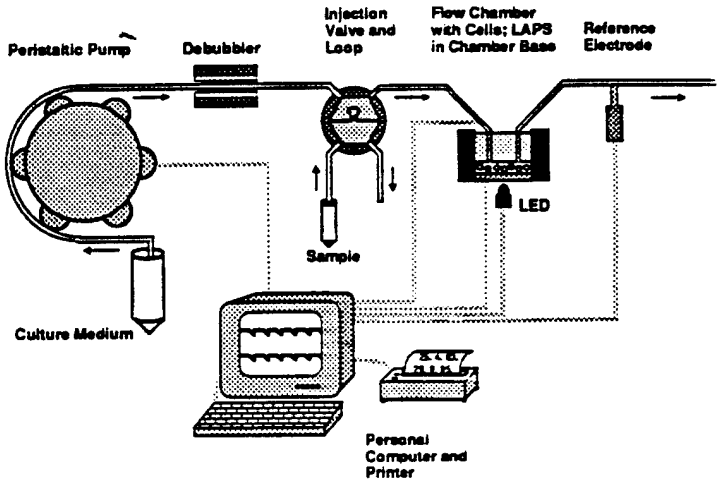

Figure 2. Schemasc diagram of microphysiometer system.

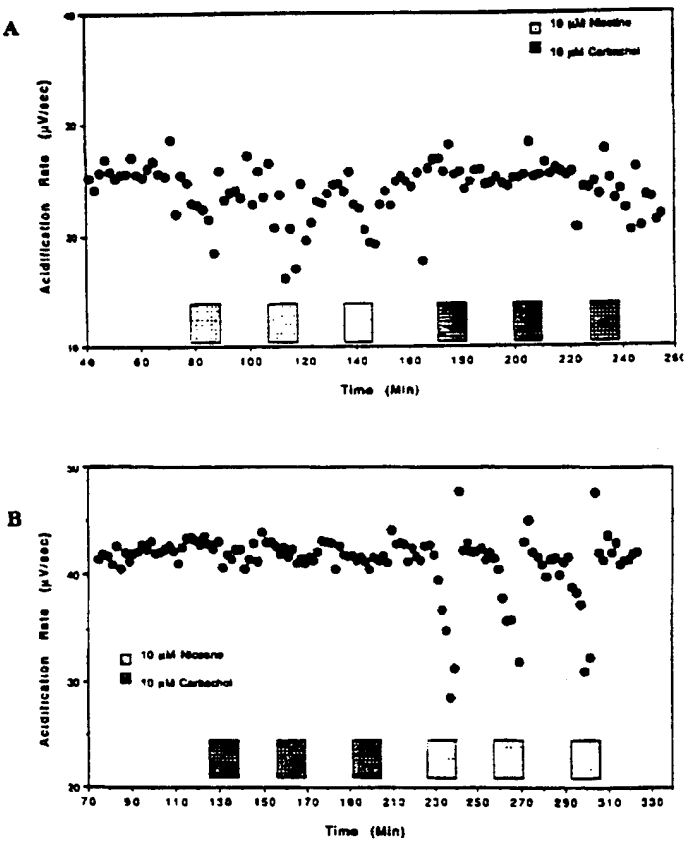

Figure 3. Individual data from one SCN culture. A) Three presentations of nicotine (10 μM) followed by three presentations of carbachol (10 μM). B) Three presentations of carbachol (10 μM) followed by three presentations of nicotine (10 μM). Note the inhibitory response to nicotine. This was the predominant response, occurring in 70% of the cultures (33/48 cultures).

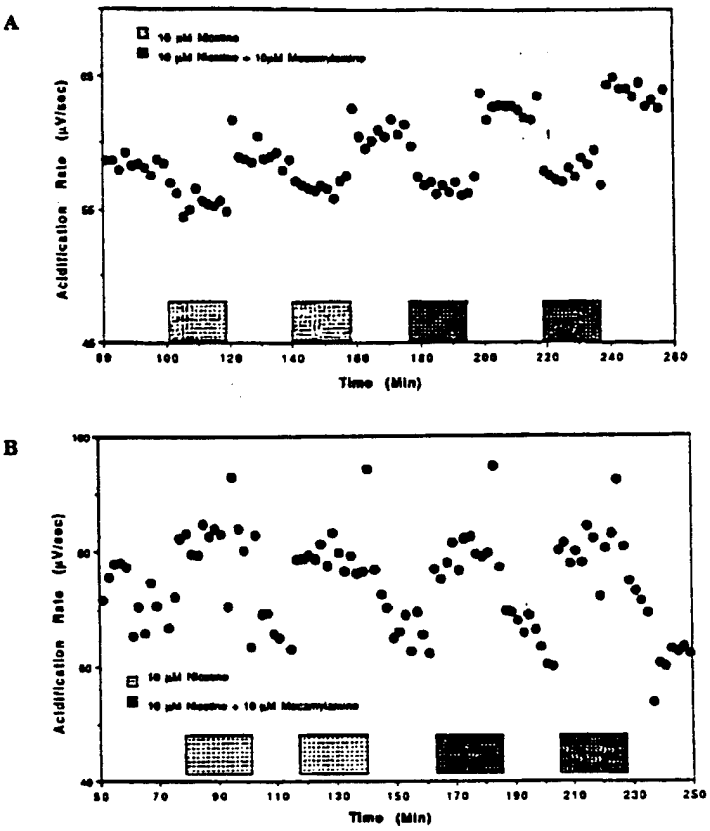

Figure 4. Individual data from one SCN culture. A) The inhibition of cellular metabolism by nicotine administration (10 µM) is not affected by coadministration of the nicotinic antagonist mecamylamine (10 µM). B) Increases in cellular metabolism induced by 10 µM nicotine (in about 20% of the cultures, 10/48 cultures) is not affected by coadministration of mecamylamine (10 µM).

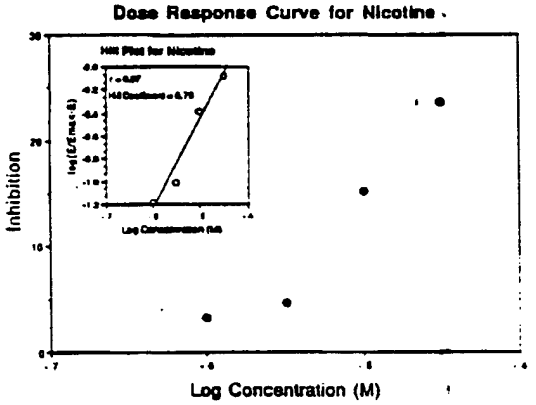

Figure 5. Dose respondent curve for nicotinic inhibition. Nicotine's effects are does dependent. The Hill plot (inset exhibits a near unitary slope, suggesting a single receptor occupancy model for the effects of nicotine.

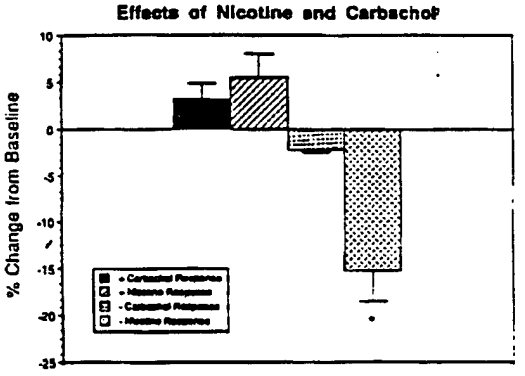

Figure 6. Effects of nicotine and carbachol (group data). Inhibition of metabolism by nicotine (10 µM) is much stronger than inhibition by carbachol (10 µM) at physiologically relevant doses.* = $p<.001$, within subjects t test comparing inhibitory effects of nicotine and carbachol. Increases in metabolism are occasionally produced by nicotine (10 µM, n = 3) or by carbachol (10 µM, n = 6), but these responses do not differ from each other. The combined positive cholinergic response (nicotine or carbachol) is significantly greater than 0 ($t = 2.9$, $df = 8$, $p<.01$).

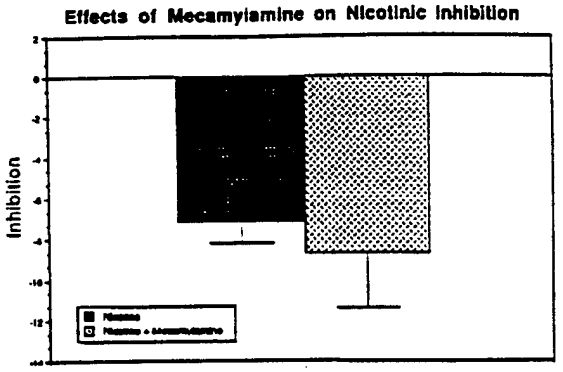

Figure 7. Effects of mecamylamine on nicotinic inhibition. Coadministration of mecamylamine does not antagonize the inhibitory effect of nicotine on cellular metabolism (n = 10, within subjects t test = 0.76, ns) or the facilitatory effect (n = 3, data not shown).

Conclusion

1. The predominant effect of nicotine in cultured SCN cells is inhibition of cellular metabolism. Carbachol, in contrast, minimally effects cellular metabolism at the same concentration.
2. The effect of nicotine is dose dependent and explainable in terms of a single occupancy model.
3. The effect of nicotine on cellular metabolism is not antagonized by the classical nicotinic antagonist, mecamylamine.
4. We suggest that nicotine may act in the SCN via a relatively low affinity binding site (µM range) with even lower affinity for carbachol. The ineffectiveness of mecamylamine further suggests that the nicotinic receptor in the SCN may be structurally different from peripheral nicotinic receptors. Molecular heterogeneity in brain nicotinic receptors and, in particular, hypothalamic nicotinic receptors has been previously reported.

This research was supported in part by a grant from the Upjohn Company.

Monitoring Changes in Proton Metabolism Enables a Functional Analysis of Inwardly Rectifying Potassium Channels Expressed in Yeast.

Soc. Neurosci. Abstr. 21: 1324 (1995)

K.M. Hahnenberger[1], S. Kurtz[2], T. Hoshi[3], and D.L. Miller[1].
1. Molecular Devices Corporation, Sunnyvale, CA 94089
2. Bristol-Myers Squibb Pharmaceutical Research Institute, Princeton, NJ 08542
3. Dept. of Physiology, University of Iowa, Iowa City, IA 52242

It has previously been shown that expression of mammalian cardiac inwardly rectifying K channels and a member of the Shaker superfamily of K channels from *Arabidopsis thaliana*, complement a defect in potassium uptake in yeast strains lacking both high and low affinity potassium transporters. In yeast, K is taken up in a 1:1 ratio with extrusion of protons. The plasma membrane H-ATPase establishes a highly negative electrical potential across the membrane, which presumably maintains the inwardly rectifying K channels in the open state.

We have utilized the tight coupling between potassium uptake and proton extrusion in yeast to analyze the function of inwardly rectifying K channels using microphysiometry. The microphysiometer is a silicon sensor-based instrument which measures the rate at which cells acidify their external environment and can be used to detect small changes in proton fluxes across the plasma membrane. Exposure to yeast cells expressing a guinea pig cardiac IRK1 homologue or the *A. thaliana* KAT1 gene to channel blockers such as Cs and TEA results in a rapid and transient decrease in proton flux. Removal of the channel blockers results in a transient increase in acidification rates. The effectiveness of the channel blockers varied; the strain expressing the inward rectifying K channel exhibits a greater response to Cs, while the strain expressing the plant Shaker channel was more affected by TEA. This system can be used to perform mutational analysis of ion channel function and to identify compounds which modulate ion channel activity.

CRYOBIOLOGY 30, 386–395 (1993)

A Metabolic View of Receptor Activation in Cultured Cells Following Cryopreservation

RICHARD C. KUO, GREGORY T. BAXTER, LIISA ALAJOKI, DONALD L. MILLER, JEFFREY M. LIBBY, AND JOHN C. OWICKI[1]

Molecular Devices Corp., 4700 Bohannon Drive, Menlo Park, California 94025

The effect of cryopreservation on agonist-induced receptor activation in mammalian cells was investigated with the Cytosensor microphysiometer, a biosensor that monitors cellular metabolic activity by measuring changes in extracellular pH. In this study, two different cell types—nonadherent TF-1 cells (from a human erythroleukemia patient) and adherent WT3 cells (CHO-K1 cells transfected with the m_1 muscarinic acetylcholine receptor)—were cryopreserved by freezing in a disposable cell capsule used in the microphysiometer. The recovery of metabolic activity by TF-1 cells was observed over ~1 h following thawing. Responses of the TF-1 cells to granulocyte–macrophage colony-stimulating factor (GM-CSF) and platelet activating factor (PAF) were measured before cryopreservation and 90 min after thawing. The GM-CSF and PAF responses retained 71 ± 14% and 73 ± 10% of maximum stimulation, respectively. Post-thaw cholinergic stimulation of WT3 cells was 73 ± 9% of its level in similarly treated but unfrozen cells. Cryopreservation caused no detectable difference in desensitization of the response due to repeated application of carbachol. These results demonstrate the feasibility of pharmacological studies with cryopreserved cells in the microphysiometer and further suggest that the microphysiometer may be useful in exploring the biological consequences of cryopreservation in the early post-thaw period.

We have reported a novel biosensor-based instrument that measures the metabolic activity of cells in a flow chamber noninvasively and in real time (13, 14, 17–19). Since the disposable capsule that houses cells in the microphysiometer is well adapted for cryopreservation, we were moved to explore two questions: Could cryopreserved cells be used in the instrument within minutes after thawing and maintain physiological responses of interest? And could the microphysiometer be used to investigate the physiological changes in cryopreserved cells while the normal physiological state is recovered after thawing? This paper reports the results of a pilot study of these questions.

To assess cellular function following freezing and thawing, cryobiologists usually examine either cellular metabolic states or reproductive capabilities (2, 4, 7, 12, 15, 20). With the microphysiometer it is possible to study the metabolic effects of cryopreservation with a time resolution and sensitivity superior to those of traditional methods such as metabolite assays, enzymatic assays, and oxygen sensors. It is further possible to study the receptor-related phenomena of stimulus response and adaptation along with metabolism in a single experiment. Although one can measure the reproductive rate of mammalian cells in the microphysiometer on the time scale of days (14), the instrument is most efficiently used to investigate faster processes.

Cellular receptors are proteins, often in the plasma membrane, that transduce intercellular signals embodied in the concentrations of messenger molecules such as hormones, neurotransmitters, and paracrine factors. Binding of one of these ligands to

Received January 27, 1993; accepted April 14, 1993

[1] To whom correspondence should be addressed. Telephone: (415) 322-4700. Fax: (415) 322-2069. E-mail: jack@moldev.com.

0011-2240/93 $5.00

its receptor generates a cascade of biochemical events that depends on the receptor and cell type but leads to a change in the physiological state of the cell. The energy needs of the cell are affected by the signal transduction process itself and by the resulting altered cell physiology (17, 19). These might include changes in energy demand (e.g., ion pump activity or anabolic synthesis) or energy supply (e.g., glycolytic activity).

The microphysiometer detects the rate of energy metabolism by measuring the rate at which cells acidify their environment (13, 14, 19). This acidification rate reflects the rate of production of acidic metabolites from aerobic and anaerobic energy metabolism, principally lactic acid from glycolysis and CO_2 from respiration. Other processes involved with cellular pH regulation exclusive of energy metabolism, such as the activity of the Na^+/H^+ antiporter protein, can also be modulated by receptor activation in a way that can be detected in the microphysiometer (13, 25). Our previous work has shown that microphysiometry detects cellular responses resulting from agonist stimulation of a wide variety of receptors, including T-cell, kainate glutamate, epidermal growth factor, m_1 muscarinic, β_2 adrenergic, and granulocyte–macrophage colony-stimulating factor (GM-CSF) (13, 14, 16, 18, 19, 21, 25).

To investigate the effects of cryopreservation on cellular response to receptor activation, we chose two unrelated mammalian cell lines, the nonadherent TF-1 and adherent WT3 cell types. The TF-1 cell line was first characterized by Kitamura *et al.* (9), who established it from the bone marrow of a human erythroleukemia patient. These cells require a cytokine such as GM-CSF for growth, thus providing a useful system for studying the effects of cytokines (8, 9). Using the microphysiometer we have obtained evidence that a Ca^{2+}-independent isoform of protein kinase C is involved in the transduction of the GM-CSF signal in TF-1 cells (24). We have also found (1) that TF-1 cells respond to platelet activating factor (PAF), through a pathway that is Ca^{2+}-dependent and separate from the signal transduction pathway of GM-CSF. In these cells, both GM-CSF and PAF transiently increase acidification rates. This response to GM-CSF has been shown to involve the activation of both the Na^+/H^+ antiporter and glycolysis (25). Similar results have been obtained for PAF (Baxter *et al.*, unpublished observations).

The WT3 cell line is a Chinese hamster ovary-K1 (CHO-K1) cell line stably transfected with the rat m_1 muscarinic acetylcholine receptor (3). The m_1 receptor is known to signal through phospholipase C activation and subsequent inositol trisphosphate production. Carbachol, an analog of acetylcholine that activates the m_1 receptor, causes a rapid and transient increase in the acidification rate of WT3 cells (18). The mechanisms of the acidification rate increase have not yet been elucidated.

Prolonged or frequently repeated activation of receptors typically leads to an adaptive decrease in cellular response termed desensitization (10). Mechanisms of desensitization include internalization of receptors from the membrane and covalent modification, typically phosphorylation, of receptors to inhibit their ability to transduce signals in the presence of bound ligands. Having observed the effects of cryopreservation on the activation of receptors by GM-CSF, PAF, and carbachol, we found that the response of WT3 cells to short-term exposure by carbachol provided a useful system for examining cellular desensitization.

In addition, we present data on one phenomenon unrelated to receptor activation. For TF-1 cells we used the microphysiometer to monitor the time course of the recovery of cellular metabolic activity from cryopreservation. These data, together with

those from the receptor activation studies, suggest that cryopreserved cells can be used in the microphysiometer for some purposes and that the microphysiometer may be useful for cyrobiological studies of early post-thaw cell physiology.

EXPERIMENTAL PROCEDURES

Cell Preparation

WT3 cells (3) were a gift of C. Fraser (NIAAA) and are available from American Type Culture Collection (CRL 1985). The cell were cultured in F12 medium supplemented with 10% horse serum (HS), 5% fetal bovine serum (FBS), and 50 μg/ml geneticin (Gibco-BRL, Gaithersburg, MD). TF-1 cells (8, 9) were obtained as a gift from S. Indelicato (Schering-Plough, Bloomfield, NJ) and were cultured in RPMI 1640 medium (Irvine Scientific, Irvine, CA) supplemented with 2 m*M* sodium pyruvate, 10% FBS, and 1 ng/ml recombinant human GM-CSF (Sandoz/Schering-Plough Corp., Bloomfield, NJ). PAF was obtained from Boehringer-Mannheim (Indianapolis, IN), while carbachol was purchased from Sigma Chemical Co. (St. Louis, MO). As noted previously (18, 25), we often observe enhanced cellular responses if the cells are "starved" for 18–20 h prior to use. Cells were starved by substituting the regular growth medium with medium lacking the necessary growth factors or serum. In the case of TF-1 cells, the starvation medium consisted of RPMI 1640 medium supplemented with 2 m*M* sodium pyruvate and 10% FBS without GM-CSF. For WT3 cells, F12 medium with 50 μg/ml geneticin, but without HS or FBS was used.

Cells were prepared for use in the microphysiometer as described previously (13, 14, 25). Because microphysiometer experiments are conducted with fluid flow, it is necessary to immobilize cells within a cell capsule (Fig. 1). With adherent cells such as the WT3 cells, natural physical attachment to the microporous membrane of the

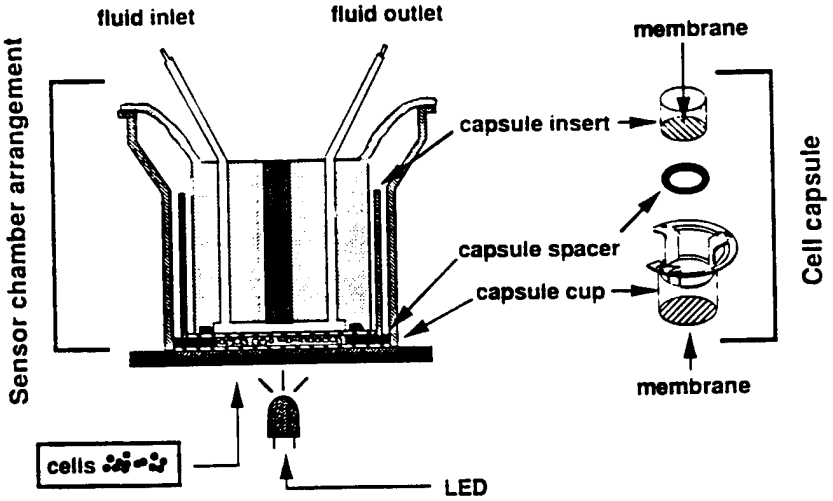

FIG. 1. Schematic diagram of the Cytosensor microphysiometer cell capsule and sensor chamber arrangement. Capsule cups are first placed in the wells of a 12-well tissue culture plate. The cells are then seeded directly on the capsule membrane or, in the case of nonadherent cells, are immobilized on the membrane within a fibrin clot. Together with the capsule cup, the spacer and insert form a microvolume disposable capsule for the cells. In the sensor chamber, the cell capsule is held directly above the region of the sensor that is sensitive to pH, i.e., the region of the sensor chip that is illuminated by an intensity-modulated infrared light-emitting diode.

capsule cup is employed. Nonadherent suspension cells (TF-1 cells in this case) are held within an inert, biocompatible, low citrate buffered fibrin matrix (Molecular Devices Corp., Menlo Park, CA). In this procedure, cells are trapped within a 50-μm-thick gel that forms when a solution containing thrombin and fibrinogen is layered on the cells in the capsule cup (25).

For experiments, capsule cups were first placed in 12-well tissue culture plates with 1 ml of culture medium in the well region outside of the capsule cup and 300–500 μl of medium within the cup of the capsule cup. Adherent WT3 cells were seeded at 300,000 cells per capsule cup and allowed to attach for 3 h prior to use. TF-1 cells were first centrifuged through cell focusers (custom made plastic funnels used to focus cells within a 2-mm central circular region on the capsule cup) at 500*g* for a final concentration of 200,000 cells per capsule cup. After centrifugation, 100 μl of a fibrinogen and thrombin clot-forming solution was added and allowed to gel for 20 min before cells were either frozen or used directly in microphysiometer experiments.

Freezing Procedure

Culture medium was aspirated from inside and outside of each capsule cup via pipeting. Five hundred microliters of freezing medium (10% Me_2SO, 90% FBS (v/v), prefiltered) at 4°C was pipeted into each capsule cup and an additional 1 ml of freezing medium into the surrounding well. The tissue culture plates containing the capsule cups were then placed into a Cryomed 1010A (New Baltimore, MI) controlled-rate freezer and frozen at 1°C/min from +4°C to −70°C. After freezing, the tissue culture plates were stored in a mechanical freezer at −70°C for 1 to 3 days prior to experimental use. The freezing and storing conditions were not optimized for cellular viability, in large part because we wished to assess the robustness of the physiological phenomena we were investigating.

Thawing Procedure

Cell well plates were moved directly from cold storage and floated in a 37°C water bath. Immediately after melting (approximately 10 min), the freezing medium was aspirated from inside and outside the capsule cup and replaced with low-phosphate-buffered RPMI 1640 culture medium (Molecular Devices Corp.) containing 1 mg/ml endotoxin-free human serum albumin (Miles Laboratories, Elkhart, IN). Capsule cups containing WT3 cells were then centrifuged at 500*g* for 5 min. Both WT3 and TF-1 cells were washed three times with the same low-phosphate-buffered RPMI 1640 to ensure that the Me_2SO-containing freezing medium was replaced. Although TF-1 cells were used immediately, it was necessary to allow WT3 cells to reattach for 3 h before being used. As noted by Smith (22), adherent cells frozen *in situ* tend to come off the surface to which they are attached as a sheet if disturbed upon thawing. We have found that careful aspiration followed by centrifugation and incubation for at least 2 h increases the number of cells that reattach to the capsule cup membrane after thawing. Cells used for experiments reported here were thawed within a week of freezing, although cells frozen more than 3 months showed no significant differences in receptor activation.

Cell Viability Measurements

The numbers of viable cells in thawed and nonfrozen cell chambers were compared by trypan blue exclusion (Gibco Laboratories, Grand Island, NY; 0.4% mixed 1:1 with cells) using a hemacytometer. TF-1 cells were harvested from cell chambers by physical disruption of the fibrin clot, and WT3 cells were released by treatment with EDTA/trypsin (Irvine Scientific, Santa Ana, CA). The conditions under which cellular viability was measured were identical to those described above except that cell

capsules were not used in the microphysiometer system.

Microphysiometry

A more detailed review of the Cytosensor microphysiometer can be found in references (13, 14, 19). In general, cells of interest are concentrated in a microvolume (approximately 2.5 μl) flow chamber, the bottom surface of which is a pH-sensitive LAPS (light-addressable potentiometric sensor) silicon chip (6). Protons excreted by the cells diffuse through the microporous membrane of the capsule cup, bind to the surface of the LAPS chip, and thereby alter the surface potential of the sensor. Surface-potential shifts are nearly Nernstian with changes in extracellular pH.

Microphysiometer experiments were conducted with low-phosphate-buffered (approximately 1 m*M*/pH at pH 7.4) RPMI 1640 at a flow rate of 100 μl/min and a temperature of 37°C. Culture medium flowed continuously through the microvolume flow chamber except during periods in which acidification rate measurements were taken. Periodic halts in the supply of fresh medium, typically 15–45 s long, cause small (<0.1 pH unit) transient decreases in the pH in the cell chamber. The acidification rate is measured as a slope calculated from a least-squares fit of the pH decrease during this time period. A valve allows switching between two fluid paths, one that contains the effector compound and one that does not.

The protocol for these experiments was flow on for 105 s and off for a total of 45 s, and acidification rates were measured for 30 s during the 45-s flow-off period. This was repeated cyclically, yielding one acidification rate every 150 s. Once a steady baseline acidification rate was obtained, sham switches of the valve between identical media were done to rule out artifacts due to valve position.

Absolute acidification rates scale with the number of cells in the region of the chamber near the sensor. Since this can vary somewhat from chamber to chamber, we present acidification rate data normalized to a basal rate for each chamber. We therefore analyze percentage changes in acidification rate. The effects of cryopreservation on maximum stimulation under Results are computed by comparing [(peak − basal)/basal] acidification rates for thawed and unfrozen cells. Statistical significance of results was computed using the two-tailed *t* test.

RESULTS

Cell Viability after Cryopreservation

The number of viable TF-1 cells recovered from cell chambers after crypreservation for less than 7 days was 82 ± 9% (mean ± SEM, $n = 2$) of the recovery of cells not subjected to cryopreservation. For WT3 cells the results was 100 ± 8% (mean ± SEM, $n = 2$). We did not attempt to correlate cell number with acidification rate. In a previous study using a different version of the microphysiometer, we established that acidification rates were proportional to the number of cells over the region of the sensor that detects pH (21). This determination is technically more difficult in the present instrument because the cells in the active region of the chamber from which pH is sensed represent a small fraction of all the cells in the chamber.

Recovery of Cellular Metabolism following Thawing

Figure 2 shows what we believe is the recovery of metabolic activity of TF-1 cells from the effects of freezing. Rapid thawing and loading of nonadherent cells on the microphysiometer require approximately 20 min. Subsequent acidification rate measurements rise dramatically over a period of ~40 min until a steady acidification rate is reached. Unfrozen cells do not show this large initial increase in acidification rates nor is this effect due to incubation in freez-

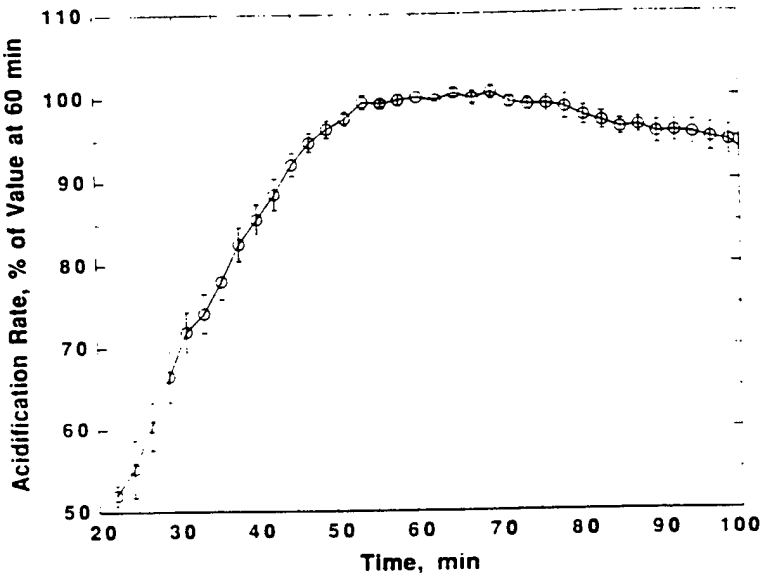

FIG. 2. Kinetics of recovery of metabolic activity of TF-1 cells after thawing. TF-1 cells were cryopreserved in microphysiometer cell capsules and, at $t = 0$, were removed from the freezer. At approximately $t = 20$ min they were inserted into the microphysiometer, and acquisition of acidification rates was begun. See Experimental Procedures for more details on cryopreservation and microphysiometry. The figure shows the recovery of stable metabolic activity by $t \sim 60$ min. Error bars represent SEM for $n = 4$.

ing medium alone (data not shown). For the adherent WT3 cells, acidification rates were substantially stable by the time the cells were loaded into the microphysiometer several hours after thawing.

Activation of GM-CSF and PAF Receptors in Nonadherent TF-1 Cells

To assess the effects of freezing on GM-CSF and PAF responses, TF-1 cells were embedded within fibrin clots, frozen, and then thawed as described under Experimental Procedures or else used fresh for comparison. After thawing, the clot remained intact, as seen by crystal violet staining. Controls consisted of unfrozen (fresh) cells. Figure 3 compares the GM-CSF response of unfrozen and thawed cells 90 min after the latter were removed from the freezer. Thawed cells retained the response, although the maximum stimulation apparently decreased to 71 ± 14% of that for the unfrozen cells (mean ± SEM, $n = 4$). Cryopreservation did not detectably alter the kinetics of the response, within the variations observed among preparations of fresh TF-1 cells. Figure 4 shows a typical response to PAF activation with unfrozen and freeze-thawed cells. Again, the cryopreservation did not detectably alter the kinetics of the response but did apparently decrease the maximum stimulation somewhat, to 73 ± 10% of that of the unfrozen cells ($n = 3$). The statistical significance of the alterations in maximum stimulation for GM-CSF and PAF is fairly weak, about $P < 0.1$ for both cases.

Activation of m_1 Muscarinic Receptors in Adherent WT3 Cells

Typical responses to 100 μM carbachol before and after freezing are shown in Fig. 5. Cryopreservation did not affect the kinetics of the response appreciably, but it did decrease the maximum stimulation to 47 ± 5% of the value for unfrozen cells

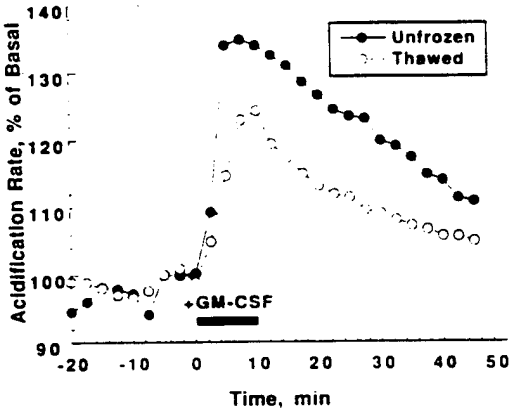

FIG. 3. Comparison of cellular response to GM-CSF between unfrozen and thawed TF-1 cells. TF-1 cells were treated with 10 ng/ml GM-CSF for 10 min beginning at $t = 0$, and the acidification rate was measured as described under Experimental Procedures. For the thawed cells, the GM-CSF was added 90 min after the cells were removed from the freezer. This experiment was repeated three times, and representative data are shown.

(mean ± SEM, $n = 5$). Most of this decrease was not, however, due to freezing per se. As noted under Cell Preparation, serum starvation enhances the response seen in the microphysiometer. The freezing

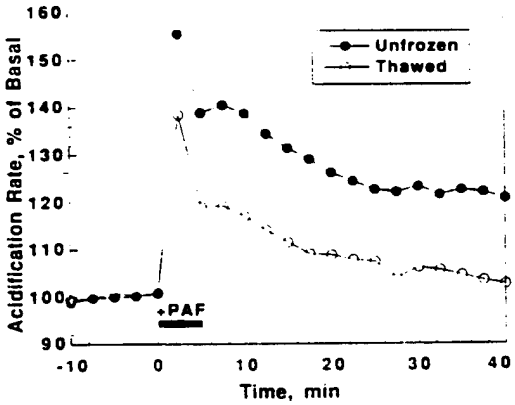

FIG. 4. Comparison of cellular response to PAF between fresh and frozen–thawed TF-1 cells. TF-1 cells were treated with 5 μM PAF for 5 min beginning at $t = 0$, and the acidification rate was measured as described under Experimental Procedures. For the thawed cells, the PAF was added 90 min after the cells were removed from the freezer. This experiment was repeated three times, and representative data are shown.

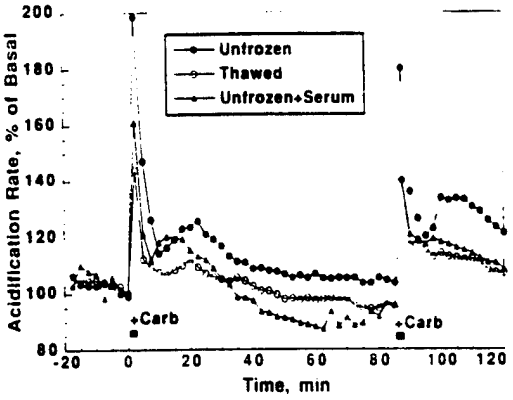

FIG. 5. Comparison of cellular muscarinic response between unfrozen and thawed WT3 cells; desensitization of the response. WT3 cells were exposed to 100 μM carbachol for 2.5 min first at $t = 0$ and then again 85 min later to observe desensitization. Acidification rates were measured as described under Experimental Procedures. Results are shown not only for unfrozen and thawed cells, but also for unfrozen cells that were exposed to the freezing medium, which contained serum. For the thawed cells, the carbachol was first added several hours after the cells were removed from the freezer. These experiments were repeated four to six times, and representative data are shown.

medium contains a high concentration of FBS (90% by volume), to which the cells are exposed for approximately 30 min before being frozen. As a control, cells were incubated with freezing medium at 4°C for 30 min before being loaded on the microphysiometer and exposed to 100 μM carbachol. As shown in Fig. 4, incubation in freezing medium without freezing causes a decrease in maximum stimulation (to 64 ± 4%, $n = 4$). Correcting for the effects of freezing medium, the maximum stimulation of thawed cells was 73 ± 9% of that of similarly treated but unfrozen cells. All the results for carbachol are highly significant ($P < 0.005$).

Figure 4 also illustrates desensitization from carbachol stimulus. Exposure to 100 μM carbachol for 2.5 min, a concentration known to cause maximum acidification response, causes a sharp increase in the acidification rate that gradually returns to its basal level over tens of minutes. After 85

min, the cells are once again exposed to 100 μM carbachol for 2.5 min. The second response is similar for all three cell treatments: a decrease in peak receptor activation (approximately 10–20%) as measured from initial basal acidification rate prior to exposure to carbachol. These results would indicate that the cellular processes involved in receptor activation, signal transduction, and adaptation remain substantially intact after freezing and thawing of these cells.

DISCUSSION

The novel method by which the microphysiometer detects changes in cellular physiology provides researchers with an instrument with which to monitor the diverse processes involved in receptor activation. We have been able to show that cryopreservation of TF-1 and WT3 cells does not greatly alter the metabolic consequences of the activation of three receptors in terms of the amplitude (although decreased 25–30%), the kinetics, and the adaptation of the response. This indicates that, at least in these cases, cellular signal transduction elements and receptor-activated processes are substantially recovered within 90 min after thawing.

There have been, to our knowledge, few explicit studies of receptor function within a few hours of thawing. However, receptor function is implicit in the well-established ability of some cellular systems to function soon after thawing. For example, it is routine to cryopreserve patients' lymphocytes prior to clinical testing for immune function that typically depends on receptor activity (5). Such tests are usually on the time scale of 24–48 h. Although not analyzing receptor function, Wood *et al.* (26) found that cryopreservation did not change the amount of cell-surface antigens in mouse embryos, as measured by fluorescence intensity; sometimes the treatment did alter the distribution of the antigens within the cell membrane. Takahashi *et al.* (23) showed that some loss of cell surface glycoproteins occurs with freezing and thawing of platelets. In addition, Takahashi *et al.* (24) found that cryopreservation of polymorphonuclear leukocytes greatly affected their surface receptor activity, but monocytes were largely unaffected by the same conditions.

The kinetics of recovery of metabolic activity following thawing of cells was also detected with the microphysiometer. This was done within 20 min of the removal of nonadherent TF-1 from cold storage; the longer post-thaw protocol for reattachment of adherent WT3 cells did not permit such a measurement. Refinements of the cryopreservation procedure, for example by freezing the cells in a minimal volume of liquid, may make it possible to observe the metabolic recovery within a few minutes of removal from storage. Further studies are required to investigate the mechanisms of the metabolic rate recovery.

Direct use of frozen cells offers many advantages over traditional methods requiring extensive post-thaw culturing as long as the physiological processes of interest are substantially functional after thawing. Frozen cells can be stored and used whenever necessary or convenient. Synchronized cell cultures can also be frozen at specific stages of differentiation or proliferation either to study development or to improve day to day reproducibility. The early events involved in thawing can be investigated pharmacologically using appropriate compounds known to affect certain stages in the freeze–thaw process.

Work in progress has shown that not only cultured cells, but also small tissue slices, can be studied with the microphysiometer. In the future it may be possible directly to examine freeze–thaw effects on the reproductive capability of eggs, sperm, or embryos. Studies are in progress further to explore new physiological systems that can be investigated with the microphysiometer.

ACKNOWLEDGMENTS

The authors thank Drs. William Rall and Boris Rubinsky for their comments and suggestions on the manuscript. We also thank Victoria Muir for her help

in arranging and organizing the manuscript. This work was supported in part by the Defense Advanced Research Projects Agency, Contract MDA 972-92-C-0005.

REFERENCES

1. Baxter, G. T., Miller, D. L., Kuo, R. C., Wada, H. G., and Owicki, J. C. PKCε is involved in granulocyte–macrophage colony-stimulating factor signal transduction: Evidence from microphysiometry and antisense oligonucleotide experiments. *Biochemistry* 31, 10950–10954 (1992).
2. Brewer, G. J., Kruckeberg, W. C., Westover, C. J., and Oberman, H. A. Erythrocyte metabolism. *In* "Clinical Uses of Frozen–Thawed Red Blood Cells" (J. A. Griep, Ed.), pp. 5–19. A. R. Liss, New York, 1976.
3. Buck, M. A., and Fraser, C. M. Muscarinic acetylcholine receptor subtypes which selectively couple to phospholipase C: Pharmacological and biochemical properties. *Biochem. Biophys. Res. Commun.* 173, 666–672 (1990).
4. Fuller, B. J., Rubinacci, A., Geboes, K., and Loecker, W. The bioenergetics of mitochondria after cryopreservation. *Cryobiology* 26, 333–340 (1989).
5. Gjerset, G., Nelson, K. A., and Strong, D. M. Methods for Cryopreserving Cells. *In* "Manual of Clinical Laboratory Immunology" (N. R. Rose, E. C. de Macario, J. L. Fahey, H. Friedman, and G. M. Penn, Eds.), fourth ed., Chap. 10, Am. Soc. Microbiol. Washington, DC, 1992.
6. Hafeman, D. G., Parce, J. W., and McConnell, H. M. Light-addressable potentiometric sensor for biochemical systems. *Science* 240, 1182–1185 (1988).
7. Innes, G. K., Fuller, B. J., and Hobbs, K. E. F. Functional testing of hepatocytes following their recovery from cryopreservation. *Cryobiology* 25, 23–30 (1988).
8. Kitamura, T., Kakaku, F., and Miyajima, A. IL-1 up-regulates the expression of cytokine receptors on a factor-dependent human hemopoietic cell line, TF-1. *Int. Immunol.* 3, 571–577 (1991).
9. Kitamura, T., Tange, T., Terasawa, T., Chiba, S., Kuwaki, T., Miyagawa, K., Piao, Y.-F., Miyazono, K., Urabe, A., and Takaku, F. Establishment and characterization of a unique human cell line that proliferates dependently on GM-CSF, IL-3, or erythropoietin. *J. Cell. Physiol.* 140, 323–334 (1979).
10. Lefkowitz, R. J., Hausdorff, W. P., and Caron, M. G. Role of phosphorylation in desensitization of the β-adrenoceptor. *Trends Pharmacol. Sci.* 11, 190–194 (1990).
11. Machen, T. E., and Negulescu, P. A. Release and reloading of intracellular Ca stores after cholinergic stimulation of the parietal cell. *Am. J. Physiol.* 254, C498–C504 (1988).
12. Mazur, P., Rall, W., and Leibo, S. Kinetics of water loss and the likelihood of intracellular freezing in mouse ova: Influence of the method of calculating the temperature dependence of water permeability. *Cell Biophys.* 6, 197–213 (1984).
13. McConnell, H. M., Owicki, J. C., Parce, J. W., Miller, D. L., Baxter, G. T., Wada, H. G., and Pitchford, S. The cytosensor microphysiometer. *Science* 257, 1906–1912 (1992).
14. McConnell, H. M., Rice, P., Wada, H. G., Owicki, J. C., and Parce, J. W. The microphysiometer biosensor. *Curr. Opin. Struct. Biol.* 1, 647–652 (1991).
15. Miyamoto, H., and Ishibashi, T. The effects of time of equilibration with cryoprotectants at 0°C prior to freezing on the survival of mouse embryos frozen by the two-step method. *Experientia* 42, 815–816 (1986).
16. Nag, B., Wada, H. G., Fok, K. S., Green, D. J., Sharma, S. D., Clark, B. R., Parce, J. W., and McConnell, H. M. Antigen-specific stimulation of T cell extracellular acidification by MHC class II-peptide complexes. *J. Immunol.* 148, 2040–2044 (1992).
17. Owicki, J. C., and Parce, J. W. Biosensors based on the energy metabolism of living cells: The physical chemistry and cell biology of extracellular acidification. *Biosensors Bioelectronics* 7, 255–272 (1992).
18. Owicki, J. C., Parce, J. W., Kercso, K. M., Sigal, G. B., Muir, V. C., Venter, J. C., Fraser, C. M., and McConnell, H. M. Continuous monitoring of receptor-mediated changes in metabolic rates of living cells. *Proc. Natl. Acad. Sci. USA* 87, 4007–4011 (1990).
19. Parce, J. W., Owicki, J. C., Kercso, K. M., Sigal, G. B., Wada, H. G., Muir, V. C., Bousse, L. J., Ross, K. L., Sikic, B. I., and McConnell, H. M. Detection of cell-affecting agents with a silicon biosensor. *Science* 246, 243–247 (1989).
20. Pegg, D. E. Viability assays for preserved cell, tissues, and organs. *Cryobiology* 26, 212–231 (1989).
21. Rayley-Susman, K. M., Miller, K. R., Owicki, J. C., and Sapolsky, R. M. Effects of excitotoxin exposure on metabolic rate of primary hippocampal cultures: Application of silicon microphysiometry to neurobiology. *J. Neurosci.* 12, 773–780 (1992).
22. Smith, K. O. Low-temperature storage of surface-attached living cell cultures. *Cryobiology* 18, 251–257 (1981).

23. Takahashi, T. A., Yakushiji, C., Segawa, K., Richter, E., and Sekiguchi, S. The loss of GPIb from platelet membrane after osmotic stress or freezing and thawing. *Cryobiology*, in press.
24. Takahashi, T., Inada, S., Pommier, C. G., O'Shea, J. J., and Brown, E. J. Osmotic stress and the freeze-thaw cycle cause shedding of Fc and C3b receptors by human polymorphonuclear leukocytes. *J. Immunol.* 134, 4062–4068 (1985).
25. Wada, H. G., Indelicato, S. R., Meyer, L., Kitamura, T., Miyajima, A., Kirk, G., Muir, V. C., and Parce, J. W. GM-CSF triggers a rapid, glucose dependent extracellular acidification by TF-1 cells: Evidence for sodium/proton antiporter and PKC mediated activation of acid production. *J. Cell. Physiol.* 154, 129–138 (1993).
26. Wood, M. J., Sjöblom, P., Lindenberg, S., and Kimber, S. J. Effect of slow and ultra-rapid freezing on cell surface antigens of 8-cell mouse embryos. *J. Exp. Zool.* 262, 330–339 (1992).

ANTIMICROBIAL AGENTS AND CHEMOTHERAPY, Oct. 1995, p. 000–000
0066-4804/95/$04.00+0

Vol. 39, No. 10

Growth Impairment Resulting from Expression of Influenza Virus M2 Protein in *Saccharomyces cerevisiae*: Identification of Novel Inhibitor of Influenza Virus

STEPHEN KURTZ,[1] GUANGXIANG LUO,[2] KAREN M. HAHNENBERGER,[3] CINDY BROOKS,[1] OKSANA GECHA,[2] KIM INGALLS,[1] KEI-ICHI NUMATA,[1] AND MARK KRYSTAL[2]*

Department of Microbial Molecular Biology, Bristol-Myers Squibb Pharmaceutical Research Institute, Princeton, New Jersey 08543[1]; Department of Virology, Bristol-Myers Squibb Pharmaceutical Research Institute, Wallingford, Connecticut 06492[2]; and Molecular Devices Corp., Sunnyvale, California 94089[3]

Received 5 May 1995/Returned for modification 6 July 1995/Accepted 31 July 1995

The gene encoding M_2, the ion channel-forming protein of influenza virus A, was expressed under the control of an inducible promoter in *Saccharomyces cerevisiae*. By using single and multicopy plasmids containing *GAL* promoter-M_2 fusions, a correlation was observed between plasmid copy number and growth in medium inducing M_2 expression. Cells expressing M_2 from multicopy plasmids have reduced growth rates, suggesting that high levels of M_2 are toxic to growth. The addition of amantadine, a compound known to block the ion channel activity of certain M_2 alleles, restores the growth rates to wild-type levels in cells expressing an amantadine-susceptible allele of M_2 but not an amantadine-resistant allele of M_2, suggesting that M_2 expression in *S. cerevisiae* results in the formation of functional M_2 ion channels. Measurements of extracellular acidification by microphysiometry suggest that proton efflux in M_2-expressing cells is altered and that the addition of amantadine permits the reestablishment of the proton gradient. The growth impairment phenotype resulting from M_2 expression was used to develop a high-capacity screening assay which identified a novel inhibitor possessing an antiviral profile similar to that of amantadine.

Functional expression of ion channels in heterologous cell types provides a general method for studying the properties of channel function. Expression in *Xenopus laevis* oocytes has provided numerous insights into ion channel function (17, 18, 35). More recently, expression of ion channels in *Saccharomyces cerevisiae* strains defective in K^+ uptake has served as a means for isolating new genes encoding functional channels (1, 29). However, expression of ion channels in yeast cells is not restricted to the restoration of uptake functions and may result in a variety of phenotypes, depending on the properties of a particular channel.

The M_2 protein of influenza virus A is one of three integral membrane proteins contained in the viral lipid envelope. The M_2 protein is a 97-amino-acid polypeptide containing a single membrane-spanning region. M_2 polypeptides associate as disulfide-linked homotetramers to form ion channels (15, 34). Direct evidence defining the ion channel function of M_2 has recently been obtained by expression studies in *Xenopus* oocytes (26, 38) and in in vitro studies (6, 28, 36). A therapeutic agent for influenza virus A infections, amantadine, has been shown to function by blocking M_2 ion channel activity (7, 12, 13, 26, 32, 33, 37, 38). Other biophysical studies have confirmed that the transmembrane portion of the molecule is the binding site and suggest that the mechanism of action is binding of the compound within the channel pore (6, 7, 27). Inhibition studies with amantadine suggest that M_2 is required at both early and late stages in the infection cycle of the virus. Early in infection, M_2 permits the flow of protons from the endosome into the virion. The resultant decrease in pH facilitates the dissociation of the matrix protein (M_1) from viral genomic ribonucleoproteins (12, 14, 20, 26) and thereby stimulates viral uncoating. In the presence of amantadine, M_1 is unable to dissociate from the viral ribonucleoproteins and transport of the ribonucleoprotein complex to the nucleus does not occur. At later stages of infection, M_2 polypeptides are abundantly expressed on the cell surface and within the cell in the endoplasmic reticulum and Golgi compartments. It is believed that M_2 functions at late stages of infection to maintain a high pH in these vesicular compartments, thereby preventing the premature activation of intracellularly cleavable hemagglutinin through a low-pH conformational change (5, 8, 9, 33).

We observed that high levels of M_2 expression in yeast cells results in growth impairment, similar to that reported for other expression systems (2, 10). Several lines of evidence suggest that the growth impairment in yeast cells results from the ion channel activity of M_2. *S. cerevisiae* strains with this phenotype allowed for the development of a high-capacity assay which identified a novel inhibitor of M_2 function with anti-influenza virus activity similar to that of amantadine.

MATERIALS AND METHODS

Strains. *S. cerevisiae* W303 (*MATa ade2-1 can1-100 his3-11,15 leu2-3,112 trp1-1 ura3-1*) was used as the recipient for transformations. The following *S. cerevisiae* strains were used in the study: SGY1442 contains the parent vector pYES2; SGY1443 contains the A/WSN/33 M_2 gene downstream of the *GAL* promoter in pYES2; SGY1444 contains the WSN gene with an asparagine-to-serine mutation at position 31 downstream of the *GAL* promoter in pYES2; SGY1492 contains the WSN M_2 gene downstream of the *GAL* promoter in the pYEUra3 vector; SGY1493 contains the Udorn M_2 gene downstream of the *GAL* promoter in pYES2.

Yeast manipulations. Standard yeast medium (yeast extract-peptone-dextrose [YEPD] and supplemented minimal medium) were used for cell growth (31). Cells were made competent for transformation by using the lithium acetate protocol of Ito et al. (16). Unless otherwise noted, transformants were maintained on selective medium containing 2% glucose (noninducing conditions) and were induced to express protein through replacement with minimal medium containing 2% galactose. Protein extracts were prepared as described previously

* Corresponding author. Mailing address: Department of Virology, Bristol-Myers Squibb Pharmaceutical Research Institute, 5 Research Parkway, Wallingford, CT 06492. Phone: (203) 284-7974. Fax: (203) 284-6088. Electronic mail address: MARK R. KRYSTAL@CCMAIL.BMS.COM.

(3). Proteins were detected by reaction with antisera to M_2 (gift of P. Rota) and a secondary antibody conjugated to alkaline phosphatase.

Construction of expression plasmids. The A/WSN/33 and A/Udorn/72 M_2 genes were modified through PCR-directed mutagenesis of cDNA by standard procedures. The A/Udorn/72 cDNA clone of the M_2 protein was a kind gift of R. Lamb (Northwestern University). The genes were cloned into the *Bam*HI-*Xba*I window of pYEUra3 (*CEN*; Clontech, Palo Alto, Calif.) or pYES2 (2μm; Invitrogen, San Diego, Calif.). Conversion of asparagine residue 31 to serine in the WSN (N31S) mutant was also accomplished by PCR-directed mutagenesis. All gene sequences were verified by DNA sequencing.

Assay for detecting M_2 inhibitors. Cultures of strains containing M_2 expression plasmids were grown overnight in minimal medium containing 2% glucose and were then shifted to inducing medium (2% galactose) at a concentration of 10^5 cells per ml and were maintained at 30°C with vigorous aeration. To identify compounds inhibiting M_2 function, cells were distributed into 96-well microtiter plates in the presence of compounds drawn from the Bristol-Myers Squibb compound collection. Compounds were judged to test positive in the assay if they allowed for the restoration of cell growth. Compounds testing positive were verified by examining M_2 protein levels by Western blot (immunoblot) analysis in order to eliminate compounds which affect the expression of M_2. When required, amantadine-HCl (Sigma Chemical Co., St. Louis, Mo.) was prepared fresh and was added to the cultures at the time of induction at the indicated concentrations. Optical density was determined at intervals by measuring the A_{600}.

Microphysiometer analysis. The extracellular acidification rates of the yeast strains containing various M_2 expression plasmids were measured with a Cytosensor microphysiometer (Molecular Devices Corp., Sunnyvale, Calif.) in which cells are immobilized in a microvolume flow chamber in contact with a pH-sensitive silicon sensor (11, 22). Approximately 4×10^5 yeast cells were immobilized in Agarose Cell Entrapment Medium (Molecular Devices Corp.) between two microporous membranes. Flow chambers at 30°C containing the immobilized cells were superfused at a rate of 100 μl/min with minimal medium containing 2% galactose or 2% glucose plus appropriate nutritional supplements. Acidification rates were measured every 80 s by interrupting the flow of medium for 10 s. Amantadine at 100 μM was introduced 20 s prior to a flow-off period. Cells were exposed to amantadine for a total of 8 min. Acidification rates are expressed as a percentage of the basal rates before exposure to amantadine.

In vivo assays. The antiviral activities of the compounds in vivo were assessed in a plaque reduction assay. Approximately 100 PFU of A/WSN/33 or A/Udorn/72 virus was added to MDCK cells in 35-mm^2 dishes, and the dishes were incubated at 37°C for 1 h. The medium was removed and the cells were covered with 2 ml of agar overlay medium containing various amounts of either amantadine-HCl or BL-1743 in the presence of 5 μg of trypsin per ml. After 2 to 3 days of incubation, the monolayer cells were stained with 0.1% crystal violet solution, and the numbers and sizes of the plaques were assessed.

RESULTS

Expression of M_2 in *S. cerevisiae*. Expression plasmids encoding sequences of the M_2 protein of influenza virus under the transcriptional control of an inducible yeast promoter (*GAL1*) were introduced into *S. cerevisiae* W303. M_2 expression was assessed in strains containing either a single copy (centromere) or a high copy (2μm ORI) number ~~and containing~~ *GAL*-M_2 fusion plasmids after incubation in noninducing (glucose) or inducing (galactose) medium. As shown in Fig. 1, expression of M_2 in *S. cerevisiae* was detectable only in extracts of cells induced with galactose (Fig. 1, lanes 5 and 7). Synthesis of M_2 protein to levels comparable to those in virus-infected MDCK cells was detected in the strain containing the high-copy-number (pYES2-derived) plasmids (Fig. 1, compare lanes 7 and 8). Low levels of M_2 protein were detected in the strain transformed with the single-copy (pYEUra3-derived) vector.

M_2 expression impairs the growth of yeast cells. In the course of culturing the various transformants, it was observed that the growth rate of the transformant expressing the M_2 gene from a high-copy-number plasmid was significantly impaired relative to those of the other strains. Studies had previously shown M_2-related toxicity in bacteria and baculovirus-infected Sf9 cells (2, 10). Consequently, growth rates were analyzed by shifting equal numbers of log-phase cells previously grown in noninducing glucose-containing medium into medium containing galactose. Growth determinations indicated a correlation between the levels of M_2 expression and growth impairment (Fig. 2). Determination of the doubling

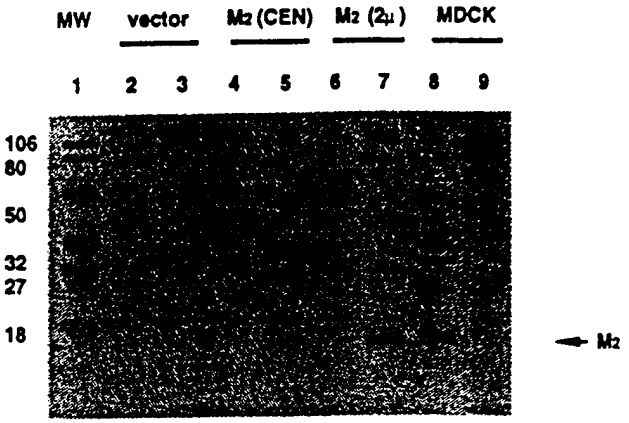

FIG. 1. M_2 is expressed at high levels in yeast cells, as shown by a Western blot indicating the levels of M_2 protein produced in yeast cells. Equivalent amounts of protein extract (100 μg) from each strain were separated on sodium dodecyl sulfate–12.5% polyacrylamide gels. The strains contained either the parental vector (SGY1442; designated vector), a single-copy centromere-containing plasmid expressing M_2 [SGY1492; designated M_2 (*CEN*)], or a high-copy-number 2μm origin-containing plasmid expressing M_2 [SGY1443; designated M_2 (2μ)]. Galactose-induced samples were loaded in lanes 3, 5, and 7, while uninduced samples were loaded in lanes 2, 4, and 6. Extracts prepared from influenza virus-infected and mock-infected MDCK cells are included as controls in lanes 8 and 9, respectively. The migrations of molecular weight standards (lane 1) are indicated.

times indicated that the strain expressing M_2 from the high-copy-number plasmid divides significantly more slowly than control strains (7.6 versus 4.0 h). This effect is observed only when the strain is grown on galactose (M_2-inducing conditions), because no growth differential is observed in medium containing glucose (noninducing conditions). However, in

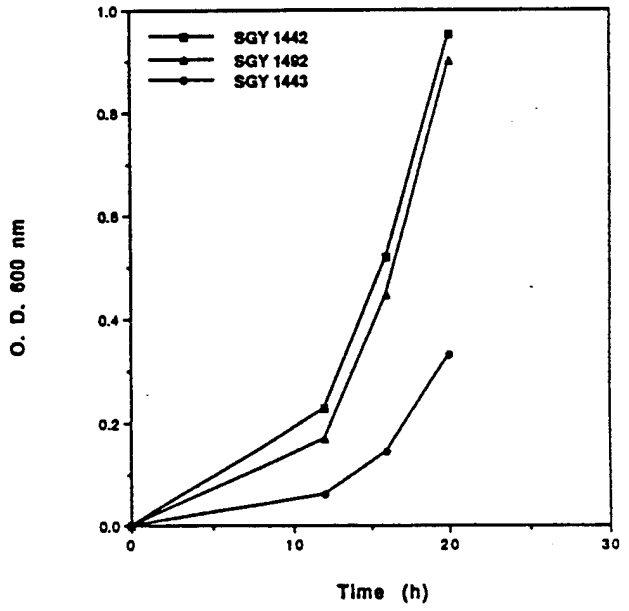

FIG. 2. Growth impairment of cells expressing M_2. Growth of cells expressing M_2 varies with plasmid copy number. Cultures of strains containing vector (SGY 1442), single-copy M_2 plasmid (SGY 1492) or high-copy-number M_2 plasmid (SGY 1443) were grown in inducing medium at 30°C with vigorous aeration. Samples were removed at various intervals, and the optical density (O.D.) at 600 nm was determined. The A_{600} is plotted versus time (in hours).

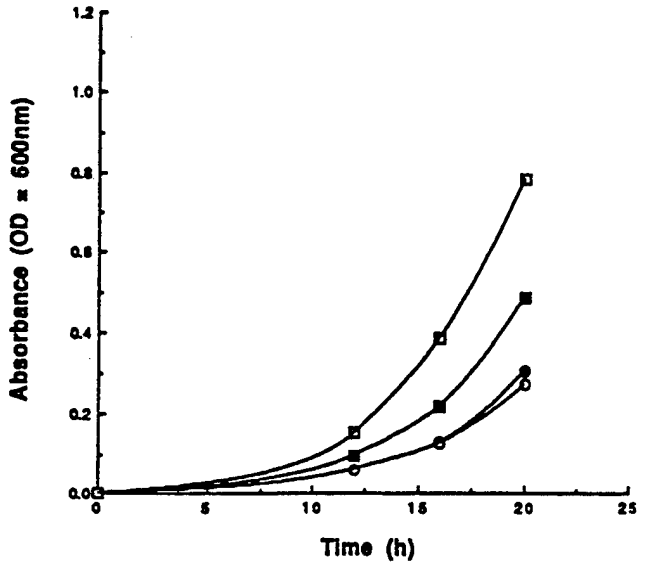

FIG. 3. Amantadine rescues the growth of cells expressing the Udorn M_2 protein. Duplicate cultures of strain SGY1443 containing the amantadine-resistant M_2 plasmid (WSN; ○, ●) or strain SGY1493 containing the amantadine-susceptible M_2 plasmid (Udorn; □, ■) were grown in inducing medium at 30°C with (○, □) or without (●, ■) amantadine. Samples were removed at various intervals, and the optical density (OD) at 600 nm was determined. The A_{600} is plotted versus time (in hours). The amantadine concentration was 100 μM.

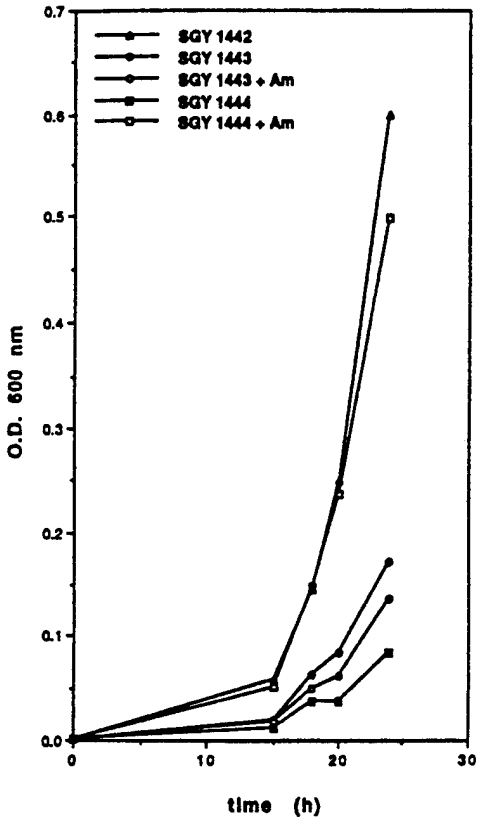

FIG. 4. Conversion of the amantadine-resistant M_2 (WSN) to amantadine (Am) susceptibility as determined by measuring the growth of strains expressing an allele of M_2 converted from amantadine resistance (WSN) to amantadine susceptibility. Cultures of a control vector-containing strain (SGY 1442, ▲); SGY 1443, the strain containing an amantadine-resistant M_2 plasmid (WSN); or strain SGY 1444, the strain containing the amantadine-susceptible M_2 [WSN (N31S)] plasmid, were grown in inducing medium at 30°C with vigorous aeration with 10 μM amantadine or without added drug. Samples were removed at various intervals, and the optical density (O.D.) at 600 nm was determined. The A_{600} is plotted versus time (in hours).

strains containing single-copy expression plasmids, no significant growth impairment was observed even after M_2 induction.

Toxicity is due to ion channel activity of M_2. One explanation to account for the impaired growth rate after M_2 induction is that the ion channel activity of the M_2 protein produced the observed toxicity. The approximate pH of the growth medium for the yeast cells is 6.0, which would be sufficient to activate the M_2 ion channel (26). To examine whether the ion channel activity is responsible for the toxicity, strains were induced for M_2 expression in the presence of amantadine, a known blocker of M_2 channel function (12, 13, 26, 33, 37). Because the M_2 gene used in this initial study was obtained from A/WSN/33 virus, which has the characteristic of amantadine resistance, a strain containing an amantadine-susceptible allele was constructed. The gene encoding the M_2 protein from an amantadine-susceptible strain, A/Udorn/72 virus (26, 37), was cloned into the pYES2 expression vector, and yeast cells were transformed with this construct. The induction of the M_2 protein of A/Udorn/72 virus results in a reduction of the growth rate (Fig. 3). The extent of growth impairment is significant, although not as great as that seen with expression of the WSN M_2 protein (Fig. 3). However, the growth rates of these transformants are substantially rescued when 100 μM amantadine is added to the culture medium at the time of induction (Fig. 3). In contrast, the growth of transformants expressing the amantadine-resistant WSN allele is not remediated with the addition of amantadine at 100 μM (Fig. 3). This result suggests that the toxicity related to M_2 expression correlates with an amantadine-responsive activity, i.e., ion channel activity.

Conversion of the WSN M_2 protein to amantadine susceptibility. The predominant mutations which result in amantadine resistance map to one of four amino acids within the membrane-spanning region of the molecule (13). Examination of the WSN M_2 protein sequence suggests that resistance in this particular molecule is conferred by an asparagine residue present at amino acid 31. Therefore, residue 31 was converted from asparagine to serine. Both WSN alleles are toxic when they are overexpressed in yeast cells; however, only the toxicity of the WSN (N31S) allele is remediated by the addition of amantadine (either 10 or 100 μM) to the growth medium (Fig. 4). In the presence of amantadine, transformants expressing the WSN (N31S) allele grow at near wild-type rates, whereas growth of the transformants expressing the amantadine-resistant WSN allele is not remediated with amantadine (Fig. 4). This experiment provides additional genetic evidence that overproduction of M_2 results in growth impairment and is a consequence of M_2 channel function. It also proves that this residue in the wild-type protein, as predicted, is responsible for resistance to amantadine.

Proton flux is altered by expression of M_2. In yeast cells, the plasma membrane H^+-ATPase establishes an electrochemical gradient by pumping protons out of the cell, which maintains ion balances and facilitates the uptake of other ions (30). Perturbations to this gradient permit leakage of essential ions and can result in cell death. We reasoned that M_2 may exert its toxic effect on yeast cells by disrupting the electrochemical proton gradient. To examine whether M_2 expression correlates with changes in proton flux, we used microphysiometry (22) to measure the rates of extracellular acidification of cells expressing this ion channel before and after exposure to the M_2 chan-

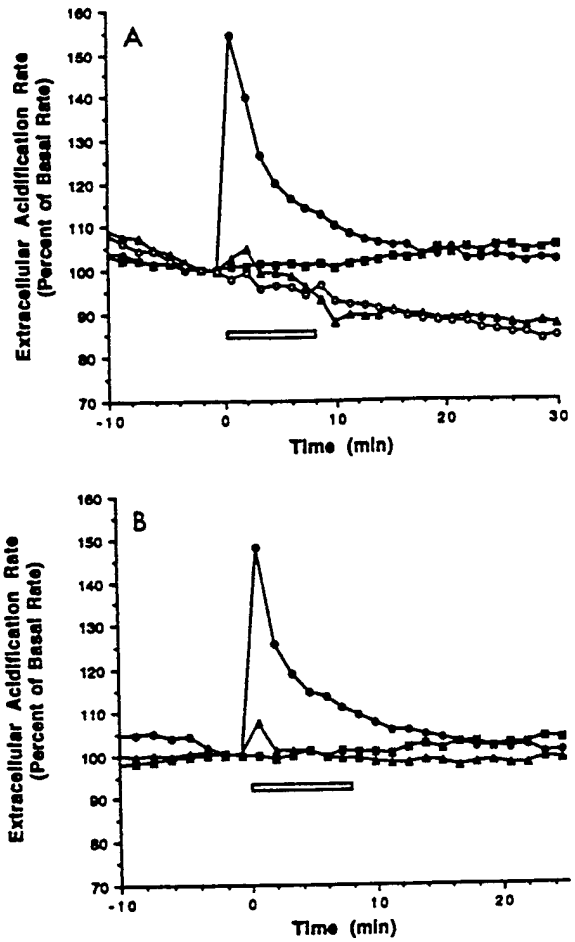

FIG. 5. Proton flux in strains expressing M_2 protein is reduced. (A) Amantadine causes a transient increase in extracellular acidification in yeast cells expressing an amantadine-susceptible channel. Control yeast cells (SGY1442; ■), cells expressing the amantadine-resistant WSN M_2 protein (SGY1443; ▲), or yeast cells expressing the amantadine-susceptible WSN (N31S) protein (SGY1444; ●) were grown overnight in medium containing galactose and were superfused with medium containing 2% galactose. After stable basal acidification rates were obtained, the cells were exposed to the same medium containing 100 μM amantadine for 8 min (indicated by the bar). Normalized extracellular acidification rates are plotted versus time (in minutes). Open circles represent SGY1444 cells grown and superfused in noninducing glucose medium. (B) Effect of amantadine on proton flux varies with external pH. Equal numbers of galactose-induced SGY1444 cells were loaded in three separate flow chambers and were superfused with minimal medium containing galactose at pH 5.5 (●), pH 6.5 (▲), and pH 7.5 (■). After stabilization of the acidification rates, cell were exposed to 100 μM amantadine for an 8-min period (indicated by the bar). Experiments were repeated at least twice, and representative data are shown.

nel blocker amantadine (Fig. 5A and B). The microphysiometer measures the rates of extracellular acidification of cells in a flow chamber by using a semiconductor-based sensor (11). These rates are sensitive to changes in metabolic activity (excretion of acidic metabolites) and to transmembrane proton flux associated with intracellular pH homeostasis (25). This technique has previously been used with mammalian cells to monitor cholinergic-stimulated changes in Na^+/K^+ ATPase activity (23) as well as activation of the nicotinic acetylcholine receptor (24). If the ion channel function of M_2 is acting to destabilize the gradient, then this should be reflected by changes in extracellular acidification.

The extracellular acidification rates of control strains SGY1442 (containing the vector only) and SGY1443 (expressing the amantadine-resistant WSN protein) are unaffected by the addition of 100 μM amantadine (Fig. 5A). However, exposure of strain SGY1444 (expressing the amantadine-susceptible M_2 protein) to 100 μM amantadine results in an immediate 50 to 60% increase in the rate of extracellular acidification, which is detected within 20 s of exposure to the drug (Fig. 5A). This increase in proton flux is transient and begins to return to basal levels even while the drug is still present. In contrast, strain SGY1444 maintained under conditions in which the M_2 gene is not expressed exhibits no effect on proton flux upon exposure to amantadine, indicating that the transient increase in acidification rates observed for SGY1444 grown under inducing conditions is a result of amantadine blockage of M_2 ion channel activity.

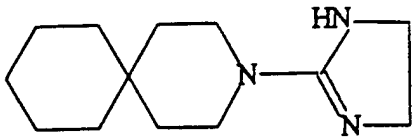

FIG. 6. Structure of BL-1743, 2-[3-azaspiro(5,5)undecano]-2-imidazoline, an inhibitor of M_2 protein function.

Previous studies of the M_2 ion channel expressed in *X. laevis* oocytes (26) or CV-1 cells (38) or reconstituted in a lipid bilayer (36) demonstrated that the activity is modulated by the external pH, with the channel being activated at low pH. We determined the effect of external pH on the activity of the M ion channel expressed in yeast cells by superfusing flow chambers containing SGY1444 with minimal medium containing 2% galactose at pHs of 5.5, 6.5, and 7.5 and then measuring the extracellular acidification rates before and after exposing the cells to 100 μM amantadine (Fig. 5B). At a pH of 5.5, the typical increase in the acidification rate of 50% was observed upon exposure to amantadine. However, at an external pH of 6.5, the observed increase in the acidification rate was less than 10%, and at pH 7.5, no change in the acidification rate was detected (Fig. 5B). This result is consistent with earlier observations that the M_2 ion channel is activated at a pH of 5 to 6 (26).

Identification of BL-1743, an inhibitor of M_2 function. The observation of M_2 expression in yeast cells was adapted into a screen format to identify compounds that inhibit the function of M_2. One compound identified in this assay is BL-1743 (Fig. 6) a spirene-containing lipophilic amine. This compound was able to rescue the growth of WSN (N31S) M_2-expressing yeast cells with a 50% effective dose (ED_{50}) of approximately 250 nM. Amantadine has an ED_{50} of 125 nM in this assay (data not shown). Interestingly, BL-1743 does not rescue the growth impairment of the wild-type WSN M_2 alleles expressed in yeast cells (data not shown), indicating that it may function in a manner similar to that of amantadine. BL-1743 also does not rescue growth by simply reducing M_2 expression in yeast cells; the levels of M_2 protein in cultures exposed to BL-1743 are comparable to those in amantadine-treated cultures (data not shown).

In vivo activity of BL-1743. BL-1743 was next examined as an inhibitor of influenza virus replication in an in vivo plaque reduction assay (Fig. 7). Amantadine was able to inhibit plaque formation in A/Udorn/72-infected cells with an ED_{50} of approximately 260 nM, although it had no effect on plaque formation in WSN-infected cells. More importantly, BL-1743 was also able to inhibit plaque formation in A/Udorn/72 virus-infected cells, with an ED_{50} of approximately 2 μM. BL-1743, as expected from the yeast rescue experiments, had no effect on A/WSN/33 plaque formation.

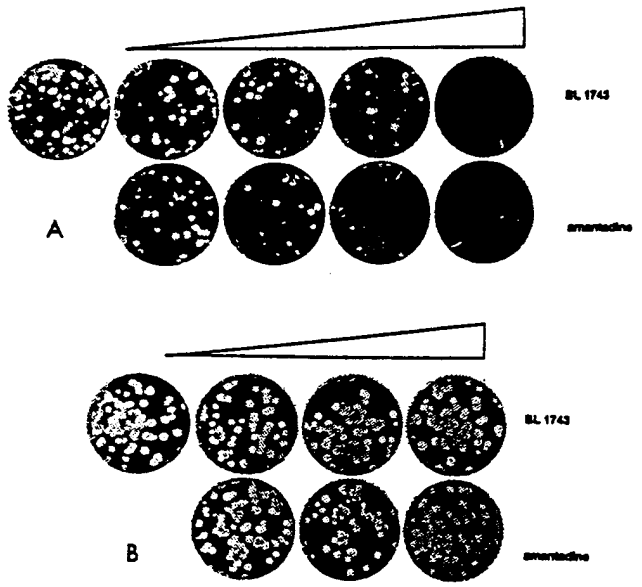

FIG. 7. Influenza virus A infection is blocked by BL-1743 in a plaque assay. A total of 50 to 100 PFU of A/Udorn/72 (A) or A/WSN/33 (WSN) (B) viruses were used in a plaque assay in the presence of increasing concentrations of either amantadine or BL-1743. For the A/Udorn/72 virus, the BL-1743 drug concentrations used were 0, 0.4, 0.8, 1.6, and 10 μg/ml, while the amantadine concentrations were 0.04, 0.08, 0.16, and 1 μg/ml. For the A/WSN/33 virus, both the BL-1743 and amantadine concentrations used were 1, 10, and 50 μg/ml.

DISCUSSION

Phenotypically, yeast cells expressing high levels of M_2 protein exhibited a consistently slower growth rate compared with that of control cells. The observation of growth impairment with M_2 expression is consistent with previous studies concerning M_2 expression in baculovirus-infected insect cells (2) and, more recently, in bacteria (10). In Sf9 cells, high levels of M_2 were produced only upon the addition of amantadine to the growth medium. One interpretation of this phenomenon is that the ion channel activity of M_2 is toxic to insect cells and that high-level expression can only be reached if this activity is blocked, perhaps because the cells remain viable and produce more protein. In our yeast system, several lines of evidence also suggest that toxicity is due to ion channel activity. Our most compelling data supporting this interpretation are from the comparison between amantadine-susceptible and amantadine-resistant alleles of M_2. Amantadine, a known inhibitor of ion channel activity, was able to rescue the growth of an amantadine-susceptible protein (the M_2 protein from A/Udorn/72 virus), but not that of an amantadine-resistant protein (A/WSN/33). In addition, when amino acid 31 of the WSN gene was altered from asparagine to serine and placed back into the yeast expression system, this transformant had a toxicity profile identical to that of the wild-type WSN protein, but the growth impairment was now responsive to amantadine. This proves that the asparagine at amino acid 31 is indeed responsible for the resistance of the WSN M_2 protein to amantadine and also strongly suggests that the toxicity associated with protein expression is directly related to the ion channel activity of the M_2 protein. The susceptibility of the WSN (N31S) M_2 protein to amantadine was also examined. This allele is extremely susceptible to amantadine, with significant rescue of growth observed at concentrations as low as 30 nM (data not shown). Growth rescue is also concentration dependent, suggesting nels. Growth rescue levels off at approximately 10 μM (unpublished data), suggesting that at this concentration all channels are blocked.

The M_2 protein may exert its toxic effect on yeast cells by destabilizing membrane function in a manner similar to that of killer toxin, a low-molecular-weight polypeptide encoded by the yeast M1 virus which forms ion channels in the lipid bilayer (4, 19, 21). In yeast cells, ion uptake is accomplished through the concerted actions of transporter proteins with ion selectivity and the electrochemical gradient established by the plasma membrane H^+-ATPase (30). Disruption of the integrity of this gradient leads to cell death by permitting the leakage of essential ions. Exposure to toxin results in a rapid inhibition of net proton pumping which reduces the proton gradient across the plasma membrane. Measurement of extracellular acidification rates of yeast strains expressing the M_2 ion channel before and after exposure to amantadine provides evidence that the open channel impairs the ability of the cell to maintain the proton gradient. Presumably, the plasma membrane H^+-ATPase is more active in the presence of the M_2 channel in order to maintain a gradient. The transient increase in proton flux observed upon exposure of cells expressing an amantadine-susceptible M_2 protein to the drug suggests that blocking the channel stops the leakage of protons into the cells. Previous studies of the M_2 channel expressed in *X. laevis* oocytes determined its cation selectivity but were unable to directly demonstrate proton flow through the channel (26). Recently however, reconstitution of recombinant M_2 into liposomes has allowed for the demonstration of M_2-mediated proton translocation in vitro (28). The microphysiometer analyses presented here suggest that the M_2-mediated proton translocation occurs in vivo in this heterologous system.

The microphysiometer analysis also indicates that, as observed in other expression systems, the activity of the M_2 channel in yeast cells is modulated by external pH (26, 36, 37). The magnitude of the increase in acidification rates due to amantadine exposure is greatest at pH 5.5, weaker at pH 6.5, and undetectable at pH 7.5, suggesting that amantadine has no effect on acidification rates at the higher pH because the channel is inactive. An alternative explanation for these results is that at the higher pH there is less proton leakage into the cell and that the M_2 channel in the open state would have less of an effect on the maintenance of the proton gradient. In this case, the addition of amantadine would be expected to have little or no effect.

The toxicity profile of M_2-expressing yeast cells allowed for the development of a screening protocol based on the rescue of cell growth in the presence of test compounds. This protocol identified BL-1743, a spirene-containing imidazole compound, as an inhibitor of M_2. BL-1743 exhibited a 50% inhibitory concentration of 250 nM in the yeast assay, whereas it exhibited a 50% inhibitory concentration of 2 μM in the virus plaque reduction assay. This disparity may result from the relative levels of M_2 protein produced in each system, differences in the solubility of BL-1743 in the two culture media, or inherent differences in the sensitivities of these assays. BL-1743 has a profile similar to that of amantadine in that it is active against an amantadine-susceptible strain (A/Udorn/72) but not against A/WSN/33, which is amantadine resistant. The same profile is observed in the yeast toxicity rescue assay. In the yeast assay, the simultaneous addition of amantadine and BL-1743 does not produce an additive effect on M_2 inhibition, suggesting that these two compounds interact with similar sites in the M_2 protein (data not shown). Also, the WSN (N31S) mutant protein, which is converted to amantadine susceptibility, is also

novel structure with an antiviral profile similar to that of amantadine.

ACKNOWLEDGMENTS

We thank Prabha Fernandes, Richard Colonno, and Jack Owicki for support and suggestions.

REFERENCES

1. Anderson, J., S. Huprikar, L. Kochian, W. Lucas, and R. Gaber. 1992. Functional expression of a probable Arabidopsis thaliana potassium channel in *Saccharomyces cerevisiae*. Proc. Natl. Acad. Sci. USA 89:3736–3740.
2. Black, R. A., P. A. Rota, N. Gorodkova, H. D. Klenk, and A. P. Kendal. 1993. Antibody response to the M2 protein of influenza A virus expressed in insect cells. J. Gen Virol. 74:143–146.
3. Brigati, C., S. Kurtz, D. Balderes, G. Vidali, and D. Shore. 1993. An essential yeast gene encoding a TTAGGG repeat-binding protein. Mol. Cell. Biol. 13:1306–1314.
4. Bussey, H., C. Boone, H. Zhu, T. Vernet, M. Whiteway, and D. Y. Thomas. 1990. Genetic and molecular approaches to synthesis and action of the yeast killer toxin. Experientia 46:193–200.
5. Clampor, F., C. A. Thompson, S. Grambas, and A. J. Hay. 1992. Regulation of pH by the M_2 protein of influenza A viruses. Virus Res. 22:247–258.
6. Duff, K. C., and R. H. Ashley. 1992. The transmembrane domain of influenza A M2 protein forms amantadine-sensitive proton channels in planar lipid bilayers. Virology 190:485–489.
7. Duff, K. C., P. J. Gilchrist, A. M. Saxena, and J. P. Bradshaw. 1994. Neutron diffraction reveals the site of amantadine blockade in the influenza A M2 ion channel. Virology 202:287–293.
8. Grambas, S., M. S. Bennett, and A. J. Hay. 1992. Influence of amantadine resistance mutations on the pH regulatory function of the M_2 protein of influenza A viruses. Virology 191:541–549.
9. Grambas, S., and A. J. Hay. 1992. Maturation of influenza A virus hemagglutinin—estimates of the pH encountered during transport and its regulation by the M_2 protein. Virology 190:11–18.
10. Guinea, R., and L. Carrasco. 1994. Influenza virus M2 protein modifies membrane permeability in E. coli cells. FEBS Lett. 343:242–246.
11. Hafeman, D. G., J. W. Parce, and H. M. McConnell. 1988. Light-addressable potentiometric sensor for biochemical systems. Science 240:1182–1185.
12. Hay, A. J. 1992. The action of adamantadines against influenza A viruses: inhibition of the M_2 ion channel protein. Semin. Virol. 3:21–30.
13. Hay, A. J., A. J. Wolstenholme, J. J. Skehel, and M. H. Smith. 1985. The molecular basis of the specific anti-influenza action of amantadine. EMBO J. 4:3021–3024.
14. Helenius, A. 1992. Unpacking the incoming influenza virus. Cell 69:577–578.
15. Holsinger, L. J., and R. A. Lamb. 1991. Influenza virus M_2 integral membrane protein is stabilized by formation of disulfide bonds. Virology 183:32–43.
16. Ito, H., Y. Fukuda, D. Murata, and A. Kimura. 1983. Transformation of intact yeast cells with alkali cations. J. Bacteriol. 153:163–168.
17. Iverson, L. E., M. A. Tanouye, H. A. Lester, N. Davidson, and B. Rudy. 1988. Expression of A-type potassium channels from *Shaker* cDNAs. Proc. Natl. Acad. Sci. USA 85:5723–5727.
18. Joho, R. H. 1992. Toward a molecular understanding of voltage-gated potassium channels. J. Cardiovasc. Electrophysiol. 3:589–601.
19. Kagan, B. 1983. Mode of action of yeast killer toxins: channel formation in lipid bilayer membranes. Nature (London) 302:709–711.
20. Martin, K., and A. Helenius. 1991. Nuclear transport of influenza virus ribonucleoproteins: the viral matrix protein (M1) promotes export and inhibits imports. Cell 67:117–130.
21. Martinac, B., H. Zhu, A. Kubalski, X. Zhou, M. Culbertson, H. Bussey, and C. Kung. 1990. Yeast K1 killer toxin forms ion channels in sensitive yeast spheroplasts and in artificial liposomes. Proc. Natl. Acad. Sci. USA 87:6228–6232.
22. McConnell, H. M., J. C. Owicki, J. W. Parce, D. L. Miller, G. T. Baxter, H. G. Wada, and S. Pitchford. 1992. The cytosensor microphysiometer: biological application of silicon technology. Science 257:1906–1912.
23. Miller, D. L., J. C. Olson, J. W. Parce, and J. C. Owicki. 1993. Cholinergic stimulation of the NA+/K+ adenosine triphosphatase as revealed by microphysiometry. Biophys. J. 54:813–823.
24. Miller, D. L., and J. C. Owicki. 1994. Long term exposure of TE671 cells to PMA induces a change in metabolic and calcium responses to nAChR activation. Can. J. Physiol. Pharmacol. 72(Suppl. 1):378.
25. Owicki, J. C., and J. W. Parce. 1992. Biosensors based on the energy metabolism of living cells: the physical chemistry and cell biology of extracellular acidification. Biosensors Bioelectronics 7:255–272.
26. Pinto, L. H., L. J. Holsinger, and R. A. Lamb. 1992. Influenza virus M_2 protein has ion channel activity. Cell 69:517–528.
27. Sansom, M. S. P., and I. D. Kerr. 1993. Influenza virus M_2 protein: a molecular modelling study of the ion channel. Protein Eng. 6:65–74.
28. Schroeder, C., C. M. Ford, S. A. Wharton, and A. J. Hay. 1994. Functional reconstitution in lipid vesicles of influenza virus M2 protein expressed by baculovirus: evidence for proton transfer activity. ●●●. ●●:●●●–●●●.
29. Sentenac, H., N. Bonneaud, M. Minet, F. Lacroute, J.-M. Salmon, F. Gaymard, and C. Grignon. 1992. Cloning and expression in yeast of a plant potassium ion transport system. Science 256:663–666.
30. Serrano, R. 1991. Transport across yeast vacuolar and plasma membranes, p 523–585. *In* J. R. Broach, et al. (ed.), The molecular biology of the yeas saccharomyces. Cold Spring Harbor Laboratory, Cold Spring Harbor, N.Y.
31. Sherman, F., G. R. Fink, and J. B. Hicks. 1983. Methods in yeast genetics. Cold Spring Harbor Laboratory, Cold Spring Harbor, N.Y.
32. Skehel, J. J. 1992. Amantadine blocks the channel. Nature (London) 358: 110–111.
33. Sugrue, R. J., G. Bahdur, M. C. Zambon, M. Hall-Smith, A. R. Douglas, and A. J. Hay. 1990. Specific structural alteration of the influenza haemagglutinin by amantadine. EMBO J. 9:346–347.
34. Sugrue, R. L., and A. J. Hay. 1991. Structural characteristics of the M_2 protein of influenza A viruses: evidence that it forms a tetrameric channel. Virology 180:617–624.
35. Timpe, L. C., T. L. Schwarz, B. L. Tempel, D. M. Papazian, Y. N. Jan, and L. Y. Jan. 1988. Expression of functional potassium channels from *Shaker* cDNA in Xenopus oocytes. Nature (London) 331:143–145.
36. Tosteson, M. T., L. H. Pinto, L. J. Holsinger, and R. A. Lamb. 1994. Reconstitution of the influenza virus M2 ion channel in lipid bilayers. J. Membr. Biol. 142:117–126.
37. Wang, C., R. A. Lamb, and L. H. Pinto. 1994. Direct measurement of the influenza A virus M2 protein ion channel activity in mammalian cells. Virology 205:1333–140.
38. Wang, C., K. Takeuchi, L. H. Pinto, and R. A. Lamb. 1993. Ion channel activity of influenza A virus M_2 protein: characterization of the amantadine block. J. Virol. 67:5585–5594.

The microphysiometer biosensor

Harden M. McConnell, Peter Rice, Garrett H. Wada, John C. Owicki and J. Wallace Parce

Stanford University, Stanford, California, USA and Molecular Devices Corp., Menlo Park, California, USA

Biosensors provide analytical information about biochemical and biological systems. One such device is a light-addressable potentiometric sensor at the heart of an instrument called a microphysiometer. The instrument detects a signal that is closely related to the cellular metabolic rate. The use of this device is discussed.

Current Opinion in Structural Biology 1991, 1:647–652

Introduction

Biosensors are broadly defined as devices that provide analytical information about biochemical and biological systems [1,2••]. Biosensors are often more narrowly viewed as small devices based on silicon-chip technology, optic fibers or electrochemistry [3]. The variety of the devices and their applications are not reviewed here. Instead we focus on one single device, a light-addressable potentiometric sensor (LAPS) [4], at the heart of an instrument called a microphysiometer [5]. Our discussion is directed to workers in the field of biotechnology who may find this device useful in their own work, rather than to readers who might be more interested in the technical details of the instrumentation.

The microphysiometer detects a signal that is closely related to the cellular metabolic rate. Measuring the metabolic rate with high sensitivity and time resolution can be a surprisingly useful and powerful technique for detecting changes in cell physiology. The many biochemical reactions that characterize the living state are highly coupled so that changes at one biochemical site propagate throughout the metabolic network, with attenuation or amplification. Energy metabolism is particularly richly coupled to this web, and so presents an attractive process to monitor. A general means of detecting physiological changes in cells can be a powerful way of detecting chemical and physical changes in cellular environments that have functional consequences.

There are several possible experimental approaches. For example, one can measure the rate of cellular oxygen consumption with an oxygen electrode [6] or the rate of heat production with a microcalorimeter [7,8]. Because the principal products of glycolysis and respiration are both acidic (lactic acid and CO_2, or carbonic acid), one can also monitor energy metabolism by measuring the rate at which cells acidify their environment. We have chosen this last method because the characteristics of the LAPS are particularly suited to this application, measuring phenomena that have been difficult to detect previously.

Operational principles

The microphysiometer uses a flow chamber into which an aqueous solution can be introduced and then removed. One wall of this chamber is formed by the LAPS. The surface of the LAPS comprises a thin ($\sim$60 nm) insulating barrier of silicon oxide and nitride which separates the silicon and the aqueous medium. When a potential is applied across the barrier by means of one electrode in the aqueous solution and a second electrode attached to the silicon, an electric field is created within the silicon. A pulse of light from a source such as a light-emitting diode can be absorbed in the silicon, generating electron-hole pairs. The electrons and holes move in the electrical field and produce a transient current that can be detected by an external circuit. When the light is pulsed, the alternating current in the external circuit can be measured by a low-impedance detecting system. The magnitude of this current depends on the bias potential across the insulating barrier. The electrostatic potential due to charged molecules and ions that bind to the insulating barrier adds in series with the applied potential. Oxynitride insulators bind protons, and this translates into a pH sensitivity of the alternating current in the external circuit. The basic LAPS structure can be modified so that it is selectively sensitive to redox potentials, or other interactions that add in series to the applied potential. The microphysiometer described here relies on the pH sensitivity of silicon oxynitride surfaces.

Abbreviation

LAPS—light-addressable potentiometric sensor.

 ISSN 0959-440X

Sensitivity and amplification

The silicon sensor together with the electronic detection system can be designed so that the potential drift in the system is $< 1\,\mu V\,s^{-1}$. The pH response on properly prepared oxynitride surfaces is Nernstian over a broad pH range, pH = 2–11, so that the drift of pH in this system is only of the order of 16×10^{-6} pH units s^{-1}. Biological components that change pH, such as enzyme–substrate combinations and biological cells, can be detected with high sensitivity in a flow chamber such as that sketched in Fig.1, provided the chamber has a sufficiently small volume. The sensitivity is ultimately limited by the buffer capacity of the solution or the solid surfaces. Sensitivity in this system has been previously discussed by Hafeman *et al.* [4] and Bousse *et al.* [9•].

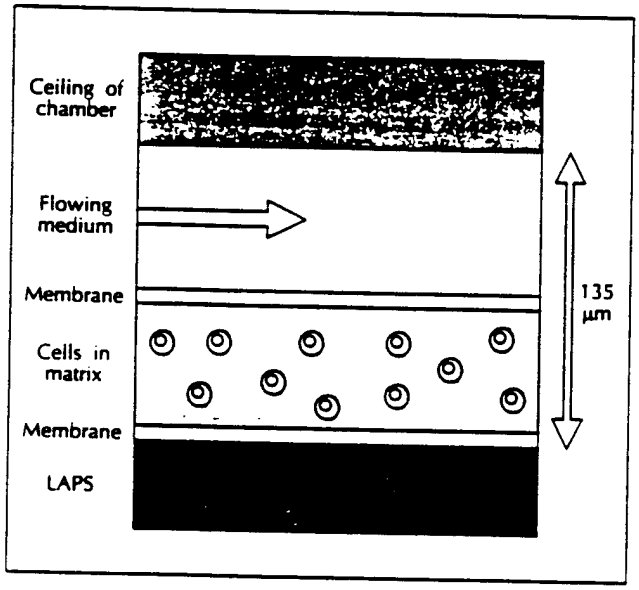

Fig. 1. Schematic diagram of the microphysiometer flow chamber. Abbreviation: LAPS, light-addressable potentiometric sensor.

The microphysiometer

The microphysiometer is designed to detect the metabolic activity of biological cells, particularly eukaryotic cells. In operation, cells are confined to a flow chamber such as the one sketched in Fig. 1. Adherent cells can be attached to either the upper or the lower surface of the chamber, or to some other supporting structure. Non-adherent cells must be constrained by means of a membrane, together with a supporting medium such as chopped collagen. In the microphysiometer under development at Molecular Devices Corp., both adherent and non-adherent cells are contained in a disposable flow capsule that is maintained in close proximity to the silicon.

The medium passing through the flow chamber is cycled, flow on and flow off, for periods of the order of 1 min each. During the flow-on cycle, the pH is essentially constant and equal to the pH of the medium. During the flow-off cycle, the medium acidifies, the acidification rate depending on the number of cells and their metabolic activity. Experimental records of the process are given in Fig. 2. A diagram of the microphysiometer system is given in Fig. 3.

Cell triggering by receptor ligands

A carefully designed microphysiometer can detect the triggering of eukaryotic cells by a wide variety of specific receptor ligands [10••,11,12]. Although this was a hoped-for result, there was no quantitative justification for this hope before construction of the microphysiometer was undertaken. Even today, there is no compelling general explanation of the observed high sensitivity of the microphysiometer for detecting the triggering of cells by receptor ligands. In the following discussion, we illustrate results obtained using various types of receptors. In these experiments, several strategies have been used to optimize the sensitivity of response. The medium bathing the cells generally has a low buffer capacity, about 1mM. The best responses from cells are often observed for 'serum starved' cells, the cells that have been maintained in medium free of serum for a period of time before the experiment [10••].

Figure 4 shows the rapid pH response of Chinese hamster ovary cells transfected with the m_1 muscarinic acetylcholine receptor to agonist and to antagonist. The response of these cells to a sudden introduction of 100 μM of the agonist carbachol takes place within the time resolution of the on (30 s) and off (60 s) cycle. Figure 4 shows that 1 μM atropine, the competitive antagonist, completely blocks the carbachol-induced response. Figure 4 also shows the pH response of Chinese hamster ovary cells to insulin. This cellular triggering may be a result of stimulation of the insulin receptor and/or the insulin-like growth factor receptor [13]. The cellular responses to both insulin and carbachol lead to a similar pH overshoot, even though the biochemical effector pathways following receptor triggering are presumably quite different.

Effector pathways

At the time of this writing, the microphysiometers under development have been used to observe the triggering of cells by about a dozen specific receptor ligands. Most of the well known second-messenger pathways have been covered in this work: the β_2-adrenergic and prostaglandin E_1 receptors respond through the stimulation of adenylyl cyclase; the d_2 dopamine response involves the inhibition of adenylyl cyclase; the m_1 muscarinic receptor response involves the activation of phosphatidylinositol hydrolysis and the opening of a G-protein-regulated K^+ chan-

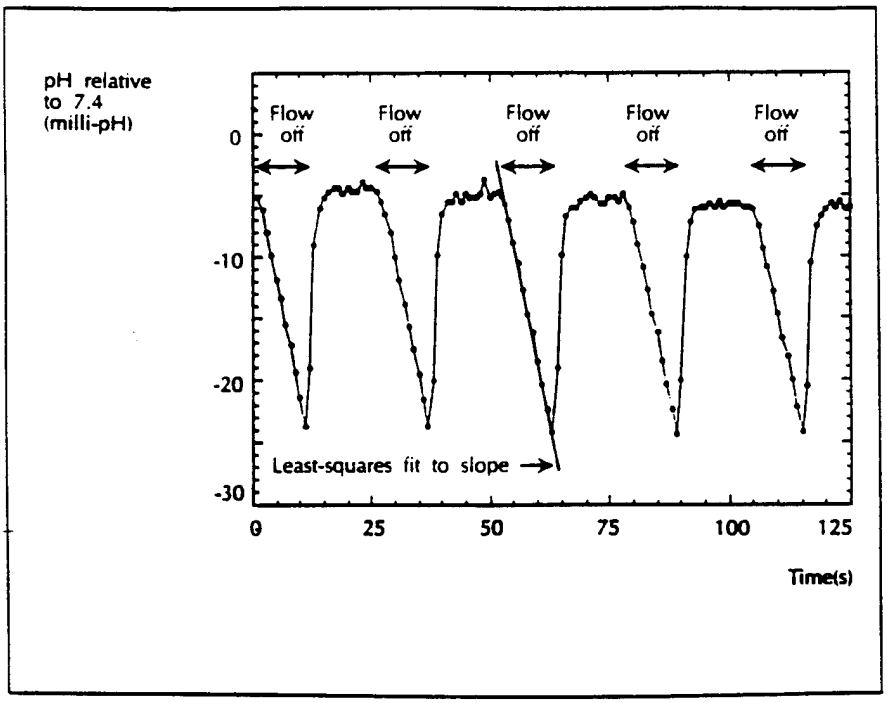

Fig. 2. Microphysiometer flow chamber pH versus time profile.

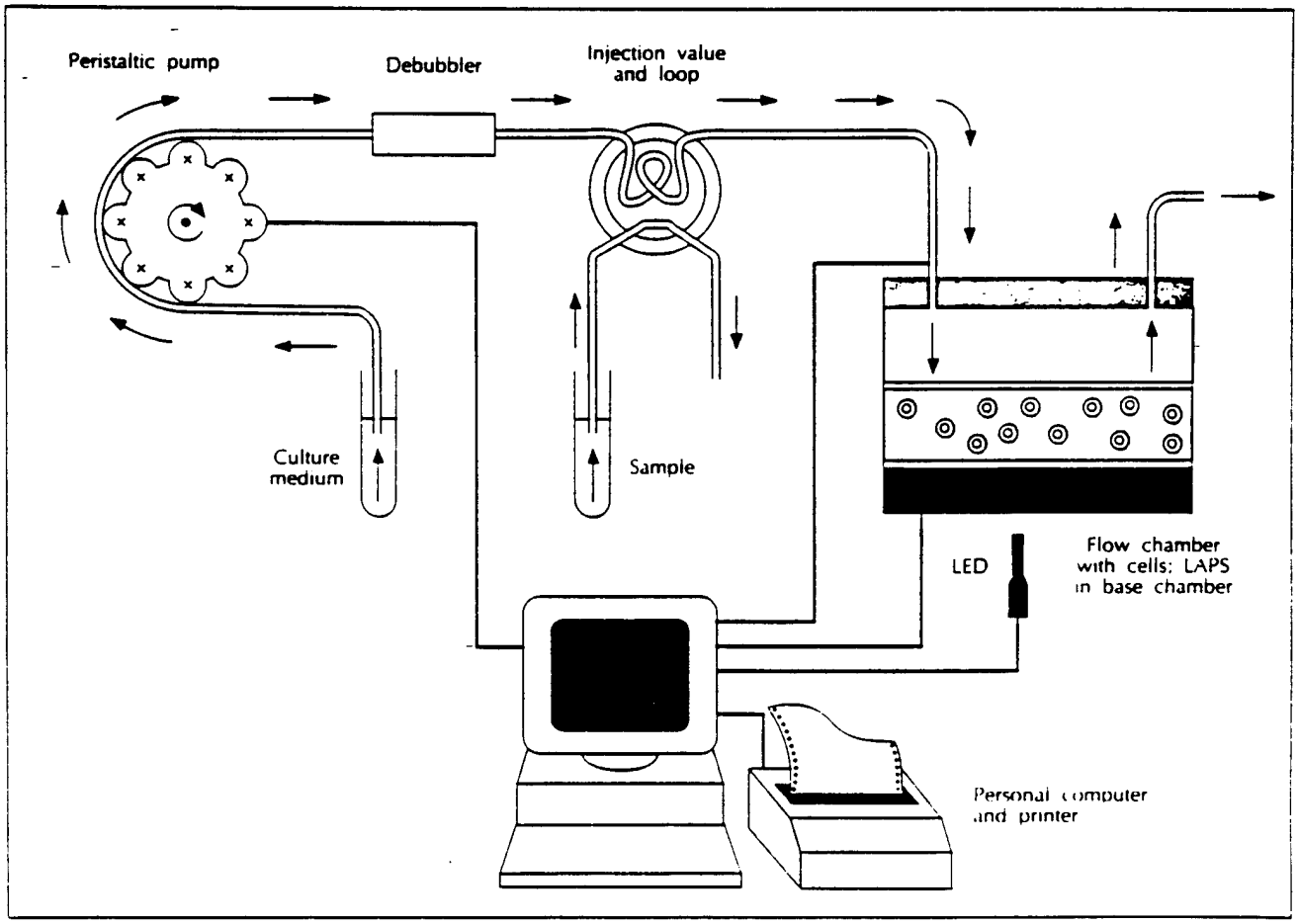

Fig 3. Diagram of the microphysiometer system. A personal computer controls the on/off cycle of the peristaltic pump and acquires data from the light-addressable potentiometric sensor (LAPS) in the flow chamber. The debubbler removes bubbles and excess gas from the culture medium so that bubbles do not form in the warm (37 °C) flow chamber. An injection loop valve is provided for the introduction of samples.

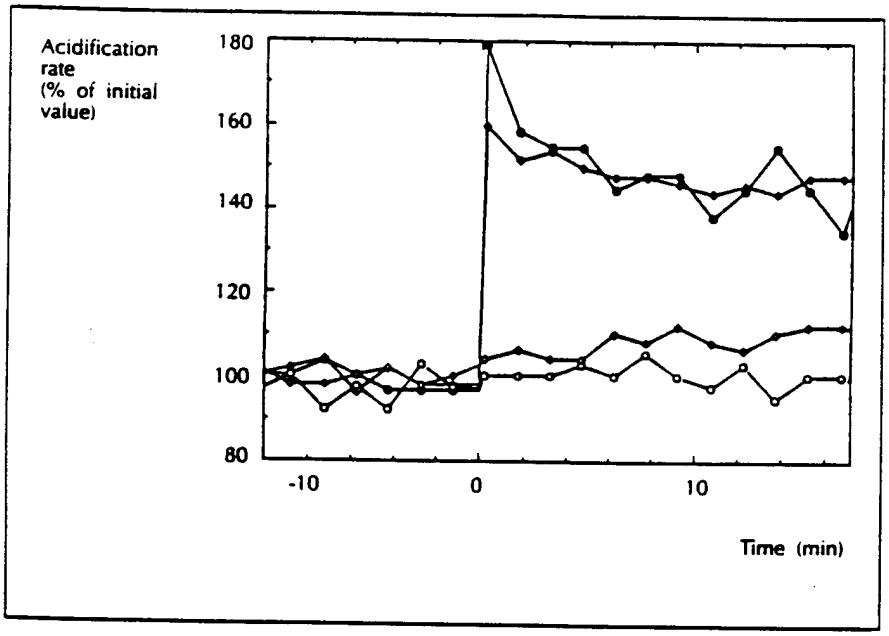

Fig. 4. Metabolic responses of Chinese hamster ovary cells transfected with the muscarinic acetylcholine receptor to the addition of agonist and antagonist. Cells in four microphysiometer chambers were exposed either to control medium (filled symbols) or control medium containing 1 μM atropine (open symbols), a muscarinic antagonist. At t = 0, 100 μM carbachol was introduced into all four chambers.

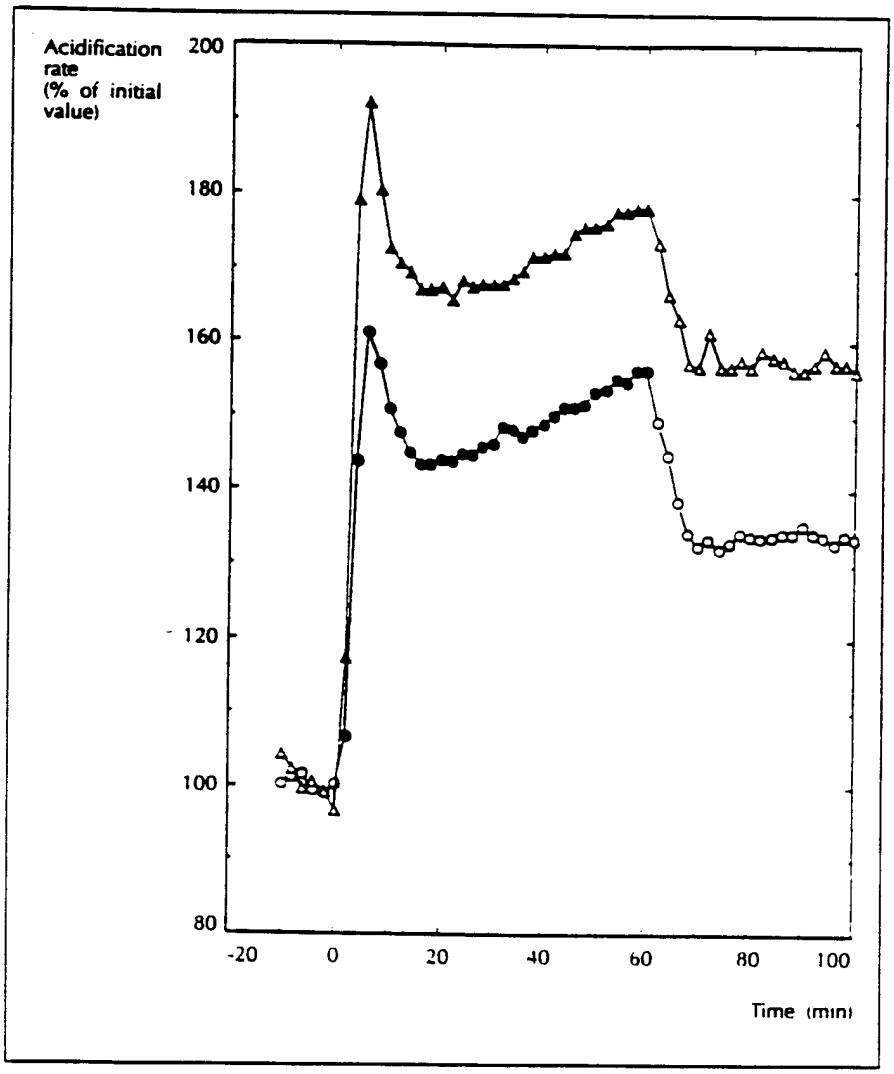

Fig. 5. Metabolic responses of Chinese hamster ovary K1 cells to insulin. Insulin at a concentration of 90 nM (●) or 900 nM (▲) was present during the period indicated by the solid symbols.

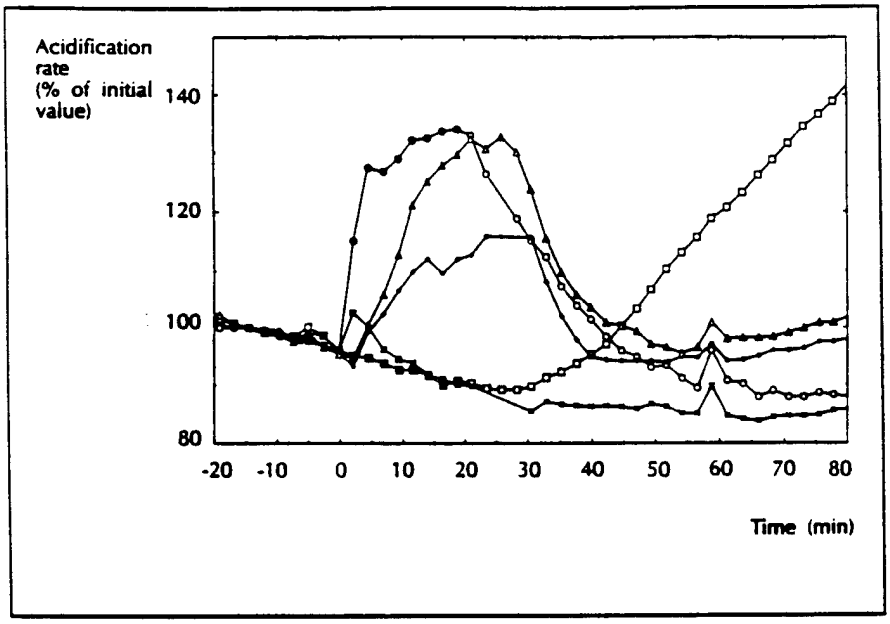

Fig. 6. Metabolic responses of Chinese hamster ovary cells containing transfected human β_2-adrenergic receptors to various agents that increase cytoplasmic cyclic AMP concentrations. The agents, 10 μM isoproterenol (○), 500 μM 8-bromo cyclic AMP (△), 10 μg ml^{-1} forskolin (■), or 1 μg ml^{-1} cholera toxin (□), were introduced during the period represented by the filled symbols. The control chamber in which no agent was introduced is represented by X.

nel; the kainate (glutamate) receptor involves a Na^+/K^+ channel intrinsic to the receptor; and, epidermal growth factor and insulin-like growth factor involve protein kinases also intrinsic to the receptors.

What specific intracellular biochemical reactions lead to the observed changes in proton production when receptors are activated? Frequently, the receptor-triggered proton flux exhibits an initial overshoot that subsequently returns to a steady-state value, as in Fig. 4. The altered steady state can be understood in terms of changes in the rates of glycolysis and respiration; in a few cases, e.g. insulin, these mechanisms are fairly well understood [14]. The transient phase probably involves enhanced ATP hydrolysis and synthesis, but the time courses of the various biochemical steps required in specific cases are not known at present. The overshoot phenomenon could be regarded simply as a transient to be expected when a system of coupled enzymatic reactions passes from one steady state to another. More mechanistically precise models involving feedback loops between ATP hydrolysis and synthesis, or changes in intracellular pH, produce overshoots qualitatively similar to those seen with the microphysiometer (JC Owicki and JW Parce, unpublished data). Another entirely different possibility is that each cell has an oscillatory proton excretion rate. Under steady-state conditions, there is generally no phase coherence among a population of the order of 1000 cells. However, it is conceivable that a pulse of receptor ligand can 'set' the phase of the cell oscillations for one, or possibly two periods, giving an initial overshoot in proton excretion. This is analogous to the phasing of yeast cells brought about by a pulse of added glucose [15,16]. The problem is not entirely theoretical, as the general aim is to provide conditions allowing a maximal enhancement of proton excretion following receptor triggering.

The microphysiometer can also be conveniently used to carry out pharmacological studies of the receptor second-messenger pathways themselves. For example, upon agonist binding, the β_2-adrenergic receptor activates a G_s protein that in turn activates adenylate cyclase, resulting in an increase in the cyclic AMP concentration within the cell [17]. The metabolic increase observed in the microphysiometer upon stimulation of this receptor is a response to the increased levels of cyclic AMP. This is shown in Fig. 5. Cellular metabolic responses are observed upon receptor-ligand interaction, upon treatment of the cells with cholera toxin (a G_s-protein activator [18]), introduction of forskolin (an activator of adenylate cyclase [19]), and upon addition of 8-bromo cyclic AMP (a stable cyclic AMP derivative [20]). The kinetics of activation and the reversibility of the response to these agents are as expected. All of the agents except cholera toxin demonstrate reversible increases in acidification rates. Cholera toxin is known to activate G_s protein irreversibly by an ADP ribosylation step [18]. Using pharmacological agents such as those described above, the second-messenger pathway to metabolic activation can be mapped. Furthermore, in the case of non-functional receptor–cell systems that occasionally occur in genetically engineered cells, the deflect point in the second-messenger pathway can be quickly identified.

Applications, and new receptor ligands

There are many potential practical applications of the microphysiometer in analytical biotechnology, for example, bioassays for specific receptor ligands. Other applications include the determination of irritancy and toxicity, which may at least partly replace animal testing [21•,22••]. Investigations of chemotherapeutic efficacy on small samples of cells are also possible [5]. From both a theoretical and a practical point of view, one of the most interesting areas of application of the microphysiometer is the

screening for new receptor ligands. The microphysiometer should serve as a useful adjunct to drug-discovery methods that involve radioactive ligand-binding assays. Perhaps the most exciting area concerns identification of receptors with unknown ligands such as the so-called orphan receptors that have been cloned by low-stringency hybridization to DNA sequences found in known receptors.

References and recommended reading

Papers of special interest, published within the annual period of review, have been highlighted as:

- • of interest
- •• of outstanding interest

1. TURNER A, KARUBE I, WILSON G (EDS): *Biosensors: Fundamentals and Applications* [book]. Oxford: Oxford University Press, 1987.

2. •• BUCK RP, HATFIELD WE, UMANA M, BOWDEN EF (EDS): *Biosensor Technology, Fundamentals and Applications [book]*. New York: Marcel Dekker Inc., 1990.

A variety of bisensor papers presented at the North Carolina Section American Chemical Society Symposium on Biosensors. Of particular interest is a very good introduction by Buck entitled 'Sensor issues for the 1990s'.

3. PARCE JW: **Biosensors and Biotechnology**. In *Advances in Applied Biotechnology Series. Vol. 3* edited by Obringer JW, Tillinghast HS. Houston: Gulf Publishing Company, 1989.

4. HAFEMAN DG, PARCE JW, MCCONNELL HM: **Light-Addressable Potentiometric Sensor for Biochemical Systems**. *Science* 1988, 240:1182–1185.

5. PARCE JW, OWICKI JC, KERCSO KM, SIGAL GB, WADA HG, MUIR VC, BOUSSE LJ, ROSS KL, SIKIC BI, MCCONNELL HM: **Detection of Cell Affecting Agents with a Silicon Biosensor**. *Science* 1989, 246:243–247.

6. LI X-M, LIANG BS, WANG HY: **Computer Aided Analysis for Biosensing and Screening**. *Biotechnol Bioeng* 1988, 31:250–256.

7. JAMES AM (ED): *Thermal and Energetic Studies of Cellular Biological Systems* [book]. Bristol: Wright, 1987.

8. SCHON A, WADSO I: **The Potential Use of Microcalorimetry in Predictive Tests of the Action of Antineoplastic Drugs on Mammalian Cells**. *Cytobios* 1988, 55:33–39.

9. • BOUSSE L, KIRK G, SIGAL G: **Biosensors for Detection of Enzymes Immobilized in Microvolume Reaction Chambers**. *Sensors Actuators* 1990, B1:555–560.

A theoretical treatment of the sensitivity of biosensors based on the measurement of pH changes produced by enzymes.

10. •• OWICKI JC, PARCE JW, KERCSO KM, SIGAL GB, MUIR VC, VENTER JC, FRASER CM, MCCONNELL HM: **Continuous Monitoring of Receptor-Mediated Changes in the Metabolic Rates of Living Cells**. *Proc Natl Acad Sci USA* 1990, 87:4007–4011.

A demonstration of the generality of changes in extracellular acidification rates that result from receptor triggering.

11. PARCE JW, OWICKI JC, KERCSO KM: **Biosensors for Directly Measuring Cell-Affecting Agents**. *Ann Biol Clin* 1990, 48:639–641.

12. WADA HG, OWICKI JC, PARCE JW: **Cells on Silicon: Bioassays with a Microphysiometer**. *Clin Chem* 1991, in press.

13. MAMOUNAS M, GERVIN D, ENGLESBERG E: **The Insulin Receptor as a Transmitter of a Mitogenic Signal in CHO-K1 Cells**. *Proc Natl Acad Sci USA* 1989, 86:9294–9298.

14. SALTIEL AR: **Second Messengers of Insulin Action**. *Diabetes Care* 1990, 13:244–256.

15. GHOSH AK, CHANCE B, PYE EK: **Metabolic Coupling and Synchronization of NADH Oscillations in Yeast Cell Populations**. *Arch Biochem Biophys* 1971, 145:319–331.

16. GHOSH A, CHANCE B: **Oscillations of Glycolytic Intermediates in Yeast Cells**. *Biochem Biophys Commun* 1964, 16:174–181.

17. FRASER CM, CHUNG F-Z, VENTER JC: **Continuous High Density Expression of Human β_2-Adrenergic Receptors in a Mouse Cell Line Previously Lacking β-Receptors**. *J Biol Chem* 1987, 262:14843–14846.

18. JOHNSON GL, KASLOW HR, BOURNE HR: **Reconstitution of Cholera Toxin Activated Adenylate Cyclase**. *Proc Natl Acad Sci USA* 1978, 75:3113–3117.

19. SEAMON KB, DALY JW: **Forskolin: A Unique Activator of c-AMP-Generating Systems**. *J Cyclic Nucleotides* 1981, 7:201.

20. FARRAR WL, EVANS SW, RAPP UR, CLEVELAND JL: **Effects of Anti-Proliferative Cyclic AMP on Interleukin 2-Stimulated Gene Expression**. *J Immunol* 1987, 139:2075–2080.

21. • BRUNER LH, KERCSO KM, OWICKI JC, PARCE JW, MUIR VC: **Testing Ocular Irritancy *in vitro* with the Silicon Microphysiometer**. *Toxicol In Vitro* 1991, in press.

An example of an approach using the microphysiometer to predict the ocular irritancy potential of various consumer products.

22. •• BRUNER LH, KAIN DJ, ROBERTS DA, PARKER RD: **Evaluation of Seven *in-vitro* Alternatives for Ocular Safety Testing**. *Fund Appl Tox* 1991, in press.

A thorough comparison of seven *in vitro* alternatives to *in vivo* ocular irritancy testing using 17 test materials.

HM McConnell and P Rice, Department of Chemistry, Stanford University, Stanford, California 94305, USA.

GH Wada, JC Owicki and JW Parce, Molecular Devices Corp., 4700 Bohannon Drive, Menlo Park, California 94025, USA.

The Cytosensor Microphysiometer: Biological Applications of Silicon Technology

H. M. McConnell, J. C. Owicki, J. W. Parce,* D. L. Miller, G. T. Baxter, H. G. Wada, S. Pitchford

A silicon-based device, dubbed a microphysiometer, can be used to detect and monitor the response of cells to a variety of chemical substances, especially ligands for specific plasma membrane receptors. The microphysiometer measures the rate of proton excretion from 10^4 to 10^6 cells. This article gives an overview of experiments currently being carried out with this instrument with emphasis on receptors with seven transmembrane helices and tyrosine kinase receptors. As a scientific instrument, the microphysiometer can be thought of as serving two distinct functions. In terms of detecting specific molecules, selected biological cells in this instrument serve as detectors and amplifiers. The microphysiometer can also investigate cell function and biochemistry. A major application of this instrument may prove to be screening for new receptor ligands. In this respect, the microphysiometer appears to offer significant advantages over other techniques.

The best known applications of silicon (Si) technology are in nonbiological realms, such as computers. This article, however, describes a biological application of Si technology: the integration of living cells with a Si-based sensor to form an instrument that detects a wide variety of molecules in the cells' environment by effects on cell physiology.

This instrument is called the microphysiometer (its manufactured version is the Cytosensor), and it differs from most other analytical instruments. Instead of reporting structural features of an analyte as do, for example, electrophoresis, nuclear magnetic resonance, and immunoassays, the microphysiometer instead reports the effects of an analyte on biological function. In other words, it is a system for performing bioassays. It is more akin to techniques that monitor cell growth and morphology, assays of biochemical change, and techniques that measure variations in transmembrane potentials and currents.

With few exceptions, cells acidify their environments because of acidic products of energy metabolism. Adenosine triphosphate (ATP) production by means of energy metabolism is tightly coupled to cellular ATP consumption such that changes in cell physiology cause changes in the rate of energy use and, hence, in the rate of extracellular acidification. In many cases, these changes are large enough to detect conveniently with the microphysiometer; typically, changes of 10 to 100% occur on a time scale of seconds to minutes. Another kind of proton-mediated signal of physiological changes arises from changes in intracellular pH, which appear as complementary changes in extracellular pH as protons are transported across the plasma membrane. These effects are the bases of the broad applicability of the instrument.

The microphysiometer uses a light-addressable potentiometric sensor (LAPS) to measure the rate at which cells acidify their environment. Figure 1 is a diagram of the LAPS and its accompanying circuitry. The LAPS is a piece of doped Si with a thin insulator on the surface. An external circuit connects an ohmic contact on the Si to an aqueous compartment that is in contact with the insulator. The function of the external circuit is twofold. It controls the potential from the Si to the aqueous solution and measures an alternating photocurrent. The photocurrent is generated when the sensor is illuminated with an amplitude-modulated light-emitting diode (LED). When the potential from Si to solution is adjusted so that the Si is forward biased, no photocurrent flows in the external circuit. When the sensor is reverse biased, a voltage gradient (depletion layer) is formed immediately below the insulator. This voltage gradient results in the separation of hole-electron pairs formed by absorption of light from the LED, and an ac-coupled photocurrent flows in the external circuit. No direct current passes through the insulator.

The applied potential (Ψ) at which photocurrent begins to flow is defined by the sum of a variety of constant potentials (that is, contact potentials) and the surface potential of the aqueous-insulator interface. Changes in the surface potential can therefore be measured by a determination of the changes in Ψ required to produce a photocurrent. The surface of the Si nitride insulator contains hydroxyl and amino functions, both of which can be titrated as a function of pH. Therefore, the surface potential at the aqueous-insulator interface is sensitive to pH. A properly prepared Si nitride surface has a sufficiently high density of titratable groups to make the pH response of the surface potential Nernstian (61 mV per pH unit at 37°C). The light-addressable nature of the sensor results from the fact that the pH is measured only at the site of illumination by the LED. Other devices have used this feature to perform several immunoassays simultaneously on one sensor (*1*). In the Cytosensor, only one LED is used

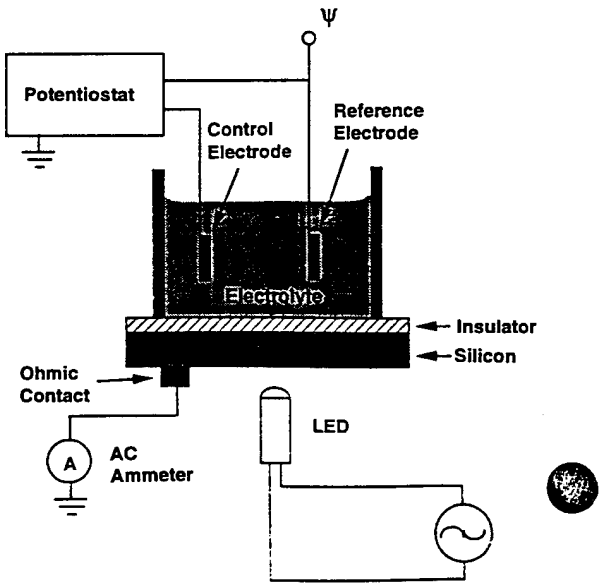

Fig. 1. Schematic drawing of the light-addressable potentiometric sensor (LAPS).

H. M. McConnell is in the Department of Chemistry, Stanford University, Stanford, CA 94305 and is a director at Molecular Devices Corporation, 4700 Bohannan Drive, Menlo Park, CA 94025. J. C. Owicki, J. W. Parce, D. L. Miller, G. T. Baxter, H. G. Wada and S. Pitchford are at Molecular Devices Corporation, 4700 Bohannon Drive, Menlo Park, CA 94025.

*To whom correspondence should be addressed.

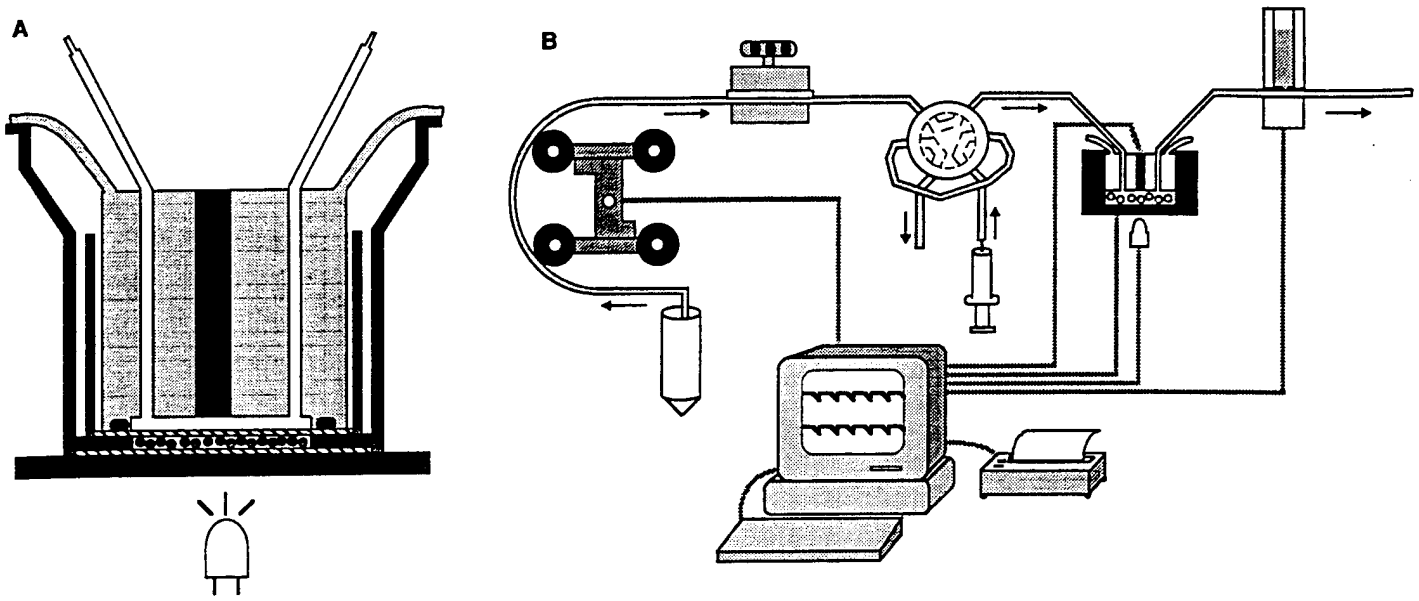

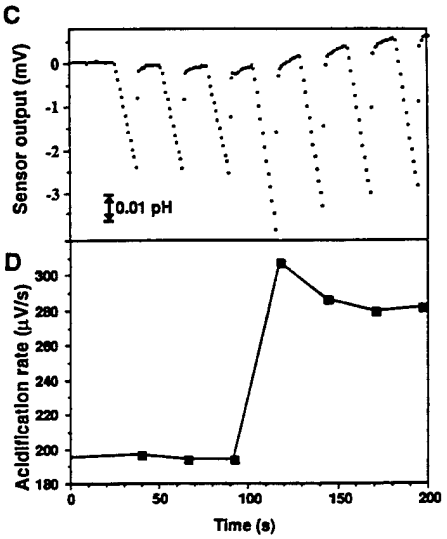

Fig. 2. Cytosensor description and operation. (**A**) Flow chamber containing cells. Cells are retained in a disk-shaped region 50 μm high and 6 mm in diameter between two track-etched microporous polycarbonate membranes, shown with diagonal hatching. The sensing surface (top) of the LAPS contacts the lower membrane, and culture medium flows tangentially across the surface of the upper membrane. An LED (bottom of figure) illuminates the non-sensing surface (bottom) of the LAPS. (**B**) Instrumentation schematic. The electronics that operates the LAPS makes three analog connections to the instrument beyond those to the LED: one to the underside of the LAPS chip, one to a controlling electrode in the ceiling of the flow chamber, and one to the reference electrode. A complete Cytosensor system contains eight flow chambers and associated components managed by one computer. (**C**) Plot of pH versus time for CHO cells transfected with the muscarinic acetylcholine receptor. Agonist (carbachol) was added at time t = 100 s. (**D**) Plot of acidification rate versus time for the data shown in (C). During each flow-off period shown in (C), the sensor data are fit to a straight line with the use of a least-squares procedure; the slope of this line is reported as the acidification rate. Numerically, 1 μV/s is close to 1 × 10^{-3} pH units per minute. In this figure, receptors on the cells were activated with an agonist midway through the period shown. The increase in acidification rate is apparent.

per sensor chamber. In this configuration, it is possible to optimize the signal-to-noise ratio of the pH measurement. At present, the instrument makes one pH reading per second in every chamber with a root-mean-square noise between 0.0005 and 0.001 pH units. This low noise feature of the LAPS is very important for the measurement of subtle changes in cell physiology in the microphysiometer.

The following paragraphs provide a more detailed description of the physical and biochemical aspects of the microphysiometer. Additional information about the LAPS can be found in (*2*); additional information about the operation of the microphysiometer can be found in (*3*) and (*4*). For a thorough discussion of quantitative aspects of cellular metabolism relative to microphysiometry, see (*5*) and references therein. We conclude with some examples of applications of the microphysiometer.

The Microphysiometer and Its Biological Basis

Cells, whether eukaryotic or prokaryotic, adherent or nonadherent, are retained by the microphysiometer in a flow chamber in aqueous diffusive contact with the pH-sensitive surface of a LAPS chip (Fig. 2A). Adherent cells attach directly to the membrane surface, whereas nonadherent cells are immobilized by, for example, entrapment within a fibrin clot. An infrared LED illuminates the underside of the LAPS chip, which defines the region of the chamber from which data are obtained. As shown in Fig. 2B, this chamber is the heart of an instrument that controls the flow of medium over the cells, the introduction of test substances, the chamber temperature, the LAPS electronics, and data management. Culture medium is pumped from a reservoir by a peristaltic pump and passes through a debubbler-degasser, a selection valve, and the flow chamber. After leaving the flow chamber, it passes a reference electrode en route to a waste receptacle. Samples for analysis can be introduced at the selection valve through an injection loop. Alternately, the tubing can be configured so that the valve controls which of two pumped streams of media enters the flow chamber. A personal computer (a Macintosh with dedicated software) controls the LAPS electronics, the pump, and the valve; it also manages data acquisition, analysis, and storage.

The extracellular acidification rate is determined by measurement of the decrease in pH that occurs as acidic metabolites build up during brief halts in the flow of media (Fig. 2, C and D). Once each second for each flow chamber, the LAPS makes a voltage measurement that is linearly related to pH (a decrease of 61 mV is approximately equal to an acidification of 1 pH unit at 37°C). During fluid flow, the sensor output is stable and reflects a pH near that of the culture medium entering the flow chamber. When the flow is briefly halted, typically for 30 to 60 s, the pH in the chamber decreases as a result of the excretion of protons by the cells. These acidifications are typically <0.1 pH unit and cause no significant perturbations of cell physiology. When the flow is resumed, the sensor output rises to the previous steady state as the mildly acidified medium is flushed out. The flow cycle is repeated continually, yielding one

measurement of acidification rate at each flow-off period. Usually, one can improve the sensitivity of the method by decreasing the buffer capacity of the culture medium to about 1 mM per pH unit by not adding strongly buffering species such as bicarbonate and Hepes to the medium.

Figure 3 shows schematically the principal cellular mechanisms by which protons are produced and excreted for a composite mammalian cell with the use of glucose as a carbon source. It further indicates how these processes can be modulated by ligand-receptor interactions, as discussed below. The main parts of the proton economy include several factors.

Proton production. Glucose enters through a glucose transport protein and is metabolized to lactic acid by glycolysis or oxidized to CO_2 by respiration. At physiological pH, both of these weak acids are predominantly dissociated.

Proton excretion. These protons cross the plasma membrane by several means, both unfacilitated and facilitated. Some of the lactic acid and CO_2 passively diffuses across the membrane. Lactic acid is also excreted through the monocarboxylic acid transporter. Bicarbonate exits by several varieties of anion transport proteins, one of which is shown (Fig. 3). Pathways for proton efflux include the Na^+-H^+ exchanger as well as various proton channels and pumps.

Regulatory mechanisms and receptor activation. Energy metabolism is largely regulated by cellular demand for ATP, which arises from diverse metabolic processes. In Fig. 3, the maintenance of transmembrane Na^+-K^+ gradients by means of Na^+, K^+-dependent adenosine triphosphatase is shown. The activation of a receptor can alter the rate of extracellular acidification by causing metabolic changes that affect demand for ATP. It can also act more directly at key regulatory points such as the Na^+-H^+ exchanger and glucose transport.

For a typical cultured mammalian cell such as a fibroblast, energy metabolism yields $\sim 10^8$ protons per second in steady state. Table 1 shows that the metabolism of all of the carbon sources commonly used in mammalian cell culture media leads to acidification. Glycolysis is by far the most acidifying process in terms of protons produced per turnover of an ATP molecule. Coupled to the fact that glycolysis is usually very active in cultured cells (in contrast to in vivo), this means that most of the protons excreted by cultured cells are usually of glycolytic origin. Data obtained with the microphysiometer to corroborate this are shown in Fig. 4A. Chinese hamster ovary–K1 (CHO-K1) cells maintained on glucose show high acidification rates that decrease significantly when the glucose is replaced by pyruvate or is simply removed from the medium.

The overshoot that occurs when pyruvate is replaced by glucose is evidence of a feature of the transport mechanisms of monocarboxylic acids: the ionized form cannot permeate a membrane, but the protonated form can be transported either by the monocarboxylic acid carrier or by unfacilitated diffusion. The addition of such weak acids extracellularly causes a pulse of alkalinization that is the result of the influx of the protonated form until transmembrane equilibrium is reached. The removal of the weak acid causes a pulse of acidification as the process is reversed. This effect is shown more clearly in Fig. 4B with oxamate, a nonmetabolizable analog of pyruvate.

The Na^+-H^+ exchange protein in the plasma membrane is an important and dynamically controlled regulatory mechanism for intracellular pH. The activity of this antiporter can be observed directly in the microphysiometer (Fig. 4C). Cells are incubated in media in which Na^+ is replaced with choline, which starves the Na^+-H^+

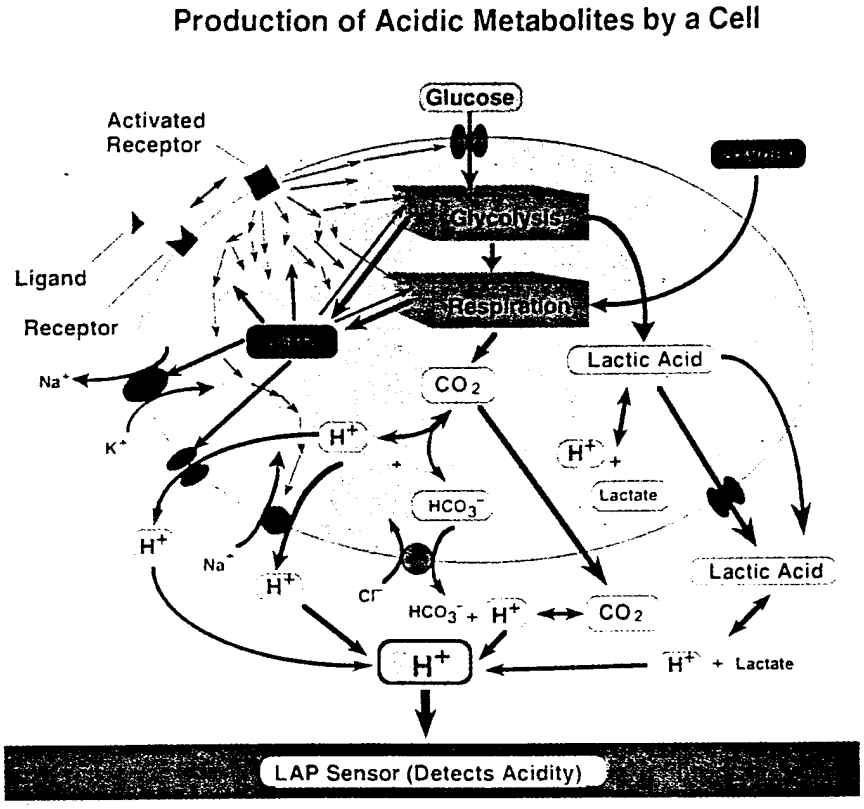

Fig. 3. The cell biology of extracellular acidification. The figure schematically shows the main features of cellular proton economy. Not all cells use all of the pathways shown in this composite figure.

Table 1. Proton yield per ATP molecule turned over during energy metabolism of representative carbon sources. ATP does not appear explicitly in the reactions because it was assumed that ATP synthesis and hydrolysis are tightly coupled. Because hydrolysis of one ATP molecule per second produces a substantial fraction of a proton, imbalances between ATP synthesis and hydrolysis can produce transient alterations in the rate of acidification.

Carbon source	Pathway	Reaction	ATP yield (per substrate molecule)	H^+ per ATP molecule
Glucose	Glycolysis	Glucose $\rightarrow$ 2 lactate$^-$ + 2 H^+	2	1.000
Glucose	Respiration	Glucose + 6 O_2 $\rightarrow$ 6 HCO_3^- + 6 H^+	36	0.167
Glutamine	Respiration	Glutamine + 9/2 O_2 + 3 H_2O $\rightarrow$ 5 HCO_3^- + 2 NH_4^+ + 3 H^+	27	0.111
Pyruvate	Respiration	Pyruvate$^-$ + 5/2 O_2 + H_2O $\rightarrow$ 3 HCO_3^- + 2 H^+	15	0.333

exchanger and causes an increase in intracellular proton concentration. When choline is replaced with Na^+, a large surge of extracellular acidification accompanies the reestablishment of homeostasis. This surge is nearly abolished by amiloride, an inhibitor of the Na^+-H^+ exchange system.

Applications

One of the major driving forces leading to the construction of the microphysiometer was the possibility of observing functional ligand receptor interactions by the monitoring of cellular metabolic rates. We have now demonstrated substantial cellular metabolic consequences that are the result of the triggering of a wide variety of receptors (Table 2). In the vast majority of ligand receptor combinations tested to date, functional receptor agonist interactions result in an increase in cellular acidification rates. There are some cases, however, where the opposite is true (6).

Table 2. Representative receptors for which acidification responses to triggering have been demonstrated in the microphysiometer. The table indicates the receptor, the superfamily to which the receptor belongs and the second messenger pathway activated by the receptor, whether the response was derived from receptors native to the cells or whether the response was derived from receptors transfected into the cells, and citations for the data. N.D., not done.

Receptor	Superfamily, pathway	Native	Transfected	Reference
m1 Muscarinic acetylcholine	G protein, inositol phosphate	N.D.	Yes	(*11*)
Muscarinic, subtype unknown	G protein	Yes	N.D.	(*18*)
β_2-Adrenergic	G protein, increasing cAMP	N.D.	Yes	(*11*)
Prostaglandin E	G protein, increasing cAMP	Yes	N.D.	(*19*)
Dopamine D1	G protein, increasing cAMP	No	Yes	(*20*)
Dopamine D2	G protein, decreasing cAMP	No	Yes	(*20, 21*)
Glutamate (kainate)	Excitatory amino acid, ion channel	Yes	N.D.	(*15*)
Insulin, insulin-like growth factor	Growth factor, tyrosine kinase	Yes	N.D.	(*22*)
Epidermal growth factor	Growth factor, tyrosine kinase	Yes	Yes	(*3, 11, 14*)
γ-Interferon	Hematopoietin	Yes	N.D.	(*23*)
Interleukin-2	Hematopoietin	Yes	N.D.	(*14*)
Interleukin-4	Hematopoietin	Yes	N.D.	(*23*)
GM-CSF	Hematopoietin	Yes	N.D.	(*8*)
T cell	T cell receptor	Yes	N.D.	(*14*)

Both the magnitude and the kinetics of the response depend on a variety of factors, including the type of receptor, the type of cell in which the receptor resides, the concentration of agonist, and the pretreatment of the cells before the introduction of agonist (7). Variations in the amplitude and kinetics of the cellular response as a function of different concentrations of granulocyte-macrophage colony-stimulating factor (GM-CSF) are illustrated in Fig. 5A. This response profile is typical of those receptors that affect cell proliferation. Low concentrations of agonist result in a gradual low-amplitude increase in acidification rate. As the agonist concentration is increased, the acidification amplitude increases and the time to reach the point of maximum acidification decreases. For the GM-CSF receptor, this response has been resolved into two components (8). The rapid component is a result of the activation of the Na^+-H^+ antiporter, and the slower is a result of the stimulation of glycolysis (9).

The diversity of responses obtained when different receptors are triggered is illustrated in Fig. 5B. The muscarinic acetylcholine (carbachol) response has a very rapid, transient component, and the maximum acidification rate is reached about 30 s after introduction of the agonist. The response decays rapidly thereafter, reaching a new plateau within a few minutes. In contrast, the response to nerve growth factor (NGF) reaches a maximum in a time that is approximately an order of magnitude longer and remains elevated for an extended peri-

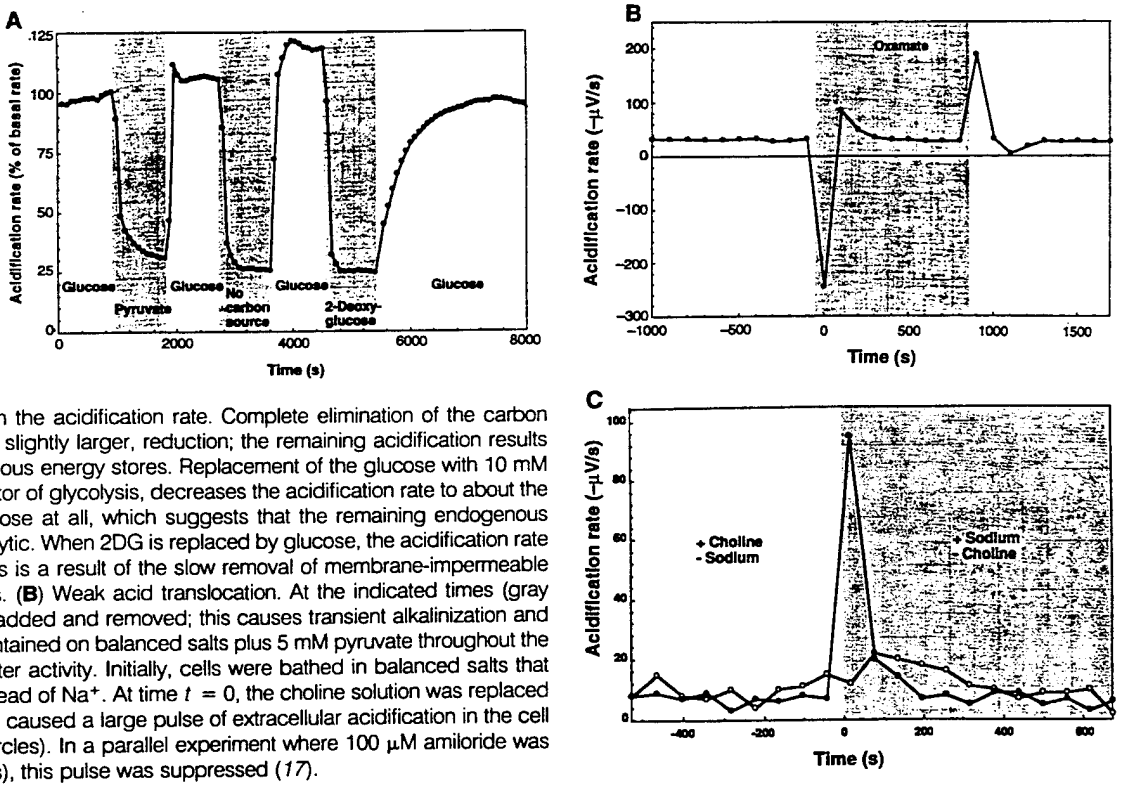

Fig. 4. Mechanisms of extracellular acidification. CHO-K1 cells were maintained in the microphysiometer in balanced salts plus the indicated carbon source. (**A**) Dependence of acidification rate on the carbon source. The replacement of 10 mM glucose by 10 mM pyruvate causes a rapid reduction in the acidification rate, which is rapidly reversible. These cells can use pyruvate as an energy source; the addition of pyruvate to glucose-containing medium also causes a significant decrease in the acidification rate. Complete elimination of the carbon source causes a similar, though slightly larger, reduction; the remaining acidification results from the metabolism of endogenous energy stores. Replacement of the glucose with 10 mM 2-deoxyglucose (2DG), an inhibitor of glycolysis, decreases the acidification rate to about the same level as that with no glucose at all, which suggests that the remaining endogenous metabolism is not strongly glycolytic. When 2DG is replaced by glucose, the acidification rate recovers slowly. Presumably, this is a result of the slow removal of membrane-impermeable 2DG-6-phosphate from the cells. (**B**) Weak acid translocation. At the indicated times (gray shading), 20 mM oxamate was added and removed; this causes transient alkalinization and acidification. The cells were maintained on balanced salts plus 5 mM pyruvate throughout the experiment. (**C**) Na^+-H^+ antiporter activity. Initially, cells were bathed in balanced salts that contained choline (130 mM) instead of Na^+. At time t = 0, the choline solution was replaced by normal balanced salts, which caused a large pulse of extracellular acidification in the cell chamber (denoted by closed circles). In a parallel experiment where 100 μM amiloride was present throughout (open circles), this pulse was suppressed (*17*).

od. A similar response rise time is observed for GM-CSF, but this response decays somewhat even in the continued presence of cytokine.

Fig. 5. Diversity of receptor responses to receptor activation. (**A**) Response versus ligand concentration. Cells from the human bone marrow cell line, TF-1, were loaded in four microphysiometer chambers. The cytokine GM-CSF was added to a final concentration of 0 ng/ml (open circles), 0.1 ng/ml (closed squares), 1 ng/ml (open squares), or 10 ng/ml (closed circles) during the period indicated by the shaded region. The acidification rates were all normalized to the average rate before the addition of cytokine. (**B**) Response characteristics of different receptors. The response of TE-671 rhabdomyosarcoma cells to 1 mM carbachol is rapid and multiphasic, and the multiphasic character of the response is reproducible. The responses of the PC-12 cells to NGF (100 ng/ml) and the response of TF-1 cells to GM-CSF (10 ng/ml) are an order of magnitude slower. The latter two responses differ in that the response to NGF is constant during a 30-min period whereas the response to GM-CSF decays to about 40% of maximum in a 30-min period.

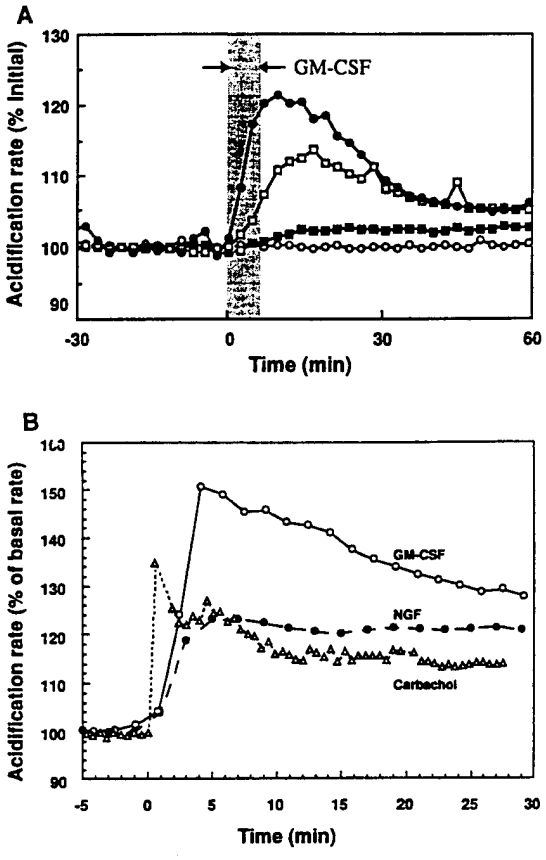

Fig. 6. Carbachol dose-response of CHO cells transfected with an m1 muscarinic acetylcholine receptor. (**A**) Extracellular acidification for sequential additions of increasing concentrations of carbachol. The transfected CHO cells were placed in the microphysiometer, and acidification rates were monitored every 2.5 min. Carbachol was introduced to the cells at the concentrations indicated in the figure for one measurement cycle per concentration (gray bars). (**B**) Amplitude of peak response versus carbachol concentration. The difference between acidification rate in the presence of carbachol and that immediately before each addition of carbachol was calculated, normalized to 100% for the largest response, and plotted as a function of carbachol concentration.

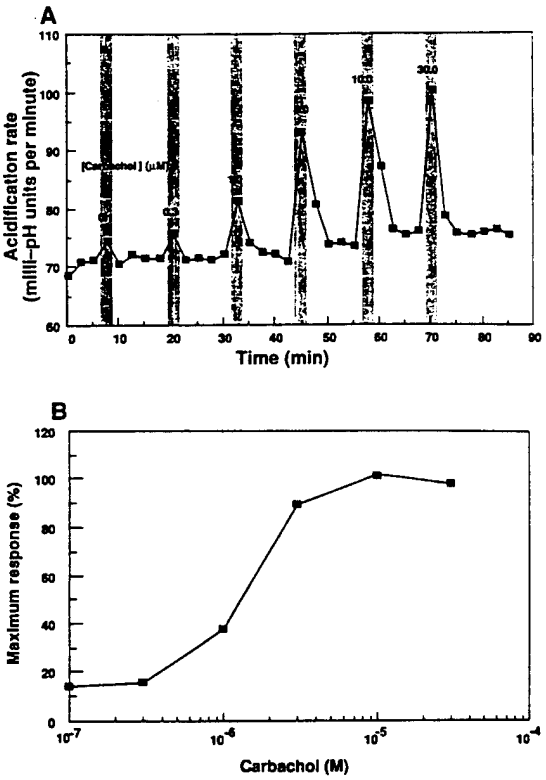

One task in the evaluation of potential pharmaceutical compounds is the determination of the efficacious concentration of the compound of interest. For receptor ligands, this is typically done with the introduction of the ligand to the cells at various concentrations and the measurement of the subsequent cellular response by biochemical assays for intermediates of second messenger pathways known to be activated by the receptor of interest. These experiments result in a dose-response curve that yields a characteristic concentration at which 50% of the maximal response is obtained (EC_{50}). Analogous experiments can be carried out in the microphysiometer. An example of the generation of a dose-response curve for a receptor agonist pair is given in Fig. 6. Here, the receptor is the rat m1 muscarinic acetylcholine receptor and the agonist is the nonhydrolyzable acetylcholine analog carbamylcholine (carbachol). The EC_{50} value for carbachol derived from this experiment is ~2 μM, which is in good agreement with the value of ~5 μM obtained by measurement of the phosphatidyl inositol hydrolysis as a function of carbachol concentration in the same cell line (*10*). We have previously reported the EC_{50} determined on the microphysiometer for triggering β-adrenergic receptors with isoproterenol (*11*). This value also compares favorably with values obtained with the use of adenosine 3′,5′-monophosphate (cAMP) measurements for the same receptor-ligand combination.

Because the acetylcholine receptor desensitizes with continued exposure to an agonist, it is necessary to limit exposure of the cells to the minimum time required to obtain a response if the same chamber of cells is to be used in order to generate the entire dose-response curve. An alternative approach is to place the cells in a set of chambers in parallel and expose them in each chamber to a different concentration of agonist. Although this approach is less efficient with regard to throughput, it is necessary for some receptor types. In the case of many of the growth factor receptors we have examined, the elevated metabolic response to a short bolus of growth factor may last for more than 1 hour (Figs. 5A and 7B). Under these conditions, the generation of dose-response curves by sequential addition of agonist to the same chamber of cells becomes impractical.

Figure 7 illustrates experiments designed to investigate second messenger pathways with the microphysiometer. Genistein inhibits tyrosine kinase activity. This effect is illustrated in Fig. 7A, where acidification that is the result of the triggering of the NGF receptor is inhibited by about 35% by typical inhibitory concentrations of genistein. The experiment illustrated in Fig. 7B was designed to determine which of several isoforms of protein kinase C is involved in the second messenger pathway triggered by GM-CSF receptors. Synthetic

antisense DNA specific for the ϵ isoform (and not the α isoform) was found to inhibit significantly the acidification response. The antisense treatment was demonstrated to diminish specifically the levels of the appropriate isoform by protein immunoblot analysis with isoform-specific antibodies (*12*).

Infection of cells with viruses often leads to major changes in cellular metabolism and eventually cell death. These metabolic changes can be monitored continuously in the microphysiometer. Figure 8A shows the effect of vesicular stomatitis virus (VSV) infection on the acidification rates of mouse fibroblasts (L cells). The control cells show a constant increase in acidification rate during the course of the experiment as a result of their normal rate of proliferation in the cell chamber. The addition of high concentrations of virus [ten plaque-forming units per L cell, or a multiplicity of infection (MOI) of 10] results in a decrease in the normal proliferative rate that can be seen in the first few hours. This is followed by a precipitous decline in acidification rate at ~9 hours after infection. As the effective dose of virus is decreased, the early effects on metabolic rate are decreased, and the time after infection at which the precipitous drop in acidification rate occurs is increasingly longer. The latter effect reflects the need for the virus to go through more replication cycles in order to infect the majority of the cells.

In contrast to the kinetics of VSV infection, the effect of human immunodeficiency virus–1 (HIV-1) infection on the acidification rate of CD4-transfected HeLa cells does not become apparent until several days after infection. Figure 8B shows the effect of administration of various concentrations of AZT (azidothymidine) on HIV-1–infected HeLa cells. The data are presented as the ratio of the acidification rates of infected cells to the acidification rates of uninfected cells. This is done to simplify the plot because the acidification rate of the uninfected cells increases over the 6-day period because of significant cell growth in the flow chambers. Microscopic examination of the infected cells removed from the cell chamber with no AZT on day 5 showed significant cytopathology, including the formation of syncytia that stained positive with antibodies to HIV (*13*). The general high sensitivity of acidification rate to cell physiology suggests that the microphysiometer may be used to screen for antiviral agents.

Conclusion

In general, robust acidification responses are observed for two large classes of receptors: the family of receptors with seven transmembrane helices (seven-helix) and the tyrosine kinase receptor family. Members of the seven-helix family studied include the β_2-adrenergic receptor and the m1 muscarinic acetylcholine receptor. The triggering of the β-adrenergic receptor by

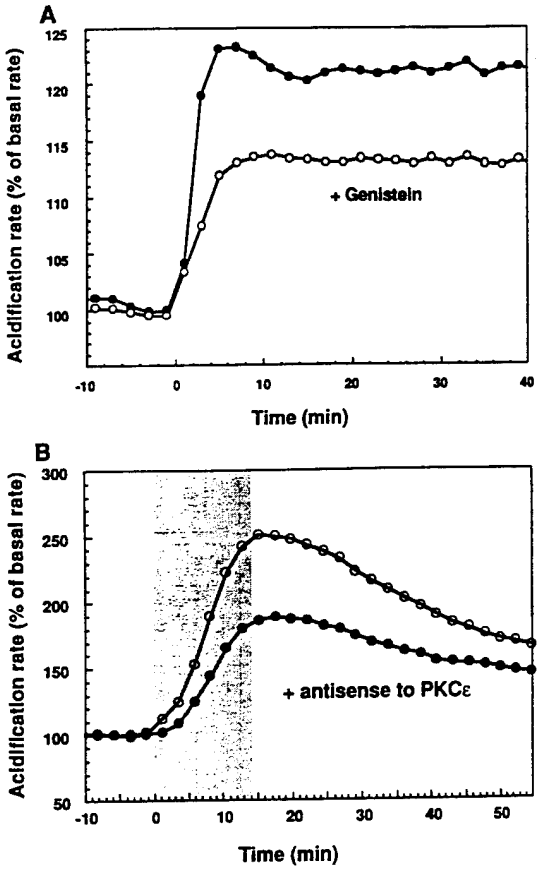

Fig. 7. Modulating second messenger pathways. (**A**) Effect of inhibiting tyrosine kinase activity on acidification response to NGF. PC-12 neuroblastoma cells were placed in two microphysiometer chambers. The medium that supplied the cells contained no additions (closed circles) or genistein (25 μg/ml) (open circles). NGF (100 ng/ml) was added at t = 0. (**B**) Effect of inhibition of protein kinase Cϵ (PKCϵ) activity on the acidification response to GM-CSF. TF-1 cells were maintained in culture for 9 days in the presence (closed circles) or absence (open circles) of 15 μM PKCϵ-antisense oligonucleotide. Cells were placed in the microphysiometer and triggered with GM-CSF (5 ng/ml) at t = 0.

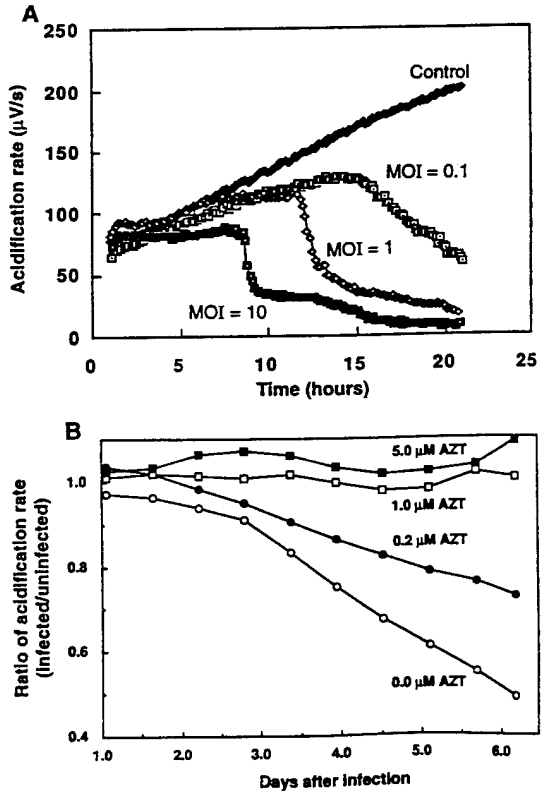

Fig. 8. Detection of viral cytopathology by the microphysiometer. (**A**) Effect of virus concentration. Mouse 929 L cells were incubated with the Indiana strain of VSV at an MOI of 0 (control), 0.1, 1, or 10 for 30 min at 5°C beginning at t = 0. The acidification rate of the cells was monitored in the microphysiometer at 37°C. (**B**) AZT inhibition of HIV-1 cytopathology. CD4-transfected HeLa cells were incubated with HIV-1 at an MOI of 1 for 1 hour at 37°C. The cells were then placed in the microphysiometer, and acidification rates were monitored for 6 days in four parallel chambers. The medium that flowed through the chambers contained AZT at the concentrations indicated in the figure. Acidification rates in (B) are presented as the ratio of the acidification rates of infected cells to those of uninfected cells.

epinephrine brings about a biochemical cascade that involves G proteins, adenylate cyclase, and protein kinase. The m1 muscarinic acetylcholine receptor also uses a G protein but stimulates phosphatidyl inositol hydrolysis and changes in K^+ conductance and can decrease cAMP levels. In view of the extensive biochemical changes that accompany agonist binding to these seven-helix receptors, it is perhaps not surprising that enhanced acidification is observed. We anticipate that large acidification rate enhancements will be observed for the majority of seven-helix receptors.

Robust acidification responses are also observed for tyrosine kinase receptors. Ligands for these receptors that result in such enhancements of acidification rates include insulin, epidermal growth factor, NGF, acidic fibroblast growth factor, GM-CSF, transforming growth factor–α, and complexes between major histocompatibility complex protein and peptide (*14*). The triggering of these receptors also leads to cascades of cellular biochemical events. In terms of monitoring the triggering of seven-helix receptors and tyrosine kinase receptors as well as screening for new receptor agonists, the microphysiometer appears to offer an efficient, convenient approach. The percentage increase in acidification rate that is the result of the triggering of many of these receptors is particularly large in the presence of glucose, which suggests a close linkage between receptor triggering and glycolysis (*8*).

A third category of receptors is the ligand-gated ion channels; examples include the nicotinic acetylcholine receptor and various glutamate receptors. The triggering of nicotinic acetylcholine receptors has not yet been detected with the Cytosensor; order-of-magnitude estimates of the ATP consumption required to pump out Na^+ ions after the triggering of this rapidly desensitizing receptor suggest that the resulting acidification may be close to the detection limit. There are a number of distinct glutamate receptors, as defined by the actions of various agonists. The triggering of the kainate (glutamate) receptor in fetal rat hippocampal neurons gives large responses in the microphysiometer (*15*).

The Cytosensor can be used to detect and analyze the triggering of a wide variety of plasma membrane receptors. It is thus of interest to consider possible applications of this instrumentation in basic research and in biotechnology. At present, it appears that the Cytosensor is ideal for screening for ligands of orphan receptors. Orphan receptors are putative receptors for which the specific ligands are not known. The β_3-adrenergic receptor may be an example of an orphan receptor of the seven-helix type. Many oncogene tyrosine kinases form a large class of orphan receptors; an example of a recently identified ligand of a tyrosine kinase receptor is heregulin, an activator of $p185^{erbB2}$ (*16*). It is likely that the sequencing of the human genome will uncover a large number of orphan receptors. Toward the discovery of the receptor ligands, it will be convenient to compare the responses of receptor-positive and otherwise identical receptor-negative cells (*11*). It should be possible to carry out such experiments with receptor-positive cells that have transient receptor transfections because the Cytosensor permits rapid bioassays to be made during the lifetime of the transfection. In some cases, the choice of the receptor-negative cell should be straightforward, but in other cases cotransfection of membrane-associated proteins, such as products of oncogenes, may be necessary.

Given a source of potential orphan receptor ligands, such as cell culture supernatants, the Cytosensor appears to have advantages over other instruments and methods for screening for these ligands. A conventional procedure for the discovery of new agonists and antagonists involves the displacement of radioactive ligands bound to plasma membrane receptors. This approach is obviously inapplicable in this case. Fluorometric detection of Ca^{2+} influx or release that is the result of ligand-receptor binding will miss cell triggering events that do not lead to changes in cytosolic Ca^{2+} concentration. [For example, the triggering of TF-1 cells by GM-CSF does not lead to a change in cytosolic Ca^{2+} concentration (*12*).] Changes in the state of membrane protein and cytosolic protein phosphorylation could undoubtedly be used to detect cell triggering by receptor ligands. However, it is difficult to imagine how this method could be used for large-scale screening in view of the radioactivity required or the associated tedious biochemical assays, or both. Inconvenience and lack of applicability for large-scale screening also apply to measurements of transmembrane potentials. Microphysiometers can be used quite generally to detect the triggering of a large number of plasma r mbrane receptors by specific ligands. This technique for the detection of cell triggering may have broad applicability in biotechnology and basic research in cell biology and may be particularly well suited to screen for the ligands of orphan receptors.

REFERENCES AND NOTES

1. J. Briggs and P. R. Panfili, *Anal. Chem.* **63**, 850 (1991).
2. D. G. Hafeman, J. W. Parce, H. M. McConnell, *Science* **240**, 1182 (1988).
3. J. W. Parce *et al.*, *ibid.* **246**, 243 (1989).
4. H. M. McConnell, P. Rice, H. G. Wada, J. C. Owicki, J. W. Parce, *Curr. Opin. Struct. Biol.* **1**, 647 (1991).
5. J. C. Owicki and J. W. Parce, *Biosens. Bioelectron.* **7**, 255 (1992).
6. For example, adrenergic agonists cause a significant decrease in acidification rate when added to the army worm ovary cell line Sf9 (B. Glaeser and S. Pitchford, personal communication).
7. The amplitude and kinetics of cell acidification response to receptor triggering depend on cell pretreatment. Because media frequently contain a variety of receptor ligands, the largest and most reproducible results are obtained with the use of cells that have been deprived of these factors for some period before the experiment. We have noted that when some cells are maintained in culture under normal growth conditions for extended periods of time, the amplitude and kinetics of the receptor-mediated acidification response can change. In contrast, cells maintained in the frozen state over extended periods give highly reproducible responses.
8. H. G. Wada *et al.*, *J. Cell. Physiol.*, in press.
9. In some experiments, it has been possible to separate in time acidification that is the result of receptor triggering and the onset of increased glycolytic rate through the sequential addition of receptor ligand and glucose.
10. C. M. Fraser, C. D. Wang, D. A. Robinson, J. D. Giocayne, J. C. Venter, *Mol. Pharmacol.* **36**, 840 (1989).
11. J. C. Owicki *et al.*, *Proc. Natl. Acad. Sci. U.S.A.* **87**, 4007 (1990).
12. G. T. Baxter *et al.*, unpublished results.
13. H. G. Wada, K. Fok, T. Nolan, W. Robinson, H. M. McConnell, paper presented at the National Institute of Allergy and Infectious Diseases Conference on Advances in Molecular Biology and Targeted Treatments for AIDS, Washington, DC, 14–18 May 1990.
14. B. Nag *et al.*, *J. Immunol.* **148**, 2040 (1992).
15. K. M. Raley-Susman, K. R. Miller, J. C. Owicki, R. M. Sapolsky, *J. Neurosci.* **12**, 773 (1992).
16. W. E. Holmes *et al.*, *Science* **256**, 1205 (1992).
17. P. Rice, thesis, Stanford University, Stanford, CA (1991).
18. D. L. Miller *et al.*, *FASEB J.* **5**, A1014 (1991).
19. J. W. Parce *et al.*, *Ann. Biol. Clin.* **48**, 639 (1990).
20. J. A. Salon *et al.*, *Soc. Neurosci. Abstr.* **17**, 86 (1991).
21. M. P. Rosser *et al.*, *ibid.*, p. 818.
22. P. A. Rice *et al.*, *FASEB J.* **5**, A1014 (1991).
23. S. R. Indelicato *et al.*, *Abstracts of the 5th International Conference on Immunopharmacology*, Tampa, FL, 27 to 30 May 1991.

24. We thank C. Venter and C. Fraser for helpful discussions concerning orphan receptors and P. Rice for some of the data in Fig. 3. Supported in part by the Defense Advanced Research Projects Agency, contract MDA972-92-C-0005.

Proc. Natl. Acad. Sci. USA
Vol. 92, pp. 2750–2754, March 1995
Immunology

Stimulation of T cells by antigen-presenting cells is kinetically controlled by antigenic peptide binding to major histocompatibility complex class II molecules

HARDEN M. MCCONNELL*†, H. GARRETT WADA‡, SUBHASHINI ARIMILLI§, KATHERINE S. FOK‡, AND BISHWAJIT NAG§

*Chemistry Department, Stanford University, Stanford, CA 94305-5080; ‡Molecular Devices Corporation, 1311 Orleans Drive, Sunnyvale, CA 94089; and §Anergen Incorporated, 301 Penobscot Drive, Redwood City, CA 94063

Contributed by Harden M. McConnell, December 7, 1994

ABSTRACT **Activation of CD4$^+$ T cells by antigenic peptide involves the interaction of major histocompatibility complex (MHC) class II–peptide complexes on the surface of antigen-presenting cells (APCs) with T-cell receptors. This report describes the kinetics of T-cell triggering by exogenous antigenic peptides in the presence of APCs. A rapid specific increase in extracellular acidification rate is observed within minutes upon exposure of A.E7 T cells (restricted for IE^k and moth cytochrome *c* peptide containing residues 88–103) and 4R3.9 T cells {restricted for IA^k and myelin basic protein peptide containing residues 1–14 [AcMBP-(1–14)]} to their cognate peptides in the presence of CH27 cells bearing both IA^k and IE^k MHC class II molecules. Pretreatment of cloned T cells, but not APCs, with herbimycin A resulted in complete inhibition of triggering events, indicating that the acidification response is mediated by T-cell second messenger pathways. This rapid assay for 4R3.9 T-cell stimulation showed increased T-cell triggering activity for AcMBP-(1–14)-A^4 and MBP-(1–14)-M^4 peptides compared to the native AcMBP-(1–14)-K^4. By using the previously determined kinetic constants for MBP-(1–14)-A^4 reactions with IA^k, it is possible to show that at the lowest peptide concentrations the kinetics of T-cell triggering are limited by the kinetics of the peptide binding to MHC class II molecules.**

The specific response of T-helper (T_H) lymphocytes to peptide antigens normally requires the participation of antigen-presenting cells (APCs) bearing class II molecules of the major histocompatibility complex (MHC) on their surfaces. A minimal requirement for T_H triggering is that a molecular complex (Mp) of peptide (p) and the class II molecule (M) form a trimolecular complex with the T-cell receptor (MpR). These trimolecular complexes are localized at the interface of T-cell and APC membranes. There is substantial interest in the physical chemical properties of these complexes. For example, it has been proposed that the avidities of class II molecule–peptide complexes for the T-cell receptor play a central role in positive and negative selection in the thymus and in the periphery (1). Another proposal is that weak binding of antigenic peptides to MHC class II molecules enables autoreactive T cells to escape negative selection and, thus, correlates weak binding to a number of autoimmune diseases (2, 3).

The two binding reactions can be represented schematically by the equilibria

$$M + p \rightleftharpoons Mp. \quad [1]$$

$$Mp + R \rightleftharpoons MpR. \quad [2]$$

The equilibrium (dissociation) constants K_1 and K_2 are then relevant to the above proposals.

$$K_1 = (M)(p)/(Mp). \quad [3]$$

$$K_2 = (Mp)(R)/(MpR). \quad [4]$$

In the present work, we show that insight into the role of these reactions in specific T_H triggering is achieved through measurements of this triggering at short times and low peptide concentrations. The parameter used to quantitate the early cellular response to T-cell triggering in the presence of APCs and antigenic peptide is the extracellular acidification rate as measured by a microphysiometer (4–6). Our analysis of these results requires knowledge of the *in vitro* rate and equilibrium constants for reaction **1**, which have been reported recently for the reaction of AcMBP-(1–14)-A^4 (where MBP is myelin basic protein) with affinity-purified IA^k in detergent (7). This work employs a kinetic analysis that minimizes problems related to the presence of endogenous peptides in MHC class II preparations and the inactivation of empty class II proteins. Such factors may be responsible for the differences reported (8, 9) in the kinetics of peptide binding to MHC molecules *in vitro* and on cell surfaces.

MATERIALS AND METHODS

Cell Culture and Preparation. IA^k-restricted 4R3.9 cloned mouse T cells (2.5×10^6 cells) specific for AcMBP-(1–14) peptide were cultured in RPMI medium 1640 containing 10% (vol/vol) fetal bovine serum (HyClone) in the presence of $0.75–8.0 \times 10^7$ freshly irradiated A/J splenocytes, recombinant human interleukin 2 (IL-2; Genzyme; 1 unit/ml), 26.6 μM AcMBP-(1–14), 10 mM Hepes, and 50 μM 2-mercaptoethanol in a final volume of 15 ml for 10 days. IE^k-restricted A.E7 cells were stimulated similarly every 20 days with freshly irradiated splenocytes from B10.A mice and pigeon cytochrome *c* at 5 μM. Prior to use in experiments, the cells were subjected to centrifugation once or twice in 19% (wt/vol) metrizamide to remove residual APCs, washed in RPMI medium 1640, and resuspended in medium containing 10% fetal bovine serum. T cells were used for experiments 10 days after antigen stimulation. CH27 cells, which express IA^k and IE^k molecules, were cultured in RPMI medium 1640 containing 10% fetal bovine serum and used in the microphysiometer as APCs. Both T cells and APCs were cultured in low-serum (2.5% fetal bovine serum) RPMI medium 1640 overnight prior to microphysiometer experiments.

The publication costs of this article were defrayed in part by page charge payment. This article must therefore be hereby marked "*advertisement*" in accordance with 18 U.S.C. §1734 solely to indicate this fact.

Abbreviations: MHC, major histocompatibility complex; APC, antigen-presenting cell; MCC, moth cytochrome *c*; MBP, myelin basic protein; T_H, T helper; % MEA, percent mean excess acidification; ED50%, the peptide concentration yielding 50% maximum stimulation; IL-2, interleukin 2.

†To whom reprint requests should be addressed.

Synthesis of Peptides. The rat MBP peptide AcMBP-(1–14)-K^4 and its analogs AcMBP-(1–14)-A^4 and AcMBP-(1–14)-M^4 with the sequences Ac-ASQKRPSQRHGSKY-NH_2, Ac-ASQARPSQRHGSKY-NH_2, and Ac-ASQMRPSQRHGSKY-NH_2, respectively, and the moth cytochrome *c* peptide containing residues 88–103 [MCC-(88–103)] with the sequence ANERADLIAYLKQATK-$CONH_2$ were synthesized by the standard solid-phase method with side-chain-protected Fmoc (*N*-9-fluorenylmethoxycarbonyl) amino acids and an Applied Biosystems 431A automated peptide synthesizer. The deprotected crude C-terminal peptide amides were purified by reverse-phase HPLC, and the homogeneity and identity of the purified peptides were confirmed by mass spectroscopic analysis.

Measurement of T-Cell Metabolic Acidification Rate. T cells were combined with APCs and loaded into Cytosensor microphysiometer cell capsules as described (6), by using low-melting-temperature agarose (Molecular Devices) to immobilize the cells. Briefly, the cells were rested from antigen stimulation for 10 days and both T cells and APCs were cultured in low-serum medium to lower their basal metabolic activity. The harvested cells were counted and mixed in serum-free loading medium (low-buffering RPMI medium 1640 containing 10 mM Hepes at pH 7.3) at a ratio typically of 10 T cells to 1 APC. The suspended cells were collected by centrifugation and resuspended at 1×10^6 T cells per 7.5 μl of loading medium. Low-melting-temperature agarose (Molecular Devices), melted and stored at 37°C, was added to the suspended cells to 2.5 μl per 7.5 μl of suspended cells, which were also held at 37°C. The agarose/cell mixture (10 μl) was immediately spotted into the center of the cell capsule cups (Molecular Devices) held in a 12-well culture plate, and 2 ml of loading medium was placed in the well, under the capsule cup. After 5 min, 0.3 ml of loading medium was placed in the capsule cup over the solidified agarose and a membrane insert was placed over the cells. The assembled cell capsule was loaded in the Cytosensor chamber maintained at 37°C and perfused at 50 μl/min with low-buffering RPMI medium 1640 containing endotoxin-free human serum albumin (Miles) at 1 mg/ml but no added Hepes or bicarbonate. Extracellular acidification measurements were made in the Cytosensor microphysiometer (Molecular Devices) as described by McConnell *et al.* (5) by collecting potentiometric measurements for 45 sec every 2 min. Acidification rate data (μV/sec) were normalized to 100% prior to cell stimulation, which allows for comparison of data from cells in separate chambers.

RESULTS

Resting mouse T-cell clones were immobilized in agarose in the presence of CH27 cells as APCs and exposed to peptides in the microphysiometer chamber to monitor their extracellular acidification rate. The method used to load the cells causes the close association of T cells with the APCs during a centrifugation step. The cells tend to aggregate at this step and remain in small clumps after resuspension, as observed by light microscopy. When exposed to their cognate peptide MCC-(88–103) at 100 μg/ml (55 μM), the A.E7 T cells were strongly activated resulting in an immediate increase in extracellular acidification rate peaking at 155% of basal rate within 5 min (Fig. 1*A*). The same cells exposed to AcMBP-(1–14)-K^4 at 100 μg/ml (60 μM) did not increase acidification rates significantly. The acidification rate increase required the presence of T cells, since the treatment of the APCs alone with the MCC peptide did not elicit the acidification rate increase. 4R3.9 T cells gave results that were consistent with the results obtained with A.E7 cells. When treated with AcMBP-(1–14)-K^4 at 100 μg/ml, the 4R3.9 cells gave a weaker increase, peaking at 108% of basal rate within 10 min of exposure to peptide (Fig. 1*B*). The weak response by 4R3.9 cells was shown to be specific

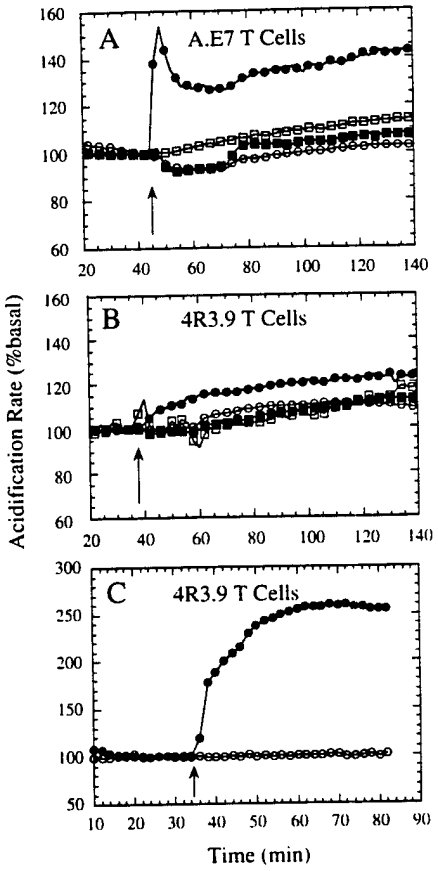

FIG. 1. Enhancement of T-cell extracellular acidification by specific peptides in the presence of APCs. Resting T cells 10 days after antigen stimulation and APCs were incubated overnight in low-serum medium and washed in serum-free low-buffering medium. T cells were mixed with APCs (CH27 cells) in a ratio of 10 T cells to 1 APC, pelleted, and resuspended in low-melting-temperature agarose for loading into Cytosensor chambers. T cells (1×10^6 cells) were monitored until basal acidification rates were stable and rates were normalized to 100% prior to exposure to peptides. (*A*) At the time indicated by the arrow, A.E7 T cells were exposed for 15 min to MCC-(88–103) at 100 μg/ml (55 μM) (●), AcMBP-(1–14)-K^4 at 100 μg/ml (60 μM) (■), or medium alone (□). A control chamber containing only APCs was exposed to MCC-(88–103) (○). (*B*) 4R3.9 T cells (1×10^6 cells) were monitored until basal acidification rates were stable. At the time indicated by the arrow, cells were exposed for 15 min to AcMBP-(1–14)-K^4 at 100 μg/ml (●) or MCC-(88–103) at 100 μg/ml (■). Control chambers containing only APCs (○) or only 4R3.9 T cells (□) were exposed to AcMBP-(1–14)-K^4. (*C*) 4R3.9 T cells prepared as described in *B* were exposed to AcMBP-(1–14)-A^4 at 100 μg/ml (62 μM) (●) or medium alone (○).

by the lack of response to MCC peptide at 100 μg/ml. Again, the presence of both 4R3.9 T cells and APCs is required for the acidification response to cognate peptide. This result agrees with our measurements of IA^k by flow cytometry that indicated no staining of 4R3.9 cells by anti-IA^k (data not shown). When 4R3.9 cells were treated with an analogue of the MBP-K^4 peptide AcMBP-(1–14)-A^4 at 100 μg/ml (62 μM), the acidification rate increase was much greater, increasing to 180% of basal rate within 5 min and peaking at 250% after 20 min (Fig. 1*C*). This is in agreement with the results from peptide-driven T-cell proliferation (2, 7) and the recent study of detergent-solubilized IA^k binding of MBP peptide analogues (7) that showed a marked increase in binding affinity for the A^4 analogue.

The effect of varying the ratio of T cells to APCs on the T-cell acidification response to cognate peptide was examined. In Fig. 2*A*, the 4R3.9 cellular response to AcMBP-A^4 was

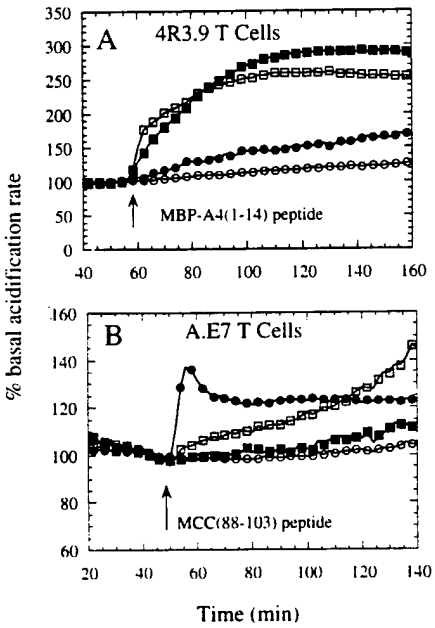

FIG. 2. Effect of T-cell/APC ratio on cell activation by peptides. 4R3.9 T cells and APCs were prepared as described in Fig. 1 and loaded into Cytosensor chambers for acidification rate monitoring. (*A*) The concentration of resting 4R3.9 T cells was held constant at 1×10^6 cells and the APC (CH27 cell) numbers were varied—1×10^5 APCs (10:1) (□), 1×10^4 APCs (100:1) (■), and 1×10^3 APCs (1000:1) (●). A control chamber containing T cells and 1×10^5 APCs was exposed to medium alone (○). T cells were monitored until basal acidification rates were stable, and rates were normalized to 100% prior to exposure to peptides. At the arrow, cells were exposed to AcMBP-(1–14)-A^4 at 1 μg/ml (0.62 μM) for 15 min, and the cells were monitored for enhanced acidification rate. (*B*) The concentration of resting A.E7 T cells was held constant (1×10^6 cells) and the APC (CH27 cell) numbers were varied—1×10^5 APCs (10:1) (●), 1×10^3 APCs (1000:1) (□), and 1×10^2 APCs (10,000:1) (■). A control chamber containing T cells and 1×10^5 APCs was exposed to medium alone (○). At the arrow, cells were exposed to MCC-(88–103) at 1 μg/ml (0.55 μM) for 15 min, and the cells were monitored for enhanced acidification rate.

measured at APC/T-cell ratios of 1:10, 1:100, and 1:1000. When the APC/T-cell ratio was 1:10, a very strong and rapid response to AcMBP-A^4 at 100 μg/ml (62 μM) was observed, which is similar to the response shown in Fig. 1*C*. At an APC/T-cell ratio of 1:100, the rate of increase of the acidification rate was slowed but the magnitude of increase was not decreased. This may be in part due to an increase in the component of the acidification rate, which is contributed by the T cells. Finally, at an APC/T-cell ratio of 1:1000, there was a large decrease in the magnitude of the peptide-induced increase in acidification rate, which indicates that the peptide–IA^k complex is limiting at this dilution. Similar results were obtained when the APC/T-cell ratio was varied by using A.E7 T cells and MCC peptide (Fig. 2*B*). When highly purified T cells were exposed to peptide in the absence of added APCs, as determined by flow cytometry (data not shown), no detectable stimulation in acidification rate was detected.

By using a constant APC/T-cell ratio, it was possible to titrate the peptide concentration required to activate T cells in the microphysiometer. Fig. 3*A* shows how A.E7 cells respond to MCC peptide at 10, 1, 0.1, and 0 μg/ml by presenting a dose–response curve. The peptide concentration corresponding to 50% maximum stimulation (ED50%) for this dose–response relationship was determined by interpolation from a plot of peptide concentration vs. the percent mean excess acidification (% MEA; 30 min) to be 30 nM (Fig. 4*A*). The % MEA is the average acidification rate of stimulated cells over

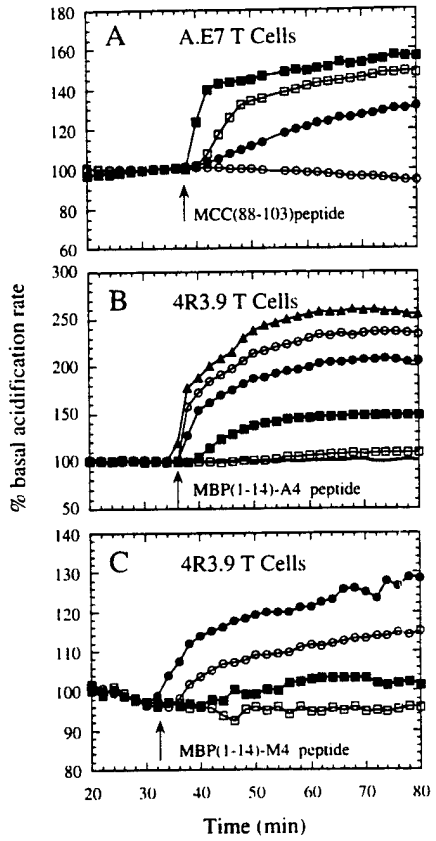

FIG. 3. Effect of peptide concentration on the acidification response of T cells. Resting T cells were prepared and loaded in Cytosensor chambers with APCs as described in Fig. 1. At the time indicated by the arrows, various doses of peptide were pumped onto the cells for 15 min, and the cells were monitored for acidification rate changes. The acidification rates were normalized to 100% prior to exposure to peptides. (*A*) A.E7 T cells were exposed to MCC-(81–104) at 0.01 μg/ml (5.5 nM) (●), MCC at 0.1 μg/ml (□), MCC at 1 μg/ml (■), or medium alone (○). (*B*) 4R3.9 T cells were exposed to AcMBP-(1–14)-A^4 at 0.01 μg/ml (6.2 nM) (□), AcMBP-A^4 at 0.1 μg/ml (■), AcMBP-A^4 at 1 μg/ml (●), AcMBP-A^4 at 10 μg/ml (○), AcMBP-A^4 at 100 μg/ml (▲), or medium alone (—). (*C*) 4R3.9 T cells were exposed to AcMBP-(1–14)-M^4 at 0.01 μg/ml (6 nM) (■), AcMBP-M^4 at 0.1 μg/ml (○), AcMBP-M^4 at 1 μg/ml (●), or medium alone (□).

a 30-min interval minus the average rate for unstimulated control cells and has been used to quantitate the sustained acidification rate response of TF-1 hemopoietic stem cells to granulocyte/macrophage colony-stimulating factor (10). It is interesting to note that the ED50% for the acidification rate response of A.E7 cells correlates very closely with the ED50% for IL-2 secretion of MCC-peptide-stimulated A.E7 cells reported by Critchfield *et al.* (11). These investigators observed that high doses of MCC peptide caused suppression of A.E7 proliferation but did not suppress IL-2 secretion, which plateaued at a high level at high peptide doses. This lack of high-dose suppression was observed here with the rapid T-cell acidification response (Fig. 4*A*). Thus, the acidification response of T cells corresponds to the initial signaling events, which lead to IL-2 secretion and do not necessarily result in cell proliferation.

Dose–response data were generated with 4R3.9 T cells and the AcMBP-A^4 peptide (Fig. 3*B*). The response of 4R3.9 cells to the AcMBP-A^4 peptide was much stronger than the response to the AcMBP-K^4 peptide, the native sequence but containing Lys-4. It was possible to interpolate an ED50% value of 360 nM from a linear plot of peptide concentration vs. % MEA (30 min) (Fig. 4*B*). The lower limit of detection was

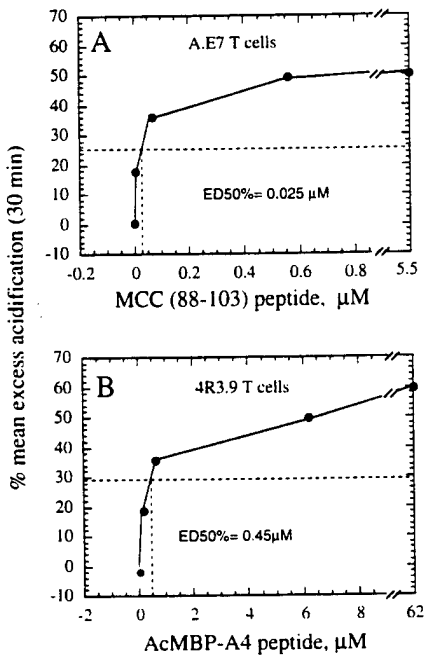

FIG. 4. Quantitation of T-cell acidification responses to peptide activation. The acidification rate increases triggered by specific peptides were quantitated by calculating the % MEA over a 30-min interval beginning at the initial time of exposure to peptide. This value is defined as the average acidification rate of stimulated cells over a 30-min interval minus the average acidification rate of unstimulated (control) cells over the same 30-min interval. (*A*) A.E7 T cells were exposed to MCC-(88–103) at 5.5, 0.55, 0.055, or 0.0055 μM, and the % MEA was determined. The ED50% was 0.025 μM. (*B*) 4R3.9 T cells were exposed to AcMBP-(1–14)-A^4 at 62, 6.2, 0.62, 0.062, or 0.0062 μM for 15 min, and the % MEA was determined for each of these concentrations. The ED50% was 0.45 μM.

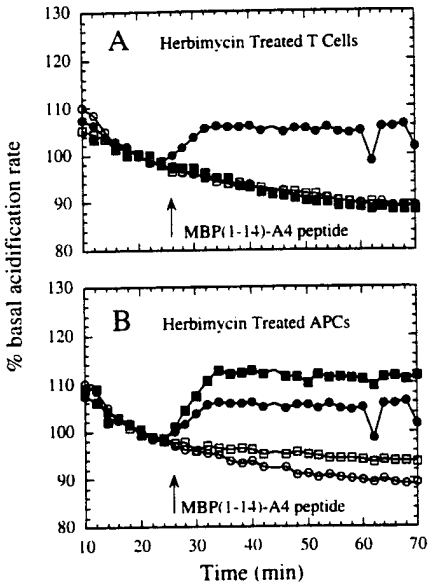

FIG. 5. Pretreatment of T cells with the tyrosine kinase inhibitor herbimycin A inhibits the peptide-activated acidification response. The effect of pretreatment of 4R3.9 T cells or APCs (CH27 cells) with herbimycin A was examined. Cells were cultured overnight in complete RPMI medium 1640 containing 2.5% fetal bovine serum and herbimycin A (0.5 μg/ml). Control cells were mock-treated in low-serum medium. (*A*) Herbimycin-treated T cells (1×10^6 cells) were mixed with 1×10^5 mock-treated APCs and loaded into Cytosensor chambers. At the arrow, AcMBP-(1–14)-A^4 at 1 μg/ml (■) or medium alone (□) was pumped onto the herbimycin-treated T cells for 15 min. Untreated T cells were also mixed with untreated APCs, loaded, and exposed to AcMBP-(1–14)-A^4 (●) or medium alone (○). (*B*) In the reciprocal experiment, herbimycin-treated CH27 cells (APCs) were mixed with mock-treated 4R3.9 T cells, loaded into Cytosensor chambers, and exposed to AcMBP-(1–14)-A^4 at 1 μg/ml (■) or medium alone (□). Again, untreated T cells were also mixed with untreated APCs, loaded, and exposed to AcMBP-(1–14)-A^4 (●) or medium alone (○). The cells were monitored for acidification rate responses, and the acidification rates were normalized to 100% prior to exposure to peptides.

6.2 nM for the AcMBP-A^4 peptide. The response of 4R3.9 cells to native AcMBP-K^4 was only detectable at 100 μg/ml (60 μM), the highest concentration tested, and it was not possible to determine an ED50% for this peptide. The response of 4R3.9 cells to the AcMBP-M^4 peptide was similar to the A.E7-cell response to MCC peptide in dose–response curves (Fig. 3*C*).

Because the microphysiometer chambers contain two populations of cells, T cells and APCs, and because the APCs (CH27 cells) were metabolically very active, with acidification rates severalfold higher than the T cells, it was important to determine whether the increase in acidification rate reflected T-cell or APC signaling and activation. For this reason, we examined the effect of inhibiting the signal transduction of the T cell by a protein tyrosine kinase inhibitor, herbimycin A (12). As shown in Fig. 5*A*, it is clear that pretreatment of 4R3.9 T cells with herbimycin completely blocks the peptide-triggered increase in acidification rate in the presence of untreated APCs. The reciprocal experiment using herbimycin-treated APCs with untreated T cells shows no inhibition of peptide-triggered acidification rate increase (Fig. 5*B*). Thus T-cell signaling and activation are required for the acidification response observed here, and APC signaling through tyrosine kinase is not required. It is possible that the B-cell metabolic activity contributes to the acidification increase; however, this must occur as a consequence of T-cell activation rather than as an independent response to ligation of class II molecules.

DISCUSSION

We have reported (6) that T_H-cell activation by peptide complexed with a purified detergent-solubilized MHC class II molecule is detectable by using microphysiometry. In the present work, we have found that this technique can also be used to study the early triggering of T_H cells by specific antigenic peptides in the presence of APCs. This has enabled the characterization of the early kinetics of T_H-cell activation that results from peptide binding to class II molecules and formation of the ternary complex of class II molecules, peptide, and T-cell receptor on the cell surfaces. At higher peptide concentrations, this early T-cell triggering is observed within 1 or 2 min after the introduction of specific peptide, and thus, intracellular events involving peptide processing are not significant. As discussed in *Results*, the enhanced acidification observed on the introduction of antigenic peptide is due to triggering of a second messenger pathway of the T_H cells. Of particular interest is the concentration dependence of the triggering of the 4R3.9 T_H cells by the AcMBP-(1–14)-A^4 peptide in the presence of APCs deploying the class II MHC molecules IA^k on their surfaces. That is, the equilibrium constant and reaction kinetics for the binding of AcMBP-A^4 to IA^k *in vitro* under conditions that avoid or minimize complicating effects due to dissociation of endogenous peptides and spontaneous inactivation of empty IA^k molecules have been determined (7). Thus, we can determine whether the observed triggering is limited by reaction **1**, the binding of AcMBP-A^4 to IA^k.

In discussing the acidification kinetics in Fig. 3*B*, we make the assumption that the acidification rate at time t and peptide concentration p is a unique function of $f = f(t, p)$, where f is the fractional occupation of the IA^k molecule by the MBP-

(1–14)-A^d peptide. If we further assume that f does not depend significantly on reaction **2** involving the T-cell receptor, then f can be calculated from the kinetics and equilibrium constant for reaction **1**, as reported (7). For reaction **1**, $k_{on} = 100$ $l \cdot M^{-1} \cdot sec^{-1}$, $k_{off} = 3.3 \times 10^{-4}$ sec^{-1}, and $K_1 = 3.3$ μM (7). The fractional occupation f is then,

$$f(t, p) = f(\infty, p)\{1 - \exp[-(k_{on}\, p + k_{off})t]\}. \quad [5]$$

To test this model, one needs to compare data points in Fig. 3*B* on the different curves for fixed values for the acidification rates—i.e., for points such that $f_c = f(t, p) = f(t', p') = f(t'', p'')$, etc. It is convenient to rewrite Eq. **5** as follows:

$$t(f_c, p) = [-1/(k_{on}\, p + k_{off})]\ln[1 - f_c/f(\infty, p)]. \quad [6]$$

Here $t(f_c, p)$ is the time required for the occupation of IA^k to reach a value $f = f_c$ when the peptide concentration is p.

At the lowest peptide concentration in Fig. 3*B*, 6.2 nM, $f(\infty, 6.2) \approx 2 \times 10^{-3}$. We may use Eq. **6** to determine the time t (2×10^{-3}, 62) at which the acidification rate for the 62 μM experiment should equal the acidification rate maximum for the 6.2 nM experiment. This is $t(2 \times 10^{-3}, 62) = 4.5$ min; it will be seen that this is remarkably close to the observed time, ≈5 min. A similar calculation for the time $t(2 \times 10^{-2}, 620)$ for acidification in the 620 nM experiment to reach the maximum acidification rate shown by the 62 nM experiment is also ≈5 min, in rough agreement with the experiment, as can be seen from Fig. 3*B*. We do not expect the one-to-one relation between f and acidification rate to hold at the largest values of f and acidification rates. Comparisons of different experiments by using Eq. **6** do show observed and calculated times $t(f_c, p)$ that are always within an order of magnitude of one another. Thus, we conclude that the assumptions leading to Eqs. **5** and **6** are plausible. In particular, reaction **2** does not drive peptide binding to be much stronger than the equilibrium constant K_1. This conclusion is consistent with the relatively weak reported binding of MHC–peptide complexes to T-cell receptors (13–16). It is also clear from our results that the kinetics of the T-cell (acidification) response is determined by the kinetics of the reaction between the MBP-(1–14)-A^d peptide and IA^k on the cell surface, particularly at the lower peptide concentrations.

There may be a discrepancy between the A.E7 T-cell response to the MCC-(88–103) peptide given in Fig. 3 and the rate constant reported for binding of this peptide to purified IE^k, 3 $l \cdot M^{-1} \cdot sec^{-1}$ at pH 7 (17). In Fig. 3*A* there is a detectable T-cell response at 4 min for MCC-(88–103) at 5.5 nM, for which we estimate that an upper limit to the fraction occupancy f is only 0.0004%. This corresponds to slightly less than one IE^k molecule occupied if there are 50,000 IE^k available molecules on the surfaces of the APCs. The origin of this discrepancy is not known but may be due to the presence of endogenous peptide in the IE^k molecules in the experiments of Reay *et al.* (17), which would give an artificially low kinetic binding constant. Of course there should be a Poisson distribution of bound peptides that may contribute to cell triggering, but f is very small and a simple calculation shows that the number of cells with more than one peptide is extremely small. Another possibility is that reaction **2** does enhance peptide binding to IE^k.

The off-rate constant for the dissociation of MBP-(1–14)-A^d from IA^k is unusually fast, and it is this corresponding lifetime that dominates the acidification kinetics at low peptide concentration. Most known peptide–class II MHC dissociation rates are very much slower, so we anticipate the possibility of significant differences in T-cell triggering at low peptide concentration for these other systems.

We thank Jeff Libby for providing the method and materials for immobilizing cells in agarose. We are indebted to Pat Jones and Ron Schwartz for the cell lines used in this work and thank Bart Beverly for his help in maintaining them. We also thank Mark Davis for helpful discussions concerning the reactions of MCC-(88–103) with IE^k. This work was supported in part by Defense Advanced Research Projects Agency Contract MDA972-92-C-0005 and by National Institutes of Health Grant 4R37 AI13587-19.

1. Ashton-Rickardt, P. G. & Tonegawa, S. (1994) *Immunol. Today* **15**, 362–366.
2. Fairchild, P. J., Wildgoose, R., Atherton, E., Webb, S. & Wraith, D. C. (1993) *Int. Immunol.* **5**, 1151–1158.
3. Joosten, I., Wauben, M. H. M., Holewijn, M. C., Reske, K., Pedersen, L. Ø., Roosenboom, C. F. P., Hensen, E. J., van Eden, W. & Buus, S. (1994) *Int. Immunol.* **6**, 751–759.
4. Parce, J. W., Owicki, J. C., Kercso, K. M., Sigal, G. B., Wada, H. G., Muir, V. C., Bousse, L. J., Ross, K. L., Sikic, B. I. & McConnell, H. M. (1989) *Science* **246**, 243–247.
5. McConnell, H. M., Owicki, J. C., Parce, J. W., Miller, D. L., Baxter, G. T., Wada, H. G. & Pitchford, S. (1992) *Science* **257**, 1906–1912.
6. Nag, B., Wada, H. G., Fok, K. S., Green, D. J., Sharma, S. D., Clark, B. R., Parce, J. W. & McConnell, H. M. (1992) *J. Immunol.* **148**, 2040–2044.
7. Mason, K. & McConnell, H. M. (1994) *Proc. Natl. Acad. Sci. USA* **91**, 12463–12466.
8. Ceppellini, R., Frumento, G., Ferrara, G. B., Tosi, R., Chersi, A. & Pernis, B. (1989) *Nature (London)* **339**, 392–394.
9. Christinck, E. R., Luscher, M. A., Barber, B. H. & Williams, D. B. (1991) *Nature (London)* **352**, 67–70.
10. Wada, H. G., Indelicato, S. R., Meyer, L., Kitamura, T., Miyajima, A., Kirk, G., Muir, V. C. & Parce, J. W. (1993) *J. Cell. Physiol.* **154**, 129–138.
11. Critchfield, J. M., Racke, M. K., Zúniga-Pflücker, J. C., Cannella, B., Raine, C. S., Goverman, J. & Lenardo, M. J. (1994) *Science* **263**, 1139–1143.
12. June, C. H., Fletcher, M. C., Ledbetter, J. A., Schieven, G. L., Siegel, J. N., Phillips, A. F. & Samelson, L. E. (1990) *Proc. Natl. Acad. Sci. USA* **87**, 7722–7726.
13. Weber, S., Traunecker, A., Oliveri, F., Gerhard, W. & Karjalainen, K. (1992) *Nature (London)* **356**, 793–796.
14. Matsui, K., Boniface, J. J., Reay, P. A., Schild, H., Fazekas de St. Groth, B. & Davis, M. M. (1991) *Science* **254**, 1788–1791.
15. Corr, M., Slanetz, A. E., Boyd, L. F., Jelonek, M. T., Khilko, S., Al-Ramadi, B. K., Kim, Y. S., Maher, S. E., Bothwell, A. L. M. & Margulies, D. H. (1994) *Science* **265**, 946–949.
16. Matsui, K., Boniface, J. J., Steffner, P., Reay, P. A. & Davis, M. M. (1994) *Proc. Natl. Acad. Sci. USA* **91**, 12862–12866.
17. Reay, P. A., Wettstein, D. A. & Davis, M. M. (1992) *EMBO J.* **11**, 2829–2839.

Cholinergic stimulation of the Na^+/K^+ adenosine triphosphatase as revealed by microphysiometry

Donald L. Miller, John C. Olson, J. Wallace Parce, and John C. Owicki
Molecular Devices Corporation, Menlo Park, California 94025 USA

ABSTRACT The activation of a wide range of cellular receptors has been detected previously using a novel instrument, the microphysiometer. In this study microphysiometry was used to monitor the basal and cholinergic-stimulated activity of the Na^+/K^+ adenosine triphosphatase (ATPase) (the Na^+/K^+ pump) in the human rhabdomyosarcoma cell line TE671. Manipulations of Na^+/K^+ ATPase activity with ouabain or removal of extracellular K^+ revealed that this ion pump was responsible for 8.8 ± 0.7% of the total cellular energy utilization by those cells as monitored by the production of acid metabolites. Activation of the pump after a period of inhibition transiently increased the acidification rate above baseline, corresponding to increases in intracellular $[Na^+]$ ($[Na^+]_i$) occurring while the pump was off. The amplitude of this transient was a function of the total $[Na^+]_i$ excursion in the absence of pump activity, which in turn depended on the duration of pump inhibition and the Na^+ influx rate. Manipulations of the mode of energy metabolism in these cells by changes of the carbon substrate and use of metabolic inhibitors revealed that, unlike some other cells studied, the Na^+/K^+ ATPase in TE671 cells does not depend on any one mode of metabolism for its adenosine triphosphate source. Stimulation of cholinergic receptors in these cells with carbachol activated the Na^+/K^+ ATPase via an increase in $[Na^+]_i$ rather than a direct activation of the ATPase.

INTRODUCTION

We recently have found that the activation of a wide variety of cellular receptors promptly leads to a significant increase in the rate at which cultured cells acidify their environment (1–4). The amplitude and kinetics of the effect vary with the receptor and cell type but typically involve a 10–100% increase in acidification rate within seconds to minutes after the application of agonist. To measure extracellular acidification rates, we have used the microphysiometer, an instrument that applies contemporary silicon technology to quantitative cell biology. The instrument uses a potentiometric semiconductor-based sensor to detect pH changes adjacent to cultured cells in a microvolume flow chamber.

At present, our understanding of the receptor pharmacology of the phenomena is greater than our understanding of the intracellular mechanisms that couple receptor activation to proton flux. The primary motivation for the present study was to gain such mechanistic information. A secondary goal was to determine whether microphysiometry could be a useful tool for cell-biology studies involving ion pumps, since it has the attractive properties of being noninvasive and providing data in real time.

What is known about how receptor activation changes the rate of extracellular acidification? In some cases, receptor activation increases the activity of the Na^+/H^+ antiporter system, causing a transient increase in extracellular acidification rate and concomitant increase in intracellular pH (5, 6). However, the most generally important source of sustained changes in extracellular acidification rate is changes in the rate of energy metabolism. The synthesis and subsequent hydrolysis of adenosine triphosphate (ATP) produce acid, typically in the form of lactic acid and CO_2. This statement is true for the carbon sources most commonly used by mammalian cells, and it holds for both glycolysis and oxidative metabolism. For a review, see Owicki and Parce (7).

The rate of energy metabolism might sometimes be increased on receptor activation by a direct modification of the activity of key regulatory enzymes involved in energy metabolism. There is evidence for this (6, 8). The rate also might be raised by increases in the rates of processes that consume ATP. In this article we examine one such process, the maintenance of the Na^+ and K^+ gradients across the plasma membrane by the Na^+/K^+ ATPase, also called the Na^+/K^+ pump. This pump, which ejects three Na^+ from the cell and imports two K^+ at the cost of one ATP hydrolyzed, is a major sink of free energy in many cell types (see the review by Clausen et al. [9]).

Using a muscle tumor cell line (the rhabdomyosarcoma TE671) as a model system, we first show that it is possible to use the microphysiometer to detect the activity of the Na^+/K^+ pump. This involves examining the coupling, through ATP turnover, between the intracellular sodium-ion concentration ($[Na^+]_i$) and extracellular acidification. Because of reports that in some cells the Na^+/K^+ pump is preferentially fueled either by glycolysis or oxidative respiration, we then investigate the effects of changes in the mode of energy metabolism on pump activity. Next, we demonstrate that part of the increase in extracellular acidification rate on activation of cholinergic receptors in TE671 cells is due to increased activity of the Na^+/K^+ pump. Finally, we present evidence that the increased pump activity results from a receptor-mediated increase in $[Na^+]_i$ rather than some more direct regulation of the pump activity.

MATERIALS AND METHODS

Materials

Culture medium was obtained from Irvine Scientific (Santa Ana, CA). The Na^+ indicator sodium-binding benzofuran isophthalate (SBFI) acetoxymethyl ester, as well as Pluronic F-127, were from Molecular Probes (Eugene, OR). All other chemicals were obtained from Sigma (St. Louis, MO).

Address correspondence to John C. Owicki.

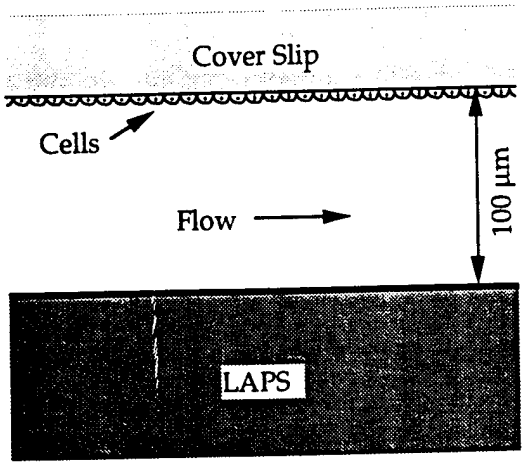

FIGURE 1 Cross-sectional view of the microphysiometer chamber. See text in Materials and Methods.

Cell culture

Cells of the adherent human rhabdomyosarcoma cell line TE671 were obtained from the American Type Culture Collection (Rockville, MD; line CRL8805). Cells were cultivated in Dulbecco's modified Eagle's medium supplemented with 2 mM glutamine, 10 mM glucose, 10% horse serum, 5% fetal calf serum, 100 U/ml penicillin, 100 μg/ml streptomycin, and buffered with bicarbonate. Cells were maintained at 37°C in 95% air/5% CO_2. Cultures were plated routinely at densities of 200/mm^2 in T-75 flasks, or onto either 12-mm-diameter cover slips coated with indium-tin oxide or uncoated 25-mm-diameter cover slips, in 12- or 6-well tissue-culture trays, respectively. The oxide-coated cover slips were used in the microphysiometer, and there were no apparent differences between cells grown on uncoated or oxide-covered cover slips. Cells were used at 90–100% confluence.

Solutions

Unless otherwise noted, all experiments were performed in the following medium, comprising balanced salts plus glucose (mM): NaCl, 138; KCl, 5; $MgCl_2$, 0.5; Na_2HPO_4, 0.81; NaH_2PO_4, 0.11; $CaCl_2$, 1.3; and glucose, 10, pH 7.4. The phosphate concentration in this solution was low to make the buffer capacity low and thus facilitate measurement of acidification rates. In experiments using pyruvate salts, the glucose was replaced by 10 mM pyruvate and 2 or 5 mM 2-deoxyglucose (2-DG).

The microphysiometer

As shown in Fig. 1 and described in more detail by Parce et al. (10) and McConnell et al. (4), the microphysiometer is based on a microflow chamber in which cells are in diffusive contact with a semiconductor-based pH sensor, the light-addressable potentiometric sensor (LAPS) (11). In this version of the instrument, the ceiling of the flow chamber was a glass cover slip that had been rendered conductive with a coating of indium-tin oxide, to which cells adhered. The sensor formed the floor of the chamber. The dimensions of the fluid channel were 100 μm high by 3.5 mm wide by 12 mm long, or 4 μl in volume. Other versions of the microphysiometer, not used in this study, use flow chambers in which the cells are retained between two microporous polycarbonate membranes rather than attached to cover slips.

The LAPS essentially reports a surface potential at the electrolyte/sensor interface that depends on pH in a Nernstian fashion (61 mV per pH unit change at 37°C). There are three electrical connections: to the base of the LAPS, to a control electrode (the conducting surface of the cover slip), and to a reference electrode downstream from the chamber. There is negligible direct current in the system. The surface potential is determined only at regions of the sensor illuminated by a light source that is intensity modulated at 5 kHz, and so the sensor signal is carried in the amplitude of a weak 5 kHz photocurrent. Since the illuminated region is only ~3 mm^2, data were obtained from a 300-nl portion of the flow chamber.

The flow of culture medium, as well as selection of fluid stream and data acquisition, was controlled by a personal computer. Extracellular acidification rates were determined as the rate of change of sensor output during periodic interruptions of fluid flow, which cause transient acidifications of <0.1 pH unit. Generally fluid flow alternated off and on (100 μl/min) for equal 15-s periods. One microvolt per second corresponds closely to an acidification rate of $-1 \cdot 10^{-3}$ pH/min. Results are reported in microvolts per second or, in the case where different chambers are directly compared, as normalized acidification rate. The latter takes into account variations in acidification rates among

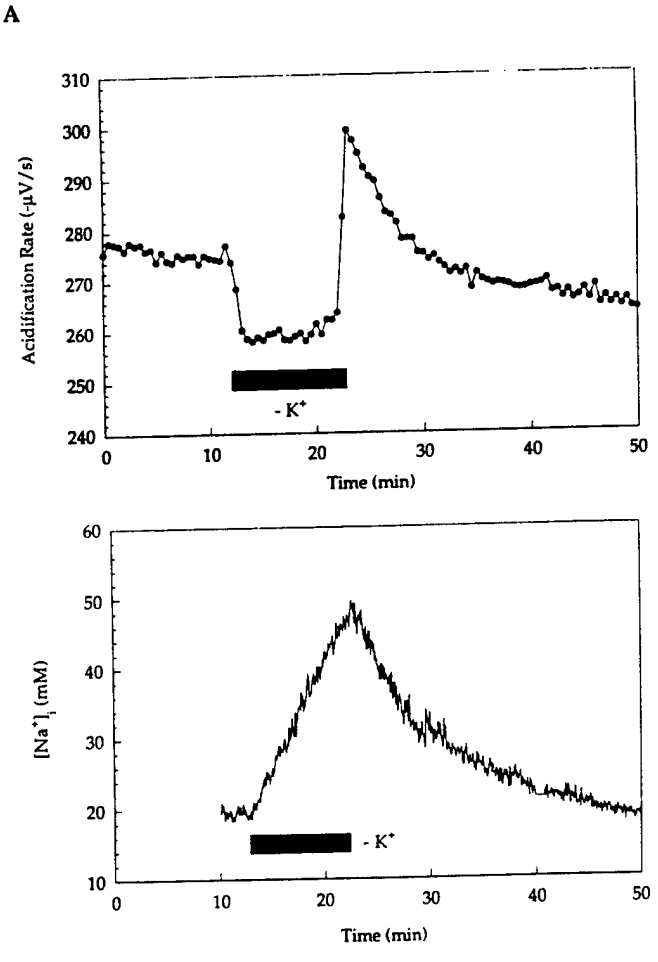

FIGURE 2 Inhibiting the Na^+/K^+ ATPase by removing extracellular K^+ changed the extracellular acidification rate. (*A*) Removal of extracellular K^+ decreased the acidification rate, and replacement of the K^+ after 10 min caused an overshoot that decayed to the original basal acidification rate. (*B*) Measurement of $[Na^+]_i$ verified that inhibiting the Na^+/K^+ ATPase caused the accumulation of Na_i^+. The kinetics of decay to basal $[Na^+]_i$ after extracellular K^+ was replenished were similar to those for the return to basal acidification rate in *A*.

chambers resulting from differing absolute numbers of cells in those chambers.

Intracellular Na^+

TE671 cells growing on 25-mm cover slips were incubated for 1 h at 37°C in medium augmented with 10 mM *N*-2-hydroxyethylpiperazine-*N'*-2-ethane sulfonic acid, containing 4 μM SBFI mixed beforehand in a 1:1 suspension with a 25% wt/vol solution of Pluronic F-127/dimethyl sulfoxide. The cover slip was then transferred to a petri dish containing fresh medium and incubated for another 30 min to allow complete de-esterification of the dye.

The cover slip was then transferred to a thermostatically controlled (37°C) closed perfusion chamber with a fluid flow path 100 μm in height by 3.4 mm across, and perfused at a rate of 50 μl/min. A switching valve placed before the chamber allowed changeover of solution in the chamber within 30 s. The geometry of the chamber, the mean flow rate, and the perfusate solutions were essentially identical to those of the microphysiometer chamber. The chamber was placed on the stage of an inverted microscope (Diaphot: Nikon Inc., Melville, NY) for viewing and fluorescence measurements.

Fluorescence was measured in a Photon Technology Inc. (model 4000; Deltascan, South Brunswick, NJ) dual-excitation spectrofluorometer. The excitation monochromators were set at 350 and 385 nm (bandwidth of 1 nm), and the fluorescence was measured at 510 nm (bandwidth 20 nm) as the ratio of the intensities resulting from excitation at 350 and 385 nm. Calibrations were usually performed at the end of each experiment, except where dye loss made calibration impossible. Calibrations were performed using the high-K^+ technique of Negulescu et al. (12), with calibration salts of 0, 20, 30, 50, and occasionally 100 mM Na^+ containing 10 μM gramicidin D. We have made no corrections for nonideality or for buffering of $[Na^+]_i$ by the fluorophore: neither should be an important effect, and so Na^+ levels are reported as concentrations. Backgrounds were initially determined by fluorescence measurements of unloaded cells, and in later experiments simply by removal of the experimental cells within the chamber via fast perfusion with distilled water (there was no significant cell autofluorescence).

The field measured typically contained ~100 cells. Thus, the signal measured was an average response of all the cells in the field, as for the microphysiometer measurements.

RESULTS AND DISCUSSION

Effects of K-free solutions and ouabain

TE671 cells were placed in the microphysiometer and perfused with medium. When the solution bathing the cells was switched to K^+-free medium to inhibit the Na^+/K^+ adenosine triphosphatase (ATPase), the acidification rates of the cells dropped quickly (<30 s) by 8.8 ± 0.7% (mean ± SEM, $n = 83$) (Fig. 2 *A*). The magnitude of the drop corresponds to the steady-state activity of the Na^+/K^+ ATPase in the balanced salt solution, which most likely is rate limited by the intrinsic "leakiness" of the cells to Na^+. This "leakiness" is the sum of all inward fluxes of Na^+, including Na^+-coupled transport, Na^+ channels, and passive membrane permeabilities. Upon restoration of extracellular K^+, the acidification rates rose quickly to values higher than those obtained before removal of K^+. The rates then decayed to the original values with an approximately exponential time course ($t_{1/2} = 272 \pm 6.5$ s, $n = 66$).

One possible explanation for this transient elevation of acidification rate is that $[Na^+]_i$ may have increased during the period in which the Na^+/K^+ pump was inhibited. Restoration of extracellular K^+ would then have resulted in increased ATP hydrolysis and corresponding increased extracellular acidification, until the normal $[Na^+]_i$ was restored. To test this hypothesis, $[Na^+]_i$ was monitored with SBFI in TE671 cells, while K^+ was transiently removed from the bathing medium. Fig. 2 *B* shows that a steady rise in $[Na^+]_i$ (~3 mM/min) occurred in the absence of extracellular K^+. Replacement of K^+ caused the $[Na^+]_i$ to return to its original value, presumably due to increased activity of the Na^+/K^+ pump. The excess $[Na^+]$ in the cell decayed with an approximately exponential time course ($t_{1/2} = 287 \pm 28$ s, $n = 16$).

The similarity of the kinetics of the return to baseline of the two processes upon replacement of K^+ indicates close coupling between acidification-rate changes and ATP-flux changes in the cells resulting from changes in the Na^+/K^+ ATPase activity. These results are quite consistent with those of other workers who have studied the effects of ouabain or K^+ removal on voltage-clamped currents (13–18). In those studies the authors looked at the current resulting from the electrogenic Na^+/K^+ pump as a fraction of the total current, analogous to our looking at the fraction of the total cellular acidification rate corresponding to the Na^+/K^+ pump activity. The metabolic analogue of the holding voltage is the cellular maintenance of a steady-state ATP level.

Although the removal of K^+ from the bathing salts is expected to inhibit the Na^+/K^+ ATPase, it may have other effects, such as a membrane hyperpolarization, that could cause changes in metabolism and thus affect acidification rates of the cells. Another way to block Na^+/K^+ ATPase activity is to use the inhibitor ouabain. As shown in Fig. 3 *A*, ouabain caused a drop in acidification rate (8%) similar to that caused by K^+ removal. Removal of ouabain resulted in a slow recovery of acidification rate, consistent with the slow rate of dissociation of ouabain from the enzyme (18). Clearly the dominant effect of removal of K^+ from the medium on the acidification rate was due to inhibition of the Na^+/K^+ ATPase. If in fact the overshoot in acidification rate upon K^+ replacement were due to enhanced Na^+/K^+ ATPase activity, then this overshoot should be inhibited by ouabain. Fig. 3 *B* shows that if ouabain was present while K^+ was reapplied to the salts after its removal for 10 min, the reactivation of acidification was indeed inhibited. Thus, both the decrease in acidification rates after removal of extracellular K^+ and the overshoot upon its replacement appear to provide a real-time measure of the Na^+/K^+ ATPase activity.

Effects of changes in $[Na^+]_i$ and Na^+ permeability, p_{Na}

Another approach to demonstrate the tight coupling between the extracellular acidification rate and Na^+/K^+ pump activity is to modulate the enzyme's activity by

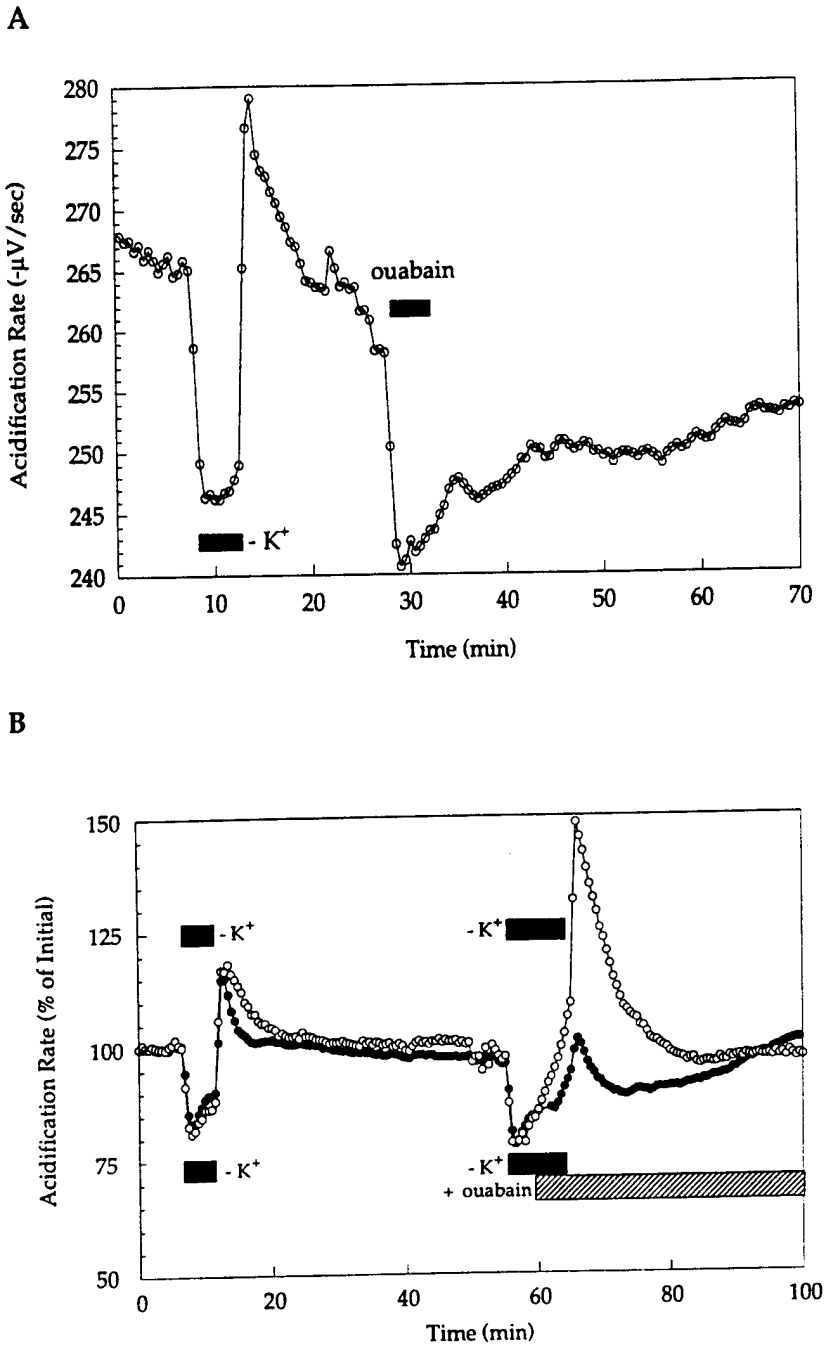

FIGURE 3 Ouabain and the removal of extracellular K^+ decreased acidification rates to similar extents, and ouabain blocked the acidification overshoot when K^+ was restored. (*A*) Extracellular K^+ was removed for 5 min, causing the acidification rate to decrease and then overshoot, as in Fig. 2 *A*. Subsequent application of 100 μM ouabain for 5 min caused a similar decrease that recovered slowly after ouabain removal, presumably due to the slow unbinding kinetics of ouabain. (*B*) In one chamber (*open circles*), extracellular K^+ was removed for first 5 min and then 10 min. In a second chamber (*closed circles*), K^+ was removed in the same fashion, but 100 μM ouabain was introduced midway through the second K^+ deprivation and remained present through the end of the experiment. Ouabain inhibited the overshoot in acidification rate, which suggests that the overshoot represents the energetic consequences of Na^+/K^+ pump activity rather than some other effect of K^+ deprivation. The rise in acidification rates during long periods of K^+ deprivation may be related to increases in $[Na^+]_i$.

changing $[Na^+]_i$. Fig. 2 *B* demonstrates that $[Na^+]_i$ can be varied by controlling the time cells are exposed to K^+-free medium. Therefore, the overshoot in acidification rates upon K^+ restoration should vary with the amount of time K^+ was withheld from the cells.

Fig. 4 *A* shows acidification rates in four chambers run in parallel with cells treated identically. The responses to increasing periods of exposure to K^+-free medium were quite similar among the four chambers: the amplitude of the decrease in acidification rate due to K^+ removal re-

A

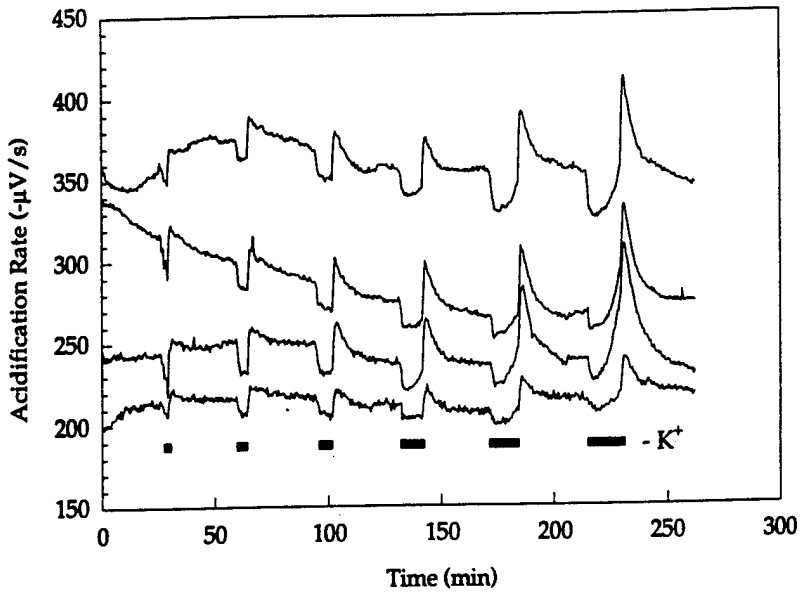

B

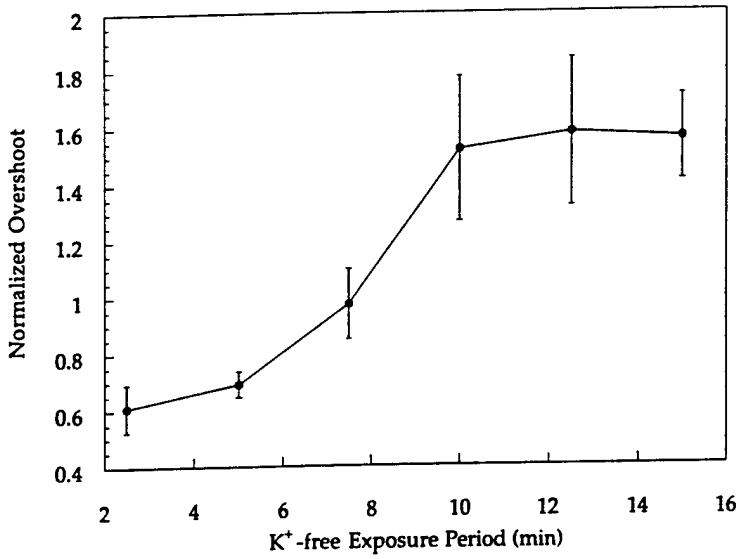

FIGURE 4 Increasing the time of K^+ deprivation increased the amplitude of the acidification overshoot. (*A*) Cells in four chambers were deprived of extracellular K^+ for increasing periods (from 2.5 up to 15 min). In each chamber the amplitude of the replenishment overshoot increased with deprivation time, as would be expected if the overshoot represents the extra activity of the Na^+/K^+ ATPase as it restores basal $[Na^+]_i$. There is some variation among the chambers in the amplitudes of the effects of K^+ deprivation. This presumably is due to differences in leakiness of the cells and, secondarily, in Na^+/K^+ pump activity. (*B*) The amplitudes of the overshoots in *A* rise monotonically with deprivation time and appear to saturate. Overshoots were measured as the amplitude of the peak upon K^+ restoration minus the difference between the basal rate just prior to K^+ removal and the value during the period of K^+ removal. The data were normalized by the decrease in acidification rate during K^+ deprivation immediately preceding the overshoot to correct for the variability in absolute response discussed above.

mained constant for a given chamber, whereas the amplitude of the overshoot increased with increasing lengths of time the Na^+/K^+ pump was off. For the longest K^+-free incubation periods, there was some increase in the acidification rate while the Na^+/K^+ pump was inhibited, probably reflecting the response of a variety of metabolic consequences of altering significantly the ionic composition of the cytoplasm. This effect is also observed during exposure of cells to ouabain with K^+ present in the medium (Fig. 3 *B*).

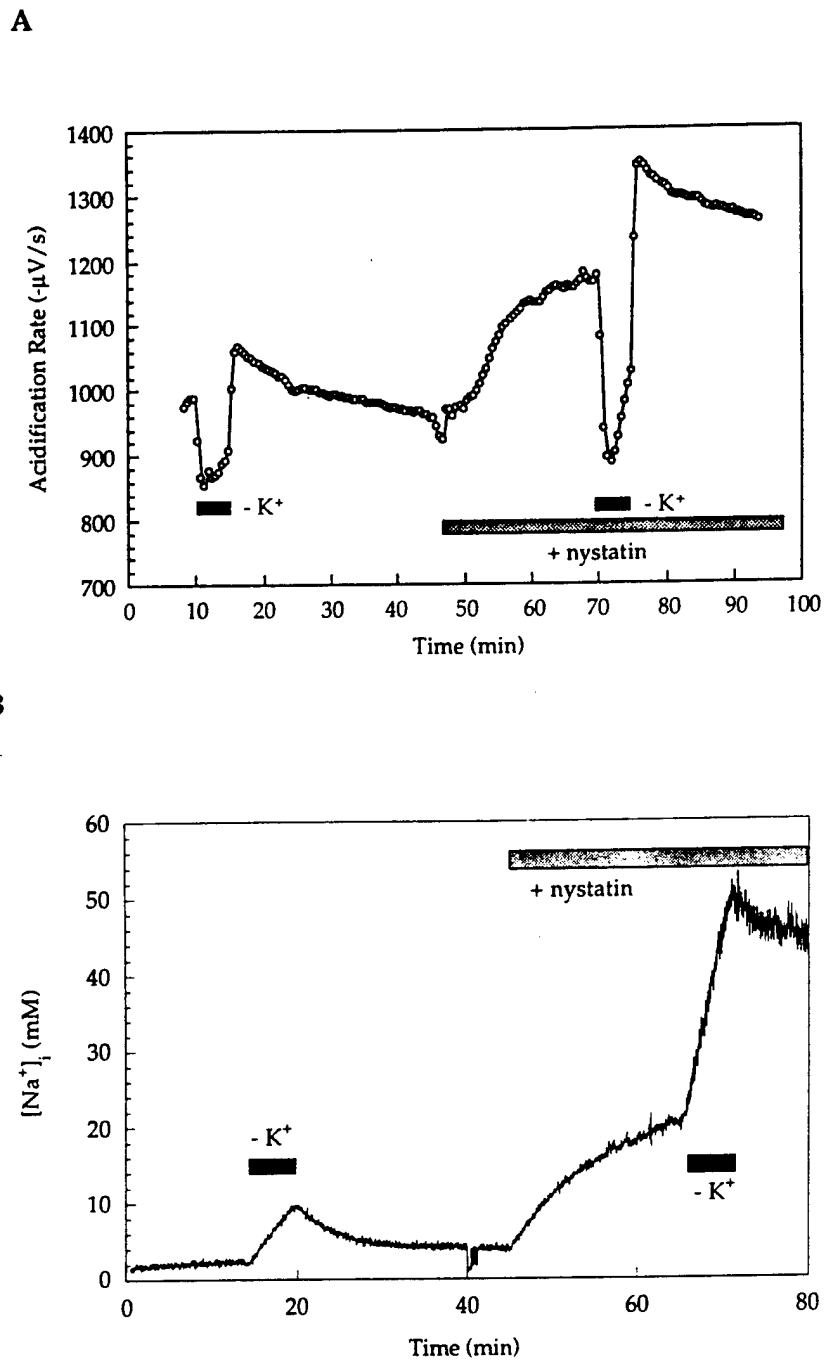

FIGURE 5 The amplitude of the acidification overshoot correlates with membrane permeability to Na^+. The permeability of the plasma membrane for Na^+ was increased by exposing the cells to 25 μg/ml of the ionophore nystatin. (*A*) Nystatin increased the acidification rate when the Na^+/K^+ ATPase was active but had little effect on the acidification rate during periods when the Na^+/K^+ ATPase was inhibited by removal of extracellular K^+. Nystatin increased the overshoot upon replenishment of K^+. These effects of nystatin are consistent with the hypothesis that the effects of K^+ deprivation on acidification rate reflect the activity of the Na^+/K^+ pump. (*B*) Intracellular Na^+ measurements confirm that nystatin increased $[Na^+]_i$ as well as the rate of increase in $[Na^+]_i$ when extracellular K^+ was removed.

Analysis of the data in Fig. 4 *A* demonstrates a correlation between the period of Na^+/K^+ pump inhibition and amplitude of the overshoot (Fig. 4 *B*). This effect appears to level off for inhibition times greater than 10 min, possibly reflecting saturation of the Na^+/K^+ pump with Na_i^+. Similar results were obtained with another adherent cell line (CHO-K1), indicating that these results are not unique to the TE671 cell line (data not shown).

Ionophores provide a second method for manipulating $[Na^+]_i$. Addition of nystatin, a monovalent cationophore, to cells in the microphysiometer caused the acidi-

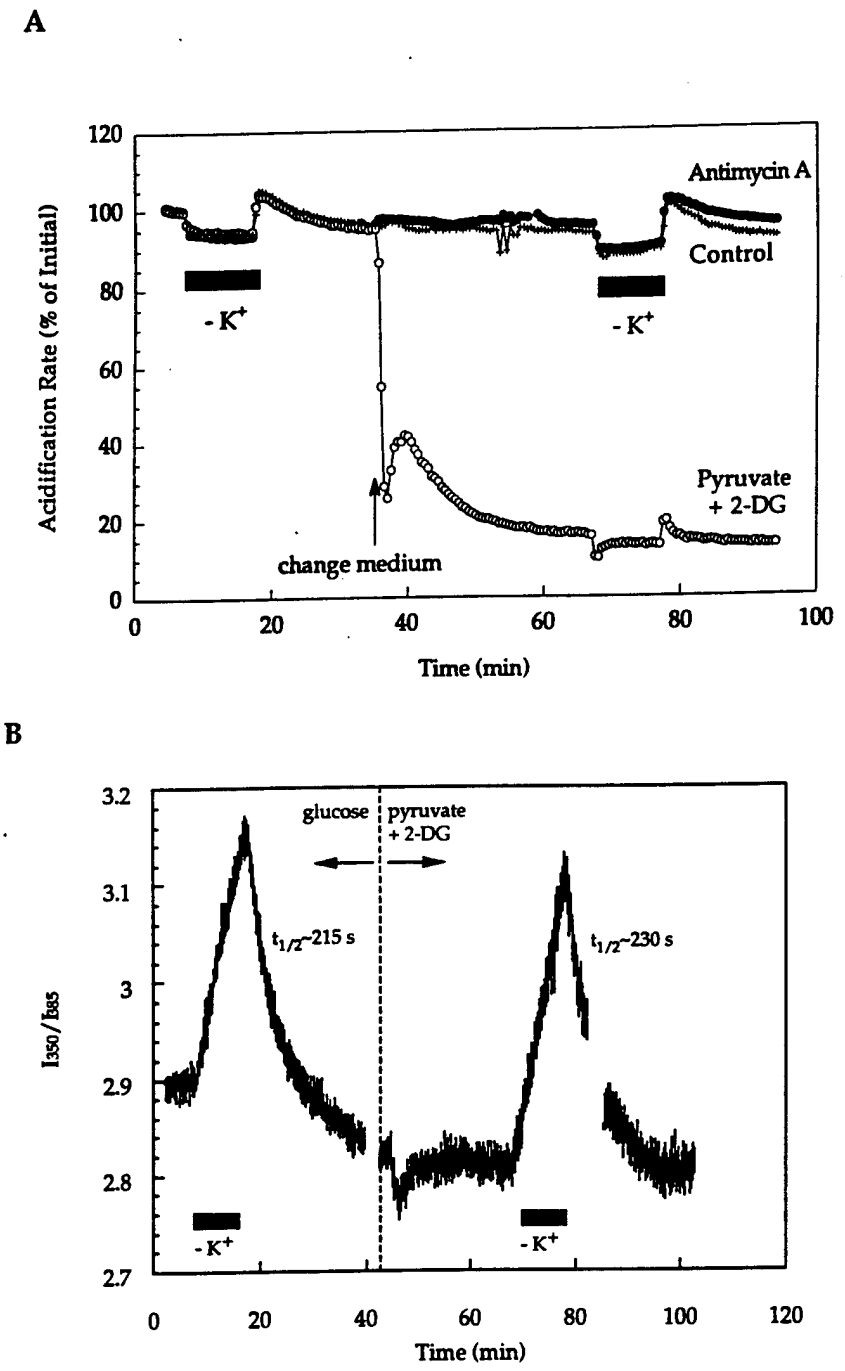

FIGURE 6 The steady-state activity of the Na^+/K^+ ATPase is independent of whether the energy metabolism of the cells is glycolytic or oxidative. (*A*) Acidification rates in three chambers responded essentially identically to a 10-min deprivation of K^+. One chamber (*solid circles*) was then forced to be completely glycolytic by exposure to 5 μM antimycin A. The second (*open circles*) was forced into purely oxidative metabolism by removal of glucose and substitution with 10 mM pyruvate and 2 mM 2-DG. The third chamber (*plus signs*) remained on glucose-containing salts as a control. Subsequent removal of extracellular K^+ for 10 min decreased the acidification rates by the same percent of the new steady-state rate for all three treatments. A representative experiment is shown. (*B*) Measurements of $[Na^+]_i$ were made on cells in a single chamber sequentially under control (predominantly glycolytic) and oxidative conditions as above. The $[Na^+]_i$ basal level did not change between the two conditions. The kinetics of recovery from 10-min deprivation of K^+, a measure of Na^+/K^+ ATPase activity, were quite similar under the two conditions. The break in the SBFI data resulted when the memory buffer on the computer became full and it was necessary to restart data accumulation (see also Fig. 7 *B*).

fication rate to rise to an elevated steady-state value (Fig. 5 *A*). Subsequent removal of K^+ resulted in an acidification rate similar to that measured in the absence of K^+ before addition of nystatin. These data indicate that the elevation in acidification rate caused by nystatin is primarily due to an increase in activity of the Na^+/K^+ pump, probably due to the increased flux of Na^+ into the cells. Analogous results were obtained in studies of monensin effects on the ouabain-suppressible clamp current in chick myocytes (18). Also consistent with a nystatin-

mediated increase in Na^+ flux into the cells is the increased acidification overshoot upon replacement of K^+. As expected, direct measurement of $[Na^+]_i$ revealed an increased steady-state concentration due to nystatin addition as well as a very rapid rise in concentration upon K^+ removal (Fig. 5 *B*). Similar results were obtained with monensin and gramicidin D (data not shown).

Thus, both the amplitude of the undershoot of acidification rates occurring during K^+ deprivation and the overshoot resulting from its replacement are indicators of changes in p_{Na} and $[Na^+]_i$. The overshoot, which reflects the time integral of Na^+ influx during K^+ removal, is the more sensitive indicator of such changes. These observations, coupled with the ouabain sensitivity of the overshoot and the similarity of the kinetics of the return of the acidification rate transient to baseline and the SBFI measurements of the kinetics of the return of $[Na^+]_i$ to baseline, argue very strongly that the changes in acidification rates seen with these manipulations do indeed track the activity of the Na^+/K^+ pump in these cells.

Dependence of the Na^+/Ka^+ pump on mode of energy metabolism

Having established that the activity of the Na^+/K^+ pump can be monitored with the microphysiometer, we next examined whether the pump activity in TE671 cells selectively depended on glycolysis or respiration as a source of ATP. These studies were motivated by reports demonstrating that different cellular processes may sometimes be fueled preferentially from one or the other of these major pathways of energy metabolism, independent of the overall balance between the two pathways in the cell. Brain and kidney are the two organs that expend the most energy on the Na^+/K^+ pump (19). Oxidative metabolism accounts for nearly all the ATP used by the pump in brain, and only part of that used in renal tubules (20), Rous-transformed hamster cells and Ehrlich ascites cells (21), or the renal cell line MDCK (22, 23). In vascular smooth muscle, Paul and collaborators (24) found that ATP derived from aerobic glycolysis was primarily used for transport functions, whereas ATP originating from oxidative metabolism was used to drive contractile processes. Similar findings were reported for the rabbit heart by Weiss and Hiltbrand (25). The conclusions above were based on experiments in which the Na^+/K^+ pump activity was manipulated and the resultant changes in O_2 consumption and/or lactate production were examined or, conversely, in which the mode of energy metabolism was changed and the effects on Na^+/K^+ pump activity were determined.

We chose the latter approach and forced the cells into one mode of energy metabolism or the other by using inhibitors of glycolysis or oxidative metabolism and by manipulating carbon source. Addition of antimycin A, a site 2 blocker of the electron transport chain and a nearly universal activator of glycolysis, caused a very slight increase in metabolic rate, as can be seen in Fig. 6 *A*. An increase is expected since completely glycolytic cells should produce six times the number of protons as cells depending completely on oxidative metabolism of glucose and assuming a constant ATP turnover rate (7). The minor increase shown here (~3%) indicates that these cells are normally almost entirely glycolytic. This is not surprising given their tumor origin and that fact that cells in culture (as opposed to in vivo) commonly are primarily glycolytic (22, 26–29).

Substitution of glucose with pyruvate and the glycolytic inhibitor 2-DG decreased the basal acid production rate by ~85% compared with that of the control cells. Since the theoretical decrease in acidification rate for a shift from glycolysis to oxidative metabolism of pyruvate at constant ATP turnover rate is 87% (7), these data are evidence that the ATP turnover rate is independent of the mode of energy metabolism.

Upon removal of K^+ from the medium, the acidification rates dropped by ~9%, regardless of whether the cells were in glycolytic ($8.1 \pm 0.9\%$; mean ± SEM, $n = 8$), oxidative ($10.0 \pm 0.8\%$, $n = 10$), or control energy-metabolism mode ($8.8 \pm 0.7\%$, $n = 83$). Assuming that the manipulations with carbon source and inhibitors did not change $[Na^+]_i$, the fact that the drop in acidification rate due to K^+ removal was nearly the same percentage in all cases implies that the ATP for the Na^+/K^+ pump is equally provided for by either glycolysis or oxidative metabolism. Fig. 6 *B* shows that the $[Na^+]_i$ indeed did not change when the cells were shifted to oxidative metabolism from a (largely) glycolytic state. Furthermore, the kinetics of the changes in $[Na^+]_i$ due to removal and replacement of extracellular K^+ were essentially identical for the two metabolic conditions. Thus, the activity of the Na^+/K^+ pump was invariant with respect to mode of energy metabolism even under conditions with slight Na^+ loading. The insensitivity of the Na^+/K^+ ATPase to the source of ATP is also demonstrated by the fact that the overshoot of acidification rate in response to K^+ replacement also scales with the basal acidification rate, independent of mode of cellular energy metabolism. This observation is also indicative of the tight coupling of ATP synthesis and hydrolysis in these cells. Since the same amount of ATP was hydrolyzed regardless of metabolic mode to remove the excess Na^+ accumulating during the period of K^+ deprivation, the same number of excess protons resulting from that hydrolysis should have been produced. These protons should have appeared outside the cells due to the cellular pH_i homeostasis mechanisms. That they did not most likely was a result of near simultaneous uptake of those protons via ATP synthesis.

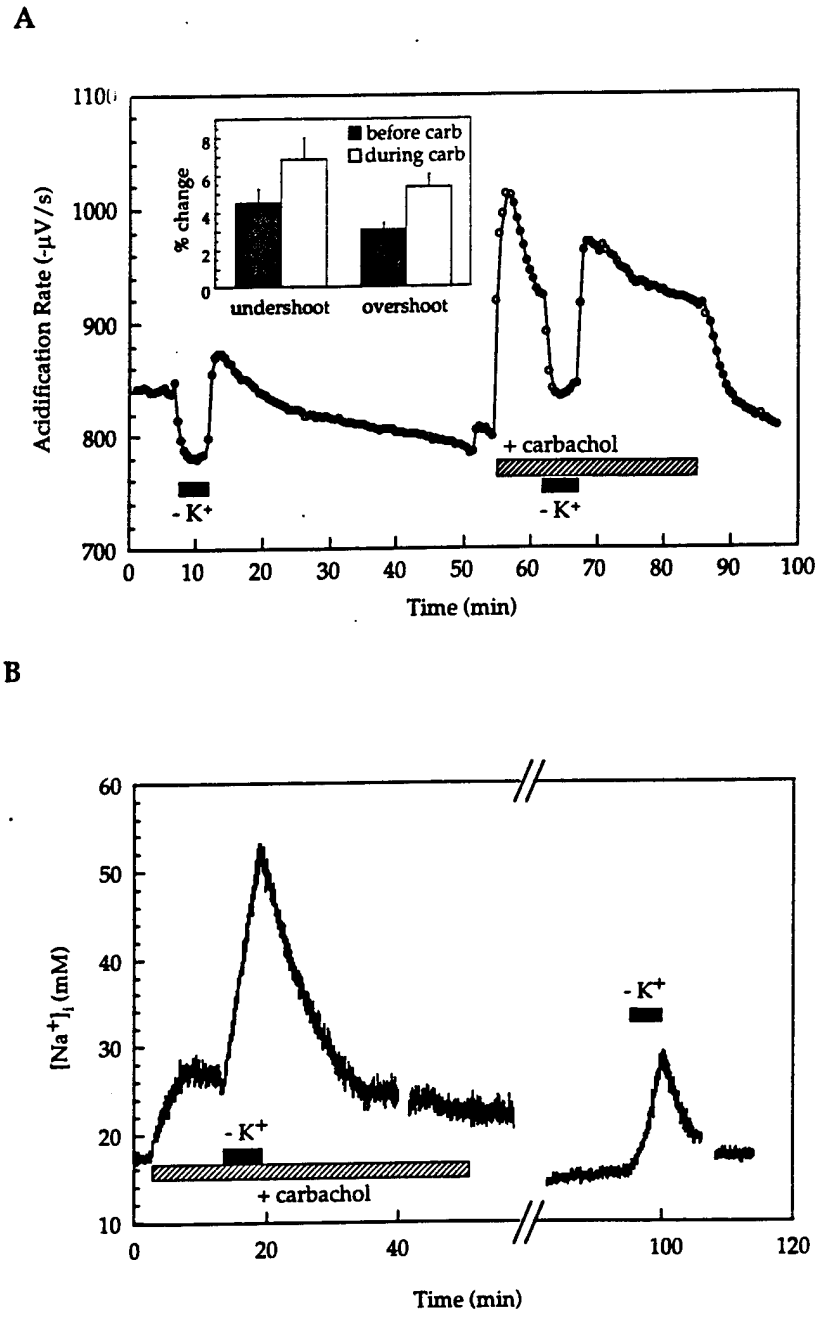

FIGURE 7 Stimulation of muscarinic receptors in TE671 cells increased the activity of the Na^+/K^+ ATPase via increase in $[Na^+]_i$. (*A*) The response of acidification rate to stimulation with 1 mM carbachol was an increase that peaked and decayed to a higher plateau while the agonist remained present. Deprivation of extracellular K^+ for 5 min during carbachol stimulation causes a larger decrease in acidification rate than deprivation before stimulation. The inset summarizes the results of six such measurements on independent chambers. (*B*) Treatment with 1 mM carbachol increased $[Na^+]_i$ and increased the rate of accumulation of Na_i^+ during deprivation of extracellular K^+ but did not alter the kinetics of return to basal $[Na^+]_i$ after the restoration of K^+.

Increase in NaK^+/K^+ ATPase activity by cholinergic stimulation

TE671 cells express both nicotinic (nAChR) and muscarinic (mAChR) acetylcholine receptors (30–33). The nAChR expressed has properties of skeletal muscle nAChR, and, based on binding studies, Bencherif and Lukas (32) have assigned the mAChR to the M_3 subclass. We have demonstrated previously that triggering acetylcholine receptors on TE671 cells with the agonist carbamyl choline (carbachol) results in immediate and significant increases in extracellular acidification rates (33). These responses are completely attributable to stimulation of the muscarinic acetylcholine receptors based on the ability of atropine to block the response. Increased acidification rates may be in part due to increased activity of the Na^+/K^+ ATPase in response to

receptor triggering. Such increases could be caused either indirectly by a rise $[Na^+]_i$ or directly by activation of the Na^+/K^+ pump. The activity of the Na^+/K^+ pump has been found to be modulated in a number of systems (34, see also 35–43), usually as a result of changes in $[Ca^{++}]_i$ and/or protein kinase C activation. Since activation of the mAChR in TE671 cells results in an increase in inositol trisphosphate concentration (32) and an increase in $[Ca^{++}]_i$ (Miller, D. L., unpublished observations), it seemed reasonable to suspect there might be some Na^+/K^+ pump modulation in these cells as well.

To determine the role of the Na^+/K^+ pump in the acidification response to receptor triggering, we tested the response of the cells to exposure to K^+-free medium before and during exposure to 1 mM carbachol (Fig. 7 *A*). The response of the cells to carbachol was robust, with the acidification rate increasing by 27.5 ± 3.0% (n = 7). Removal of K^+ from the medium resulted in a larger decrease in acidification rate in the presence of carbachol (6.8 ± 1.2% versus 4.5 ± 0.7% before carb, n = 6), indicating enhanced Na^+/K^+ pump activity due to receptor triggering. Replacement of K^+ resulted in a larger acidification-rate overshoot, suggesting that carbachol-enhanced pump activity is due to an increased flux of Na^+ into the cells (3.1 ± 0.4% before carbachol versus 5.4 ± 0.7% after, n = 6).

To confirm this hypothesis, we examined changes in $[Na^+]_i$ directly with SBFI during the carbachol response (Fig. 7 *B*). As expected, carbachol increased $[Na^+]_i$ as well as the rate of Na_i^+ accumulation upon removal of K^+. The presence of carbachol did not alter the kinetics of the removal of Na_i^+ in response to K^+ replacement ($t_{1/2}$ = 245 s, n = 2). The $[Na^+]_i$ remained elevated all the while the carbachol was present, and decayed slowly to its original value after carbachol removal (not shown). Thus, the permeability of the cells to Na^+ due to receptor triggering is not transiently enhanced but rather remains elevated throughout the period of exposure of the cells to agonist. The mechanism by which Na^+ permeability is enhanced by muscarinic receptor activation is currently under investigation. In other systems Na^+ influx increases due to receptor activation have been attributed to activation of the Na^+/H^+ antiporter; however, preliminary experiments have indicated that is not the case in these cells (unpublished observations).

CONCLUSIONS

We have determined that the activity of the Na^+/K^+ ATPase is closely coupled to the rate of production of acidic metabolites by the human rhabdomyosarcoma cell line TE671. Manipulation of the activity of the ATPase caused changes in the metabolic flux in these cells that were measurable noninvasively in real time with a microphysiometer. Parallel measurements of changes in $[Na^+]_i$ with a ratiometric fluorescence technique corroborated the results from the microphysiometer. Use of both techniques indicated that the pool of ATP used by the pump is derived nonpreferentially from either glycolysis or oxidative metabolism. Furthermore, we were able to demonstrate that the Na^+/K^+ ATPase is activated when carbachol stimulates cholinergic receptors in these cells. The activation of the ATPase is secondary to an increase in $[Na^+]_i$ that is caused by increased Na^+ influx during receptor stimulation. We are continuing to investigate the source of the increase in Na^+ influx.

This work was supported in part by the Defense Advanced Research Projects Agency, contract MDA972-92-C-0005.

Received for publication 1 September 1992 and in final form 9 November 1992.

REFERENCES

1. McConnell, H. M., P. Rice, H. G. Wada, J. C. Owicki, and J. W. Parce. 1991. The microphysiometer biosensor. *Curr. Opin. Struct. Biol.* 1:647–652.
2. Nag, B., H. G. Wada, K. S. Fok, D. J. Green, S. D. Sharma, B. Clark, J. W. Parce, and H. M. McConnell. 1992. Antigen-specific stimulation of T cell extracellular acidification by MHC class II-peptide complexes. *J. Immunol.* 148:2040–2044.
3. Raley-Susman, K. M., K. R. Miller, J. C. Owicki, and R. M. Sapolsky. 1992. Effects of excitotoxin exposure on metabolic rate of primary hippocampal cultures: application of silicon microphysiometry to neurobiology. *J. Neurosci.* 12:773–780.
4. McConnell, H. M., J. C. Owicki, J. W. Parce, D. L. Miller, G. T. Baxter, H. G. Wada, and S. Pitchford. 1992. The Cytosensor microphysiometer. *Science (Wash. DC).* 257:1906–1912.
5. Baxter, G. T., D. L. Miller, R. C. Kuo, H. G. Wada, and J. C. Owicki. 1992. PKCε is involved in GM-CSF signal transduction. Evidence from microphysiometry and antisense oligonucleotide experiments. *Biochemistry.* 31:10950–10954.
6. Wada, H. G., S. R. Indelicato, L. Meyer, T. Kitamura, A. Miyajima, G. Kirk, V. C. Muir, and J. W. Parce. 1993. GM-CSF triggers a rapid glucose dependent extracellular acidification by TF-1 cells. Evidence for sodium/proton antiporter and PKC mediated activation of acid production. *J. Cell Physiol.* 154:129–138.
7. Owicki, J. C., and J. W. Parce. 1992. Biosensors based on the energy metabolism of living cells: the physical chemistry and cell biology of extracellular acidification. *Biosens. & Bioelectronics.* 7:255–272.
8. Rice, P. A. 1991. Biophysics of Monolayers and Cellular Responses. Ph.D. thesis, Stanford University, Stanford, CA. 236 pp.
9. Clausen, T., C. van Hardeveld, and M. E. Everts. 1991. Significance of cation transport in control of energy metabolism and thermogenesis. *Physiol. Rev.* 71:733–774.
10. Parce, J., J. Owicki, K. Kercso, G. Sigal, H. Wada, V. C. Muir, L. Bousse, K. Ross, B. Sikic, and H. M. McConnell. 1989. Detection of cell-affecting agents with a silicon biosensor. *Science (Wash. DC).* 246:243–247.
11. Hafeman, D. G., J. W. Parce, and H. M. McConnell. 1988. Light-addressable potentiometric sensor for biochemical systems. *Science (Wash. DC).* 240:1182–1185.
12. Negulescu, P. A., A. Harootunian, R. Y. Tsien, and T. E. Machen. 1990. Fluorescence measurements of cytosolic free Na concentration, influx, and efflux in gastric cells. *Cell Regul.* 1:259–268.

13. Gadsby, D. C., and P. F. Cranefield. 1979. Electrogenic sodium extrusion in cardiac Purkinje fibers. *J. Gen. Physiol.* 73:819–837.

14. Eisner, D. A., W. J. Lederer, and R. D. Vaughan-Jones. 1981. The dependence of sodium pumping and tension on intracellular sodium activity in voltage-clamped sheep Purkinje fibres. *J. Physiol. (Lond.)*. 317:163–187.

15. Daut, J., and R. Rudel. 1982. The electrogenic sodium pump in guinea-pig ventricular muscle: inhibition of pump current by cardiac glycosides. *J. Physiol. (Lond.)*. 330:243–264.

16. Daut, J. 1983. Inhibition of the sodium pump in guinea-pig ventricular muscle by dihyro-ouabain: effects of external potassium and sodium. *J. Physiol. (Lond.)*. 339:643–662.

17. Cohen, I. S., N. B. Datyner, G. A. Gintant, N. K. Mulrine, and P. Pennefather. 1987. Properties of an electrogenic sodium-potassium pump in isolated canine Purkinje myocytes. *J. Physiol. (Lond.)*. 383:251–267.

18. Stimers, J. R., N. Shigeto, and M. Lieberman. 1990. Na/K pump current in aggregates of cultured chick myocytes. *J. Gen. Physiol.* 95:61–76.

19. Erecinska, M., and I. A. Silver. 1989. ATP and brain function. *J. Cereb. Blood Flow Metab.* 9:2–19.

20. Chamberlin, M., and L. J. Mandel. 1987. Na^+-K^+-ATPase activity in medullary thick ascending limb during short-term anoxia. *Am. J. Physiol.* 252:F838–F843.

21. Balaban, R. S., and J. P. Bader. 1984. Studies on the relationship between glycolysis and (Na^+ + K^+)-ATPase in cultured cells. *Biochim. Biophys. Acta.* 804:419–426.

22. Lynch, R. M., and R. S. Balaban. 1987. Energy metabolism of renal cell lines, A6 and MDCK: regulation by Na-K-ATPase. *Am. J. Physiol.* 252:C225–C231.

23. Lynch, R. M., and R. S. Balaban. 1987. Coupling of aerobic glycolysis and Na^+-K^+-ATPase in renal cell line MDCK. *Am. J. Physiol.* 253:C269–C276.

24. Paul, R. J., M. Bauer, and W. Pease. 1979. Vascular smooth muscle: aerobic glycolysis linked to sodium and potassium transport processes. *Science (Wash. DC)*. 206:1414–1416.

25. Weiss, J., and B. Hiltbrand. 1985. Functional compartmentation of glycolytic versus oxidative metabolism in isolated rabbit heart. *J. Clin. Invest.* 75:436–447.

26. Gebhardt, R., P. Bellemann, and D. Mecke. 1978. Metabolic and enzymatic characteristics of adult rat liver parenchymal cells in non-proliferating primary monolayer cultures. *Exp. Cell Res.* 112:432–441.

27. Lopez, M. P., M. J. Gomez-Lechon, and J. V. Castell. 1988. Active glycolysis and glycogenolysis in early stages of primary cultured hepatocytes: role of AMP and fructose 2,6-bisphosphate. *In Vitro (Rockville)*. 24:511–517.

28. Dickman, K. G., and L. J. Mandel. 1989. Glycolytic and oxidative metabolism in primary renal proximal tubule cultures. *Am. J. Physiol.* 257:C333–C340.

29. Dickman, K. G., and L. J. Mandel. 1990. Different effects of respiratory inhibitors on glycolysis in proximal tubules. *Am. J. Physiol.* 258:F1608–F1615.

30. Lukas, R. J. 1986. Functional nicotinic acetylcholine receptors on the clonal cell line, TE671. *Trans. Am. Soc. Neurochem.* 17:286.

31. Lukas, R. J. 1986. Characterization of curaremimetic neurotoxin binding sites on membrane fractions derived from the human medulloblastoma clonal line, TE671. *J. Neurochem.* 46:1936–1941.

32. Bencherif, M., and R. J. Lukas. 1991. Ligand binding and functional characterization of muscarinic acetylcholine receptors on the TE671/RD human cell line. *J. Pharmacol. Exp. Ther.* 257:946–953.

33. Miller, D. L., J. C. Owicki, and J. W. Parce. 1991. Real-time detection of agonist-induced acetylcholine receptor (AChR) activation in TE671 cells with a silicon-based biosensor. *FASEB (Fed. Am. Soc. Exp. Biol.) J.* 5:1600*a* (Abstr.)

34. Yingst, D. R. 1988. Modulation of the Na,K-ATPase by Ca and intracellular proteins. *Annu. Rev. Physiol.* 50:291–303.

35. Lynch, C. J., P. B. Wilson, P. F. Blackmore, and J. H. Exton. 1986. The hormone-sensitive hepatic Na^+-pump. Evidence for regulation by diacylglycerol and tumor promoters. *J. Biol. Chem.* 261:14551–14556.

36. Lowndes, J. M., M. Hokin-Neaverson, and P. J. Bertics. 1990. Kinetics of phosphorylation of Na^+-K^+-ATPase by protein kinase C. *Biochim. Biophys. Acta.* 1052:143–151.

37. Hootman, S. R., M. E. Brown, and J. A. Williams. 1987. Phorbol esters and A23187 regulate Na^+-K^+-pump activity in pancreatic acinar cells. *Am. J. Physiol.* 252:G499–G505.

38. Bertorello, A., and A. Aperia. 1989. Regulation of Na^+-K^+-ATPase activity in kidney proximal tubules: involvement of GTP binding proteins. *Am. J. Physiol.* 256:F57–F62.

39. Knudsen, T., and T. Johansen. 1989. The mode of inhibition of the Na^+-K^+ pump activity in mast cells by calcium. *Br. J. Pharmacol.* 98:1119–1126.

40. Gupta, S., N. B. Ruderman, E. J. Cragoe, Jr., and I. Sussman. 1991. Endothelin stimulates Na^+-K^+-ATPase activity by a protein kinase C-dependent pathway in rabbit aorta. *Am. J. Physiol.* 261:H38–H45.

41. Borin, M., and W. Siffert. 1991. Further characterization of the mechanisms mediating the rise in cytosolic free Na in thrombin-stimulated platelets. *J. Biol. Chem.* 266:13153–13160.

42. Navran, S. S., G. Allain, H. F. Garcia, J. C. Allen, and C. L. Seidel. 1991. Serotonin-induced Na^+/K^+ pump stimulation in vascular smooth muscle cells. Evidence for coupling to multiple receptor mechanisms. *J. Pharmacol. Exp. Ther.* 256:297–303.

43. Aperia, A., I. Ibarra, L.-B. Svensson, C. Klee, and P. Greengard. 1992. Calcineurin mediates α-adrenergic stimulation of Na,K-ATPase activity in renal tubule cells. *Proc. Natl. Acad. Sci. USA.* 89:7394–7397.

0022-1767/92/1487-2040$02.00/0
THE JOURNAL OF IMMUNOLOGY

Vol. 148, 2040–2044, No. 7, April 1, 1992
Printed in U.S.A.

ANTIGEN-SPECIFIC STIMULATION OF T CELL EXTRACELLULAR ACIDIFICATION BY MHC CLASS II-PEPTIDE COMPLEXES

BISHWAJIT NAG,[1]* H. GARRETT WADA,† KATHERINE S. FOK,† DONNA J. GREEN,* SOMESH D. SHARMA,* BRIAN R. CLARK,* J. WALLACE PARCE,† AND HARDEN M. McCONNELL†

*From *Anergen Incorporation, Redwood City, CA 94063; †Molecular Devices Corporation, Menlo Park, CA 94025; and ‡Stauffer Laboratory for Physical Chemistry, Stanford University, Stanford, CA 94305*

A specific T cell response to a preformed complex of detergent-solubilized MHC class II molecule and cognate antigenic peptide was observed by monitoring the extracellular acidification. An increase in this rate was observed when the resting 4R3.9 T cell clone specific for the peptide fragment MBP(1–14) of myelin basic protein was exposed to preformed detergent-solublized IA^k-MBP(1–14)A^4 complexes. MBP peptide alone, IA^k alone, or complexes of IA^a-proteolipid protein(139–151) and IA^d-OVA(323–339), did not cause significant increases in the acidification rates of the MBP(1–14)-restricted 4R3.9 T cell clone. In addition, BW 5147 T lymphoma cells, which lack TCR, did not show any increase in rate when exposed to IA^k-MBP(1–14)A^4 complexes. Similar increases in acidification rate were observed in the presence of IL-2, anti-CD3 and anti-TCR antibodies. The enhanced acidification responses were blocked by genistein, a tyrosine kinase inhibitor.

In recent work, it has been found that the in vitro triggering of a wide variety of cells by specific receptor ligands can be detected and monitored using sensitive measurements of medium acidification (1, 2). The present work was undertaken to determine whether acidification rates can also be used to detect specific cell triggering by ligands that bind to TCR. The triggering of Th cells by complexes of class II MHC molecules and cognate antigenic peptides can be observed using a variety of techniques (3–7). The acidification rate technique differs from most other methods in that it provides a continuous probe of the early events in cellular triggering. We are particularly interested in ligands that may be responsible for the induction of anergy (8, 9).

MATERIALS AND METHODS

Cells, antibodies, and chemicals. The 4R3.9 T cell clone specific for N terminus acetylated MBP[2](1–14) was obtained from the laboratory of Dr. Patricia Jones, Stanford University, Stanford, CA. The BW 5147 T lymphoma cell line lacking TCR was obtained from the American Type Culture Collection (Bethesda, MD). The 4R3.9 T cell clone was maintained by stimulation with irradiated AJ spleen cells, 26.4 μM MBP(1–14) peptide and 1 U/ml human rIL-2 every 10 days. T cells were harvested at day 10 after Ag pulsing, and were cultured overnight at a cell density of 1×10^6 cells/ml in RPMI 1640 medium containing 2.5% FCS. Cells were washed in serum-free loading medium (RPMI 1640 with 1 mM sodium phosphate, 10 mM HEPES buffer, pH 7.4, penicillin, and streptomycin, without bicarbonate) just before use. Receptor-transfected CHO cells HB2 (β2-adrenergic) and WT3 (m1-muscarinic) were from Craig Venter, National Institutes of Health (Bethesda, MD). The CHO cells were cultured in F12 medium containing 10% serum, penicillin, and streptomycin. The EGF receptor-transfected 3T3 cells, DHER-14, were obtained from Joseph Schlessinger, New York University Medical Center (New York, NY). The DHER-14 cells were cultured in Dulbecco's modified Eagle's medium containing 10% FCS and antibiotics. Both CHO and 3T3 cells were maintained in serum-free medium for a period of at least 12 h immediately before use in the microphysiometer. Adherent cells were removed from culture flasks by incubating cells with 5 mM sodium EDTA in PBS for 5 min at 37°C. The cells were washed in serum-free medium and were used for experiments. Anti-CD3 and anti-TCR-αδ IgG mAb were affinity purified from hybridoma cell supernatant using a protein A Sepharose column. The anti TCR-αδ-producing hybridoma cells, H57-597, were from Ralph Kubo, National Jewish Medical Center (Denver, CO). Anti-CD3-producing hybridoma cells, E500A2, were from Jim Allison, University of California (Berkeley, CA). Anti-CD4 IgG mAb was purchased from Olympus Corporation (Lake Success, NY). Human rIL-2 was purchased from Genzyme (Boston, MA). Genistein (4′,5,7-trihydroxyisoflavone) was purchased from BioMol Research Labs. (Plymouth Meetings, PA) and was dissolved in DMSO. TGF-α was from Rick Harkins, Berlex Biosciences (Alameda, CA). (−) Isoproterenol and carbamoyl choline chloride (carbachol) were purchased from Sigma Chemical Co. (St. Louis, MO).

Synthesis of peptide analogs. The rat MBP peptide MBP(1–14)A^4, with the sequence Ac-ASQARPSQRHGSKY-NH2 (lysine at position 4 is replaced by alanine), the OVA peptide, OVA(323–339), with the sequence, ISQAVHAAHAEINEAGR-NH_2, and proteolipid peptide, PLP(139–151), with the sequence, TSLGKWLGHPDKF-NH_2, were synthesized by standard solid phase methodology using side chain-protected Fmoc amino acids and a MilliGen 9050 or Applied Biosystems 431A (Foster City, CA) automated peptide synthesizer. Deprotected, crude peptide amides were purified by reverse phase HPLC, and the homogeneity and identity of the purified peptides were confirmed by mass spectroscopic analysis.

Affinity purification of IA^k, IA^d, and IA^s MHC class II molecules. IA^k and IA^s were purified from an NP-40 extract of membranes prepared from cultured CH27 cells and SJL mice spleen cells, respectively, using an affinity support prepared by coupling mAb, 10-2.16 (specific for both IA^k and IA^s), with Sepharose 4B beads by the standard cyanogen bromide-coupling method. Similarly, IA^d was purified from A20.1.11 cells using a support containing MKD6 mAb. Briefly, a high speed (100,000 × *g*) membrane fraction was detergent extracted in a buffer containing 10 mM Tris-HCl, pH 8.3, 0.5% NP-40, 0.1 M NaCl, 5 mM EDTA, 0.02% sodium azide, and 1 mM PMSF, and the lysate was recycled over the preequilibrated antibody column at 4°C for 16 h. The column was washed with 10-bed volumes of deoxycholate buffer containing 10 mM Tris HCl, pH 8.3, 0.5% deoxycholate, 0.1 M NaCl, 5 mM EDTA, 0.02% sodium azide, and 1 mM PMSF followed by 5-bed volumes of PBS containing 1% OG buffer. Finally, the Ia molecules were eluted with 20 mM phosphate

Received for publication November 21, 1991.
Accepted for publication January 7, 1992.
The costs of publication of this article were defrayed in part by the payment of page charges. This article must therefore be hereby marked *advertisement* in accordance with 18 U.S.C. Section 1734 solely to indicate this fact.

[1] Address correspondence and reprint requests to Bishwajit Nag or A. Garrett Wada, Anergen Corporation, 301 Penobscot Drive, Redwood City, CA 94063.

[2] Abbreviations used in this paper: MBP, myelin basic protein; PLP, proteolipid protein; OG, *n*-octyl *d*-D-glucopyranoside; EGF, epidermal growth factor; CHO, chinese hamster ovary; TGF-α, transforming growth factor-α.

buffer, pH 11, containing 0.1 M NaCl, 1% OG, 0.02% sodium azide, and 1 mM PMSF. Each fraction was immediately neutralized with acetic acid to a final concentration of 12 mM, and the MHC class II was concentrated using an Amicon Centriprep-10 concentrator. Affinity-purified Ia molecules were characterized by 12% one-dimensional SDS-PAGE.

Preparation of class II-peptide complex. Affinity-purified Ia molecules at 400 to 500 μg/ml were incubated at 37°C for 48 h with 50-fold molar excess of peptides in a buffer containing 10 mM Tris HCl, pH 8.3, 0.02% sodium azide, 1 mM PMSF, and 1% OG. The excess peptide was removed by extensive dialysis of the complex against bicarbonate-free, low buffering RPMI 1640 medium, pH 7.4, containing 1 mM sodium phosphate, penicillin, and streptomycin. The final preparation of complex used in these experiments contains monomers and aggregates as measured by high speed centrifugation and gel filtration chromatography of [^{125}I]-IA^k and unlabeled MBP(1–14)A4 peptide complexes.

Loading of cells into cell capsule. T cells were loaded into disposable cell capsules for metabolic monitoring in the CytoSensor microphysiometer (Molecular Devices Corp., Menlo Park, CA) as described by McConnell et al. (10) (Fig. 1). Cells were pelleted at 500 × *g* for 5 min and resuspended in serum-free loading medium (low buffering RPMI 1640 medium containing 10 mM HEPES buffer, pH 7.4) at a cell density of 10×10^6 cells/ml. Using sterile technique in a laminar flow hood, capsule cups were placed in a 12-well microplate and loaded with 1 mg of particulate collagen (cross-linked collagen, 200-μm particles, Molecular Devices Corp.) suspended in 0.5 ml of loading medium. A 50-μm thick capsule spacer ring was added to the cup before addition of the collagen. After the collagen settled for 10 min, 5×10^6 cells in 0.5 ml were added to the membrane cups. The cups were then transferred into plate wells containing 2 ml of loading medium and centrifuged at 500 × *g* for 5 min in order to deposit cells onto the collagen-particle coated membrane. A capsule insert was then placed in the capsule cup and sunk through the overlying medium by wetting the top surface of the insert membrane with several drops of loading medium. The resulting configuration is termed the "cell capsule." This is made up of the capsule cup containing cells and collagen, sandwiched between lower cup membrane and upper capsule insert membrane, separated by a 50-μm thick capsule spacer ring (see Fig. 1). The cell capsule was then filled with loading medium and assembled into the sensor chamber.

Loading of cell capsules into sensor chambers. The sensor chambers were cleaned and disinfected using a pyrogen-removing detergent/oxidizing solution for 1 h and rinsed four times with sterile water and once with loading medium. With 1 ml of medium in the sensor chamber, a cell capsule was lowered into the chamber, and a sterile plunger primed with loading medium was lowered onto the cell capsule, sealing it into the sensor chamber. The sensor chamber was then connected to the inlet and exit tubing of the microphysiometer with the pumps running to exclude air from the sensor chamber during connection.

Measurement of cellular metabolic rates. A low buffering RPMI 1640 running medium containing 1 mg/ml endotoxin-free human serum albumin (Miles Laboratories, Elkhart, IN) was pumped through each sensor chamber at 50 μl/min. The acidification rate of cells was measured by stopping the flow of medium through the sensor chamber and collecting potential measurements for 1 min. A change of 1 μV/s in potential corresponds to 1 mpH U/min change in pH because of the Nernstian response (59 mV/pH unit) of the silicon sensor (11). Typically, resting T cells at the described cell density give rates of 10 to 20 μV/s. Restarting the flow of medium for a 1-min interval reestablished the pH in the sensor chamber to that of the medium, and replenished nutrients and removed waste products in order to maintain the cells in viable condition. Acidification rate data is mathematically normalized to a 100% value at a time before cell stimulation. This allows the direct comparison of changes in rates collected from cells in separate chambers with different initial rates in μV/s. The microphysiometer was equipped with 200-μl sample loops for the injection of MHC complexes and other effector agents such as rIL-2, which were diluted into running medium or dialyzed against low buffering medium.

RESULTS

Ag-specific stimulation of T cell acidification rates. Mouse T cell clone 4R3.9 was cultured overnight in medium containing 2.5% serum and washed with serum-free medium before measurements were made. After loading into the microphysiometer, the cells were monitored for acidification rate until a stable or slowly increasing base line was obtained before the injection of complex. Specific stimulation in the presence of IA^k-MBP(1–14)A^4 and not in the presence of IA^k alone is shown in Figure 2*A*. An increase of 12 to 15% in acidification rate over control cells was observed within 2 to 3 min after sample injection. The increase in acidification rate over controls slowly increased to 20% 45 min after injection of the complex. Cells treated with IA^s-PLP (139–151) complex did not show any significant increase in rate. A very similar result, i.e., no increase in the acidification rate, was obtained when BW 5147 T lymphoma cells were exposed to IA^k-MBP(1–14)A^4 complex. These results are presented in Figure 2*B*. Similarly, treatment of 4R3.9 T cells with either 10 μg/ml concentration of MBP(1–14)A^4 peptide alone or with complexes of IA^d-OVA(323–339) showed no increase in the metabolic rate (data not shown). The stimulation of T cell acidification rate was sustained for a long period of time. Although the acidification rate decreased after 4 h in the microphysiometer, the difference in the stimulation obtained with cells

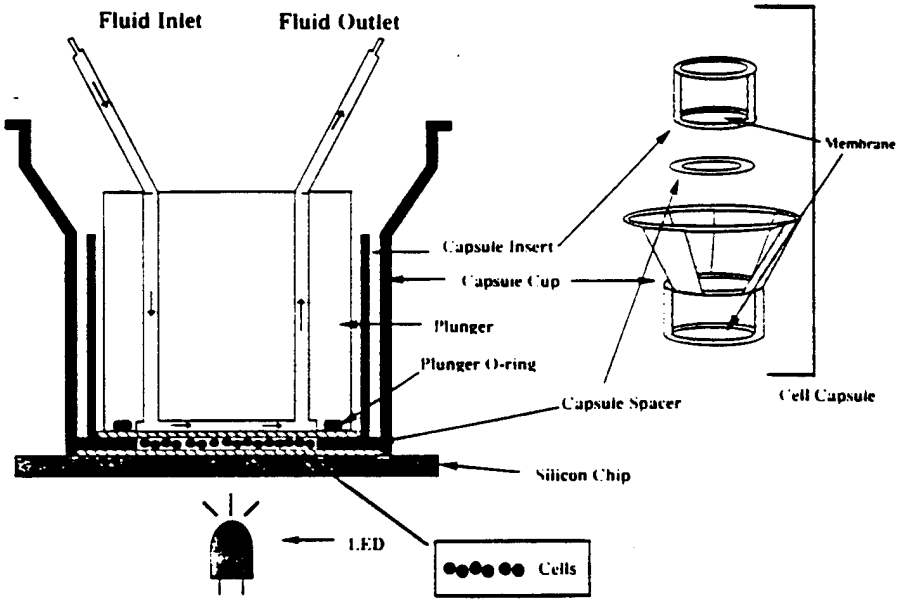

Figure 1. Microphysiometer cell capsule and plunger. Schematic illustration of "cell-capsule" and sensor chamber assembly.

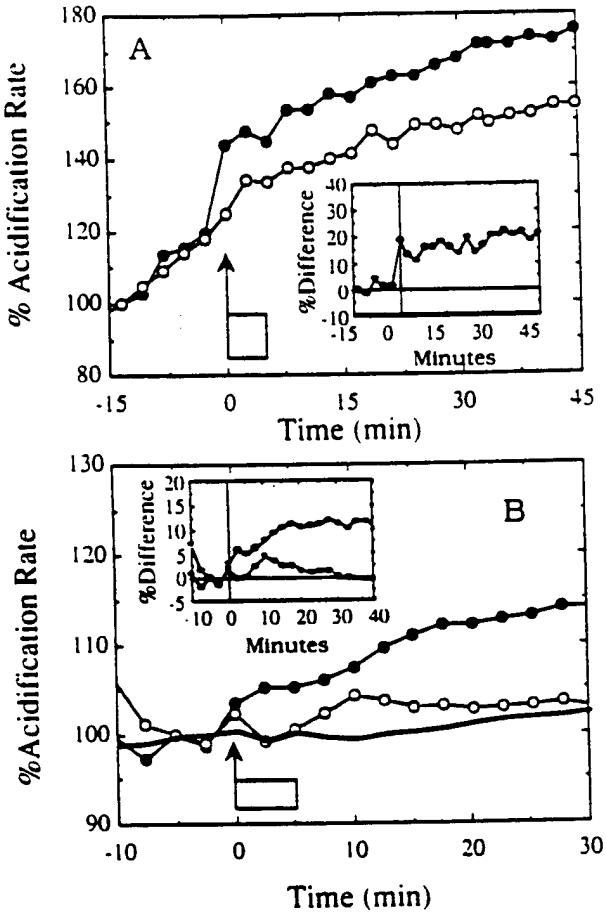

Figure 2. Stimulation of acidification rate of T cells in the presence of soluble MHC II-peptide complex. Resting 4R3.9 T cells at day 10 after Ag pulsing were prepared as described in *Materials and Methods*. The cells were rested overnight in low serum (2.5%) medium and washed in serum-free RPMI 1640 loading medium just before use. The cells were monitored for acidification rate for 30 min, and then samples were injected using a 200-μl sample injection loop. In *A*, either IA^k alone (*open circles*) or IA^k-MBP(1–14)A^4 complex (*closed circles*) at 500 μg/ml were injected into separate chambers at time zero. The acidification rates for each channel were normalized to 100% at 1 h after cell loading. The box indicates the time of sample exposure. The *inset graph* displays the difference in the rate between IA^k-MBP(1–14)A^4 complex and IA^k. In *B*, 200 μl of either IA^k-PLP(139–151) (*open circles*) or IA^k-MBP(1–14)A^4 complex (*closed circles*) at a concentration of 500 μg/ml were injected into the chambers. In a separate chamber BW 5147 cells were exposed to 200 μl of IA^k-MBP(1–14)A^4 complex (*solid line*) at a concentration of 500 μg/ml. The *inset graph* displays the difference in rate between the BW cells and 4R3.9 cells with either IA^k-MBP(1–14)A^4 complex (*closed circles*) or IA^k-PLP(139–151) complex (*open circles*).

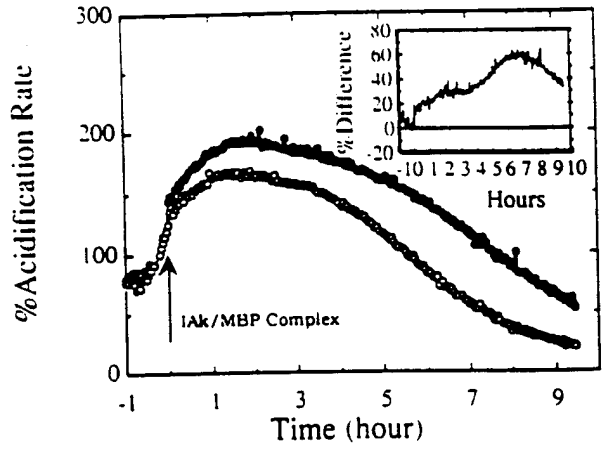

Figure 3. The sustained stimulation of T cell acidification rate by soluble MHC II-peptide complex. 4R3.9 T cells at day 10 after Ag pulsing were loaded per cell capsule for running in microphysiometer chambers. The cells were monitored for acidification rate, and at time zero 200 μl of either IA^k alone (*open circles*) or IA^k-MBP(1–14)A^4 complex (*closed circles*) at a concentration of 500 μg/ml were injected into two separate chambers. The rates were continually monitored for up to 10 h. The *inset graph* displays the difference in rate between the cells treated with IA^k and IA^k-MBP(1–14)A^4 complex.

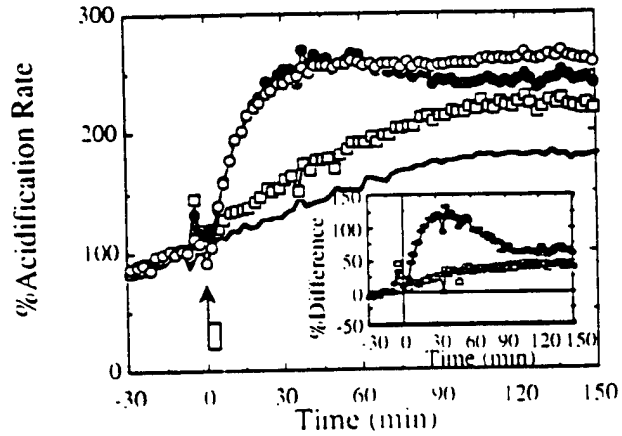

Figure 4. Effect of rIL-2 on the metabolic rate of T cells. T cells were prepared and loaded in cell capsules. Human rIL-2 at 0 (*solid line*), 10 (*open squares*), 100 (*closed circles*), and 1000 (*open circles*) U/ml was injected at time zero. The *inset graph* displays the difference in rate between the cell exposed to no IL-2 and cells exposed to 10 U/ml (*open squares*) and 100 U/ml (*closed circles*). The acidification rates were normalized to 100% at 1 h and were continually measured for a period of 6 h.

treated with IA^k alone and that obtained with cells treated with IA^k-MBP(1–14)A^4 persisted for 10 h as shown in Figure 3.

Effect of IL-2 on the acidification rate of T cell clone. IL-2 activates T cells (12). The effect of IL-2 on the acidification rate of the 4R3.9 T cell clone is shown in Figure 4. When cells were exposed to varying concentrations of human rIL-2 for 5 min, an increase of 50% and 100% in the rate was observed at IL-2 concentrations of 10 U/ml and 100 U/ml, respectively. Further increasing IL-2 concentration (1000 U/ml) did not show additional increase in the rate. The rate increased immediately upon exposure to IL-2 and stabilized at a maximum value within 20 min of exposure. The elevated rate of IL-2-treated cells, like that obtained upon treatment with complex, was sustained for at least 10 h after exposure to the lymphokine (data not shown).

Genistein blockade of Ag-specific, IL-2, and anti-CD3 and anti-TCR antibody stimulation of T cell acidification rates. T cells were loaded into the microphysiometer for measurement of acidification rate. The microphysiometer was run with medium alone or with 40 μg/ml genistein for 30 to 60 min to allow cellular acidification rates to stabilize. Figure 5*A* shows an increase of approximately 44% in acidification rate in response to complex injection after 30 min. In the presence of genistein, metabolic stimulation is completely blocked. Exposure of T cells to rIL-2 (Fig. 5*B*) causes an increase in acidification rate that reaches approximately 60% in 30 min. This IL-2 stimulation is also blocked by genistein.

Increases in acidification rate were also observed when T cells were exposed to anti-CD3 and anti-TCR mAb at a concentration of 10 μg/ml as shown in Figures 5*C* and 5*D*. The response to antibody was similar to the Ag-specific response, although the increase in metabolic rate occurred more slowly, reaching 40% for anti-CD3 and

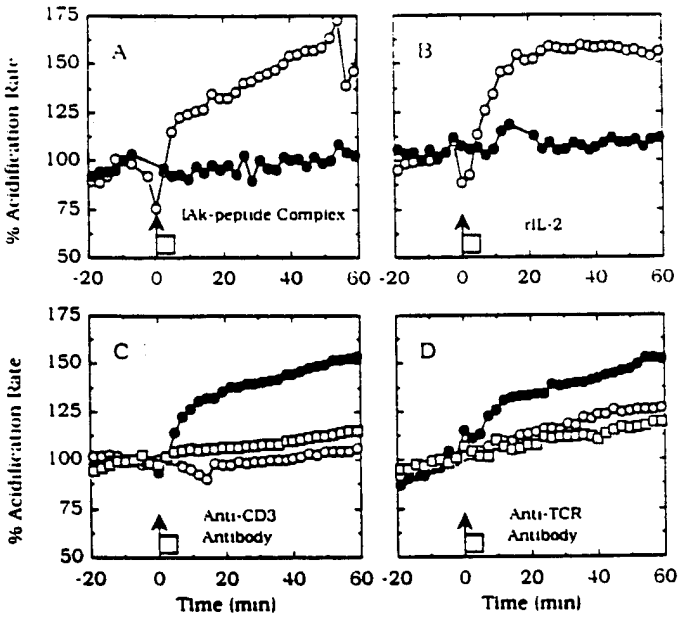

Figure 5. Inhibition of T cell responses to MHC-peptide complex, rIL-2, and specific anti-CD3 and anti-TCR antibody by genistein. T cells were prepared and loaded in cell capsules. In *A*, the cells were equilibrated in the microphysiometer with medium containing no additives (*open circles*) or 40 μg/ml genistein (*closed circles*). The DMSO concentration was held constant at 0.8%. Acidification rates were monitored for ~50 min before injection of IAk/MBP complex (500 μg/ml) at time zero. The acidification rates for each channel were normalized to 100% 10 min before complex injection. The box indicates the time of sample exposure. In *B*, the cells were equilibrated with no additives (*open circles*) or 40 μg/ml genistein (*closed circles*). The acidification rates were monitored before injection of rIL-2 (1000 U/ml) at time zero. Five minutes before sample injection, the acidification rates for each channel were normalized to 100%. In *C*, 10 μg/ml anti-CD3 antibody was injected into chambers equilibrated with (*open squares*) or without (*closed circles*) 40 μg/ml genistein. The box indicates the period of exposure of cells. Ten micrograms per milliliter anti-CD4 was also injected without genistein (*open circles*). In *D*, 10 μg/ml anti-TCR antibody was injected into chambers equilibrated with (*open square*) or without 40 μg/ml genistein (*closed circle*). A control chamber of cells without genistein was mock injected with medium (*open circles*).

TABLE I

Effect of genistein on T cell acidification response

Stimulus (Concentration)	% Increase[a]	
	− Genistein	− Genistein (40 μg/ml)
IA^k-MBP complex (500 μg/ml)	44	0
rIL-2 (1000 U/ml)	60	5
Anti-CD3 antibody (10 μg/ml)	40	8
Anti-TCR antibody (10 μg/ml)	20	−6
Anti-CD4 antibody (10 μg/ml)	0	ND

[a] % Increase is the difference between stimulated and initial (100%) T cell acidification rates, measured 30 min after stimulus.

20% for anti-TCR at 30 min. When genistein was added before antibody exposure, the anti-CD3 and anti-TCR stimulations of T cells were both inhibited. Exposure to anti-CD4 mAb did not cause an increase in acidification rate (Fig. 5C). These results are summarized in Table I.

The response of Hβ2 cells, CHO cells transfected with the β2-adrenergic receptor, to agonist was not inhibited in the presence of 40 μg/ml genistein. The effect of 40 μg/ml of genistein on the agonist stimulation of DHER-14 cells, 3T3 fibroblasts stably transfected with EGF receptor, on the other hand, showed complete inhibition by genistein. These results are summarized in Table II. Stability of the acidification rates during all of these

TABLE II

Inhibition of transfected receptor responses by genistein

Receptor (Agonist)	% Increase[a]	
	− Genistein	− Genistein (40 μg/ml)
β2-Adrenergic (10 μM isoproterenol)	36	30
EGF (10 ng/ml TGF-α)	28	0

[a] % Increase is the difference between stimulated and initial (100%) cell acidification rates, measured at the peak of agonist response.

experiments clearly indicates that genistein treatment did not cause any cell death. This was further confirmed in the case of T cells by dye exclusion viability measurements.

DISCUSSION

Results presented in this report demonstrate an increase in T cell acidification rate as a specific response to interaction with cognate MHC class II-peptide complex. Similar increases in the acidification rate were observed in the presence of rIL-2 and during TCR ligation by anti-CD3 and anti-TCR antibodies. The increase in acidification rate of other cell types upon binding of receptor-specific ligands has been described earlier (1, 2). We have extended these studies to T cell clones. The 4R 3.9 T cell clone used in this study is specific for the acetylated N-terminal 1–14 peptide fragment of rat myelin basic protein. A specific increase in acidification rate was obtained by treatment with a complex of IA^k-MBP(1–14)A^d. We used the MBP(1–14) peptide analog containing an alanine substitution at position 4, which has been shown to result in increased binding of this peptide to IA^k (12). The increase in the acidification rate of 4R3.9 T cells in the presence of IA^k-MBP(1–14)A^d was shown to be highly specific, because cells exposed to only MBP peptide, IA^k, IA^d-PLP(139–151) or IA^d-OVA(323–339) complexes showed no significant increase in the acidification rate. A similar result was obtained with another T cell clone, AJ1.2, specific for the same antigenic determinant of the MBP molecule (result not shown). The specificity of the rate increase was further confirmed by the lack of response of BW5147 cells, a T lymphoma cell line with no TCR. The T cells exhibited a very strong acidification response to rIL-2. The effect of rIL-2 on T cell acidification rate is dose dependent, and the increased rate of acidification saturated at 100 U/ml concentration of rIL-2. T cells either treated or untreated with complex and then exposed to rIL-2 showed a strong increase in acidification rate.

In all of the experiments the increase in acidification rate was sustained long after the initial rapid rise. We have observed, however, a decrease in the overall rate 5 to 7 h after cell loading into chambers. The drop is most likely caused by the decreased viability of cells exposed to serum-free medium for an extended period of time. The cell stimulation experiments presented here are conducted within the first 3 h of the microphysiometer run, while cells show no loss of viability.

The T cell clones we used in this study seem to be sensitive to serum-free medium. Storage in 2.5% serum at a cell density of 1×10^6 cells/ml was preferable for maintaining cell viability; the cells were >95% viable

under these conditions, stored overnight. The metabolic responses are best observed in resting cells that have been maintained in 2.5% serum overnight. This observation can be compared with a previous study that reported CHO cells transfected with the m1-muscarinic receptor require overnight serum starvation to produce a surge in acidification rate upon stimulation with carbamoylcholine, an agonist for that receptor (2). The specific T cell response to cognate MHC-Ag complexes was significantly increased when the stimulation was conducted in serum-free, low buffering medium, as opposed to a very weak or no increase when conducted in medium containing 10% serum. The magnitude of the increase in acidification rate ranged from 15 to 100% of the prestimulation value. The response amplitude depends on the cell density and the concentration of MHC II-peptide complex or IL-2 used to stimulate the cells. Exposure time may also influence the amplitude of the response; however, that parameter was held constant in this series of experiments.

It was observed that the acidification rates of the resting T cells gradually increase during the first 2.5 to 3 h. This initial increase in rate of cells loaded into the microphysiometer has been observed for a variety of T cell lines as well as the T cell clone used in the present work (unpublished observation). The origin of this increase is not understood, but may be related to autocrine or nonspecific stimulation of the cells that are held at relatively high density in the cell capsules. The inclusion of albumin in the serum-free, running medium used for microphysiometer experiments appears to decrease the unstimulated cell rise in acidification rate. Perhaps irritancy effects of the cell capsule environment are reduced by inclusion of the protein. Irritancy by agents with low toxicity was found in earlier studies to cause a nonspecific increase in acidification rate (1).

T cell activation has been shown to be blocked by genistein (13, 14), a tyrosine kinase inhibitor (15). Therefore, the effect of genistein on the acidification responses of 4R3.9 T cells was studied. At a concentration of 40 μg/ml, genistein inhibited the stimulation of T cells by Ag, IL-2, anti-CD3, or anti-TCR antibodies, and no signs of genistein cytotoxicity were observed. This concentration has been previously shown to inhibit the activation of phospholipase C and phosphoinositol release during TCR ligation by anti-CD3 antibody (16). Our results obtained with the microphysiometer are in agreement with these previously reported results using genistein treatment of T cells. Additional evidence for the specificity of the genistein inhibition of acidification enhancement was provided by testing cells transfected with the EGF receptor, a tyrosine kinase receptor (17), and the β2-adrenergic receptor, an adenylate cyclase G-protein-linked receptor (18). As expected, genistein blocked the EGF receptor response and not the β2-adrenergic receptor response.

It is known that the specific binding of cognate MHC II-peptide complex to T cells can result in either activation and proliferation, or induction of tolerance, depending on the presence of co-stimulation signals (8, 9, 19). Measurement of the increase in the acidification rate obtained with a soluble class II-peptide complex provides a noninvasive and rapid in vitro method for examining the specificity of T cell response. Whether such response is linked to the induction of anergy or proliferation is yet to be determined.

Acknowledgments. The authors thank Patricia Jones for providing T cell clones; Craig Venter and Joseph Schlessinger for receptor transfected cells; Ralph Kubo and Jim Allison for hybridoma cells; Rick Harkins for TGF-α; David Passmore, David Kopa, Masami Hattori, and Dario Slavazza for technical assistance; Greg Kirk, Jeff Libby, Victoria Muir, and the entire CytoSensor product team for the research prototype and supplies; and John Owicki and Gillian Humphries for critical reading of the manuscript.

REFERENCES

1. **Parce, J. W., J. C. Owicki, K. M. Kercso, G. B. Sigal, H. G. Wada, V. C. Muir, L. C. Bousse, K. L. Ross, B. I. Sikic, and H. M. McConnell.** 1989. Detection of cell-affecting agents with a silicon biosensor. *Science 246:243.*
2. **Owicki, J. C., J. W. Parce, K. M. Kersco, G. B. Sigal, V. C. Muir, J. C. Venter, C. M. Fraser, and H. M. McConnell.** 1990. Continuous monitoring of receptor-mediated changes in the metabolic rates of living cells. *Proc. Natl. Acad. Sci. USA 87:4007.*
3. **Gratzner, H. G.** 1982. Monoclonal antibody to 5-bromo- and 5-iodo deoxyuridine: a new reagent for detection of DNA replication. *Science 218:474.*
4. **Mosmann, T.** 1983. Rapid colorimetric assay for cellular growth and survival: application to proliferation and cytotoxicity assays. *J. Immunol. Methods 65:55.*
5. **Gillis, S., M. M. Ferm, W. Ou, and K. A. Smith.** 1978. T-cell growth factor: parameters of production and a quantitative microassay for activity. *J. Immunol. 120:2027.*
6. **Watts, T. H., A. A. Brian, J. W. Kappler, P. Marrack, and H. M. McConnell.** 1984. Antigen presentation by supported planar membranes containing affinity-purified IAd. *Proc. Natl. Acad. Sci., USA 81:7564.*
7. **Quill, H., L. Carlson, B. S. Fox, J. N. Weinstein, and R. H. Schwartz.** 1987. Optimization of antigen presentation to T-cell hybridomas by purified Ia molecules in planar membranes. Ia molecule polymorphism determines the antigenic fine specificity of the response to cytochrome c peptides. *J. Immunol. Methods 98:29.*
8. **Mueller, D. L., M. K. Jenkins, and R. H. Schwartz.** 1989. Clonal expansion versus functional clonal inactivation: a costimulatory pathway determines the outcome of T-cell antigen receptor occupancy. *Annu. Rev. Immunol. 7:445.*
9. **Schwartz, R. H., D. L. Mueller, M. K. Jenkins, and H. Quill.** 1989. T-cell clonal anergy. *Cold Spring Harbor Symp. Quant. Biol. vol. LIV, part 2, p. 605.*
10. **McConnell, H. M., P. Rice, H. G. Wada, J. C. Owicki, and J. W. Parce.** 1991. The microphysiometer biosensor. *Curr. Opin. Struct. Biol. 1:647.*
11. **Hafeman, D. G., J. W. Parce, and H. M. McConnell.** 1988. Light-addressable potentiometric sensor for biochemical systems. *Science 240:1182.*
12. **Watson, J.** 1979. Continuous proliferation of murine antigen specific helper T lymphocytes in culture. *J. Exp. Med. 150:1510.*
13. **Norton, S. D., D. E. Hovinen, and M. K. Jenkins.** 1991. IL-2 secretion and T-cell clonal anergy are induced by distinct biochemical pathways. *J. Immunol. 146:1125.*
14. **Klausner, R. D., and L. E. Samelson.** 1991. T-cell antigen receptor activation pathways: The tyrosine kinase connection. *Cell 64:875.*
15. **Tetsu, A., J. Ishida, S. Nakagawa, H. Ogawara, S. Watanabe, N. Itoh, M. Shibuya, and Y. Fukami.** 1987. Genistein, a specific inhibitor of tyrosine-specific protein kinases. *J. Biol. Chem. 262:5592.*
16. **Mustelin, T., K. M. Coggeshall, N. Isakov, and A. Altman.** 1990. T-cell antigen receptor-mediated activation of phospholipase C requires tyrosine phosphorylation. *Science 247:1584.*
17. **Honegger, A. M., T. J. Dull, S. Felder, E. Van Obberghen, F. Bellot, D. Szapary, A. Schmidt, A. Ullrich, and J. Schlessinger.** 1987. Point mutation at the ATP binding site of EGF receptor abolishes protein-tyrosine kinase activity and alters cellular routing. *Cell 51:199.*
18. **Fraser, C. M., F.-Z. Chung, and J. C. Venter.** 1987. Continuous high density expression of human β2-adrenergic receptors in a mouse cell line previously lacking β-receptors. *J. Biol. Chem. 262:14843.*
19. **Quill, H., R. H. Schwartz.** 1987. Stimulation of normal inducer T-cell clones with antigen presented by purified Ia molecules in planar lipid membranes: specific induction of a long-lived state of proliferative nonresponsiveness. *J. Immunol. 138:3704.*

Annu. Rev. Biophys. Biomol. Struct. 1994. 23:87–113

THE LIGHT-ADDRESSABLE POTENTIOMETRIC SENSOR: Principles and Biological Applications

John C. Owicki, Luc J. Bousse, Dean G. Hafeman, Gregory L. Kirk, John D. Olson, H. Garrett Wada, and J. Wallace Parce

Molecular Devices Corporation, Menlo Park, California 94025

KEY WORDS: LAPS, sensor, immunoassay, bioassay, receptor

CONTENTS

INTRODUCTION 88
PRINCIPLES OF THE LIGHT-ADDRESSABLE POTENTIOMETRIC SENSOR 88
Measurement of pH 89
The Photoeffect 90
Light Addressability 93
Measurement of Other Chemical Species 93
THE LAPS AS A SENSOR IN AN ANALYTICAL SYSTEM 94
Electrical Measurement of Phospholipid Membranes 94
Discrete Sensor Arrays 94
LAPS as an Imaging Sensor 94
Microvolume Systems 95
The Sensor as a Structural Element of Analytical Systems 96
Data Analysis in LAPS Systems 96
APPLICATIONS FOR BIOCHEMICAL ASSAYS 98
Measurement of Enzyme Substrates and Inhibitors 98
Enzyme-Linked Immunoassays 98
APPLICATIONS FOR CELL-BASED BIOASSAYS: THE MICROPHYSIOMETER 102
Biological Basis 102
Instrumental Characteristics 102
Applications of Microphysiometry 105
Prospects 108
CONCLUDING PERSPECTIVE 109

1056-8700/94/0610-0087$05.00

INTRODUCTION

Semiconductor technology and biotechnology are two major technical disciplines that have large practical ramifications. This review describes the fruits of a research and development project that combines the two fields: the light-addressable potentiometric sensor (LAPS) and its bioanalytical applications.

Our focus on this particular device prevents us from describing in detail other noteworthy work at the interface (both intellectual and physical!) between semiconductor technology and biology. Such studies include the work of Fromherz et al on using field-effect transistors to sense action potentials (25) and others on the fabrication of microelectrodes (18, 21, 57). Several groups have used photolithography to pattern the chemical or physical properties of cell-culture substrates to control the patterns of adhesion or migration of cells (17, 20, 32, 66). The work of Fodor et al combining photolithographic chemical synthesis with optical sensing (24) is also worth reading about.

Here, we first present the principles of operation of the LAPS without relying too heavily on solid-state physics. Next we indicate how the LAPS can be integrated into sensitive analytical systems, stressing the sensor's usefulness for microvolume applications. Finally, we survey the two primary applications of the LAPS to date: an enzyme-linked immunosorbent assay (ELISA) system and a system for performing bioassays on living cells, the microphysiometer.

PRINCIPLES OF THE LIGHT-ADDRESSABLE POTENTIOMETRIC SENSOR

The LAPS, as currently used in analytical instrumentation, consists of lightly doped silicon with a thin silicon nitride insulator that contacts an aqueous solution (Figure 1). The accompanying electronic equipment serves two purposes. It controls the potential (Ψ) applied from the noninsulated side of the silicon to the solution and measures an alternating photocurrent (I_p) generated when a light source, such as one of the light-emitting diodes (LEDs) pictured in Figure 1, flashes rapidly. Both chemical sensing and signal transduction occur immediately adjacent to the insulator layer, at the solution-insulator interface, and the silicon-insulator interface respectively.

Figure 2 is a schematic of the LAPS showing the changes in potential that occur as the circuit is traced from solution through the sensor and back through the electronics to the solution again. Ground potential is chosen as the potential of the noninsulated side of the silicon chip.

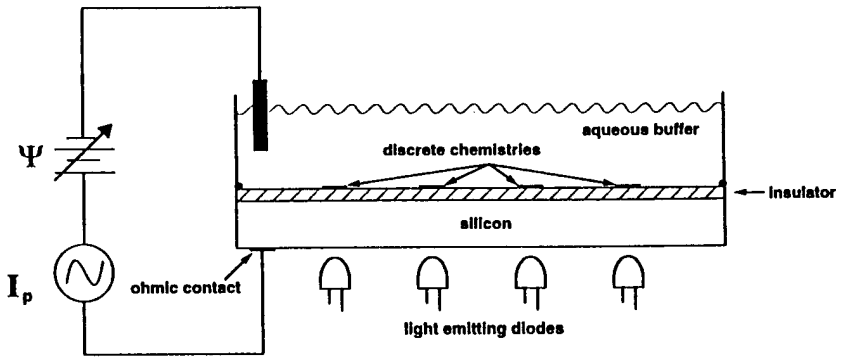

Figure 1 Schematic representation of a LAPS device and circuit components. In this case, the electrode placed in the aqueous buffer serves both as a controlling and a reference electrode. See text for details.

Beginning at the left side of the figure, this potential is changed by a potentiostat, depicted here as a variable potential, Ψ, such that the solution is negative with respect to the potential of bulk silicon. Scanning through solution toward the right, the potential remains essentially constant up to within a few nanometers of the insulator surface.

Measurement of pH

The silicon nitride surface contains primarily silanol groups with a small percentage of silamine groups (9, 10). The silanol groups titrate with

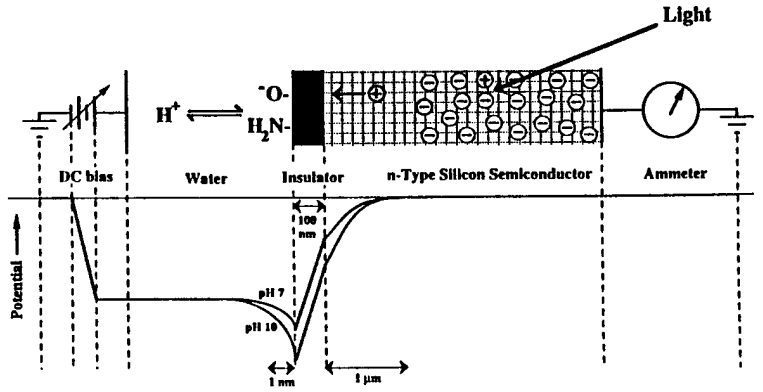

Figure 2 Physical principles of LAPS operation. This is a schematic view of the change in potential around the circuit depicted in Figure 1. Circled minuses and pluses represent electrons and holes, respectively, in the silicon. The bold-outlined circles represent electron-hole pairs created by the absorption of light. Note that the lateral dimensions are not to scale.

protons from solution and exist as either negatively charged SiO^- or neutrally charged SiOH functions. Likewise the silamine groups can exist as neutral or positively charged functions. The surface is neutrally charged at a pH of ~3.5 (point of zero charge). Therefore at neutral pH the surface is negatively charged as depicted in the figure, and the potential of solution becomes more negative as the surface is approached. The distance over which the solution potential deviates from that of the bulk is determined by the ionic strength of solution. At physiologic ionic strength, ~150 mM, the $1/e$ distance for the exponential decay of the surface potential is approximately 1 nm. Also as depicted in the figure, the difference in potential between bulk solution and the insulator surface is pH dependent, and therefore the potential at the surface is more negative at pH 10 than at pH 7. The pH dependence of the surface potential is Nernstian, ~59 mV/pH unit at room temperature (5, 27). This is the attribute of the sensor that enables measurement of solution pH. Nernstian responses require a high density of titratable groups on the sensor surface. Based on the relatively short shielding distance in physiologic saline in relation to the size of a typical globular protein, one would predict that adsorbed proteins would have little influence on sensor performance. In fact, the LAPS has been used to measure the pH of whole blood without experiencing any fouling problems (D Hafeman, personal communication).

Progressing through the insulator, the potential rises back toward that of the bulk silicon. In the silicon adjacent to the insulator, a depletion layer (space-charge region) may be formed owing to the electrostatic repulsion of majority charge carriers (electrons in n-type silicon). This region, in which the potential decays to that of the bulk silicon, is ~1 μm thick for the densities of phosphorus dopant used in the LAPS (~10 Ωcm silicon). It is the electric field (voltage gradient) in this region that is sensed electronically to determine changes in the surface potential and therefore changes in the solution pH. Completing the circuit on the right hand side is an ammeter used to measure alternating current.

As can be seen, the LAPS belongs to the family of electrolyte-insulator–silicon field–effect sensors. This family also includes the ion-selective field–effect transistors, sometimes called ChemFETs (4, 30). The differences between these devices result from the different mechanisms used to detect changes in the potential at the silicon-insulator interface.

The Photoeffect

The presence of a depletion layer in the sensor can be determined by shining light on the silicon and measuring the current in the ammeter.

When silicon absorbs light of the appropriate wavelength, hole-electron pairs are generated. These pairs become separated in the electric field in the depletion layer. Electrons move toward the silicon bulk, and holes accumulate at the silicon-insulator interface. This charge separation results in a compensatory capacitatively coupled movement of charge in the external circuit that the ammeter can detect. Figure 3*a* shows the current generated in the external circuit by illuminating a sensor with an LED as depicted in Figure 1. When the light is turned on, the current rises as holes diffuse from their point of generation near the back of the sensor and are separated in the electric field in the depletion layer (drift current). Holes accumulate at the silicon-insulator interface until a steady state is reached at which the rate of diffusion of holes back toward the bulk silicon (diffusion current) equals the drift current. At that point, the current in the external circuit has decayed to zero. When the LED is turned off, the diffusion current now predominates, and current flows transiently in the opposite direction as the light-induced charge separation is reversed. Because there is no flow of direct current through the insulator, the areas under the charg-

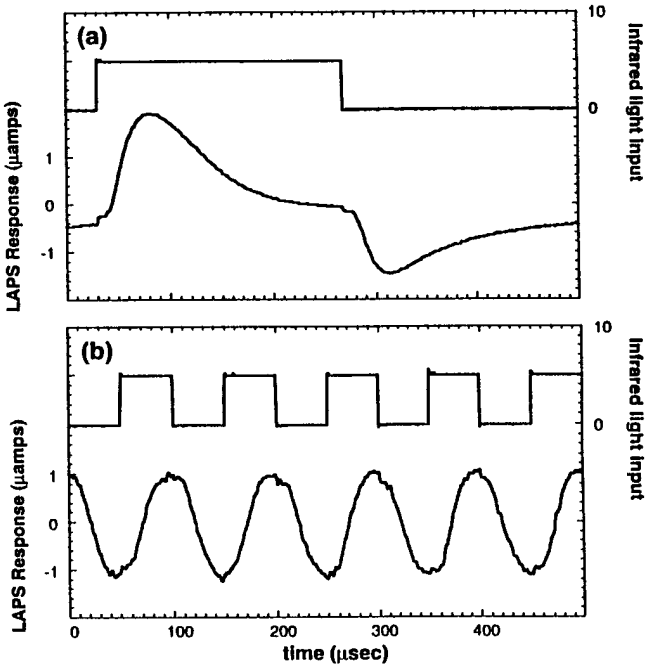

Figure 3 Photocurrents in the LAPS. (*a, lower trace*) Transient photocurrents resulting from initiating and ceasing sensor illumination (*upper trace*, in arbitrary units). (*b*) The continuous response to a 10-kHz square-wave modulation of the light intensity.

ing and discharging curves in Figure 3*a* are equal. To generate a more useful signal, in practice the LED is flashed rapidly with respect to the decay processes, resulting in the signal shown in Figure 3*b*. This signal is rectified to give to give a root mean square (rms) amplitude for the AC photocurrent (I_p).

The photocurrent described above only exists when a depletion layer is present in the silicon. If the potential applied to the solution becomes sufficiently positive, the depletion layer collapses and no photocurrent is generated. This effect appears in Figure 4, where I_p is plotted versus the applied potential (Ψ). Note that the three photoresponse curves shown for three different solution pH values are identical except for shifts on the potential axis. This is because the potential sensed in the silicon is the sum of any fixed potentials in the series circuit, Ψ, and the surface potential at the insulator-aqueous interface. As mentioned previously, the surface potential depends on the solution pH. Change in pH can be measured by determining the shift in the photoresponse curve from its position at any starting pH value. The value of Ψ at which the inflection point ($d^2I_p/d\Psi^2 = 0$) occurs in the photoresponse curve is called Ψ_{pip} and is used to monitor the shift on the potential axis.

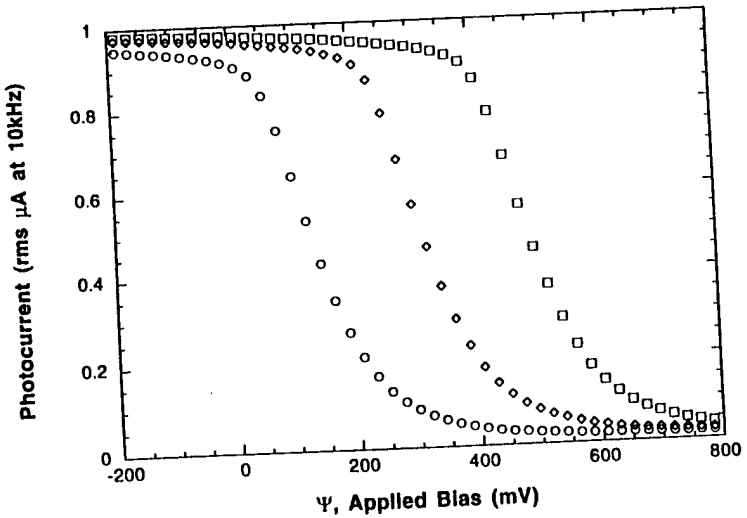

Figure 4 Photocurrent-voltage curves in LAPS and the effects of pH. The potential from solution to the silicon bulk, as determined by a Ag/AgCl reference electrode, was swept from −200 mV to +800 mV while the light intensity was modulated at 10 kHz and the photocurrent was recorded. The curves represent pH 4.0 (*circles*), pH 7.0 (*diamonds*), and pH 10.0 (*squares*).

Light Addressability

As shown in Figure 1, the pH of solution is only measured where the sensor is illuminated. Thus the four LEDs can be energized one at a time and used to measure local changes in pH due to the discrete chemistries adjacent to the sensor surface. By multiplexing the LEDs, one can use this light addressability to perform many measurements practically simultaneously with a single sensor and a single set of accompanying electronics.

Measurement of Other Chemical Species

Our discussion so far has focused on sensing pH. However, the LAPS is a generic potentiometric sensor, and as such can be configured to sense a variety of species (27). Figure 5 shows near Nernstian responses of the LAPS for the sensing of pH, redox potential, and potassium ions. The redox potential of a solution of ferri- and ferrocyanide was determined using a LAPS with a thin gold spot evaporated onto the solution side of the insulator. For determining [K^+], a polyvinyl chlo-

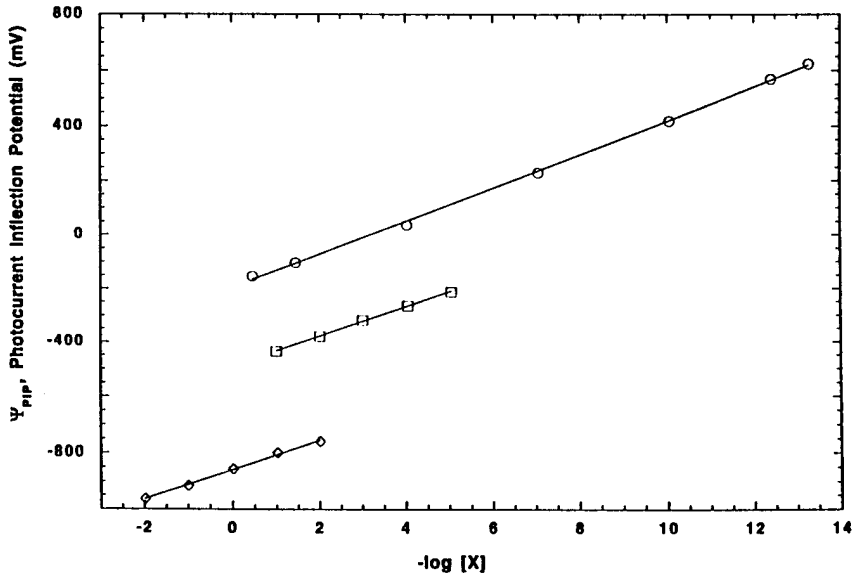

Figure 5 Detection of pH, redox potential, and [K^+] with LAPS. Three different LAPS devices were used to perform these measurements: for pH measurements (*circles*), the silicon nitride insulator contacted solution; for determination of redox potential (*diamonds*), a thin layer of gold was evaporated on the insulator surface; for measurements of potassium (*squares*), a thin membrane of polyvinylchloride containing valinomycin was pressed onto the LAPS insulator surface by means of an o-ring.

ride membrane containing the potassium ionophore valinomycin was deposited on the surface of the sensor.

THE LAPS AS A SENSOR IN AN ANALYTICAL SYSTEM

As discussed above, the LAPS displays a variety of novel attributes. From an analytical point of view, a sensor is only as good as the system in which it is incorporated. The remainder of this article focuses on measurement systems designed to take advantage of the LAPS's capabilities.

Electrical Measurements of Phospholipid Membranes

An early use of the LAPS was to measure the electrical properties of phospholipid bilayer membranes. Transmembrane potentials, as well as membrane capacitance and conductance, were all determined using a black-lipid membrane (BLM) configuration (65). Although this configuration has not been pursued further, it should be possible to combine phospholipid membranes with micromachined structures on LAPS to construct novel sensor systems. Membrane stability is of paramount importance.

Discrete Sensor Arrays

One of the first analytical applications of the LAPS, proposed originally by Hafeman et al (27), was an array of sensors for different analytes, fabricated by placing an ion-selective membrane at the solution-insulator interface over each sensing spot. Investigators have explored this type of LAPS application in several systems to measure potentiometric responses of arrays of different chemical sensors. Examples include the recent work of Kanai et al (31) on taste sensors and of Sato et al (63) on gas sensing. As we discuss later, an array of sensing sites has also been used to increase the parallelism in a LAPS-based immunoassay system.

LAPS as an Imaging Sensor

Several research groups have used LAPS devices to make potentiometric images of the front surface by scanning light from an LED or a laser on the backside of the silicon chip or wafer. This amounts to an extension of the discrete sensor arrays, in which the number of sensor spots becomes very large. This concept was first demonstrated by Lundstrom et al in 1991 using arrays of gas-sensitive materials (37), and it is being further developed to generate artificial olfactory images

(38, 72). Another type of recently demonstrated imaging involves enzyme reactions (64). Here, different enzymes are immobilized on the surface of the LAPS to measure concentrations of the enzyme substrates (glucose and urea). Iwasaki et al (45), investigating the spatial resolution of such imaging LAPS systems, concluded that with backside illumination, resolution is approximately equal to the wafer thickness. Clearly, this whole area is still in its infancy and is being actively developed.

Microvolume Systems

The most important applications of LAPS devices to date have been to measure time-varying chemical concentrations in very small volumes (11). A LAPS device especially suits this application because the silicon front surface is extremely flat, and it has no metallization leads or bond wires with their required encapsulation. The microvolumes used are typically on the order of 1 mm by 1 mm by 100 μm, or 100 nl. However, even thinner chambers are relatively easy to make, and a goal of 10 nl could be met if needed. In most work so far, the chemical quantity monitored has been either pH or redox potential.

Molecular Devices Corporation has pursued two families of microvolume applications in which different agents cause a pH change. One application is an ELISA based on a pH-changing enzyme. In the other, the excretion of acidic metabolites by living cells provides a means to measure metabolic activity. Both cases are discussed in more detail below, but here we note that the measured quantity is the rate of pH change, not pH itself. Clearly, for a given number of protons or hydroxyl ions added to the system, the resulting rate of pH change will be larger if the total volume is smaller. A general expression for the rate of pH change in a microvolume is

$$\frac{dpH}{dt} = \frac{R}{V\beta_V + S\beta_S}, \qquad 1.$$

where R is the rate at which H^+ or OH^- ions are generated (positive for OH^- ions and negative for H^+ ions); V and S are the volume and surface area of the reaction chamber, and β_V and β_S are volumetric and surface buffer capacities (11). Rapid equilibration of the pH in an unstirred microvolume chamber requires that the chamber be thin, customarily 100–200 μm thick, and that most of the buffer capacity be contributed by diffusing species rather than by bound species. Thus $V\beta_V$ should be at least a factor of 10 greater than $S\beta_S$. The volumetric buffer capacity β_V is determined by the concentration of buffer present; at a pH equal to the pK of the buffer, $\beta_V(\max) = 0.576c$ for monovalent

buffers, where c is the buffer concentration. When pH is different from pK, β_V decreases from this maximal value. The term in Equation 1 corresponding to surface buffering is very important in the immunoassay applications, in which a membrane is used to capture and immobilize the immunocomplexes. This membrane has a large surface area, and because of its own composition as well as adsorbed protein, it can contribute significantly to the total buffer capacity. A 100-μm-thick nitrocellulose membrane coated with biotinylated bovine serum albumin has a surface buffer capacity equivalent to the buffer capacity of ~2–3 mM sodium phosphate near its pK_a in the same volume (6).

The principles for measuring rate of redox potential change are exactly the same as for pH except that the sensing area on the LAPS has a noble metal surface for sensing redox potential rather than a pH-sensing surface (27). An equation analogous to Equation 1 can be defined for redox measurements. For useful membrane materials and in biological systems, the buffer capacity for redox is usually much lower than that for pH (J Song, personal communication), which renders redox detection much more sensitive than pH detection as long as the detection limits are set by the size of the potentiometric signal.

The Sensor as a Structural Element of Analytical Systems

The front side of a LAPS device has no metallizations or transistor structures. Photocurrent is measured from the device through a single electrode in the conductive solution, with a single wire lead from the backside of the device. The requirements of electronic and micromachining steps in the fabrication of chemical sensors often conflict. Therefore, the relatively minor electronic constraints on LAPS fabrication make this device quite useful for applications requiring micromachining. Micromachining has been used in some microphysiometer applications to make 50 × 50 × 50 μm wells in which nonadherent cells can be sedimented (12, 53) and to etch flow channels for multichannel microphysiometer chips (7, 8).

Data Analysis in LAPS Systems

When examining data obtained in a system using a LAPS device, one should understand the hierarchy of the different data levels. The first level consists of the measured photocurrent as a function of bias voltage, as shown in Figures 4 and 6*a*. The exact relationship between photocurrent and bias voltage is complex and has been used to study the presence of fixed charges and electron-accepting or -donating states at the silicon-insulator interface (26). Several efforts to model LAPS photocurrent/bias-voltage curves have been published (11, 39, 61, 62).

The details of this structure are unimportant for potentiometric sensing applications; as described earlier, potentiometric measurements usually only quantify the shift in this relationship along the bias-potential axis, typically in the form of the photocurrent inflection potential (Ψ_{pip}), as shown in Figure 6*a*. Adami et al (1) have described another

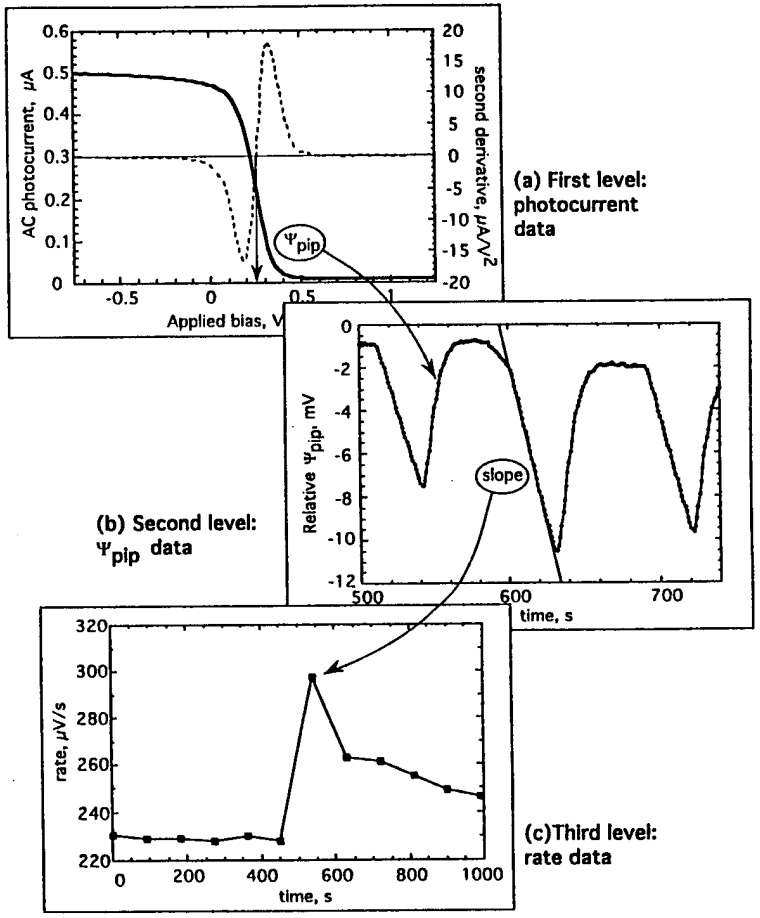

Figure 6 Data-analysis hierarchy. (*a*) The photoresponse curve (*solid line*). The inflection point of the photoresponse curve (Ψ_{pip}) is determined by finding the zero crossing of the second derivative (*dashed line*). (*b*) A typical experiment in which the voltage (Ψ_{pip}) is plotted versus time as some change in surface potential shifts its value. (*c*) The rate of change in the surface potential is determined by a least-squares fit of the χ_{pip} data. The data shown are from a microphysiometer, and the change in pH is caused by the build-up of excreted acidic substances during a brief halt in the flow of culture medium past the cells; the increase in acidification rate results from the addition of an agonist for muscarinic receptors on the cells in the microphysiometer chamber.

method for measuring this shift using a dual LAPS device. In commercially available sensor systems, this first level of data analysis is made invisible to the user, and the Ψ_{pip} data are shown as sensor-output data. The Ψ_{pip} data (Figure 6*b*) constitute the second level of data, which are equivalent to the voltages that would be measured by a pH-sensitive glass electrode. Where the rate of pH change is desired, these Ψ_{pip} data over time are fit by linear regression, giving the rate of potential change (Figure 6*c*). With a Nernstian response of 60 mV/pH unit, 1 μV/s corresponds to a rate of pH change of about 1 milli-pH unit per min.

APPLICATIONS FOR BIOCHEMICAL ASSAYS

Measurement of Enzyme Substrates and Inhibitors

To measure various compounds in a solution, LAPS devices have been coupled with enzymes that produce either pH or redox potential changes. Enzymes have been immobilized directly onto the surface of the LAPS to measure the concentration of enzyme substrates, urea and glucose, via pH changes (64). In this particular application, the sensor response depends on the pH buffer capacity of the medium in which it is immersed (16). These devices can be used in cases where a constant buffer capacity is expected, such as in a fermentation tank, and the pH response can be calibrated to the concentration of substrate. Enzymes have also been used in conjunction with the LAPS to measure specific enzymatic inhibitors such as anticholinesterase insecticides (23).

The major use of enzymes with LAPS has been in enzyme-linked immunoassays, as detailed below. Urease has been used most often as an enyme label; the catalyzed hydrolysis of urea increases pH at a rate proportional to enzymatic activity. Enzymes that catalyze reactions that change redox potential have also been used. For example, Wada et al have coupled the horseradish peroxidase-catalyzed oxidation of tetramethyl benzidine and the alkaline phosphatase-catalyzed hydrolysis of 5-bromo-4-chloro-3-indolylphosphate to the redox potential mediators hexacyanoferrate or ruthenium pentamine pyridine (71).

Enzyme-Linked Immunoassays

Most immunoassays involve the binding of enzyme-linked antibodies to ligands and separation of bound and free enzymes. These assays can be set up in two formats. First, multiepitopic ligands can be sandwiched between two antibodies (or other binding proteins): one to attach the ligand to the solid surface, and one to attach it to the enzyme label. Second, small haptens can be attached to the solid surface to compete with haptens in solution for binding sites on enzyme-labeled antibodies.

The surface of the sensor itself can be used as the solid phase for separation, or an alternative support can cause the separation and then be transferred to the sensor. Because solid phases can dramatically affect the performance of enzyme immunoassays (54), one should use a solid phase and assay protocol that minimally perturb the binding reaction and the signal detection.

Microporous membranes such as nitrocellulose are ideal solid supports for use with the LAPS. The monolithic nature of the sensor allows presentation of membranes to the LAPS surface under conditions that maintain a precise microvolume for measurement. The act of capturing the enzyme complex on a membrane also concentrates the complex into a small volume (47). The nitrocellulose filter membrane (0.45 μm pore size) is ~120 μm thick and ~30% solid. Capture by filtration through a spot 3 mm in diameter defines a solution volume of approximately 0.64 μl in which the enzyme changes the pH or redox potential.

Microporous capture membranes also have the advantage that reactants can be filtered rapidly with efficient, high-capacity capture because of the large surface area of the membrane (~150 cm^2 per 1 cm^2 of planar surface). This high surface area has its drawbacks, however. Proteins tend to adsorb to surfaces, and unwanted (nonspecific) binding of the enzyme to the solid phase can reduce assay sensitivity (22). Furthermore, high surface-buffer capacity reduces the signal obtained per enzyme molecule.

A commercial application of the LAPS for immunoassays (Threshold®) uses a biotinylated nitrocellulose capture membrane and streptavidin to capture specific binders and urease (41). The binding reactions involving the antibodies are performed in solution, followed by filtration through the membrane for rapid separation (Figure 7*a*). The sensor chamber, or reader, is designed to accept the membrane mounted across an aperture on a plastic stick, align the filtration spots with the light-interrogated areas of the LAPS, and create a microvolume by pressing the membrane against the sensor (Figure 7*b*). Eight samples are assayed in parallel on a membrane stick, taking advantage of the light addressability of the sensor.

Table 1 lists several ligands that have been detected with the LAPS and membrane capture. The analytes in the various assays were bound by specific antibodies (for protein antigens and haptens), DNA-binding proteins (for total DNA), or DNA probes (for specific-sequence DNA).

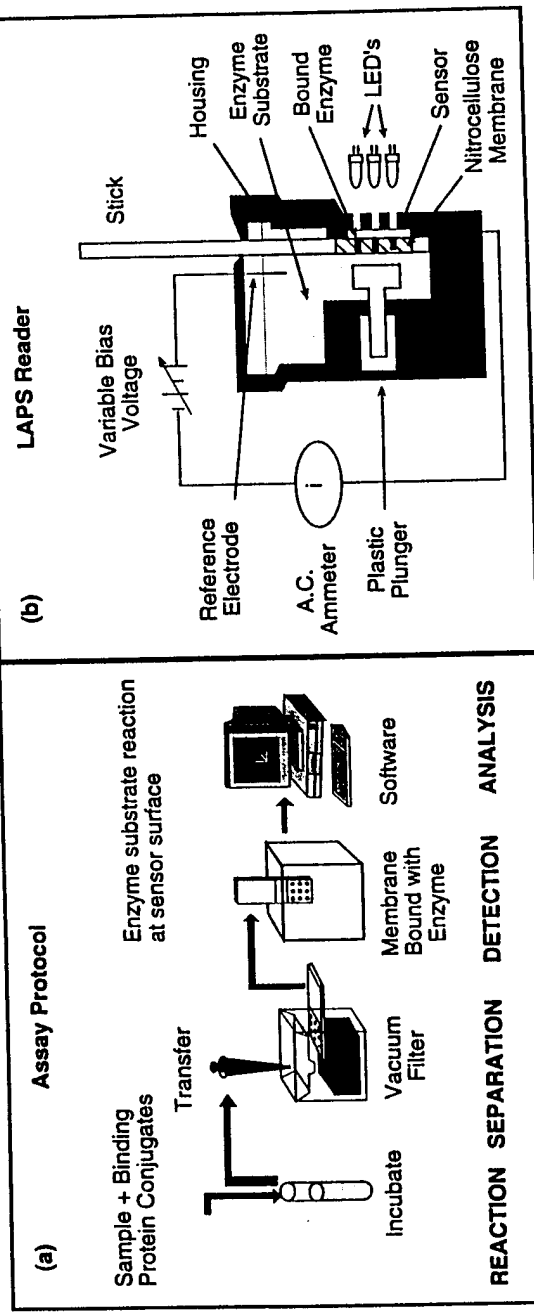

Figure 7 Solution-phase binding of enzyme conjugate and ligand is determined by vacuum filtration of the reagents, including a biotinylated component with streptavidin, through multiple spots on a biotinylated capture membrane. (*a*) The membrane is transferred to a LAPS reader (*b*), which aligns the filtration spots with the LEDs. A plunger presses the membrane against the sensor, creating individual microvolumes at each filtration spot for the captured enzyme complexes. Either pH or redox changes are sensed in the microvolumes.

Table 1 Lower limit of detection and assay time for various analytes in a LAPS-based immunoassay

Analyte	Sensitivity	Assay time	Reference
Total DNA	2 pg	2 h	14
Specific-sequence DNA	2×10^7 molecules	1 h	48
Tick anticoagulant protein	2.5 pg	2.5 h	58
Protein A	10 pg	4 h	41
Human chorionic gonadotropin	10 pg	20 min	47
Anti-PreS2 antibody	750 pg	overnight	29
Nicotinic acetylcholine receptor	1 ng	<10 min	59
Chlamydia trachomatis	600 cells	30 min	70
Neisseria meningitidis	800 cells	30 min	35
Yersinia pestis	4000 cells	30 min	35
Newcastle disease virus	130 pg	6 min	33a
	40 ng	65 min	
T-2 mycotoxin	1.0 ng	3 min	36
Saxitoxin	1.5 ng	3 min	73

In the case of the nicotinic acetylcholine receptor, biotinylated bungarotoxin was used to capture the receptor on the membrane (59). The incubation time and binding affinity of the reactants affect assay sensitivity. Assays listed in the table were optimized either for sensitivity or speed (or, in the case of the anti-PreS2 antibody assay, were run in parallel with an overnight radioimmunoassay).

Affinity constants for binding pairs have been determined using this assay configuration (K Dill & D Hafeman, personal communication). The rapid-filtration system allows equilibration to take place in the solution phase and minimizes the time of binder-receptor exposure to the solid phase. The affinity constants are thus unperturbed by the presence of the solid phase. In some other solid-phase measurement systems, as in most microplate determinations, equilibrium is established on the solid phase, or the time of contact between solution and solid phases is long enough for binding to the solid phase to perturb the solution-phase equilibrium and lower the measured affinity constant (28).

Other instruments have been developed that use the filtration/sensor system described above to run enzyme-linked assays. One such system applies the attributes of the Threshold® system in an automated form (36, 51). Here, the membrane is mounted on a continuous tape that is automatically transferred from a chemistry station, where regents have been automatically metered and filtered, to a reader. This system is

designed for unattended continuous monitoring, for example in environmental applications.

APPLICATIONS FOR CELL-BASED BIOASSAYS: THE MICROPHYSIOMETER

Biological Basis

The hydrolysis of an ATP molecule in a cell liberates about 0.7 H^+ ions, whereas the synthesis of an ATP may produce or consume H^+, depending on the carbon source and catabolic pathway, but it usually does so in smaller amounts. ATP synthesis and hydrolysis must be balanced in the long term (typically minutes), and so the net effect of energy metabolism is to produce acid. This typically appears as the excretion of lactic acid or CO_2, through glycolysis or respiration. Hence, the rate of extracellular acidification is a measure of catabolic activity that is similar in principle to the rate of glucose or O_2 consumption, or to the rate of lactate, CO_2, or heat production. Extracellular acidification has, however, some instrumental advantages.

An additional component of extracellular acidification is independent of energy metabolism. Intracellular pH (pH_i) is altered during a variety of physiological processes, including the activation of many growth-factor receptors. The transition from one steady-state pH_i to a higher steady-state pH_i involves the transfer of protons from the cytoplasmic buffer to the environment as a pulse during the transition.

We summarize the relationships of some of the biological processes in Figure 8 and have discussed them in more detail elsewhere (49). Monitoring the extracellular acidification rate can in principle be used as a relatively generic method of detecting physiological changes, because many such changes alter pH_i, and most alter the use or generation of metabolic (free) energy. A LAPS-based instrument called a microphysiometer provides a practical means for doing so.

Instrumental Characteristics

Figure 9 indicates how the LAPS can be placed within proton-diffusion distance of living cells to sense extracellular pH changes in a microvolume flow chamber. Acidification rates are determined by measuring the rate of pH change during periodic brief halts in the flow of culture medium through the flow chamber, as in Figure 6, during which the pH drops transiently by ~0.1 unit. To reduce buffering, typical media buffers such as $NaHCO_3$ and HEPES are omitted from the medium;

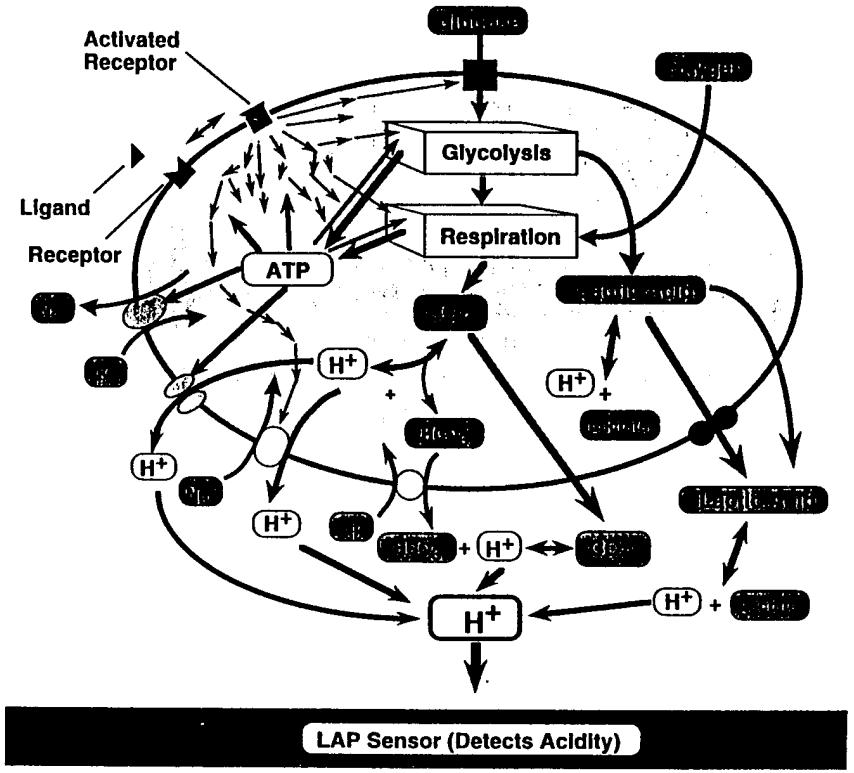

Figure 8 Relationships between cell physiology and extracellular acidification. Cellular energy metabolism is the principal ongoing source of protons; changes in intracellular pH can modify this flux transiently. The activation of cellular receptors can alter extracellular acidification by acting directly on energy metabolism, by changing the demand for ATP, and by changing the regulation of intracellular pH.

the remaining buffers (phosphate, amino acids) typically contribute ~1 mM/pH unit to the buffer capacity. The rms noise on individual pH measurements (one per second) is 5×10^{-4} to 1×10^{-3} pH units. The standard deviation of successive acidification-rate measurements is typically ~2%. The best time resolution of this version of the microphysiometer is about 30 s, which is approximately the minimum time between acidification-rate data points and is also about the time it takes for the concentration of a test substance to stabilize within the chamber after the fluid-selection valve is switched. Vertical diffusional equilibration of protons and buffer species within the chamber is not kinetically limiting.

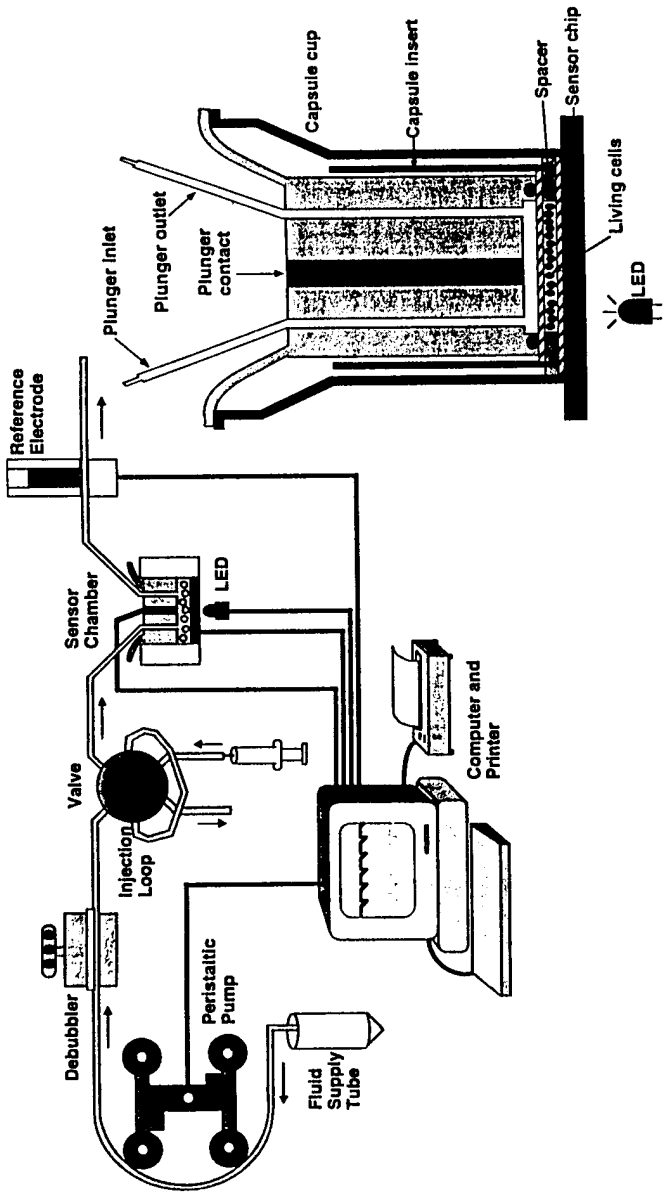

Cross-section of a Cell Capsule in a Sensor Chamber

Figure 9 Schematic diagram of the Cytosensor® microphysiometer. Culture medium is pumped by a peristaltic pump through a debubbling/degassing device, through a fluid-switching valve, into the cell-containing flow chamber, and then out past a reference electrode to waste. The valve selects one of two fluid streams or, as is shown, controls an injection loop. Cells are retained in the flow chamber between two track-etched polycarbonate membranes, either by natural adherence to one of the membranes or by immobilization, e.g. in a fibrin clot. The LAPS device forms the floor of the flow chamber. The superfused volume is a disk-shaped region 135 μm high and 6 mm in diameter (4 μl), and culture medium typically flows at ~100 μl/min. A microcomputer controls fluidics and data acquisition. A complete instrument has four or eight chambers operating in parallel.

Applications of Microphysiometry

MEASURING METABOLIC ACTIVITY Extracellular acidification rate depends on carbon source (e.g. glucose or pyruvate) and on metabolic inhibitors (40, 52), and this finding is consistent with elementary considerations of intermediary metabolism (49). The microphysiometer has also been used to record the recovery of metabolic activity in cells recently thawed from cryopreservation (33).

Sapolsky and coauthors have used the microphysiometer to study how 24-h exposure to glucocorticoids affects fibroblast metabolism. Pretreatment with 1 nM corticosterone, but not 1 μM estradiol, progesterone, or testosterone, significantly decreased the acidification rate (56). These authors concluded that this inhibition was caused by decreased rates of glucose transport and protein synthesis in the cells, which are well established effects of glucocorticoids on fibroblasts. In another study that included microphysiometry, this group discovered that virally transformed fibroblasts were resistant to such metabolic inhibition (60). The authors proposed that stress, which causes the secretion of glucocorticoids, accelerates the growth of some types of tumors by this mechanism.

The Na^+/K^+-ATPase, or sodium pump, is a major user of ATP in many cell types. The acidification rate of TE671 rhabdomyosarcoma cells was decreased by 9% when this pump was inhibited either with ouabain or the removal of extracellular K^+ (42). In the same work, stimulation of the Na^+/K^+-ATPase by activation of a muscarinic receptor was shown to be mediated by an increase in intracellular $[Na^+]$.

PHARMACOLOGY A surprising observation, now established for most major classes of plasma-membrane receptors and transduction mechanisms, is that receptor activation typically changes the extracellular acidification rate by 10–100% (40). We next describe how this phenomenon can be used to construct a relatively generic assay for receptor activation, temporarily deferring questions about the mechanisms of these acidification-rate changes.

Most pharmacological assays measure either the binding of a drug to a macromolecule or some functional consequence of that binding. The latter category includes extracellular acidification measured by microphysiometry, which is often similar in sensitivity and information content to other functional assays for receptor activation such as cAMP, protein phosphorylation, or mitogenesis. An important difference is that most assays are restricted in application to a limited range of receptors operating by the mechanism being probed; microphysiom-

etry can be applied to a wider range of receptors because the cellular proton economy operates at a very high level of physiological integration.

Among the receptors whose activation has been detected under pharmacologically relevant conditions are protein tyrosine kinases such as epidermal growth factor (50, 53), ligand-gated ion channels such as the kainate glutamate receptor (55), hematopoietin-family receptors such as that for granulocyte-macrophage colony-stimulating factor (GM-CSF) (69), the T-cell receptor (43, 44), and receptors that are linked to G proteins, including β_2-adrenergic receptor through G_s (50), the D_2 dopamine receptor through G_i (13, 46), and the m_1 muscarinic receptor through G_q (40, 50). Figure 10 shows an example of the concentration-response data that can be obtained.

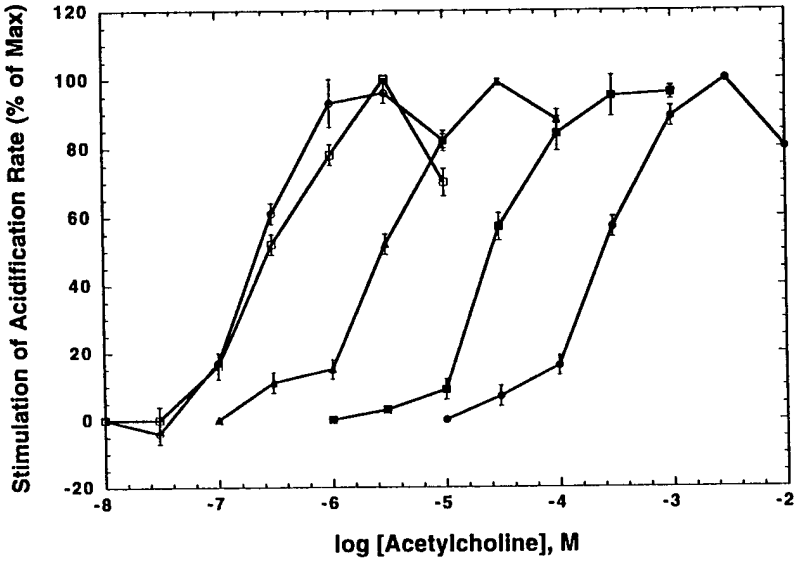

Figure 10 Concentration-response curves for the cholinergic stimulation of mouse pancreatic acinar cells as detected in the microphysiometer (19). Cells in a microphysiometer chamber were exposed to successively higher concentrations of acetylcholine, generating a sigmoid concentration-response curve as shown in the figure (*open circles* and *open squares* for two experiments, normalized to the highest stimulation of acidification rate). Fifty percent of maximum response was elicited by 0.20 ± 0.04 μM acetylcholine. When the experiment was repeated in the presence the muscarinic cholinergic antagonist atropine, the curve was shifted to the right to an extent depending on the concentration of atropine (10 nM, *filled triangles;* 100 nM, *filled squares;* 1 μM, *filled circles*). Schild analysis gave a pA_2 of 9.2, which is the negative logarithm of the concentration of antagonist sufficient to shift the curve rightward by a factor of two. Error bars indicate the standard error of the mean (SEM) based on n = 4–6.

When receptor activation is not strongly coupled to cell physiology, changes in extracellular acidification rate may not be observed. Changing the host cell or its physiology may induce responsiveness. Thus the responses seen by microphysiometry are characteristic of the combination of receptor and host cell, not of the receptor alone.

SIGNAL TRANSDUCTION The metabolic pathways by which receptor activation alters extracellular acidification can be identified by observing the effects of modulating their activity on acidification rate. To date this has been done primarily by using specific inhibitors. Figure 11 shows, for example, that a component of the acidification response to GM-CSF in TF-1 erythroleukemia cells depends on the presence of extracellular sodium, implicating the Na^+/H^+ exchanger. Further studies demonstrated that the response is initiated by protein kinase activity and results from increased rates of glycolysis as well as activation of the Na^+/H^+ exchanger (69). In the same system antisense oligonucleotides were used to show that the ϵ isoform of protein kinase C is involved in the acidification response (3).

TOXICOLOGY Extracellular acidification rate, as a measure of overall metabolic activity, lends itself naturally to in vitro toxicology. A close

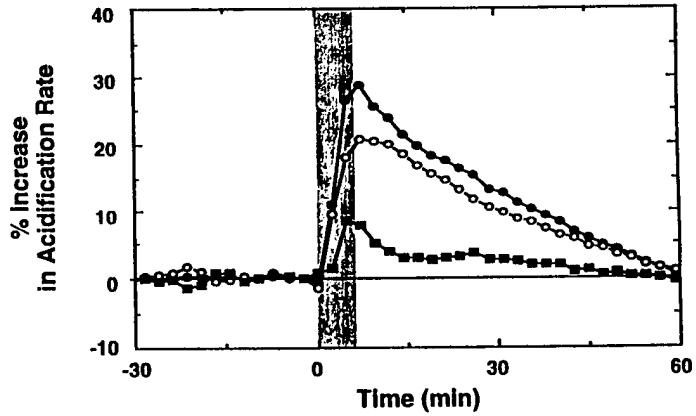

Figure 11 Demonstration that the Na^+/H^+ antiporter causes part of the acidification-rate increase observed when TF-1 erythroleukemia cells are stimulated with GM-CSF (69). The cells in the microphysiometer are stimulated with 10 ng/ml GM-CSF during the shaded period either under normal conditions (*filled circles*) or with sodium in the extracellular medium replaced by choline (*open circles*), which is not transported by the antiporter. The difference (*filled squares*) represents the contribution of the antiporter; when the experiment is repeated in the presence of amiloride, an inhibitor of the antiporter, the difference disappears (data not shown).

correlation has been established between the severity of ocular irritants, such as detergents and organic solvents, and the concentrations at which brief exposure to these compounds inhibits the acidification rates of fibroblasts or keratinocytes in the microphysiometer by 50% (2, 15, 53). In some cases the cells recover from the toxic insult (15). The ability to monitor recovery indicates that the microphysiometer measures a metabolic disturbance more subtle than cell death.

Medically relevant results for pharmacological toxicology are more difficult to obtain in vitro, because here the toxic compound acts by a tissue-specific mechanism. This case minimally requires a match between the toxic compound and type of responding cell. The only study of this type yet based on microphysiometry demonstrated excitotoxicity of a glutamate analogue in cocultures of hippocampal rat neurons and glia (55).

OTHER CELLULAR PREPARATIONS Nearly all published microphysiometry results have used cultured mammalian cells. The metabolism of intact tissue, for example gastric glands (67) or organ slices (R Kuo & A Harris, personal communication) also may be monitored. Immobilized microbial cells can also be studied, as has been shown for bacteria and yeasts (34; J Libby & K Hahnenberger, personal communication). Free-swimming ciliates such as *Tetrahymena thermophila* can be studied (J Libby, personal communication), as can the slime mold *Dictyostelium discoideum* (R Metzger, personal communication). Finally, the cytopathic effects of viruses on mammalian cells have been demonstrated in the microphysiometer, both with fast-acting viruses such as vesicular stomatitis virus (~8 h) (53), and with slow-acting viruses such as HIV-1 (~4 days during 6 days of continuous culture in the microphysiometer) (40).

Prospects

The microphysiometer has been established as a useful tool in the cell-biology and pharmacology laboratory, providing functional information with a combination of promptness, convenience, and generality of application. It has applications in screening for drug discovery, though its throughput is not sufficient for truly large-scale screening. In some cases it should be possible to achieve $\sim 10^4$ tests per year with an eight-channel instrument (R Metzger, personal communication). The microphysiometer should be particularly useful for identifying ligands for so-called orphan receptors, proteins of unknown function that are presumed to be receptors, based on loose sequence homology to known receptors.

Clinical applications are as yet essentially unexplored. Some nonclinical data suggest that microphysiometry may be useful for detecting patterns of resistance of patients' tumors to chemotherapeutic agents (53). Given the published results for T-cell activation (43, 44), microphysiometry might be useful in monitoring the immune status of immunosuppressed patients. Finally, the ability of the microphysiometer to detect cellular metabolic activity sensitively and in real time may make it suitable for clinical microbiology.

Many of these additional applications will require substantial improvements in instrumentation. In particular, we are constructing research prototypes based on LAPS chips that have been extensively micromachined and include a microfluidics system. The benefits of miniaturization include reduced sample consumption and increased time resolution. They also include higher throughput via an increase in the number of parallel measurements, which will facilitate applications such as screening for new therapeutic drugs.

CONCLUDING PERSPECTIVE

The LAPS is a chemical sensor that, when used for biological applications, may be called a biosensor. It has been noted correctly that this field has had its share of hyperbole and unfulfilled expectations (68); one test of a technology's significance is the extent to which it migrates outside the laboratory of its creators, and the number of biosensors that pass that test has been disappointingly small. An important root of the problem is the highly interdisciplinary nature required of the research and development effort: biology, physical science, and engineering must be thoroughly intertwined. How to construct an atmosphere that nurtures this synthesis is an important question, but one beyond the scope of this review. We have, however, tried to convey the spirit of the endeavor by emphasizing the LAPS as a component of an analytical system, rather than the LAPS as a device.

ACKNOWLEDGMENTS

Much of the work on the immunological and cellular applications of LAPS would not have been possible without the support of ARPA, Contracts DAAL03-86-C-0009 (with USA/CRDEC) and MDA972-92-C-0005. We thank P Lam and S Mostarshed for help with the illustra-

tions, and J Denyer for the data in Figure 10 (from the study reported in Ref. 19).

Literature Cited

1. Adami M, Sartore M, Baldini E, Rossi A, Nicolini C. 1992. New measuring principle for LAPS devices. *Sens. Actuators B* 9:25–31
2. Bagley DM, Bruner LH, de Silva O, Cottin M, O'Brien KAF, et al. 1992. An evaluation of five potential alternatives in vitro to the rabbit eye irritation test in vivo. *Toxicol. Vitro* 6:275–84
3. Baxter GT, Miller DL, Kuo RC, Wada HG, Owicki JC. 1992. PKCε is involved in GM-CSF signal transduction. Evidence from microphysiometry and antisense oligonucleotide experiments. *Biochemistry* 31:10950–54
4. Bergveld P, Sibbald A. 1988. *Analytical and Biomedical Applications of Ion-Selective Field-Effect Transistors*. Amsterdam: Elsevier
5. Bousse L, Hafeman D, Tran N. 1990. Time dependence of the chemical response of silicon nitride surfaces. *Sens. Actuators B* 1:361–67
6. Bousse L, Kirk G, Sigal G. 1990. Biosensors for detection of enzymes immobilized in microvolume reaction chambers. *Sens. Actuators B* 1:555–60
7. Bousse L, McReynolds RJ, Kirk G, Dawes T, Lam P, et al. 1993. Micromachined multichannel systems for the measurement of cellular metabolism. In *Proceedings of Transducers 93, 7th Int. Conf. on Solid-State Sensors and Actuators*. pp. 916–20. Yokohama, Japan: Inst. Electr. Eng. Japan
8. Bousse L, McReynolds RJ, Kirk G, Lam P, Parce JW. 1993. Integrated fluidics for biosensors used to measure cellular metabolism. In *Proceedings of the Symposium on Chemical Sensors II, Proceedings of the Electrochemical Society Hawaii*, pp. 742–45. Pennington, NJ: Electrochem. Soc.
9. Bousse L, Mostarshed S. 1991. The zeta potential of silicon nitride thin films. *J. Electroanal. Chem.* 302:269–74
10. Bousse L, Mostarshed S, Hafeman D. 1992. Combined measurement of surface potential and zeta potential at insulator/electrolyte interfaces. *Sens. Actuators B* 10:67–71
11. Bousse L, Owicki JC, Parce JW. 1992. Biosensors with microvolume reaction chambers. In *Chemical Sensor Technology*, ed. S Yamauchi, 4:145–66. Amsterdam: Elsevier; Tokyo: Kodansha
12. Bousse L, Parce JW, Owicki JC, Kercso KM. 1990. Silicon micromachining in the fabrication of biosensors using living cells. In *Technical Digest, IEEE Solid State Sens. Actuator Workshop*, pp. 173–76. Piscataway, NJ: Inst. Electr. Electron. Eng.
13. Bouvier C, Salon JA, Johnson RA, Civelli O. 1993. Dopaminergic activity measured in D_1- and D_2-transfected fibroblasts by silicon-microphysiometry. *J. Receptor Res.* 13:559–71
14. Briggs J, Panfili PR. 1991. Quantitation of DNA and protein impurities in biopharmaceuticals. *Anal. Chem.* 63:850–59
15. Bruner LH, Miller KR, Owicki JC, Parce JW, Muir VC. 1991. Testing ocular irritancy in vitro with the silicon microphysiometer. *Toxicol. Vitro* 5:277–84
16. Caras SD, Janata J, Saupe D, Schmitt K. 1985. pH-Based enzyme potentiometric sensors. Part I. Theory. *Anal. Chem.* 57:1917–20
17. Chehroudi B, Gould TR, Brunette DM. 1990. Titanium-coated micromachined grooves of different dimensions affect epithelial and connective-tissue cells differently in vivo. *J. Biomed. Mater. Res.* 24:1203–19
18. Connolly P, Clark P, Curtis AS, Dow JA, Wilkinson CD. 1990. An extracellular microelectrode array for monitoring electrogenic cells in culture. *Biosens. Bioelectr.* 5:223–34
19. Denyer JC, Thorn P, Bountra C, Jordan CC. 1993. Acetylcholine and cholecystokinin induced acid extrusion in mouse isolated pancreatic acinar cells as measured by the microphysiometer. *J. Physiol. (London)* 459:390P

20. Dulcey CS, Georger JH Jr, Krauthamer V, Stenger DA, Fare TL, Calvert JM. 1991. Deep UV photochemistry of chemisorbed monolayers: patterned coplanar molecular assemblies. *Science* 252:551–54
21. Edell DJ, Toi VV, McNeil VM, Clark LD. 1992. Factors influencing the biocompatibility of insertable silicon microshafts in cerebral cortex. *IEEE Trans. Biomed. Eng.* 39:635–43
22. Ekins R. 1990. Immunoassay design and optimisation. In *Principles and Practice of Immunoassay*, ed. CP Price, DJ Newman, pp. 96–153. New York: Stockton
23. Fernando JC, Rogers KR, Anis NA, Valdes JJ, Thompson RG, et al. 1993. Rapid detection of anticholinesterase insecticides by a reusable light addressable potentiometric biosensor. *J. Agric. Food Chem.* 41:511–16
24. Fodor S, Read JL, Pirrung MC, Stryer L, Lu AT, Solas D. 1991. Light-directed, spatially addressable parallel chemical synthesis. *Science* 251:767–73
25. Fromherz P, Offenhäusser A, Vetter T, Weis J. 1991. A neuron-silicon junction: a retzius cell of the leech on an insulated-gate field-effect transistor. *Science* 252:1290–93
26. Hafeman DG. 1988. Method of analyzing semiconductor systems. *US Patent No. 4,758,786*
27. Hafeman DG, Parce JW, McConnell HM. 1988. Light-addressable potentiometric sensor for biochemical systems. *Science* 240:1182–85
28. Hetherington S. 1990. Solid phase disruption of fluid phase equilibrium in affinity assays with ELISA. *J. Immunol. Methods* 131:195–202
29. Hurni WM, Miller WJ, Zuk RF, Kung VT. 1991. Detection of antibody to the PreS2 sequence of the hepatitis B virus envelope protein using an immuno-ligand assay with a silicon sensor detection system. *J. Immunol. Methods* 145: 19–26
30. Janata J. 1989. *Principles of Chemical Sensors*. New York: Plenum
31. Kanai Y, Shimizu M, Uchida H, Maekawa H, Nakahara H, Zhou CG, Katsube T. 1993. Integrated taste sensor with surface photovoltage technique. In *Proc. Transducers 93, 7th Int. Conf. Solid-State Sensors and Actuators*, pp. 407. Yokohama, Japan: Inst. Electr. Eng. Japan
32. Kleinfeld D, Kahler KH, Hockberger PE. 1988. Controlled outgrowth of dissociated neurons on patterned substrates. *J. Neurosci.* 8:4098–4120
33. Kuo RC, Baxter GT, Alajoki L, Miller DL, Libby JM, Owicki JC. 1993. A metabolic view of receptor activation in cultured cells following cryopreservation. *Cryobiology* 30:386–95
33a. Lee WE, Thompson HG, Hall JG, Fulton RE, Wong JP. 1993. Rapid immunofiltration assay of Newcastle disease virus using a silicon sensor. *J. Immunol. Methods* 166:123–31
34. Libby JM, Miller DL, Humphries GM. 1989. Determination of metabolic activity and antibiotic sensitivity of *E. coli* with a silicon-based biosensor. *Natl. Meeting Am. Soc. Microbiol., New Orleans, LA*. Abstr. C-385
35. Libby JM, Wada HG. 1989. Detection of *Neisseria meningitidis* and *Yersinia pestis* with a novel silicon based sensor. *J. Clin. Microbiol.* 27:1456–59
36. Lucas ME, Huntington MF, Regina FJ, Bolts JM, Alter SC, et al. 1990. Rapid, filtration-based immunoassays performed with a silicon biosensor. In *Biosensor Technology, Fundamentals and Applications*, ed. RP Buck, WE Hatfield, M Umana, EF Bowden, pp. 351–65. New York:Marcel Dekker
37. Lundstrom I, Erlandsson R, Frykman U, Hedborg E, Spetz A, et al. 1991. Artifical 'olfactory' images from a chemical sensor using a light-pulse technique. *Nature* 352:47–50
38. Lundstrom I, Sundgren H, Winquist F. 1993. Physics of artificial olfactory images produced by catalytic sensing surfaces. *Proc. Transducers 93, 7th Int. Conf. Solid-State Sensors and Actuators*, pp. 416–19. Yokohama, Japan: Inst. Electr. Eng. Japan
39. Massobrio G, Martinoia S, Grattarola M. 1992. Light-addressable chemical sensors: modelling and computer simulations. *Sens. Actuators B* 7:484–87
40. McConnell HM, Owicki JC, Parce JW, Miller DL, Baxter GT, et al.. 1992. The Cytosensor microphysiometer: biological applications of silicon technology. *Science* 257:1906–12
41. Merrick H, Hawlitschek G. 1992. Threshold™—a complete system for quantitative analysis of total DNA, protein impurities and relevant proteins. *Biotech. Forum Eur.* 6/92:398–403
42. Miller DL, Olson JC, Parce JW, Owicki JC. 1993. Cholinergic stimulation of the Na^+/K^+ ATPase as revealed by microphysiometry. *Biophys. J.* 64:813–23
43. Nag B, Wada HG, Deshpande SV, Pass-

more D, Kendrick T, et al. 1993. Stimulation of T cells by antigenic peptide complexed with isolated chains of major histocompatibility complex class II molecules. *Proc. Natl. Acad. Sci. USA* 90: 1604–8
44. Nag B, Wada HG, Fok KS, Green DJ, Sharma SD, et al. 1992. Antigen-specific stimulation of T cell extracellular acidification by MHC class II–peptide complexes. *J. Immunol.* 148:2040–44
45. Nakao M, Yoshinobu T, Iwasaki H. 1993. Scanning-laser-beam semiconductor pH-imaging sensor. In *Proc. Transducers 93, 7th Int. Conf. Solid-State Sensors and Actuators (late news papers)*. pp. 52–53. Yokohama, Japan: Inst. Electr. Eng. Japan
46. Neve KA, Kozlowski MR, Rosser MP. 1992. Dopamine D_2 receptor stimulation of Na^+/H^+ exchange assessed by quantification of extracellular acidification. *J. Biol. Chem.* 267:25748–53
47. Olson JD, Panfili PR, Armenta R, Femmel MB, Merrick H, et al. 1990. A silicon sensor-based filtration immunoassay using biotin-mediated capture. *J. Immunol. Methods* 134:71–79
48. Olson JD, Panfili PR, Zuk RF, Sheldon EL. 1991. Quantitation of DNA hybridization in a silicon-based system: application to PCR. *Mol. Cell. Probes* 5:351–58
49. Owicki JC, Parce JW. 1992. Biosensors based on the energy metabolism of living cells: the physical chemistry and cell biology of extracellular acidification. *Biosens. Bioelectr.* 7:255–72
50. Owicki JC, Parce JW, Kercso KM, Sigal GB, Muir VC, et al. 1990. Continuous monitoring of receptor-mediated changes in the metabolic rates of living cells. *Proc. Natl. Acad. Sci. USA* 87: 4007–11
51. Parce JW, Kirk GL. 1989. High sensitivity silicon biosensors designed for continuous environmental monitoring. *Int. Chemical Congr. Pacific Basin Soc. Honolulu, Hawaii*. Section 01, Abstract #150
52. Parce JW, Owicki JC, Kercso KM. 1990. Biosensors for directly measuring cell-affecting agents. *Ann. Biol. Clin.* 48: 639–41
53. Parce JW, Owicki JC, Kercso KM, Sigal GB, Wada HG, et al. 1989. Detection of cell affecting agents with a silicon biosensor. *Science* 246:243–47
54. Pesce AJ, Michael JG. 1992. Artifacts and limitations of enzyme immunoassay. *J. Immunol. Methods* 150:111–19
55. Raley-Susman KM, Miller KR, Owicki JC, Sapolsky RM. 1992. Effects of excitotoxin exposure on metabolic rate of primary hippocampal cultures: application of silicon microphysiometry to neurobiology. *J. Neurosci.* 12:773–80
56. Redish DM, Raley-Susman KM, Sapolsky RM. 1993. Inhibition of acidification rate in cultured fibroblasts by glucocorticoids: application of silicon microphysiometry to endocrinology. *Hormone Metabol. Res.* 25:262–65
57. Regehr WG, Pine J, Rutledge DB. 1988. A long-term in vitro silicon-based microelectrode-neuron connection. *IEEE Trans. Biomed. Eng.* 35:1023–32
58. Robinett RSR, Herber WK. 1993. Nanogram quantitation of secreted protein in a recombinant yeast fermentation using an immuno-ligand assay. *J. Immunol. Methods* 159:229–34
59. Rogers KR, Fernando JC, Thompson RG, Valdes JJ, Eldefrawi ME. 1992. Detection of nicotinic receptor ligands with a light addressable potentiometric sensor. *Anal. Biochem.* 202:111–16
60. Romero LM, Raley-Susman KM, Redish DM, Brooke SM, Horner HC, Sapolsky RM. 1992. Possible mechanism by which stress accelerates growth of virally derived tumors. *Proc. Natl. Acad. Sci. USA* 89:11084–87
61. Sartore M, Adami M, Nicolini C. 1992. Computer simulation and optimization of a light addressable potentiometric sensor. *Biosens. Bioelectr.* 7:57–64
62. Sartore M, Adami M, Nicolini C, Bousse L, Mostarshed S, Hafeman D. 1992. Minority carrier diffusion length effects on light-addressable potentiometric sensor (LAPS) devices. *Sens. Actuators A* 32:431–36
63. Sato T, Shimizu M, Uchida H, Maekawa H, Katsube T. 1993. Light addressable suspended gate gas sensor. In *Proc. Transducers 93, 7th Int. Conf. Solid-State Sensors and Actuators*, pp. 438–41. Yokohama, Japan: Inst. Electr. Eng. Japan
64. Shimizu M, Uchida H, Zhou CG, Maekawa H, Matsuda I, Katsube T. 1993. Integrated biosensor employing a surface photovoltage technique. In *Proc. Transducers 93, 7th Int. Conf. Solid-State Sensors and Actuators*, pp. 495–98. Yokohama, Japan: Inst. Electr. Eng. Japan
65. Sigal GB, Hafeman DH, Parce JW, McConnell HM. 1989. Electrical properties of phospholipid bilayer membranes measured with a light addressable potentiometric sensor. In *Chemical Sensors and Microinstrumentation, ACS Symposium Series 403*, ed. RW Murray, RE Dessy, WR Heineman, J Janata, WR Seitz, pp. 46–64. Washington, DC: Am. Chem. Soc.
66. Ternaux JP, Wilson R, Dow J, Curtis AS, Clark P, et al. 1992. Dendritic processing: using microstructures to solve a hitherto intractable neurobiological problem. *Med. Biol. Eng. Comput.* 30: CE37–41
67. Thibodeau A, Kuo RC, Yao X, Owicki JC, Forte JG. 1993. Real-time measurement of extracellular acidification rate in isolated gastric glands using a microphysiometer. *FASEB J.* 7:A576
68. Vadgama P. 1993. Biosensors in clinical biochemistry. *Ann. Clin. Biochem.* 30: 337–40
69. Wada HG, Indelicato SR, Meyer L, Kitamura T, Miyajima A, et al. 1993. GM-CSF triggers a rapid, glucose dependent extracellular acidification by TF-1 cells: evidence for sodium/proton antiporter and PKC mediated activation of acid production. *J. Cell. Physiol.* 154:129–38
70. Wada HG, Libby JM, Rice LS, Masino RS, Kasper KC, et al. 1989. Detection of *C. trachomatis* in clinical specimens using a silicon-based sensor. *Annu. Meeting of Am. Soc. Microbiol., 89th, New Orleans, LA*. Abstr. C-122
71. Wada HG, McConnell HM, Hafeman DG. 1990. Polyredox couples in analyte determinations. *US Patent No. 4,942,127*
72. Winquist F, Sundgren H, Hedborg E, Spetz A, Lundstrom I. 1992. Visual images of gas mixtures produced with field-effect structures. *Sens. Actuators B* 6:157–61
73. Dill K, Lin M, Poteras C, Fraser C, Hafeman DG, et al. 1994. Antibody-antigen binding constants determined in solution phase with the Threshold® membrane-capture system. Binding constants for anti-fluorescein, anti-saxitoxin, and anti-ricin antibodies. *Anal. Biochem.* In press

Signal Transduction by the Truncated *trk*B Isoform, *trk*B.T1.

Soc. Neurosci. Abstr. **20**: 37 (1994)

[1]Monte J. Radke, [1]Gregory Baxter, [1]Richard Kuo, [3]Angelica Medina-Selby, [3]Doris Coit, [3]Pablo Valenzuela, and [1]Stuart C. Feinstein.
[1]Neuroscience Research Institute, Univ. of California, Santa Barbara, CA 93106: [2]Molecular Devices Corporation, Menlo Park, CA 94205 and [3]Chiron Corporation, Emeryville, CA 94608.

The *trk* family of proteins serve as receptors for the neurotrophin family of ligands. Alternative splicing of *trk*B mRNA generates three known *trk*B isoforms, each possessing the same extracellular and transmembrane domains but varying intracellularly. While "full length" trkB (trkB.FL) has a tyrosine kinase domain and initiates typical tyrosine kinase responses, the "truncated" *trk*B isoforms *trk*B.T1 and *trk*B.T2 have extremely small intracellular domains (23 and 21 amino acids, respectively) and appear not to elicit typical tyrosine kinase responses.

Several possible functions have been suggested for the truncated receptors. They might reduce responsiveness of expressing cells by acting as "sponges" to remove excess or unwanted BDNF ligand, or by acting as naturally occurring dominant negative effectors of *trk*B.FL. They might serve to present ligand to *trk*B.FL. Alternatively, they could transduce a signal, but by presently unknown mechanism(s). To assess this latter possibility, we used a Cytosensor Microphysiometer to compare the ability of and DNA transfixed to signal intracellular events. The Cytosensor microphysiometer is a biosensor-based instrument that detects changes in the physiological state of cultured cells by monitoring the rate at which they cells release acidic metabolic products. BDNF treatment of *trk*B.FL cells induces a biphasic response characteristic of other known receptor tyrosine kinases, i.e. an initial transient acidification burst followed by a sustained increase in metabolic activity. Non-transfected controls showed no effect. Most importantly, BDNF treatment of *trk*B.T1 transfected cells induces a marked change in the media acidification rate, similar to the long term component of the *trk*B.FL response but without the initial burst of acidification. We conclude that the *trk*B.T1 isoform of the *trk*B receptor mediates BDNF signal transduction via an unknown mechanism and will discuss possible implications.

Supported by grants from the NSF (BN-9120836) and ARPA (MDA-972-92-C-0005).

The Journal of Neuroscience, March 1992, 12(3): 773–780

Effects of Excitotoxin Exposure on Metabolic Rate of Primary Hippocampal Cultures: Application of Silicon Microphysiometry to Neurobiology

Kathleen M. Raley-Susman,[1] Karen R. Miller,[2] John C. Owicki,[2] and Robert M. Sapolsky[1]

[1]Department of Biological Sciences, Stanford University, Stanford, California 94305 and [2]Molecular Devices Corporation, Menlo Park, California 94025

Increasing evidence implicates glutamate receptor overstimulation in the neurotoxicity associated with a host of metabolic insults, including seizures and hypoxia-ischemia. To begin to understand more completely the role of energy metabolism in the mechanism of neuron death following excitatory amino acid exposure, we investigated the effects of kainic acid exposure on metabolic rate in cultured hippocampal cells using a recently developed silicon microphysiometer. The device gives a continual real-time measure of metabolism in relatively small numbers of cells, as assessed by efflux of protons generated at least in part by ATP hydrolysis and lactic acid production. In the first half of this report, we characterize the feasibility of using this device for measuring cellular metabolism in hippocampal cultures. Metabolic rate in both astrocytes and neurons was readily detectable, with a high signal-to-noise ratio. The rate was proportional to the number of cells and was sensitive to metabolic enhancement or depression. We then utilized this device to study metabolic responses to the excitotoxin kainic acid. We observed a receptor-mediated, dose-dependent increase in metabolic rate upon stimulation by kainic acid, with an EC_{50} of ~100 μM. Exposure to toxic levels of kainic acid for 10 min produced an initial elevation (for 2 hr) in metabolic rate and then a gradual decline in metabolism over the next 8 hr that preceded a measurable loss of cell viability. This study further delineates a time window for the onset of kainic acid–induced damage. The results clearly show the feasibility of using silicon microphysiometry for assessing metabolism of brain cultures and for exploring the relationship between metabolism and synaptic activation.

Activation of glutamate receptors is thought to stimulate neuronal energy consumption for the operation of the cells' energy-dependent ion homeostatic mechanisms. However, the metabolic consequences of glutamate exposure under normal conditions are not well understood, largely because direct measurement of metabolic rate in healthy brain tissue is technically difficult. For example, while *in vivo* studies have measured metabolic parameters, such as ^{14}C-2-deoxyglucose uptake (Cremer et al., 1988) (which affords excellent cellular resolution), the time resolution necessary for responses to receptor activation is quite poor. Further, studies with brain slices measuring oxygen consumption in response to bath application of glutamate receptor agonists (Nishizaki et al., 1988) suffer from limitations relating to the diffusion of oxygen from the center of tissue whose edges are damaged. These technical difficulties also limit the ability to measure directly the effects of toxic concentrations of excitatory amino acids such as glutamate. This determination is important because it is generally thought that exposure to excitatory amino acids is damaging when energy stores are excessively taxed because of overstimulation of receptors (Choi, 1988; Novelli et al., 1988). This excitotoxicity hypothesis rests on the assumption that the mechanism of neuron damage is energetic in nature, and yet few direct assessments of the metabolic effects of excitotoxin exposure have been undertaken to test this assumption.

In the present study, we measured the metabolic rate in primary hippocampal cultures in response to kainic acid using a silicon microphysiometer, a novel device that allows for real-time, sensitive measurement of cellular metabolism (Parce et al., 1989; Owicki et al., 1990). The silicon microphysiometer, a semiconductor-based instrument, detects the extrusion of acidic metabolic products of glycolysis, respiration, and ATP hydrolysis (Parce et al., 1989), including lactic acid, CO_2, and protons. In addition, the device may detect transient proton fluxes such as those caused by imbalances between ATP synthesis and hydrolysis, or by changes in intracellular pH (Owicki and Parce, in press). Previous work has demonstrated the usefulness of the microphysiometer for screening cellular responses to therapeutic drugs, growth factors, and hormone/neurotransmitter receptors transfected into cell lines (Parce et al., 1989; Owicki et al., 1990). The present report demonstrates the usefulness of using silicon microphysiometry for studying neurotransmitter receptor activation in primary neuronal cultures and demonstrates a correlation between neurotransmitter exposure and neuronal metabolism.

We show that the microphysiometer is sensitive to the metabolic status of hippocampal cultures. In addition, we observe that acute exposure to kainic acid increases metabolic rate in a receptor-specific, dose-dependent manner. Further, we observe that toxic concentrations of kainic acid cause a delayed decline in metabolic rate that precedes cell death.

Received May 28, 1991; revised Oct. 1, 1991; accepted Oct. 7, 1991.

This work was supported by an American Heart Association, Santa Barbara Chapter, postdoctoral fellowship (K.M.R.-S.) and by NIH Grant R01-AG06633 (R.M.S.). Partial support was also provided by U.S. Army CRDEC and DARPA programs (to Molecular Devices, Inc.). We thank G. Tombaugh and Dr. L. Jacobson for helpful comments about the manuscript, and the members of the Sapolsky lab for assistance with tissue culture procedures.

Correspondence should be addressed to Dr. Kathleen M. Raley-Susman, Department of Biology, Vassar College, Poughkeepsie, NY 12601.

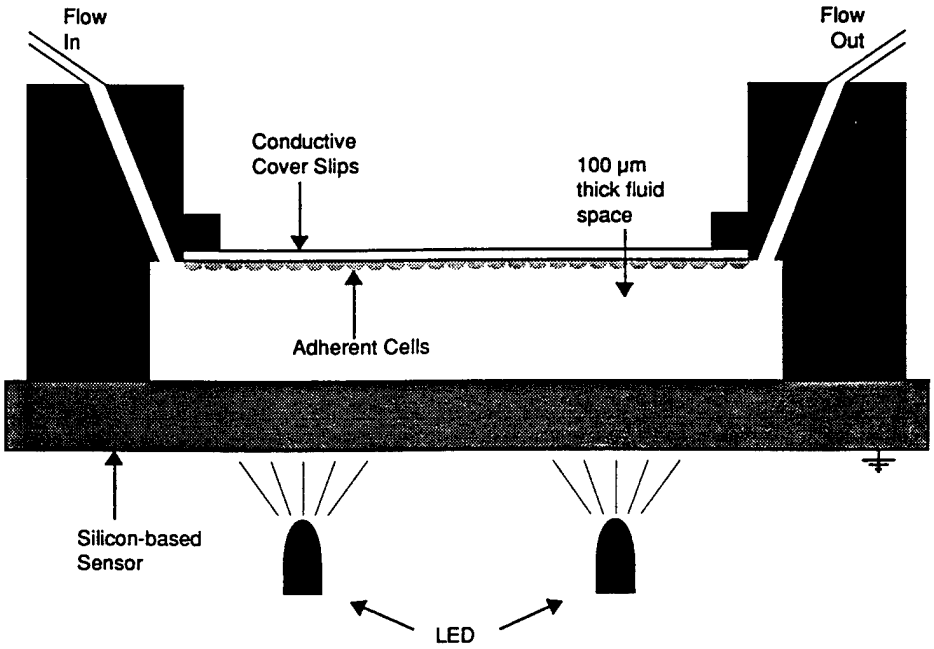

Figure 1. Schematic diagram of cell-containing chamber. Metabolic rate determinations are obtained from cells directly above the region illuminated by the LED (see text). Perfusion of experimental medium is under computer control. The silicon-based sensor forms the bottom of the cell chamber, while the conductive coverslip forms the top of the chamber.

Materials and Methods

Buffers. Cell cultures were maintained in Dulbecco's modified Eagle's medium (DMEM; GIBCO, Grand Island, NY) containing 5.55 mM glucose, 10% fetal calf serum (FCS; GIBCO), and 1% penicillin, 1% streptomycin (GIBCO). Twenty-four hours prior to some experiments (see Results), the medium was changed with two washes of DMEM (Sigma) containing the concentrations of glucose indicated in Results. For metabolic rate determinations, microphysiometer perfusates consisted of a modified DMEM lacking bicarbonate to reduce the buffering capacity of the extracellular medium to 1 mM (Owicki et al., 1990). The concentrations of glucose and other constituents are as indicated in Results.

Culture preparation. Cultured hippocampal neurons were isolated according to Banker and Cowan (1977) and prepared as described previously (Sapolsky et al., 1988) with modifications. Briefly, 50–100 hippocampi from day 18 fetal rats were dissected from the brain, washed, and enzymatically and mechanically dispersed with 0.05% trypsin (GIBCO) or 0.4% collagenase II (Worthington Biochemicals, Freehold, NJ) and DNase II (Sigma) in 0.1% BSA (Calbiochem) in HEPES-buffered Hank's balanced salt solution (GIBCO). Cells were plated to a density of approximately 1–2 × 10^5 cells/cm^2 and maintained in high-glucose HEPES-buffered DMEM (GIBCO) with 5% FCS (Hyclone Laboratories, Logan, UT). The cells were grown on poly-D-lysine–coated conductive glass coverslips. The coverslips were coated on the cellular side with indium-tin oxide to provide a conductive surface. The coating did not affect the adherence properties or the viability of the cultures. Cultures were maintained for 10 d in DMEM (with 5 mM glucose) with 5% FCS at 37°C in an incubator equilibrated with 10% CO_2. Cells were refed on day 5 with fresh medium containing 30 μg/ml uridine (Sigma) and 15 μg/ml fluoro-deoxyuridine (Sigma) to retard glial proliferation.

At the time of experimentation (10–15 d), mixed cultures consisted of 50–60% glia, which form a flat, discontinuous monolayer of polygonal cells along the bottom of the coverglass, and 40–50% neurons, which are phase bright and overlie the glial monolayer. Morphological criteria for neurons and glia were determined previously based on immunocytochemical analysis with antisera to neuron-specific enolase and glial fibrillary acidic protein (Horner et al., 1990). As noted above, 24 hr prior to experimentation, cells were pretreated with DMEM lacking serum and containing different concentrations of glucose.

Glia-enriched cultures were obtained by omitting the mitotic inhibitors and refeeding the cultures every 3–4 d for 4 weeks. This treatment resulted in a confluent layer of flat, polygonal-shaped cells and no overlying phase-bright neuronal cells.

Measurement of cellular metabolic rate. Metabolic rates of hippocampal mixed cultures were measured using the silicon microphysiometer, as has been described in detail elsewhere (Parce et al., 1989; Owicki et al., 1990). Briefly, coverslips containing cells were placed in a low-volume flow chamber, one side of which is a silicon-based light-addressable potentiometric sensor that measures small changes in extracellular medium pH. The other side of the chamber is the cell-bearing coverslip, which is coated with indium-tin oxide to create a conductive surface. Cultures were perfused with a low-buffering-capacity (1 mM) medium at 15 μl/min for 150 sec, followed by a 100 sec period of halted flow. The perfusion/halt cycle was controlled by an IBM PC interface.

Metabolic rate was determined as the rate of acidification of the external medium during the brief halt (100 sec) in the perfusion. Previous studies have shown that the rate of acidification of the external medium is a sensitive index of metabolic rate in various cell types (Parce et al., 1989) and correlates well with other indices of metabolism, including lactate production and oxygen consumption. Acidification rates of the medium were measured at regions of the silicon/electrolyte interface using a light-emitting diode (Fig. 1). The rate of acidification was determined as the slope of a linear least-squares fit to the relation of pH versus time (sec). The perfusion then resumed, allowing the pH of the medium to return to basal levels (within 10–15 sec of perfusion onset). Multiple determinations of the acidification rate were obtained, and the data are expressed as the average of 5–10 such determinations at a given time point (see Results).

In some experiments, we used a version of the microphysiometer that utilized an He-Ne laser beam, projected through the optics of a microscope (Parce et al., 1989), to illuminate a total sensing region of 1 mm^2 of the silicon light-addressable sensor. This setup allowed us to select fields with particular cell densities and that were enriched with particular cell types (astrocytes or neurons).

Drug treatments. As indicated above, for experiments investigating the effects of substrate availability on basal metabolic rate, cultures were pretreated 24 hr prior to experimentation with the indicated glucose concentration. The effects of cyanide or kainic acid on metabolic rate were studied by injecting the indicated solutions into the tubing leading to the cell chambers on the microphysiometer. All solutions were warmed to 37°C and adjusted to pH 7.4 with NaOH or HCl. Cells were exposed to the solutions for the times indicated in Results.

LDH assay. At the conclusion of some experiments, coverslips were removed from the microphysiometer and placed in lysis buffer (0.1% Triton X-100) overnight at 4°C. Cell lysates were assayed for lactate dehydrogenase (LDH) activity as described previously (Sapolsky et al., 1988). Cellular lysates could be stored at 4°C for several days with no

significant loss of activity. Enzyme activity was measured as a decrease in absorbance (corresponding to the amount of NADH present) at 340 nm in a Beckman DU-64 spectrophotometer (Sapolsky et al., 1988). LDH is a biologically stable marker whose activity correlates linearly with cell number (Koh and Choi, 1987). We measured residual LDH remaining in undamaged cells (Sapolsky et al., 1988).

Data analysis and statistics. Data are presented as either the average metabolic rate (an average of 5–10 rate determinations prior to experimental manipulation, mean ± SEM) or as the percentage of the average basal metabolic rate for the cells on a single coverslip, as indicated. Statistical analyses are delineated in Results and figure captions.

Results

Assessment of microphysiometry for measurement of metabolic rate in primary hippocampal cultures

The metabolic rate, as measured by the rate of acidification of the medium, was 27.7 ± 3.7 μV/sec when the total sensing region was filled with confluent cultures of astrocytes, and 114.3 ± 10 μV/sec when the sensing region was focused on primarily neuronal clusters in mixed culture (Table 1). These rates represented cellular responses, as cell-free coverslips and coverslips whose cells were lysed and removed with either water or 0.2% trypsin showed background noise of 1.25 ± 0.31 μV/sec. Further, the metabolic rate was proportional to the percentage of the total sensing field covered by cells (Fig. 2). A specific cellular signal (i.e., above the 95% confidence interval of the signal from cell-free background) was detectable when as little as 20% of the 1 mm² total sensing region was occupied with mixed cultures at the stated plating density (see Materials and Methods).

Pretreatment of cultures with different concentrations of glucose altered the basal metabolic rate (Fig. 3*A*). Hyperglycemic conditions significantly enhanced metabolic rate, while 24 hr pretreatment with 0 mM glucose substantially reduced the metabolic rate. Visual inspection of these cultures revealed an essentially complete loss of overlying neurons in this aglycemic state, although some glia remained. The remaining metabolic rate recorded under these circumstances agreed well with what would be expected from a pure astrocyte culture (see Table 1).

Cyanide (2 mM) in the perfusate for 2 hr reduced metabolic rate 32% (Fig. 3*B*), indicating the sensitivity of the cultures to disruption of oxidative metabolism. Thus, these experiments show that the microphysiometer is sensitive to changes in the metabolic status of mixed cultures. Treatments that increase the supply of glucose increase the metabolic rate in a dose-dependent manner, while treatments that interfere with metabolism decrease the metabolic rate.

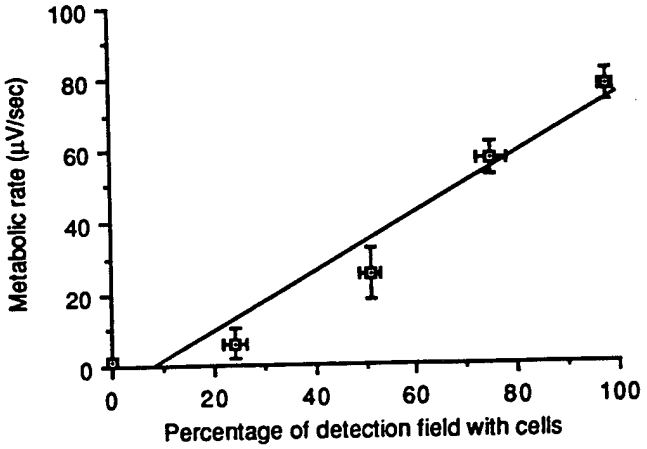

Figure 2. Metabolic rate measurements are proportional to cell density. Mixed hippocampal cultures were plated on coverslips in a concentrated area using a cloning ring. A low-volume flow chamber containing the coverslip was mounted on a microscope stage, and the beam from an He-Ne laser was projected through the optics of the microscope as described by Parce et al. (1989). Acidification rates were thus recorded from cells directly over the 1 mm² region of the silicon light-activated sensor illuminated by the laser. We could move the microscope stage and thus manipulate the portion of the coverslip from which we gathered metabolic rate data. The cells were plated in the center of the coverslip, so that a sharp boundary existed between coverslips with and without cells. We moved the stage so that an increasing fraction of the illuminated field contained cells. The microscope stage was moved by predetermined amounts to vary the percentage of the fixed measurement area containing cells. The fraction of the measurement area containing cells was estimated using an ocular grid. Data represent the average metabolic rate determinations for three separate experiments. Linear regression analysis: $r^2 = 0.955$; $p < 0.01$.

Table 1. Effect of kainic acid on metabolic rate in mixed and pure astrocytic cultures

	n	Average basal rate (μV/sec)	Average rate in treatment (μV/sec)	Percentage increase in basal rate
Mixed cultures				
500 μM KA	4	114.3 ± 10	191.4 ± 12***	71.4 ± 9[a,b]
500 μM KA + 1 mM KYN acid	4	96 ± 18	104.5 ± 17	9.8 ± 2[b]
Astrocyte cultures				
500 μM KA	7	27.7 ± 3.7	36.6 ± 5***	31.7 ± 4.9[a]

Mixed hippocampal cultures (see Materials and Methods) or pure astrocyte cultures (see Materials and Methods) were loaded into microphysiometer chambers and exposed to kainic acid (KA) as described in Figures 2 and 4. The mixed culture data are presented from clusters of primarily neurons isolated with the laser procedure described in Materials and Methods and in the caption to Figure 2. The astrocytic culture data were obtained from pure astrocyte cultures.

*** Significant ($p < 0.001$) increase in metabolic rate when compared with the basal rate using Student's *t* test for paired samples. ANOVA comparison of the percentage increase in basal rates across treatments was statistically significant ($p < 0.001$).

[a] Statistically significant difference ($p < 0.05$) between the percentage increase in basal rate of neurons as compared with glial cultures using the Fisher PLSD test.

[b] Statistically significant ($p < 0.05$) difference between the neuronal responses to KA in the absence as compared to the presence of kynurenic acid (KYN) using the Fisher PLSD test.

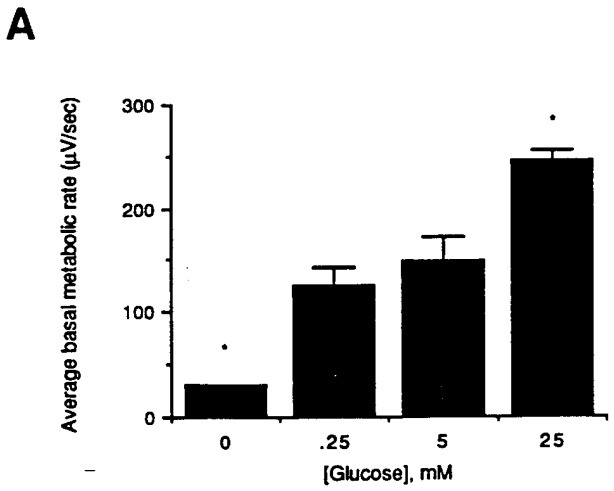

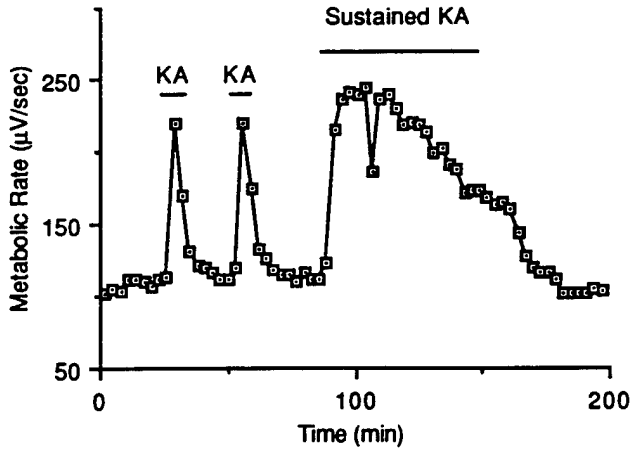

Figure 4. Kainic acid increases metabolic rate. Coverslips containing mixed hippocampal cultures were loaded into chambers of the microphysiometer. Regions of predominantly neurons were focused upon using the laser setup described in Materials and Methods and the caption to Figure 2. A steady basal metabolic rate was determined for the first 30 min to 1 hr after chamber assembly. Where indicated, a 500 μM kainic acid (*KA*) solution (in bicarbonate-free DMEM, pH 7.4) was injected into the chambers using a 750 μl injection loop. Measurements in response to acute (3–5 min) exposures were obtained, and the solution was switched to normal bicarbonate-free DMEM lacking the drug. Sustained exposure to kainic acid was obtained by switching the bathing solution. Data are representative of three similar experiments.

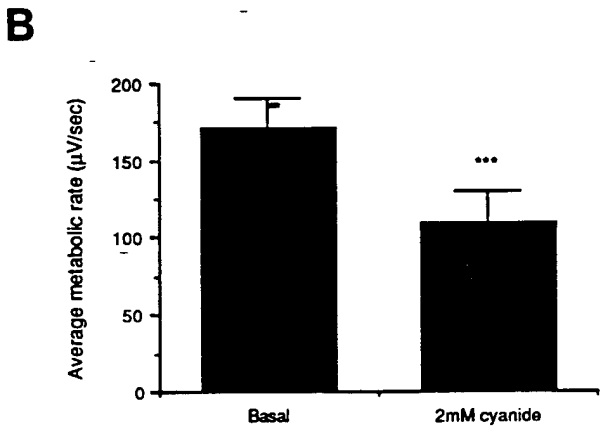

Figure 3. Metabolic rate is sensitive to substrate availability. *A*, Mixed hippocampal cultures were pretreated 24 hr prior to the experiment with DMEM containing different concentrations of glucose (0, 0.25, 5, or 25 mM). Metabolic rate determinations were made in bicarbonate-free DMEM with the same concentrations of glucose. ANOVA revealed a significant glucose effect ($p < 0.0001$). *, $p < 0.05$ when compared against the normal (5 mM) glucose group with the Fisher PLSD test. *B*, Cells were acutely exposed to 2 mM cyanide for 2 hr during the metabolic rate determinations. Rates were compared with basal rates using a paired Student's *t* test (***, $p < 0.0001$). Data in both figures represent average metabolic rate (μV/sec; see Materials and Methods) determinations for five to seven separate experiments.

Effects of kainic acid on metabolic rate of hippocampal mixed cultures

Acute exposure (5–10 min) of mixed cultures to 500 μM of kainic acid increased metabolic rate (Fig. 4, Table 1). Upon removal of the kainic acid, the metabolic rate returned to basal levels. Repeated exposures evoked similar changes in metabolic rate. With more prolonged kainic acid exposure, the metabolic response eventually began to wane (Fig. 4). The response included both neuronal and glial components, as pure astrocyte cultures were also responsive to the drug (Table 1). Parallel experiments (using the laser setup described in the caption to Fig. 2, with which it is possible to focus on isolated clusters of neurons, relatively free from the presence of glia) indicated that neurons were more responsive to kainic acid than glia (Table 1).

The response to kainic acid appeared glutamate receptor mediated, as it was prevented by 1 mM kynurenic acid (Fig. 5, Table 1). It is important to note that 1 mM kynurenic acid blocks all subtypes of the glutamate receptor (Ganong et al., 1983). Thus, these results do not distinguish between a direct action of kainic acid on the kainate receptor subtype to increase metabolic rate or a secondary effect from depolarization and subsequent activation of additional glutamate receptor subtypes (such as the NMDA receptor). Finally, the metabolic response to kainic acid was dose dependent (Fig. 6), with an estimated EC_{50} of ~100 μM in this paradigm.

Overstimulation of glutamate receptors, including the kainic acid receptor, is neurotoxic (Coyle et al., 1981; Rothman et al., 1987; Frandsen et al., 1989). Presumably, such overstimulation produces ion imbalances with which the cell cannot cope because energy-dependent ion homeostatic mechanisms are not fueled sufficiently with ATP. These ideas predict that overstimulation of kainic acid receptors should produce an initial stimulation of cellular metabolism, which the cells cannot maintain; this was observed when cells were exposed continuously to a toxic dose (2.5 mM) dose of kainic acid for up to 8 hr (Fig. 7).

Because a sustained exposure to kainic acid is a rather severe and unphysiological insult, we next exposed cells to a 10 min pulse of 2.5 mM kainic acid (an exposure that is still toxic) and allowed cells to recover in normal perfusate lacking the drug (Fig. 8). At 5 hr recovery, when the metabolic rate was significantly decreased relative to baseline (Fig. 8), LDH measurements indicated no significant loss of cell viability relative to unexposed cultures (Fig. 8 inset). Thus, a decrease in metabolism appears to precede measurable cell loss.

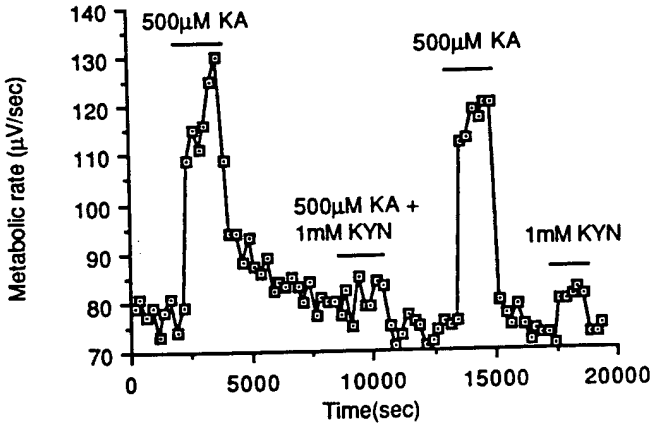

Figure 5. The kainic acid–induced increase in metabolic rate is receptor mediated. Coverslips containing mixed hippocampal cultures were loaded into chambers of the microphysiometer, and a steady basal metabolic rate from predominantly neurons (see the caption to Figure 4) was determined. Where indicated, a 500 μM kainic acid (*KA*) solution (pH 7.4) in the presence or absence of 1 mM kynurenic acid (*KYN*), a glutamate receptor antagonist, was injected using injection loops of 750 μl vol. Several measurements were obtained, and the solution was returned to normal bicarbonate-free DMEM lacking drugs. Kynurenic acid at 1 mM had only a very small effect (see Table 1) on metabolic rate. Data shown are representative of three separate experiments.

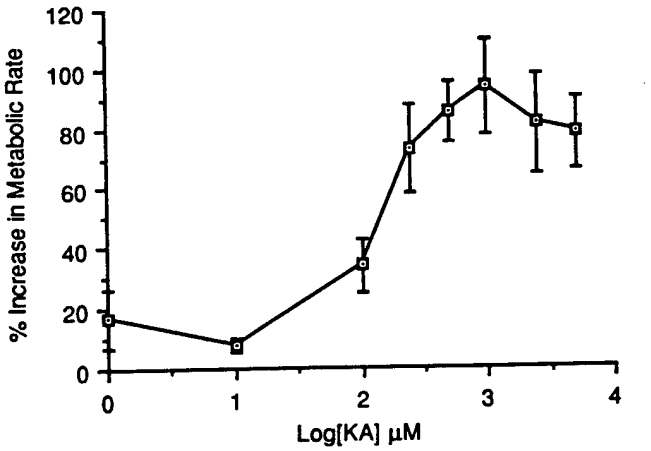

Figure 6. The kainic acid–induced increase in metabolic rate is dose dependent. Mixed hippocampal cultures were exposed to sequential (from lowest to highest concentrations) injections of different concentrations of kainic acid (*KA*; pH 7.4). Several measurements at each concentration were obtained, and the cells were allowed to recover in normal bicarbonate-free DMEM until a steady basal rate was again obtained between each injection of the drug. Responses were calculated as the percentage of the basal metabolic rate for each coverslip and presented versus the log of the kainic acid concentration. Data shown are the average of $n = 6$ similar experiments.

Discussion

Application of silicon microphysiometry to neurobiology

We used a silicon microphysiometer to measure the metabolic rate of mixed hippocampal cultures. Our data indicate some of the advantages and likely limitations of this technology when applied to neuronal cultures. Previous studies have shown that this device, which measures the rate of acidification of the extracellular perfusate, provides a sensitive index of overall cellular metabolic rate; the acidification rate is proportional to lactate production and oxygen consumption (Parce et al., 1989; Owicki et al., 1990). In this study, we demonstrated the sensitivity of this device for use with primary hippocampal cultures. Basal metabolic rates far above background could be detected in pure astrocytic cultures and in detection fields filled primarily with neurons. The neuronal metabolic rate was approximately four times higher than the astrocytic rate (this is likely to be an underestimate because of the presence of some astrocytes in the primarily neuronal fields, and the fact that such neuron-rich clusters did not fill the total sensing region). The smaller rate in astrocyte cultures compared with neuronal clusters could reflect a different cell density, as glia are flattened and take up a greater surface area on the coverslips than do the neurons. It was not possible in this study to determine metabolic rate on a per cell basis; a more detailed analysis of these differences is under way. The rate of acidification of the external medium was proportional to the size of the cell-containing field overlying the light-addressable potentiometric sensor, and the rate represents cellular acid extrusion, as the rate was abolished when the cells were lysed.

The acidification rate comprises a summation of all cellular processes involving acid extrusion. In most cells, this measure would indicate lactate and CO_2 production/extrusion, proton production/extrusion from ATP hydrolysis, and proton extrusion mechanisms unrelated to energy metabolism. Previous work with other cell types demonstrated that the acidification rate was quite similar to the rate of O_2 consumption and the rate of lactate production (Parce et al., 1989). Those data indicated that the acidification rate includes both aerobic and anaerobic metabolism components. Indeed, our results with cyanide, used at

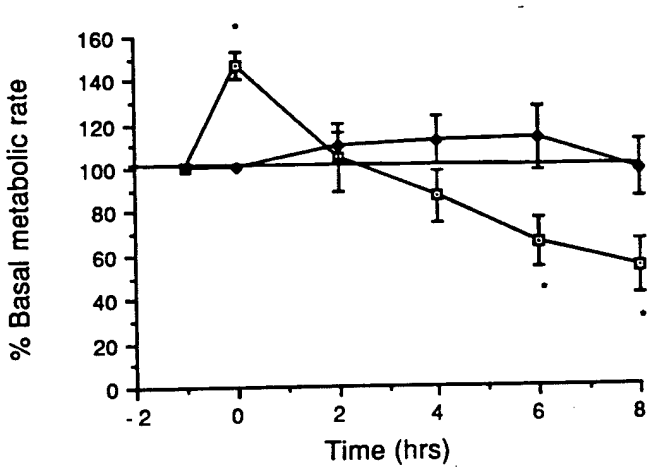

Figure 7. Effect of sustained exposure to kainic acid. Mixed hippocampal cultures were exposed to 2.5 mM kainic acid (pH 7.4) beginning at $t = 0$ hr. The average metabolic rate was determined at the times indicated and presented as a percentage of the average basal metabolic rate (see Materials and Methods). Data represent the averages of $n = 8$ separate experiments. Average basal metabolic rate was 160.6 ± 18 μV/sec. *Open symbols* indicate mixed cultures exposed to 2.5 mM kainic acid at $t = 0$, and the *solid symbols* indicate control cultures not exposed to kainic acid. Two-factor ANOVA revealed a significant effect of kainic acid over time, when compared with untreated cultures ($p \leq 0.0005$). The *asterisk* indicates a significant difference between the response to kainic acid and the basal metabolic rate ($p < 0.05$) with the Fisher PLSD test. There was no significant effect of time on metabolic rate in untreated cultures.

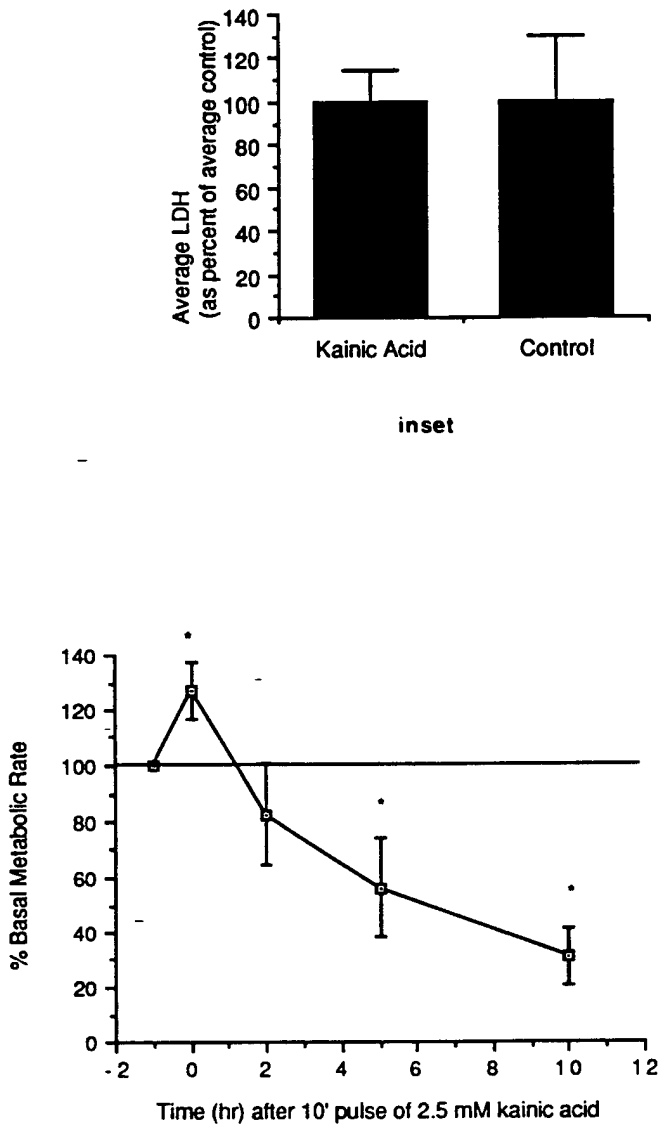

Figure 8. Effect of 10 min exposure to 2.5 mM kainic acid. Mixed hippocampal cultures were exposed to 2.5 mM kainic acid (pH 7.4) for 10 min at $t = 0$ and then returned to normal perfusion medium for the recovery times indicated. Data represent the average of $n = 3$ separate experiments. Data are presented as the average metabolic rate (μV/sec); see Materials and Methods. Average basal metabolic rate was 213.3 ± 29 μV/sec. ANOVA revealed a significant decline in metabolic rate ($p < 0.0037$). The *asterisk* indicates statistical significance ($p < 0.05$) when compared with basal rates ($t = -1$ hr) using Fisher PLSD test. *Inset,* Cultures were exposed to 2.5 mM KA or vehicle (DMEM) for 10 min as described above, and at 5 hr after the exposure, coverslips were removed and prepared for LDH determination as described in Materials and Methods. LDH values are presented relative to the average control value in $n = 6$–8 separate experiments. No statistical difference when compared using Student's t test for unpaired samples.

a concentration sufficient to interfere maximally with oxygen-dependent metabolism (Olesen, 1986), indicate that a proportion, but by no means all, of the acidification rate represents aerobic metabolism in hippocampal mixed cultures. The actual contribution of aerobic metabolism to the metabolic rate measured in this study may be an underestimate because anaerobic metabolism may have been stimulated to compensate for the cyanide-induced loss of oxidative ATP production. Thus, from this study, the actual percentage of the measurement that is lactate production is unknown for hippocampal mixed cultures.

ATP hydrolysis produces protons, which are extruded by several membrane transport mechanisms (Roos and Boron, 1981), including the Na^+/H^+ exchanger in hippocampal neurons (Raley-Susman et al., 1991). There are additional, HCO_3-dependent mechanisms; however, the nominally HCO_3-free perfusion medium precludes the contribution of these transport mechanisms. We have shown previously that in nominally HCO_3-free solutions, the primary mechanism of acid extrusion is an Na^+/H^+ exchanger (Raley-Susman et al., 1991). Therefore, an important consideration of the metabolic rate measurement in this study is the effect of neurotransmitters and hormones on this acid extruder. For example, direct activation of the Na^+/H^+ antiport would produce an apparent increase in metabolic rate using the microphysiometer. Indeed, growth factors, phorbol esters, and various receptor agonists have been shown in other cell types to activate Na^+/H^+ exchange activity (Moolenaar, 1986; Grinstein et al., 1989). While such an effect cannot be ruled out in the present study, glutamate analogs transiently (30 sec) decreased intracellular pH, when measured with a fluorescent pH indicator; this effect was very brief and presumably reflects direct proton influx via channel opening, or decreased activity of the Na^+/H^+ exchanger (K. M. Raley-Susman, unpublished observations). Thus, the extracellular acidification rates, occurring during and after the brief effect on intracellular pH, most probably represent a true increase in metabolic rate.

Another important consideration in this study is the effect of conditions in the microphysiometer on mixed hippocampal cultures. Silicon microphysiometry necessitates the use of solutions with very low buffering capacity (1 mM PO_4, nominally bicarbonate free) in order to detect sensitively acidification of the medium due to cellular acid extrusion. Although the cells do not appear to be extremely sensitive to low bicarbonate concentrations (Raley-Susman et al., 1991), the long-term effects of such low-buffering-capacity solutions are unknown and may affect the normal response of neurons and glia. In fact, in contrast to other cell types (Wada et al., 1991), we found that metabolic rate in control cultures began to decrease after 10 hr or more of constant perfusion with low buffering medium. This decreased rate could reflect cell loss or hampered metabolism resulting from prolonged time periods in low buffering medium or from the shear stress (1 dyne/cm^2) caused by the perfusion. Although this shear stress causes minimal changes in some cell types (Levesque et al., 1989), the effects on neuronal cultures are unknown. Further work is ongoing to characterize more fully the effects of low buffering medium and perfusion shear force in hippocampal mixed cultures.

Thus, secondary measurements of cell viability, such as LDH determination, are necessary to distinguish between a true decrease in metabolic rate and a decrease resulting from loss of cells. However, the advantages afforded by the sensitive, time-integrated measurements of metabolism enable increased time resolution of metabolic events evoked by neurotransmitter activation.

Effects of kainic acid on cellular metabolism

This is the first direct demonstration that kainic acid increases metabolic rate (~80%) in hippocampal mixed cultures in a dose-dependent and receptor-mediated manner. This increase most likely reflects the depolarization-induced activation of energy-dependent ion extrusion pumps, since kainic acid has been shown

to induce changes in Na^+, K^+, H^+, and Ca^{2+} fluxes (Biziere and Coyle, 1978; Lothman and Collins, 1981; Ben-Ari, 1985; Lazarewicz et al., 1986; Kobayashi et al., 1990). The estimated EC_{50} for kainic acid in this study (100 μM) agrees quite well with that for electophysiological responses to excitatory amino acid exposure in culture (Koroshetz et al., 1990). Pure astrocytic cultures also exhibited an increased metabolic rate upon exposure to kainic acid, although the increase was less than half the magnitude of that seen with primarily neuronal clusters. Astrocytes *in vitro* express kainic acid receptors (Backus et al., 1989). The difference in the intensity of the metabolic response to kainic acid is intriguing and could relate to differences in receptor density or to differences in sensitivity to the excitatory amino acid (amount of depolarization, changes in calcium, etc.). Further, the responsiveness of glia to kainic acid in mixed culture could be modified indirectly by the presence of neurons.

Early work suggested that neurons expend more than half of their ATP for the maintenance of ion homeostasis (Siesjo, 1978). Thus, activation of kainic acid receptors, leading to influx of Na^+, would be expected to activate energy-dependent ion extruders, such as the Na^+/K^+ ATPase and Na^+/Ca^{2+} exchange mechanism, and subsequently activate cellular metabolism. With increasing doses of kainic acid, the depolarization of neurons would be sufficient to open voltage-dependent calcium channels, further activating ion extruders. The large increase in metabolism is quite striking and suggests that, under conditions of energy failure, the brain's ability to withstand neurotransmitter activation could be altered.

In the present study, we used a concentration of kainic acid that has been shown to be neurotoxic in other *in vitro* studies (Frandsen et al., 1989; Galarraga et al., 1990) and continuously monitored the metabolic response to this exposure. We found that, following the initial metabolic excitation, metabolic impairment began as little as 4 hr after a brief (10 min) or a continuous exposure to kainic acid. At these early times, the decreased metabolic rate preceded measurable cell lysis, based on LDH measurements. Thus, the decline in rate most likely represents a true decrease in metabolic rate. At later time points, LDH measurements also declined, indicating measurable cell lysis contributing to the decline in metabolic rate. Is the decline in metabolic rate (extracellular acidification) a reflection of decreased energy (ATP) availability or a decreased cellular demand for energy? *In vivo* studies have demonstrated that excitotoxin exposure produces a sustained increase in electrophysiological excitability (McGregor et al., 1990), increased oxygen and glucose utilization (Franck et al., 1986; Ingvar, 1986; Siesjo et al., 1986), and a marked decrease in ATP concentration (Ingvar, 1986). Similarly, excitotoxins such as kainic acid cause a decrease in ATP levels in striatal slices (Biziere and Coyle, 1978). While these parameters have not been measured in primary hippocampal cultures over the time course utilized in this study, this literature suggests that the decrease in metabolic rate would seem to be secondary to a decline in substrate availability, rather than to decreased cellular demand. This scenario is certainly consonant with current thinking regarding the role of energy depletion in excitotoxin-induced neuron death.

Another important finding mentioned above is that the measured decrease in metabolic rate, whether because of decreased demand or decreased supply, preceded cell death, as assessed by LDH measurement. These data suggest that metabolic impairment is detectable soon after excitotoxin exposure and may serve as a sensitive index of neurotoxicity. While we have not yet shown conclusively that this is the case, earlier *in vivo* studies have demonstrated that the indices of hypermetabolism and substrate depletion precede overt cell degeneration (Franck et al., 1986; Ingvar, 1986; Siesjo et al., 1986; Woolf, 1987; McGregor et al., 1990).

In summary, we have shown the feasibility of using novel silicon microphysiometry for assessing metabolism in brain cultures. Given the caveats discussed, the sensitivity of this approach and its capacity to provide real-time data suggest a broad array of potential uses. Microphysiometry affords the advantage of being able to couple continual time-integrated monitoring of metabolic rate with measurements of toxicity and/or substrate availability, in order to test hypotheses of the relationships among these variables. In a first application of this technology, we have demonstrated that an excitotoxin initially stimulates metabolic rate in hippocampal mixed cultures (in a dose-dependent, receptor-mediated manner) and then causes a decline in metabolism that precedes cell loss. These results delineate a time-window for the onset of excitotoxin-induced damage *in vitro*.

References

Backus KH, Kettenmann H, Schachner M (1989) Pharmacological characterization of the glutamate receptors in cultured astrocytes. J Neurosci Res 22:274–282.

Banker G, Cowan W (1977) Rat hippocampal neurons in dispersed cell culture. Brain Res 126:397–425.

Ben-Ari Y (1985) Limbic seizure and brain damage produced by kainic acid: mechanisms and relevance to human temporal lobe epilepsy. Neuroscience 14:375–403.

Biziere K, Coyle JT (1978) Effects of kainic acid on ion distribution and ATP levels of striatal slices incubated *in vitro*. J Neurochem 31: 513–520.

Choi DW (1988) Glutamate neurotoxicity and diseases of the nervous system. Neuron 1:623–634.

Coyle JT, Bird SJ, Evans RH, Gulley RL, Nadler JV, Nicklas WJ, Olney JW (1981) Excitatory amino acid neurotoxins: selectivity, specificity, and mechanism of action. Neurosci Res Prog Bull 19:329–427.

Cremer JE, Seville MP, Cunningham VJ (1988) Tracer 2-deoxyglucose kinetics in brain regions of rats given kainic acid. J Cereb Blood Flow Metab 8:244–253.

Franck G, Sadzot B, Salmon E, Depresseux JC, Grisar T, Peters JM, Guillaume M, Quaglia L, Delfiore G, Lamotte D (1986) Regional cerebral blood flow and metabolic rates in human focal epilepsy and status epilepticus. Adv Neurol 44:935–948.

Frandsen A, Drejer J, Schousboe A (1989) Direct evidence that excitotoxicity in cultured neurons is mediated via *N*-methyl-D-aspartate (NMDA) as well as non-NMDA receptors. J Neurochem 53:297–299.

Galarraga E, Surmeier DJ, Kitai ST (1990) Quinolinate and kainate neurotoxicity in neostriatal culture is potentiated by co-culturing with neocortical neurons. Brain Res 512:269–276.

Ganong AH, Lanthorn TH, Cotman CW (1983) Kynurenic acid inhibits synaptic and acidic amino acid–induced responses in the rat hippocampus and spinal cord. Brain Res 273:170–174.

Grinstein S, Rotin D, Mason MJ (1989) Na/H exchange and growth factor-induced cytosolic pH changes: role in cellular proliferation. Biochim Biophys Acta 988:73–97.

Horner HC, Packan D, Sapolsky RM (1990) Glucocorticoids inhibit glucose transport in cultured hippocampal neurons and glia. Neuroendocrinology 52:57–64.

Ingvar M (1986) Cerebral blood flow and metabolic rate during seizures. Ann NY Acad Sci 462:194–206.

Kobayashi S, Kikuchi H, Ishikawa M, Hashimoto K (1990) Regional changes of tissue pH and ATP content in rat brain following systemic administration of kainic acid. Brain Res 514:352–354.

Koh JY, Choi DW (1987) Quantitative determination of glutamate mediated cortical neuronal injury in cell culture by lactate dehydrogenase efflux assay. J Neurosci Methods 20:83–90.

Koroshetz WJ, Freese A, Difiglia M (1990) The correlation between excitatory amino acid–induced current responses and excitotoxicity in striatal cultures. Brain Res 521:265–272.

Lazarewicz JW, Lehmann A, Hagberg H, Hamberger A (1986) Effects

of kainic acid on brain calcium fluxes studied *in vivo* and *in vitro*. J Neurochem 46:494–498.

Levesque JM, Sprague EA, Schwartz CJ, Nerem RM (1989) The influence of shear stress on cultured vascular endothelial cells: the stress response of an anchorage-dependent mammalian cell. Biotech Prog 5:1–8.

Lothman EW, Collins RC (1981) Kainic acid induced limbic seizures: metabolic, behavioural, electroencephalographic and neuropathological correlates. Brain Res 218:299–318.

McGregor IS, Menendez JA, Atrens DM (1990) Metabolic effects obtained from excitatory amino acid stimulation of the sulcal prefrontal cortex. Brain Res 529:1–6.

Moolenaar WH (1986) Regulation of cytoplasmic pH by Na/H exchange. Trends Biochem Sci 11:141–143.

Nishizaki T, Yamauchi R, Okada Y (1988) Enhancement of the oxygen consumption in the hippocampal slices of the guinea pig induced by glutamate and its related substances. Neurosci Lett 85:61–64.

Novelli A, Reilly JA, Lysko PG, Henneberry RC (1988) Glutamate becomes neurotoxic via the *N*-methyl-D-aspartate receptor when intracellular energy levels are reduced. Brain Res 451:205–212.

Olesen SP (1986) Rapid increase in blood–brain barrier permeability during severe hypoxia and metabolic inhibition. Brain Res 368:24–29.

Owicki JC, Parce JW (in press) Biosensors based on the energy metabolism of living cells: the physical chemistry and cell biology of extracellular acidification. Biosens Bioeng, in press.

Owicki JC, Parce JW, Kercso KM, Sigal GB, Muir VC, Venter JC, Fraser CM, McConnell HM (1990) Continuous monitoring of receptor-mediated changes in the metabolic rates of living cells. Proc Natl Acad Sci USA 87:4007–4011.

Parce JW, Owicki JC, Kercso KM, Sigal GB, Wada HG, Muir VC, Bousse LJ, Ross KL, Sikic BL, McConnell HM (1989) Detection of cell-affecting agents with a silicon biosensor. Science 246:243–247.

Raley-Susman KM, Cragoe EJJ, Sapolsky RM, Kopito RR (1991) Regulation of intracellular pH in cultured hippocampal neurons by an amiloride-insensitive Na^+/H^+ exchanger. J Biol Chem 266:2739–2745.

Roos A, Boron WF (1981) Intracellular pH. Physiol Rev 61:296–434.

Rothman SM, Thurston JH, Hauhart RE (1987) Delayed neurotoxicity of excitatory amino acids *in vitro*. Neuroscience 22:471–480.

Sapolsky RM, Packan DR, Vale WW (1988) Glucocorticoid toxicity in the hippocampus: *in vitro* demonstration. Brain Res 453:367–371.

Siesjo BK (1978) Brain metabolism. New York: Wiley.

Siesjo BK, Ingvar M, Wieloch T (1986) Cellular and molecular events underlying epileptic brain damage. Ann NY Acad Sci 462:207–223.

Wada HG, Owicki JC, Parce JW (1991) Cells on silicon: bioassays with a microphysiometer. Clin Chem 37:600–601.

Woolf CJ (1987) Excitatory amino acids increase glycogen phosphorylase activity in the rat spinal cord. Neurosci Lett 73:209–214.

AATEX 1, 154–164 (1992)

Measurement of Cellular Responses to Toxic Agents using a Silicon Microphysiometer

H.G. WADA[1*], J.C. OWICKI[1], L.H. BRUNER[2], K.R. MILLER[3], K.M. RALEY-SUSMAN[4], P.R. PANFILI[1], G.M.K. HUMPHRIES[1] & J.W. PARCE[1]

[1]*Molecular Devices Corp, Menlo Park, CA 94025,*
[2]*Procter & Gamble Co., Miami Valley Lab., Cincinnati, OH 45239–8707*
[3]*Microbiological Associates, Rockville, MD 20850*
[4]*Vassar College, Poughkeepsie, NY 12601*
[*]*to whom correspondence should be addressed*

The silicon microphysiometer monitors cellular metabolism *in vitro* and has been used to detect and study biological responses to xenobiotics. This instrument uses a light addressable potentiometric sensor to measure millipH changes in micro-flow chambers maintained at 37°C. Cells are immobilized in the flow chambers. Cell proton excretion can be measured as the acidification of the medium when medium flow through the chamber is stopped. The rate of acidification is a measure of catabolism, which produces lactic and carbonic acids. Through continual cycling of on and off periods of flow, non-destructive metabolic measurements may be made every few minutes. When a cell affecting agent is introduced into the fluid stream a change in acidification rate indicates either the stimulatory or toxic effect of the agent on the cells. Thus, rapid cellular responses to chemical agents can be detected within minutes and quantitated by the magnitude of acidification rate change.

Receptor-mediated cell activation by specific ligands, such as hormones, neurotransmitters, and growth factors, causes increases in acidification rate within minutes of receptor-ligand binding. This provides a receptor-specific response that can be monitored during exposure to materials as a possible indicator of cell-type specific toxicity. Receptor specific toxicity in hippocampal neurons has also been tested using extracellular acidification as the measurement of the toxicity of glutamate receptor overstimulation.

In tests for chemotherapeutic efficacy, antiviral drug activity and toxicity, acidification rates have been used as the cell activity and viability indicator. Agents, such as detergents, that produce irritancy or other non-specific toxicity have been evaluated for their effects on extracellular acidification rate and found to decrease acidification rate. Concentrations at which acidification rates are reduced by 50% were determined for test substances and correlated with animal ocular irritation test results. Recovery after insult is readily measured and may be an important index of irritancy or toxicity. These examples illustrate the broad range of cell affecting agents that cause cellular responses detectable in the microphysiometer using extracellular acidification rate.

Introduction

Toxicologic assays and other bioassays seek to test, predict and characterize the effects of substances upon organisms. *In vitro* cellular assays simplify this inherently complex task by measuring single, defined endpoints and by reducing the number of cell types tested. Since the object is to mimic events taking place in the intact organism, both the cell type studied and the endpoint measured may impose significant limitations on the assay system if prediction of irritancy is the object. One solution is to assay cells by a wide variety of endpoints. A recently developed instrument system, the Cytosensor™ silicon microphysiometer provides a novel means to monitor cellular responses to test substances. This system is based on a biosensor that measures a parameter that is central to the complex network of metabolic pathways[1,2]. Thus, it provides a broad screen for diverse agents that alter cellular metabolism by varied mechanisms.

The silicon microphysiometer measures changes in the metabolic rate of cells upon exposure to xenobiotics. Principal excreted products of carbohydrate, fat and amino acid metabolism are acids, and the rate of acidification of the minimally buffered culture medium reflects the rate of metabolic energy production[3]. Initial studies showed that the effects of agents such as hormones, neurotransmitters, growth factors, and toxic compounds on acidification rate could be detected rapidly and directly[1,4,5,6]. Activation of receptors by agonists increases metabolic activity, which is detected as increased acidification rate. The physiological changes associated with this increased metabolic activity are yet to be identified conclusively, but they are thought to include alterations of ionic homeostasis and proliferation rate[3]. In contrast to receptor activation, exposure to chemicals at levels that are toxic by other criteria, such as decreased viability and proliferation, usually decreases metabolic activity in the microphysiometer.

The advantages offered by the silicon microphysiometer include speed, precision, reproducibility, detection of a broad spectrum of effects of chemical agents on metabolically active cells, and suitability for virtually any cell capable of growth or maintenance in culture. Specificity is introduced through selection of appropriate blocking agents such as antibodies, antagonists, specific transduction pathway blockers, or by the use of cells with transfected receptors. Since the technique is nondestructive, cells may be removed from chambers and subsequently tested by other assays. In addition, information on the recovery of cells from initial metabolic response to effector agents can be obtained[4,6,7]. The time required to recover to basal metabolic activity from treatments with agents that either activate or reduce metabolic rate may be a useful parameter for characterizing cell-affecting agents.

Materials and Methods

The Silicon Microphysiometer:

Cells are grown and tested in a compact flow chamber into which metered volumes of liquids can be introduced and then removed. The pH of the culture medium is measured with a light addressable potentiometric sensor (LAPS), which serves as one wall of the flow chamber. The LAPS is a silicon semiconductor device that detects changes in the surface potential at the interface between electrolyte and an insulating layer on the surface of the silicon chip[8]. This insulating surface contains silicon nitride and silicon oxide groups that can be protonated; thus, the pH of the culture medium affects surface charge. The sensor detects changes in surface potential, which depends on pH in a Nernstian way (61 mV per pH unit at 37°C), similar to a glass pH electrode. Data are obtained only from illuminated regions of the sensor, which permits spatial selectivity in some applications.

Figure 1 shows the components of the system. The fluidics system includes a pump to deliver medium to the low-volume culture chamber via a debubbling device. The temperature of the culture chamber is regulated. Fluid flow, electronics for the LAPS, and data acquisition and computation are controlled by a microcomputer.

The microphysiometer measures net metabolic activity of small numbers of cells in real time. The cell chamber contains 10^5 to 10^6

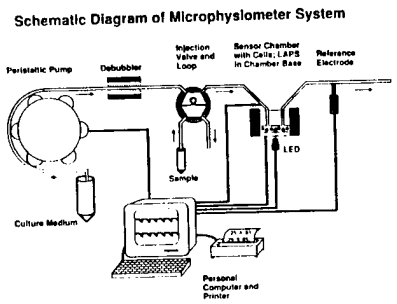

Fig. 1. Diagram of the microphysiometer system. A personal computer controls the on/off cycle of the peristaltic pump and acquires data from the light addressable potentiometric (LAP) sensor in the sensor chamber. The debubbler removes bubbles and excess gas from the culture medium so that bubbles do not form in the warm (37°C) flow chambers. An injection loop valve is provided for the introduction of samples [after H.M. McConnell, et al.,[4]].

cells, although only a fraction, as few as 3000 cells, are actually monitored in the instrument. The time necessary to introduce a compound and measure the cellular response can be on the order of a few minutes. The flow of medium alternates on and off, and one determination of acidification rate is made during each flow-off period. When flow is on, the pH at the sensor is close to that of the fresh medium entering the sensor chamber. When flow ceases, the lactic and carbonic acids secreted by the cells build up in the chamber; the pH drops at a rate that is proportional to the number, size, and metabolic activity of the cells.

Cells and chemicals:

Human keratinocytes (Clonetics, San Diego, CA) were cultured using the vendor's growth medium. Cells from the human uterine sarcoma lines, MES-SA and Dx5 (from Branimir Sikic, Stanford University, Stanford, CA) were cultured in RPMI 1640 medium supplemented with 10% fetal bovine serum (FBS), 50 units/ml penicillin and 50 mg/ml streptomycin (pen/strep). Mouse fibroblastic L 929 cells from Frank Lee (DNAX Research Institute, Palo Alto, CA) were cultured in Dulbecco's Modified Eagle's Medium (DMEM) supplemented with 10% FBS and pen/step. CD4-transfected HeLa cells, HT4–6C, from William Robinson (Stanford University, Stanford, CA) were cultured in RPMI 1640 supplemented with 10% FBS, pen/strep, and 50 μg/ml geneticin. Hippocampal neurons were prepared from fetal rat brains as described by Raley-Susman, et al.[9] and maintained in high glucose HEPES-buffered DMEM supplemented with 5% FBS. TF-1 cells were from Toshio Kitamura (DNAX Research Institute, Palo Alto, CA). These nonadherent cells were cultured in RPMI 1640 supplemented with 2 mM sodium pyruvate, 50 μM β-mercaptoethanol, 1 ng/ml granulocyte/macrophage colony stimulating factor (GM-CSF) from Sandoz/Schering-Plough (Bloomfield, NJ), pen/strep, and 10% FBS.

Certain responses may be enhanced by replacing complete medium with serum-free medium 12–24 hours prior to placement into the microphysiometer. Serum contains growth factors, insulin, and other cytokines that can elevate basal metabolic rate and decrease the net metabolic response to stimulus. Low buffering tissue culture medium is use in the microphysiometer to make acidification rate measurements; we routinely use a buffer at approximately 1–2 mM buffering capacity such as sodium bicarbonate-free RPMI 1640, 1 mM phosphate (Irvine Scientific, Irvine, CA) supplemented with pen/strep. Bicarbonate buffer is avoided to reduce buffering and simplify pH control.

Loading of cells into cell capsules; metabolic measuerments:

The Cytosensor silicon microphysiometer and associated cell capsule parts and reagents are manufactured by Molecular Devices Corporation, Menlo Park, CA. Cells are confined to the sensor chamber by growth on membranes in disposable cell capsules (Figure 2). Adherent cell scan be seeded onto these surfaces and maintained in a 12-well cell culture plate in an incubator until needed. The diameter of the membrane is 12 mm, but

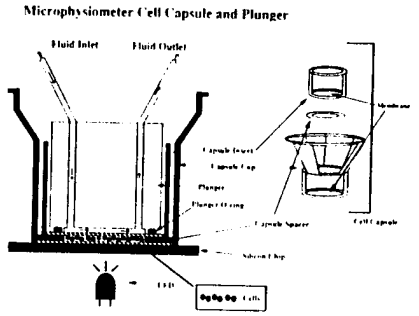

Fig. 2. Diagram of the disposable cell capsule used to immobilize cells in the microphysiometer sensor chamber. Cells are grown on the lower capsule cup membrane and enclosed using a capsule spacer with a capsule insert membrane. Non-adherent cells require an immobilizing matrix such as a fibrin gel to hold the cells onto the lower capsule membrane.

the sensor only collects data from a central region of 2 mm diameter. An added capsule spacer ring separates the cells growing on one surface from the other surface, which in the preferred method is a second microporous membrane on a capsule insert. The capsule insert is sunk over the cells and enclosed by a sealing plunger, thereby creating the low volume culture chamber.

Cells are at about 60–95% confluence when the chambers are used. Early versions of the microphysiometer, not commercially available, employed indium tin oxide coated coverslips on which adherent cells were grown. Non-adherent cells, such as the TF-1 cells, can also be confined using the double membrane system described above. These cells are embedded in a collagen particle matrix or a fibrin gel to immobilize them in the cell capsule. Many elements of the Cytosensor (LAPS, tubing, and cell capsule housing) are reusable. The system is decontaminated by cycling Cytosensor sterilant, an oxidant plus detergent solution, through the assembled system (minus the cell capsule assembly), to sterilize and depyrogenate the system, and then rinsing with sterile distilled water followed by sterile phosphate buffered saline or medium.

Sample handling:

Samples are usually water-soluble substances. Water-insoluble or viscous materials pose delivery problems; however, dimethylsulfoxide has been used to increase solubility since it is non-toxic at relatively high doses (1%). Samples are diluted in the same low buffered medium used for acidification-rate measurements. Matrix controls must be run to estimate the contribution of the vehicle in medium to the cytotoxicity observed.

Determination of the 50% Metabolic Reduction Dose (MRD50):

The concentration of test substance that reduces the metabolic rate to 50% of the initial rate (MRD50) has been used to characterize the irritancy of test substances. The MRD50 is measured using the protocol previously described by Bruner et al.[6] and depicted in Figure 3, which shows one cycle of the assay protocol. The flow rate of medium, the introduction of test substance into the cell culture chamber, and the net change in medium pH are displayed. A 300 μl sample bolus is introduced in a sample loop using injection valves. The sample flows into the chamber for 120 sec, flow halts for a 200 sec incubation, and the sample is washed out for 380 sec. The nominal time that the cells are exposed to the sample is 380 sec (300 μl/100 μl/min+200 sec). Following washout, the acidification rate is determined while flow is halted for 200 sec. It is simple to vary sample exposure time, the time of subsequent wash with fresh medium, and the time for reading acidification rate. Typically, in this protocol acidification rate is measured only after the sample is washed out to avoid possible changes in buffer capacity and pH of the medium due to the sample itself. Endpoints are calculated after testing a series of dilutions of the test substance, starting with the greatest dilution and continuing until the acidification rate (measured in μV/s) is reduced by >50%. The *in vitro* irritancy is often expressed as −log (MRD50), or pMRD50.

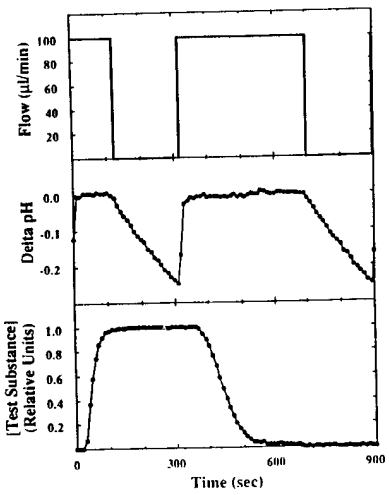

Fig. 3. One cycle of the assay protocol for ocular irritancy. The top figure shows the liquid flow rate over the 900 sec cycle. The net change in medium pH is shown in the middle figure. The second stopped flow time period is used to measure the acidification rate. The bottom figure shows the actual introduction of test substances into the cell culture chamber [after L.H. Bruner, et al., [6]].

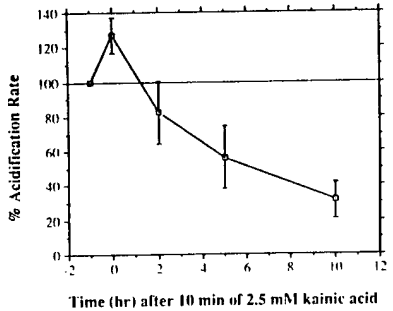

Fig. 4. Effect of glutamate receptor stimulation of mixed hippocampal cultures. Hippocampal cultures were exposed to 2.5 mM kainic acid for 10 min at time 0, then returned to normal perfusion medium. Data represents the average acidification rate (µV/sec) of 3 experiments. The average, initial acidification rate was 213+-29 µV/sec, and expressed as 100% acidification rate. Statistical analysis of the decline in rate after kainic acid stimulation indicated high degree of significance, $p<0.0037$ level, using the Fisher PLSD test [after Raley-Susman et al., [9]].

Results

Stimulus-induced neurotoxicity:

Glutamate is an important excitatory neurotransmitter in the central nervous system. There is much evidence that overstimulation of the glutamate receptor leads to the neurotoxicity associated with a host of metabolic insults, including seizures and hypoxia-ischemia, because of the disruption of metabolism-dependent homeostatic mechanisms[10]. The microphysiometer was used to monitor the toxicity of glutamate receptor stimulation by the agonist kainic acid, using co-cultures of hippocampal neurons and glia that were isolated from fetal rats and maintained in culture as previously described[11]. These cells were tested in the microphysiometer after serum starvation for 24 hr. Exposure to kainate caused a prompt (<1 min) increase in acidification rate of up to 100%, with half-maximal stimulation at 2 µM kainate. As is shown in Figure 4, transient (10 min) exposure to 2.5 mM kainate, a level known to be neurotoxic, led to a depression of acidification rate within 5 hr. This decrease in metabolic activity was not due to cell loss since cell-associated lactate dehydrogenase was not significantly decreased in cells treated with kainate, in parallel experiments, and untreated control cells did not show the decrease in metabolic activity (data not shown).

Inhibition of receptor-activated cellular response by a protein kinase C inhibitor:

Another type of receptor-specific toxicity that can be measured by the microphysiometer is the interference with intracellular signal transduction pathways. The effect of an enzyme inhibitor on the activation of TF-1 cells by granulocyte-macrophage colony stimulating factor (GM-CSF) was examined. Exposure of TF-1 cells to GM-CSF causes a rapid increase in extracellular acidification rate[12]. Protein kinase C (PKC) is activated by a number of colony stimulating factors[13], including GM-CSF, and depletion of PKC

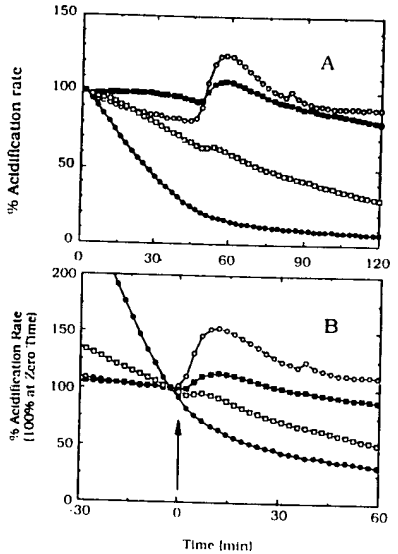

Fig. 5. Calphostin C inhibits the GM-CSF acidification response in TF-1 cells. Panel A shows the acidification rate of cells treated with 0 (open circles), 12.5 nM (closed squares), 25 nM (open squares), and 50 nM (closed circles) of calphostin C for 1 hr under fluorescent lighting prior to loading into the microphysiometer chamber using the fibrin gel method. At about 50 min, the cells were exposed to GM-CSF at 5 ng/ml for 6 min. Panel B shows the acidification rates of the same TF-1 cells in panstell A, normalized to 100% at the time of GM-CSF exposure.

blocks GM-CSF dependent cell proliferation as well as other cellular responses. The effects of calphostin C, an irreversible photoactivated protein kinase C inhibitor[14], on the GM-CSF activation of TF-1 cells was evaluated as was calphostin general toxicity. Cells were exposed to calphostin C under fluorescent lights for 1 hr prior to being loaded into the microphysiometer. Figure 5A shows that cytotoxicity was observed at calphostin concentrations as low as 25 nM, as measured by the decrease in acidification rate monitored for 2 hr after treatment. The effect of calphostin on the GM-CSF response was observed at a lower concentration, 12.5 nM, which caused a 66% decrease in the activation of acidification rate (Figure 5B). The onset of cellular

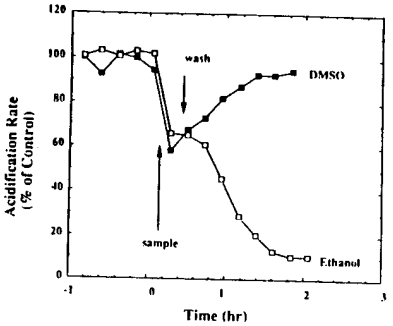

Fig. 6. Recovery of human keratinocytes from exposure to irritating test materials. Keratinocytes were exposed to DMSO or to ethanol at concentrations corresponding to the MRD50 for 5 minutes. The first arrow indicates the time of exposure to test sample, and the second arrow indicates the start of sample washout. The cells treated with DMSO (solid squares) and ethanol (open squares) were monitored for acidification rates for an additional 90 min [after J.W. Parce et al., [7]].

toxicity could in this way be differentiated from the inhibition of GM-CSF signal transduction. This example shows how receptor activation of acidification rate may be used to test for agents that interfere with cellular signaling pathways.

Recovery from toxic insult:

Physiological responses to toxic insult can be characterized both by intensity and duration, most *in vitro* toxicological assays measure intensity. The microphysiometer is well suited to measure not only intensity, but also duration of alterations of cellular metabolic activity. Two pilot experiments in the microphysiometer have tested the relationship between *in vivo* irritancy and recovery from insult.

The *in vivo* irritancy of dimethylsulfoxide (DMSO) is less than that of ethanol, and DMSO accordingly has a lower pMRD50 than does ethanol (0.1 vs. 0.8)[1]. Human keratinocytes were exposed to each compound for 5 minutes at its MRD50 concentration, to equalize acute effects, and then metabolic activity was monitored for 2 hours (Figure 6)[15]. The acidification rate of keratinocytes

exposed to DMSO returned to its initial control value within the observation period, suggesting complete recovery. In contrast, the acidification rate of the cells exposed to ethanol continued to decline, reaching about 10% of the control value by 2 hours after exposure.

Another experiment of similar design compared recovery from exposure to triethanolamine and heavy-duty laundry detergent[6]. Triethanolamine is the less irritating *in vivo* and in the microphysiometer (pMRD50=1.77 vs. 3.78 for the detergent). Keratinocytes exposed to triethanolamine recovered their initial acidification rates, while those exposed to the detergent did not.

In vitro irritancy testing

Initial studies using human keratinocytes grown on coverslips tested half-log serial dilutions of eight irritants previously characterized as having *in vivo* ocular irritancy ranging from mild to severe[1]. Cells were exposed to irritants for 5 min in a protocol similar to that described in Materials and Methods, and MRD50 was determined as shown in Figure 7. There was high rank correlation between the *in vivo* irritancy and the MRD50. There was a 4 log range of MRD50 values between the most mild (DMSO) and most severe (benzalkonium chloride) chemicals (Table 1). Reproducibility of the MRD50 value was within a factor of 2 over a period of several months using different lots of primary keratinocytes.

Bruner et al[6] tested seventeen product formulations and chemicals well characterized with historical data obtained at Procter and Gamble Co. using the rabbit Low Volume

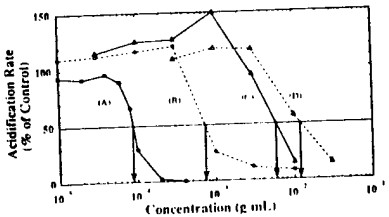

Fig. 7. Analysis of test substances for irritancy using reduction of metabolic rate. Two-fold serial dilutions of materials were sequentially tested, starting with the least concentrated samples. As the concentration of irritating substances was increased the acidification rate decreased. The concentration causing a 50% decrease in rate (MRD50) was interpolated for each test substance. In this study, heavy-duty laundry detergent (A) was the most irritating, MRD50=8.6×10^{-5} g/ml, and triethanolamine (D) was the least irritating, MRD50=1.2×10^{-2} g/ml [after L.H. Bruner, et al., [6]].

Eye Test (LVET). These materials represent the range of activities commonly encountered in ocular irritancy testing of cleaning products: soaps, shampoos, detergents, fabric softener, and 4 single chemicals. Keratinocytes grown on coverslips were also used in the microphysiometer to determine MRD50. MRD50 ranged from 2.50 10^{-4} g/ml [most irritating] to 1.8×10^{-2} g/ml [least irritating]. The correlation was r=0.86, p<0.0001 with the LVET maximum average scores (MAS), illustrated in Figure 8. It was noted that the metabolic rate of the cells increased at sub-inhibitory concentrations for some of the test materials, before higher concentration caused decreased rates. It was also noted that metabolic rate recovered to the basal rate after removal of some irritants which decreased rate. In a later study, Catroux et al., using L

Table 1. Comparison of the in vivo ocular irritancy to MRD50

ID#	Substance	-log MRD_{50}	In vivo irritancy
1	Dimethyl sulfoxide	0.1	Mild
2	Propylene glycol	0.5	Mild
3	Methanol	0.7	Moderate to mild
4	Ethanol	0.8	Moderate to mild
5	Acetone	0.9	moderate to mild
6	n-Butanol	1.7	moderate
7	Na dodecyl sulfate	3.9	Severe to moderate
8	Benzalkonium Cl	4.1	Severe

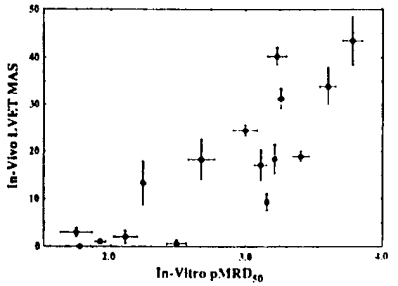

Fig. 8. Correlation of *in vitro* and *in vivo* results. The *in vivo* test was the Low Volume Eye Test (LVET); Maximum Average Scores (MAS) were determined for 17 test substances. The arithmetic mean of the negative log of the MRD_{50}, the $pMRD_{50}$, is plotted versus the LVET MAS value. There is significant positive correlation between the two data sets (correlation coefficient r=0.85, p<0.0001). The vertical and horizontal error bars show the SEM from at least three replicates for both assays [after L.H. Bruner, et al., [6]].

929 cells grown on the polycarbonate membrane of a capsule cup, evaluated the MRD50 of 19 surfactants (representing the cationic, anionic, nonionic and amphoteric classes) using a sample exposure time of 380 sec[16]. This panel of substances had been characterized by *in vivo* ocular irritancy testing and had maximum average scores (MAS) ranging from 3.8 to 54.0. Microphysiometer MRD50 values ranged from 40 to 200,000 μg/ml. A plot of MAS versus the pMRD50 yielded r=0.89, which was comparable to the Bruner study[6] using keratinocytes grown on coverslips.

Chemotherapeutic susceptibility testing:

Closely related to toxicity testing is chemotherapeutic susceptibility testing. A human uterine carcinoma cell line, MES-SA, which is sensitive to doxorubicin and vincristine, and a cell line, Dx5, derived by selection to be resistant to these drugs [17] by virtue of the P-glycoprotein transporter were tested in the microphysiometer for susceptibility to 1 μM doxorubicin and 100 μM vincristine. Figure 9A[1,7] shows that compared to MES-SA cells, which show 50% reduction in net metabolic activity in response to doxorubicin after 15 hr,

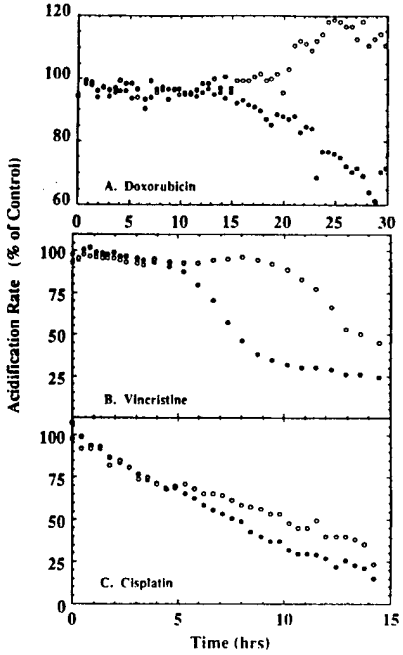

Fig. 9. The sensitivity of two human sarcoma cell lines to chemotherapeutic drugs. Acidification rates are presented as percent of rates before the drug was introduced into the microphysiometer. In panel A, MES-SA cells (solid circles) and Dx5 cells (open circles) were treated with 1 μM doxorubicin beginning at time 0. In panel B, these same cells were treated with 100 μM vincristine. In panel C, the cells were treated with 100 μM cisplatin [after Parce et al., [17]].

the Dx5 cells are resistant to this chemotherapeutic drug. Vincristine at 100 μM shortens the time to cytotoxic effects to 5 hr for MESSA cells. The Dx5 cells were shown in Figure 9B to be differentially sensitive in a much shorter time. Figure 9C shows that both cell lines are similarly sensitive to cisplatin.

Anti-viral drug testing:

The detection of viral ytopathic effects with the microphysiometer was first demonstrated using mouse L cells infected with vesicular stomatitis virus[1]. Ribavirin treatment of infected cells inhibited the viral cytopathic effect of decreases in acidification rate and

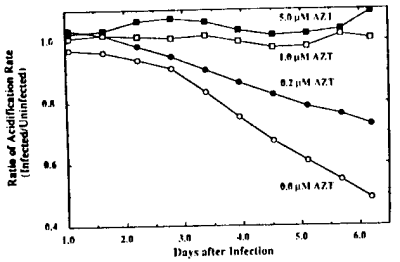

Fig. 10. The metabolic consequences of infection of cells with human immunodeficiency virus (HIV-1). Acidification rate data are presented as the ratio of the acidification rates of infected and uninfected cells. CD4 transfected HeLa cells were infected on coverslips by incubation for 1 hr at 37°C with 100 μl of viral innoculum, 1×10^5 infectious units/ml, prior to loading into microphysiometer. The perfusing medium contains the indicated concentrations of AZT [after Wada et al., [17]].

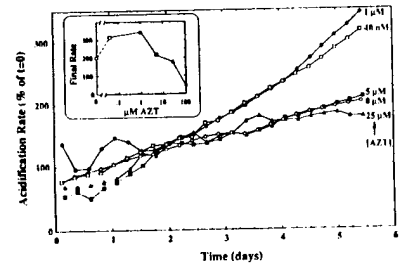

Fig. 11. Toxic effect of AZT on uninfected cells. CD4 transfected HeLa cells were perfused with medium containing various concentrations of AZT. A stimulation of acidificaton rate growth is seen at low concentrations of AZT. The insert figure shows the final acidification rate as a function of AZT concentration [after Wada et al., [17]].

delayed their on-set. Later, the infection of CD4 transfected HeLa cells, HT4–6C, with HIV-1 was detected in the microphysiometer (Figure 10)[7,18]. Six days were required for the HIV effects to be fully manifest, as a drop in the ratio of acidification rates of infected versus uninfected cells. The inhibition of viral cytopathic effects was demonstrated using 0 to 5 μM concentrations of 3'-azido-3'-deoxythymidine (AZT). The dose causing 50% inhibition of the HIV cytopathic effects (ED50) was 0.23 μM. The toxicity of AZT on the same CD4 transfected, uninfected cells was evaluated in the microphysiometer. As shown in Figure 11, AZT caused an increase in rate at low levels and a decrease at higher levels in uninfected cells relative to untreated controls over the 6 day treatment period. The dose causing a 50% reduction in acidification rate (TD50) was 67 μM. Testing of a panel of four compounds showed a rank order of anti-HIV potency of AZT ED50=0.23 μM<2', 3'-dideoxyinosine (DDI) ED50=8.3 μM<chloramine T ED50=19.2 μM<mannitol (no activity), which is in agreement with their known *in vitro* anti-HIV properties[17]. The ratio of TD50/ED50 was determined as a measure of *in vitro* anti-HIV selectivity, and the rank order was the same, AZT = 291 > DDI = 66 > chloramine T = 30>mannitol ≈ 0.

Discussion

In vitro toxicology can be considered to comprise two types of activities: safety assessment screening and studies of mechanism. The former seeks replacements for animal (or human) testing, typically for ocular and skin irritation. The most critical attribute of any *in vitro* alternative must be high predictive value: results for an unknown compound should provide an index of irritancy *in vivo*. The latter activity, mechanistic study, seeks to identify the molecular mechanism of toxicity. In this type of study, toxicity is already demonstrated and one investigates the target of the toxic effect, as toxicokinetics and toxicodynamics. The silicon microphysiometer is suitable for both types of study, as demonstrated by the above examples. Basic research in signal transduction has broadened the areas of toxicology.

An important parameter of both irritancy screening and mechanistic study, recovery from toxic insult, is uniquely measurable in the silicon microphysiometer. Results in three studies show good correspondence between pMRD50 and rabbit eye irritation scores. Two prelimary tests of recovery using essentially identical protcols were each able to demonstrate recovery (DMSO and triethanolamine) and failure to recover (ethanol and heavy duty laundry detergent) after a toxic insult corresponding to the MRD50. For this small study, the pMRD50 did not correlate unequivocally with inability to recover: the ranking of pMRD50 (with recovery in parentheses) is DMSO (yes) < ethanol (no) > triethanolamine (yes) < detergent (no). Recovery apparently does measure a different property from MRD50, and more work is necessary to relate it to the behavior of irritants *in vivo*. This is a little investigated area of *in vitro* toxicology and promises to be a powerful tool for screening and mechanistic studies.

The prospects for advanncing *in vitro* toxicology include the monitoring of receptor-specific toxic events, and elucidating mechanism(s) of cytotoxicity by studying cell-affecting agents in the microphysiometer. An illustration of neurotoxicity mediated through the glutamate receptor was provided by the work of Raley-Susman, et al.[9], who demonstrated the toxic effects of kainic acid, a glutamate receptor agonist, on hippocampal neurons using acidification rate to monitor the metabolic activity of the neuronal cell cultures as well as detect the rapid activation of glutamate receptors in these cells. The decreased metabolic activity is thought to be due to depletion of the cellular energy stores preceding overt cell degeneration[10]; alternatively, it may be due to leakage of essential low molecular weight metabolites through damaged membranes. Other tissue specific toxicity mediated through either inappropriate receptor activation or interruption in normal receptor mediated signaling processes could be evaluated using metabolic monitoring. Calphostin C inhibition of GM-CSF signaling provides an example of this type of toxicity. The interruption of the GM-CSF activation of bone marrow cells was detected by acidification rate monitoring, and this form of toxicity was also kinetically distinguished from the general cytotoxicity of higher levels of calphostin C. It should be possible to select other receptor systems characteristic of various tissue types to establish tests for other forms of tissue specific toxicity.

The measurement of toxicity is an important aspect of drug testing. In the case of chemotherapeutics, the efficacy of the drug is measured by the sensitivity of tumor cells to the therapeutic agent. This measurement can be made on relatively few cells which may make testing of tumor biopsies possible. By using elevated concentrations of the chemotherapeutic agents in the microphysiometer, the time required to determine drug susceptibility of tumor cells could be shortened. Evaluation of drugs for anti-viral activity requires the evaluation of toxicity as well as the measurement of vial inhibition, since inhibition of viral replication is closely tied to host cell metabolism. The general technique of acidification rate monitoring is capable of making both measurements, using infected or uninfected cells in the same series of assays.

The use of acidification rates to monitor the metabolism of cells exposed to irritating substances has been evaluated using human keratinocytes and mouse L cells and found to correlate well with *in vivo* measurement of ocular irritancy (r=0.86 and 0.89). Bruner et al. also compared 7 *in vitro* methods for ocular safety testing[19] including the microphysiometer, neutral red assay, total protein assay *Tetrahymena thermophila* motility assay, bovine eye/chorioallantoic membrane assay, and the EYTEX system and found significant correlation between *in vivo* ocular irritation and all *in vitro* methods except the EYTEX system. These authors noted that the microphysiometer method of monitoring recovery of cells after exposure to irritating test substances may be useful in differentiating innocuous irritants from more irritating materials.

Several features suggest that the silicon microphysiometer will be useful for irritancy testing as well as for mechanistic studies of toxicity. These factor include screening for multiple sites of toxic actions, real time

results, the possibility of both dosage and recovery studies, and suitability for a broad range of cell types.

Acknowledgements

The authors would like to thank B. Sikic, W. Robinson, F. Lee, and T. Kitamura for providing cells used in these studies. A. Goldberg for reviewing the manuscript, and the entire Cytosensor product group of Molecular Devices Corp. for providing the research prototype instrument system and supplies.

References

1) Parce J.W., Owicki J.C., Kercso K.M., Sigal G.B., Wada H.G., Muir V.C., Bousse L.J., Ross K.L., Sikic B.I., and McConnell H.M. (1989) Detection of cell-affecting agents with a Silica Biosensor. *Science*, 246: 243–247.

2) Parce J.W., Owicki J.C. and Kercso K.M. (1990) Biosensors for directly measuring cell affecting agents. *Annales de Biologie Clinique*, 48: 639–641.

3) Owicki J.C. and Parce J.W. (1992) Biosensors based on the energy metabolism of living cells: The physical chemistry and cell biology of extracellular acidification. *Biosensors and Bioelectronics*, 7: 255–272.

4) McConnell H.M., Rice P., Wada H.G., Owicki J.C., and Parce J.W. (1991) The microphysiometer biosensor. *Current Opin. Struc. Biol.*, 1: 647–652.

5) Owicki J.C., Parce J.W., Kercso K.M., Sigal G.B., Muir V.C., Venter J.C., Fraser C.M. and McConnell H.M. (1990) Continuous monitoring of receptor-mediated changes in the metabolic rates of living cells. *Proc. Natl. Acad. Sci. USA*, 87: 4007–4011.

6) Bruner L.H., Kercso K.M., Owicki J.C., Parce J.W. and Muir V.C. (1991) Testing ocular irritancy in vitro with the silicon mycrophysiometer. *Toxicol. in Vitro*, 5: 277–284.

7) Parce J.W., Owicki J.C., Wada H.G. and Kercso K.M. Cells on Silicon: The Microphysiometer. (In Press) vol. 8 of the *Alternative Methods in Toxicology* book series titled "In Vitro Toxicology Mechanisms and New Technology" Mary Ann Liebert, Inc., Publishers, 1651 Third Avenue, New York, NY.

8) Hafeman D.G., Parce J. W. and McConnell H.M. (1988) Light-addressable potentiometric sensor for biochemical systems. *Science*, 240: 1182–1185.

9) Raley-Susman K.M., Miller K.R., Owicki J.C., and Sapolsky R.M. (1992) Effects of excitotoxin exposure on metabolic rate of primary hippocampal cultures: Application of silicon microphysiometry to neurobiology. *J. Neuro-Sci.*, 12: 773–780.

10) Choi D.W. (1988) Glutamate neurotoxicity and diseases of the nervous system. *Neuron*, 1: 623–634.

11) Sapolsky R. M., Packen D.R. and Vale W.W. (1988) Glucocorticoid toxicity in the hippocampus: in vitro demonstration. *Brain Res.*, 453: 367–371.

12) DeVries J.K, Indelicato S.R., Meyer L. and Wada H.G. (1991) The real time assessment of cellular metabolism from GM-CSF mediated stimulation of TF-1 cells as measured by a microphysiometer. Abstract presented at *3rd Internatl. Workshop on Cytokines*, Stresa, Italy, November 10–14.

13) Gino V. and Hamilton J.A. (1991) Signalling through CSF receptor. *Immunol. Today* 12: 362–369.

14) Bruns R.F., Miller F.D., Merriman R.L., Howbert J.J., Health W.F., Kobayashi E., Takahashi I., Tamaoki T. and Nakano H. (1991) Inhibition of protein kinase C by calphostin C is light-dependent. *Biochem Biophys. Res. Comm.*, 176: 288–293.

15) Parce J.W., Sigal G.B., Kercso K.M. and Owicki J.C. (1990) *in* "Biosensor technology: Fundamentals and Applications," (Eds. Buck R.P., Hatfield W.E., Umaña M. and Bowden E.F.), p. 367–373. Marcel Dekker, Inc, New York.

16) Catroux P., Cottin M., Dossou K.G. and Rougier A. (1991) The silicon microphysiometer: a new tool for testing ocular irritancy in vitro. Abstract presented at the *3rd colloquium of Société de Pharmaco-Toxicologie Cellulaire*, Paris, France, October 18.

17) Harker W.G. and Sikic B.I. (1985) Multidrug (pleiotropic) resistance in doxorubicin-selected variants of the human sarcoma cell line MES-SA. *Cancer Res.*, 45: 4091–4096.

18) Wada H.G., Fok K, Nolan T., Robinson W. and McConnell H.M. (1990) Application of the MDC microphysiometer to the detection of HIV-mediated effects on host cell metabolism and anti-HIV activity. Abstracts of the *N.I.A.I.D. Conference on Advances in Molecular Biology and Targeted Treatments for AIDS*. Washington, D.C., May 14–18.

19) Bruner L.H., Kain D.J., Roberts D.A. and Parker R.D. (1991) Evaluation of seven in vitro alternatives for ocular safety testing. *Fundam. Appl. Toxicol.*, 17: 136–149.

JOURNAL OF CELLULAR PHYSIOLOGY 154:129–138 (1993)

GM-CSF Triggers a Rapid, Glucose Dependent Extracellular Acidification by TF-1 Cells: Evidence for Sodium/Proton Antiporter and PKC Mediated Activation of Acid Production

H. GARRETT WADA,* STEPHEN R. INDELICATO, LORRAINE MEYER, TOSHIO KITAMURA, ATSUSHI MIYAJIMA, GREGORY KIRK, VICTORIA C. MUIR, AND J. WALLACE PARCE

Molecular Devices Corporation, Menlo Park, California 94025 (H.G.W., G.K., V.C.M., J.W.P.); Schering-Plough Research, Bloomfield, New Jersey 07003 (S.R.I., L.M.); DNAX Research Institute, Palo Alto, California 94304 (T.K., A.M.)

The extracellular acidification rate of the human bone marrow cell line, TF-1, increases rapidly in response to a bolus of recombinant granulocyte-macrophage colony stimulating factor (GM-CSF). Extracellular acidification rates were measured using a silicon microphysiometer. This instrument contains micro-flow chambers equipped with potentiometric sensors to monitor pH. The cells are immobilized in a fibrin clot sandwiched between two porous polycarbonate membranes. The membranes are part of a disposable plastic "cell capsule" that fits into the microphysiometer flow chamber. The GM-CSF activated acidification burst is dose dependent and can be neutralized by pretreating the cytokine with anti–GM-CSF antibody. The acidification burst can be resolved kinetically into at least two components. A rapid component of the burst is due to activation of the sodium/proton antiporter as evidenced by its elimination in sodium-free medium and in the presence of amiloride. A slower component of the GM-CSF response is a consequence of increased glycolytic metabolism as demonstrated by its dependence on D-glucose as a medium nutrient. Okadaic acid (a phospho-serine/threonine phosphatase inhibitor), phorbol 12-myristate 13-acetate (PMA, a protein kinase C (PKC) activator), and ionomycin (a calcium ionophore) all produce metabolic bursts in TF-1 cells similar to the GM-CSF response. Pretreatment of TF-1 cells with PMA for 18 h resulted in loss of the GM-CSF acidification response. Although this treatment is reported to destroy protein kinase activity, we demonstrate here that it also down-regulates expression of high-affinity GM-CSF receptors on the surface of TF-1 cells. In addition, GM-CSF driven TF-1 cell proliferation was decreased after the 18 h PMA treatment. Short-term treatment with PMA (1–2 h) again resulted in loss of the GM-CSF acidification response, but without a decrease in expression of high-affinity GM-CSF receptors. Evidence for involvement of PKC in GM-CSF signal transduction was obtained using calphostin C, a specific inhibitor of PKC, which inhibited the GM-CSF metabolic burst at a subtoxic concentration. Genistein and herbimycin A, tyrosine kinase inhibitors, both inhibited the GM-CSF response of TF-1 cells, but only at levels high enough to also inhibit stimulation by PMA. These results indicate that GM-CSF activated extracellular acidification of TF-1 cells is caused by increases in sodium/proton antiporter activity and glycolysis, through protein kinase signalling pathways which can be both activated and down-regulated by PMA.

Granulocyte-macrophage colony stimulating factor (GM-CSF) is a glycoprotein belonging to a family of cytokines that have stimulatory effects on proliferation and maturation of hemopoetic/myeloid progenitor cells (Gasson, 1991; Miyajima et al., 1992). A variety of cellular responses to GM-CSF receptor ligation have been demonstrated. These include activation of ras p21 protein, diacylglycerol release, translocation and activation of protein kinase C (PKC), sodium/proton antiporter activation, increased glucose uptake, and subsequent DNA synthesis and gene expression (Vario and Hamilton, 1991). Despite all of this information, the basic mechanism by which the GM-CSF signal is transduced has not been determined. A low-affinity cell surface receptor for human GM-CSF was cloned and

Received February 3, 1992; accepted July 14, 1992.

To whom reprint requests/correspondence should be addressed.

expressed in COS7 cells by Gearing et al. (1989). Hayashida et al. (1990) cloned a second component that conferred high-affinity binding to hGM-CSF when co-transfected with the low-affinity receptor. This indicates that the structure of the GM-CSF receptor is probably similar to that of the interleukin-2 (IL-2) receptor, which is composed of α- and β-subunits. Competitive binding between interleukin-3 (IL-3) and GM-CSF suggests that the receptors for these cytokines share the same β-subunit. In fact, Kitamura et al. (1991b) demonstrated that hIL-3 and hGM-CSF receptors share a common β-subunit by cloning c-DNA for the hIL-3 receptor α-subunit, which reconstituted the high-affinity IL-3 receptor when co-transfected with the hGM-CSF receptor β-subunit. Since there is evidence for early GM-CSF and IL-3 induced tyrosine phosphorylation in hemopoetic cells (Isfort and Ihle, 1990; Evans et al., 1990) and no consensus tyrosine kinase sequences were found in the cloned receptor subunits (Hayashida et al., 1990), it has been suggested that additional signal transducing elements are associated with the IL-3/GM-CSF receptor complex.

To further study the mechanism by which the GM-CSF signal is transduced, we have used a rapid, non-invasive method for measuring cellular responses to GM-CSF. This method involves measuring the rate of extracellular acidification in a device called a microphysiometer (Parce et al., 1989; McConnell et al., 1992). The cell line used, TF-1, is a human bone marrow cell line obtained from an erythroleukemia patient. It is dependent upon GM-CSF, IL-3, or erythropoetin for growth (Kitamura et al., 1989) and expresses about 2,000 high-affinity GM-CSF receptors per cell (Kitamura et al., 1991a). We have previously shown that activating TF-1 cells with GM-CSF or IL-3 results in a rapid and dramatic increase in extracellular acidification rate (De Vries et al., 1991). This result is consistent with previous studies that have shown activation of a variety of receptors for hormones, growth factors, and neurotransmitters to result in a rapid increase in the rate of extracellular acidification (Parce et al., 1989; Owicki et al., 1990; McConnell et al., 1991; Wada et al., 1991; Raley-Susman et al., 1992; Miller et al., 1991).

In this study, the GM-CSF response was resolved into two components: a rapid component that corresponds to the activation of the sodium/proton antiporter and a slower component that is independent of the antiporter and dependent upon glucose metabolism. We propose that both components of the increase in acidification rate are triggered by protein kinase activation. Experiments with phorbol 12-myristate 13-acetate (PMA), a PKC inhibitor (calphostin C), a protein phosphatase inhibitor (okadaic acid), a calcium ionophore (ionomycin), and tyrosine kinase inhibitors (genistein and herbimycin A) were conducted, and we report their effects on acidification rates of TF-1 cells and the GM-CSF activated acidification burst. The correlation between GM-CSF driven cell proliferation and the GM-CSF activated acidification burst is also presented.

MATERIALS AND METHODS

Cells and chemicals

TF-1 cells were established from bone marrow of a patient with erythroleukemia by T. Kitamura et al. (1989). They were cultured in RPMI 1640 medium supplemented with 10% fetal bovine serum (FBS), 2 mM sodium pyruvate, 50 μM β-mercaptoethanol, and 1 ng/ml recombinant hGM-CSF from Sandoz/Schering-Plough Corp. (Bloomfield, NJ). Cells were deprived of GM-CSF for 4–24 h prior to testing in the microphysiometer by incubation in RPMI containing 5–10% FBS. PMA and 4-α-PMA were obtained from LC Services corporation (Woburn, MA) or Sigma (St. Louis, MO); ionomycin, calcium salt from Calbiochem Corp. (La Jolla, CA); genistein from BioMol (Philadelphia, PA); herbimycin A from BRL (Bethesda, MD); and calphostin C from Kamiya Biochem. Co. (Thousand Oaks, CA). Inhibitors and enzyme activators were dissolved in solvent vehicle at 100× working concentration. Controls were treated with solvent vehicle alone.

Trapping cells in fibrin clots and loading them into sensor chambers

TF-1 cells were immobilized in a thin fibrin clot in a cell capsule from Molecular Devices Corp. (Menlo Park, CA) comprising two polycarbonate membranes separated by a 50 μ thick plastic spacer. The cell capsule, a disposable sterile plastic assembly in which cells are immobilized, was described earlier (McConnell et al., 1991; Nag et al., 1992). The spacer was placed in the capsule cup; then 100 μl of a suspension of GM-CSF deprived cells was centrifuged at 500g into the capsule cup. The cells were suspended at a density of 1×10^6/ml in RPMI containing no bicarbonate or serum, with 10 mM HEPES added. A cell focusing device (a funnel shaped plastic insert) was used to direct the cells into a circular area (3.7 mm in diameter) at the center of the capsule membrane. For some experiments, 1×10^6 cells were centrifuged into the capsule cup without the cell focuser. The centrifuged cells were overlaid with 50 μl of a fibrinogen/thrombin mixture, which would clot in 5–10 min, immobilizing the cells in the capsule cup. A capsule insert, containing the top membrane, was placed in the cup and allowed to sink through the overlying medium onto the fibrin clot; then the assembled cell capsule was loaded into the sensor chamber.

Measuring acidification rates and introducing cell-affecting agents

Once the cells were loaded into the sensor chambers, Low Buffer RPMI (LB-RPMI) was pumped through the sensor chambers at 50 μl per min. LB-RPMI is made without bicarbonate or serum, and contains 1 mM sodium phosphate, penicillin/streptomycin, and 1 mg/ml endotoxin-free human serum albumin (Miles Labs, Elkhart, IN). Acidification rates in the sensor chambers were measured by stopping the flow of medium for 20 seconds, then monitoring the pH for an additional 60 seconds with the pump still off. The pump was then run for 60 seconds to return the sensor chambers to the pH of the LB-RPMI and remove waste products (Parce et al., 1989). By repeating the on-off cycle, rate measurements were made every 2.3 min. The acidification rates were measured in μV/sec, which is approximately equivalent to millipH/min. Before being plotted the data were normalized to the initial acidification rate (i.e., the average rate prior to sample introduction). In experiments in which medium components were re-

moved or other components were added, a balanced salt solution (130 mM sodium chloride, 3 mM potassium chloride, 1 mM potassium phosphate, 0.6 mM magnesium chloride, 0.3 mM calcium chloride, and 10 mM D-glucose) was used in place of LB-RPMI medium. When sodium-free medium was used, choline chloride was substituted for sodium chloride in the balanced salt solution. A 200 μl sample injection loop and a valve were used to introduce cell affecting agents during three pump-on cycles, exposing the cells to the agents for 7 min.

Radiolabeled GM-CSF cell binding assays

Recombinant hGM-CSF produced in *E. coli* was iodinated using the Bolton and Hunter (1973) reagent with minor modifications as described by Hayashida et al. (1990). Binding assays were performed as follows: the cells were incubated with iodinated hGM-CSF at 4°C for 2 h, and cell-bound radioactivity was separated from free ligand by centrifugation through n-butyl phtalate.

TF-1 cell proliferation assays

Cellular proliferation was measured as described by Mossman (1983) with slight modifications. TF-1 cells were taken from 48 h cultures and washed in assay medium (RPMI 1640 supplemented as described above, containing no GM-CSF and only 5% FBS). Cells were diluted to 2×10^5 cells/ml in aliquots of assay medium containing a range of PMA concentrations from 1×10^{-6} to 1.6×10^{-11} M, then distributed into wells of a 96-well microtiter plate. A control without PMA was also run. The plates were incubated for 18 h at 37°C, 5–6% CO_2. Following the initial incubation in PMA, GM-CSF (4 ng/ml) was added to selected wells of the assay plates and the plates were further incubated for 24 h. Following the second incubation, MTT (3-(4,5-dimethylthiozol-2-yl)-2,5-diphenyl-tetrazolium bromide) was added to the plates to a final concentration of 1.25 mg/ml. The cells were incubated for an additional 6 h before the reaction was stopped and the formazan product solubilized with 100 μl/well of 10% sodium dodecylsulfate solution in 0.01 N hydrochloric acid (Tada et al., 1986). Optical density was measured with a microplate reader at 570 nm with background reading at 650 nm subtracted from the results.

RESULTS

Acidification response of TF-1 cells to GM-CSF

When TF-1 cells that had been deprived of GM-CSF for 18 h were exposed to the cytokine for 7 min, a dose dependent increase in acidification rate was observed (Fig. 1A). Pre-incubation of the GM-CSF with 10 μg/ml anti–GM-CSF antibody completely blocked the cytokine induced increase in acidification rate (Fig. 1B). Subsequent addition of GM-CSF to the cells that had been previously exposed to the antibody-cytokine complexes resulted in a normal acidification response, demonstrating that the immune complexes had no adverse effect on the cells' ability to respond to cytokine. The amplitude of the response shown in Figure 1B was considerably larger than that shown for the highest concentration of GM-CSF in Figure 1A. This amplitude variation appears to be related to the number of days since GM-CSF containing medium was last added to the culture and the length of time the cells were maintained in the complete absence of GM-CSF prior to microphysiometer experiments. GM-CSF deprivation arrests TF-1 cell growth and depresses the basal acidification rate. The extent to which cells are deprived of cytokine determines the degree to which the basal rate is depressed and, therefore, the magnitude of the GM-CSF response which is expressed as a percentage of basal rate. The use of normalized values, percent of basal acidification rate, was necessary since there was some variation (±20%) in absolute rate (millipH units/min) due to variation in numbers of cells loaded into the reading area of the instrument. Optimum re-

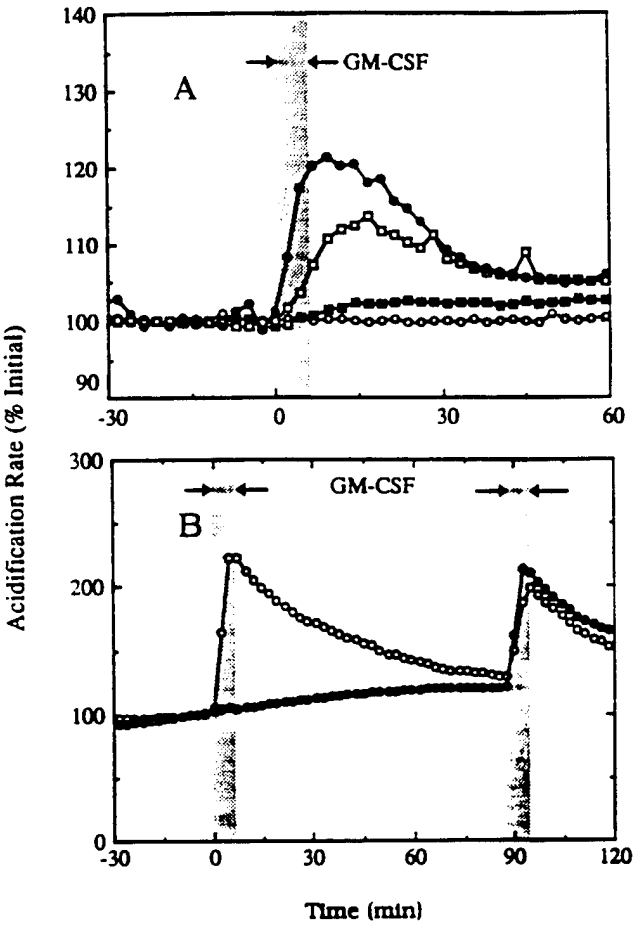

Fig. 1. Stimulation of extracellular acidification rate by hGM-CSF. TF-1 cells were cultured overnight in medium without GM-CSF. Cells were loaded into sensor chambers as described in Materials and Methods; then the acidification rates were monitored for 1 h until they stabilized. A: The cells were exposed at time zero to a bolus of GM-CSF for 7 min, as indicated by the gray bar. Each sensor chamber was exposed to a different concentration of GM-CSF: 0 ng/ml (open circles), 0.1 ng/ml (closed squares), 1 ng/ml (open squares), and 10 ng/ml (closed circles). Before being plotted the rates were normalized to the basal acidification rate (i.e., the average rate prior to sample introduction). B: Cells were exposed at time zero to a 6 min bolus of 10 ng/ml GM-CSF that had been pre-incubated with 10 μg/ml purified anti–GM-CSF sheep antibody for 30 min at 37°C (closed circles). In a second chamber, cells were exposed to a bolus of 10 ng/ml GM-CSF that had undergone a sham incubation with medium (open circles). In a second treatment, cells in both chambers were exposed to a bolus of 10 ng/ml GM-CSF. The data presented here are from a single experiment, representative of two separate runs.

sponse to cytokine was obtained after 3 days in culture with 1 ng/ml GM-CSF followed by 18 to 24 h of GM-CSF deprivation (data not shown). Variation in response between sensor chambers using the same cell preparation was minimal. TF-1 cells from a single culture flask were divided and placed in 3 parallel chambers. All three chambers were exposed to 5 ng/ml GM-CSF. The basal acidification rate ranged from 90 to 120 μV/s, and the average percent increase in rate due to GM-CSF addition was 28% with a 2% SEM. In earlier studies using CHO cells transfected with the β2-adrenergic receptor (Owicki et al., 1990), variation of the acidification response to agonist as measured by the microphysiometer was found to be 2.5% SEM for 6 runs conducted over 16 days.

Evidence for activation of the sodium/proton antiporter

The acidification response of TF-1 cells to GM-CSF can be resolved kinetically into two components at high concentrations of cytokine: a low amplitude short-lived response and a higher amplitude longer-lived response. This was demonstrated by exposing TF-1 cells to a bolus of GM-CSF in the presence and absence of sodium, as shown in Figure 2A. The characteristic profile of the GM-CSF metabolic response was obtained using balanced salts supplemented with D-glucose. When sodium was omitted from the solution and replaced with choline to maintain osmotic balance, the response lost the short-lived component. This component of the response is represented in Figure 2A by plotting the difference between responses obtained in the presence and absence of sodium. However, the difference between the GM-CSF responses with and without sodium disappeared (Fig. 2B) when amiloride was present at a concentration known to block the sodium/proton antiporter (Paris and Pouyssegur, 1983).

Glucose dependence of the GM-CSF activated acidification response

The glucose dependence of the GM-CSF metabolic burst was investigated using balanced salt solution with or without 10 mM glucose. The cells were loaded into the microphysiometer using LB-RPMI medium, then monitored until the acidification rates had stabilized. At this time, the LB-RPMI was replaced with balanced salt solution, with or without D-glucose. As shown in Figure 3, in the absence of glucose the acidification rates dropped to 50% of the initial rate, while in the presence of glucose the rates remained at a level similar to that obtained with LB-RPMI medium. When exposed to GM-CSF the cells perfused with glucose gave a strong response, whereas the cells without glucose gave a weak response. The weak response was similar kinetically and in magnitude to the component of the GM-CSF response attributed to activation of the sodium/proton antiporter. Subsequent addition of glucose to cells that had been exposed to GM-CSF in the absence of glucose resulted in large increases in acidification rate to levels greater than that of cells stimulated with GM-CSF in the presence of glucose. This overshoot in rate may be due to an energy deficit which occurred during the glucose-free GM-CSF stimulation of the cells.

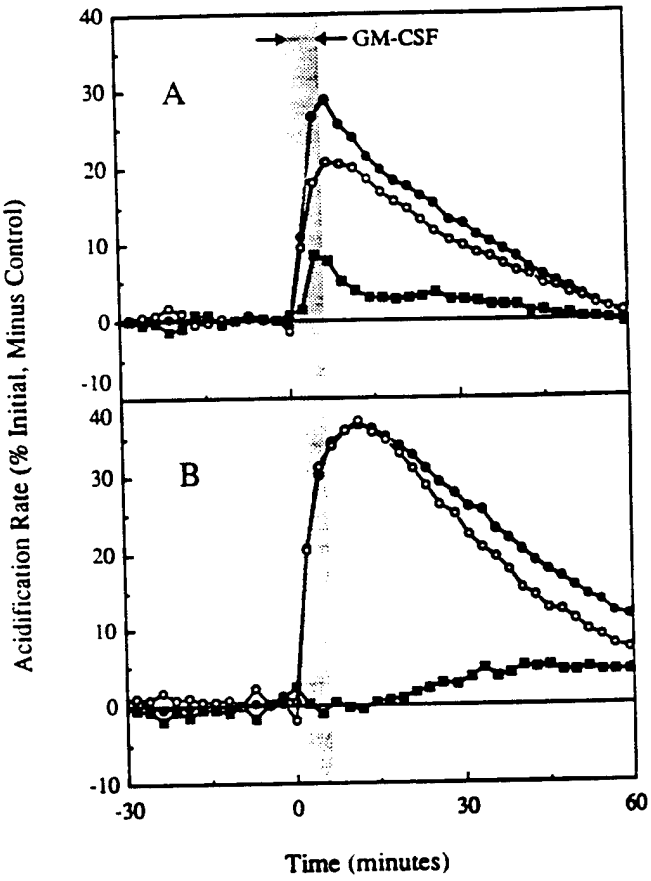

Fig. 2. GM-CSF activation of the sodium/proton antiporter. TF-1 cells were deprived of GM-CSF overnight, then loaded into cell capsules. A: Two chambers were perfused with balanced salts containing 130 mM sodium chloride and two chambers were perfused with balanced salts containing 130 mM choline chloride instead of sodium chloride. At time zero one chamber with and one chamber without sodium were exposed to a 7 min bolus of 10 ng/ml GM-CSF. The other two chambers were treated with medium alone. Acidification rates were monitored for 1 h after sample injection and normalized to the initial rate to GM-CSF exposure. To control for effects of sodium removal, the rates from control chambers (treated with balanced salts alone) were subtracted from the rates from chambers exposed to GM-CSF in the presence of sodium (closed circles) or in the absence of sodium (open circles). The difference in rate between the GM-CSF treated chambers with and without sodium was also calculated and plotted (closed squares). B: The same experimental conditions as described for A were reproduced with the addition of 0.1 mM amiloride to the balanced salts with sodium (closed circles) or without sodium (open circles). The difference in rate between the GM-CSF injected chambers with and without sodium was again calculated and plotted (closed squares). The rates were normalized to the basal acidification rate, and the data presented here are from a single experiment, representative of two separate runs.

Involvement of protein kinases in activation of TF-1 cell acidification rate

To evaluate the possibility that PKC participates in the signal transduction pathway that mediates the GM-CSF metabolic burst, TF-1 cells were exposed to a bolus of the PKC activator, PMA, or the protein phosphatase inhibitor, okadaic acid. Figure 4A,B shows that both PMA and okadaic acid cause an increase in acidification rate, presumably by enhancing phosphorylation levels of regulatory proteins or enzymes. Protein

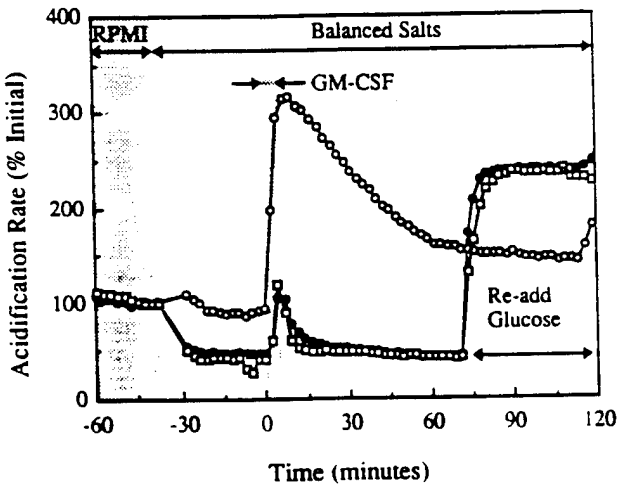

Fig. 3. Glucose dependence of GM-CSF stimulation of acidification rate. TF-1 cells were deprived of GM-CSF overnight and loaded into three sensor chambers. After the rates stabilized, the media in the chambers were changed to balanced salts (closed circles), balanced salts plus 2 mM L-glutamine (open squares), and balanced salts plus 10 mM glucose (open circles). After 30 min of exposure to the new medium, the cells were exposed to a bolus of 10 ng/ml GM-CSF, at time zero. After 70 min, the balanced salt solution lacking glucose was changed to balanced salts plus 10 mM glucose. The data presented here are from a single experiment, representative of two separate runs.

kinase inhibitors have been used to study involvement of these enzymes in signal transduction pathways. Figure 4C shows the effect of calphostin C (Kobayashi et al., 1989; Bruns et al., 1991), a light-activated specific inhibitor of PKC, on the GM-CSF acidification response. The GM-CSF response was inhibited 66% bya sub-toxic dose of 12.5 nM calphostin C. Two tyrosine kinase inhibitors, 166 μM genistein (Tetsu et al., 1987) and 2.4 μM herbimycin A (Uehara et al., 1989; June et al., 1990), were also tested and found to partially inhibit GM-CSF's stimulation of acidification rate (45–47%) as shown in Table 1. When PMA was used to stimulate the TF-1 cells, calphostin and the tyrosine kinase inhibitors gave a similar level of inhibition for PMA stimulation as was observed for GM-CSF stimulation.

Effect of PMA pre-treatment on TF-1 cells' metabolic response to GM-CSF

TF-1 cells were treated with 16 μM PMA for 18 h, a procedure known to deplete PKC activity in human lymphocytes (Farrar and Linnekin, 1990) and to down-regulate phorbol ester binding sites in IL-3 dependent hemopoietic stem cell lines (Whetton et al., 1988). Dramatic morphological changes occurred in the TF-1 cells after several hours of incubation, including a ruffled appearance of the cell surface and a significant increase in adhesion of the normally non-adherent cells to the plastic culture flask. Figure 5A shows that 18 h pre-treatment to PMA caused the TF-1 cells to lose their response to GM-CSF. The cells pre-treated with PMA did respond, however, to a bolus of ionomycin. Ionomycin produced an immediate increase in acidification rate, which then quickly returned to the initial rate after the ionomycin was removed. The ionomycin response of control cells was kinetically distinguishable from that of PMA pre-treated cells. In control cells, the rate of decrease in acidification rates upon ionomycin removal was much slower and its kinetics were characteristic of the normal GM-CSF response. The effect of short-term exposure of TF-1 cells to PMA on the GM-CSF activated metabolic burst was further investigated. TF-1 cells were pre-treated for 1 or 2 h with 1 nM

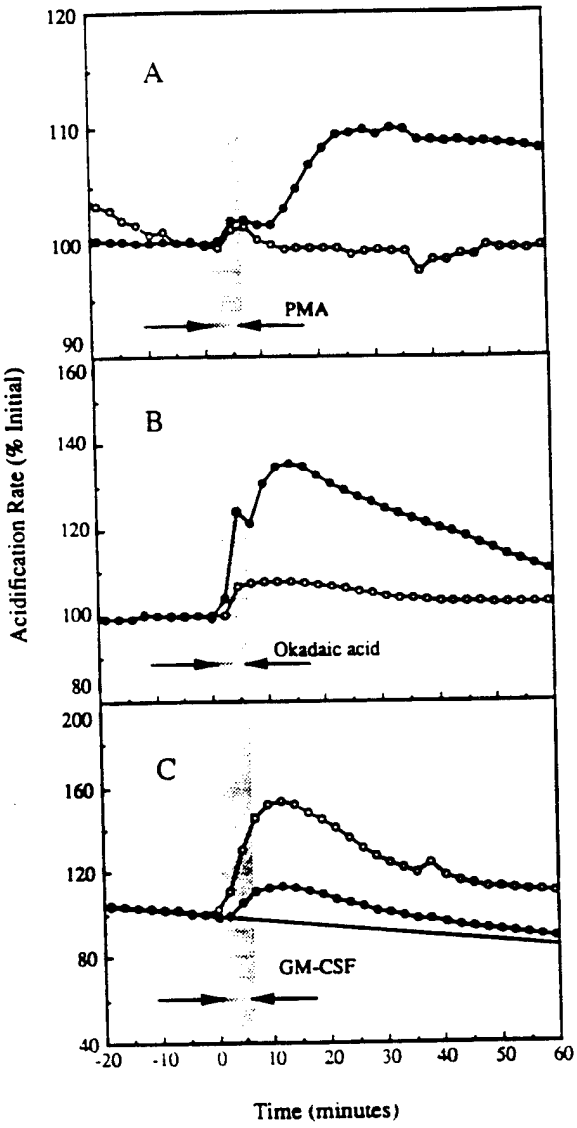

Fig. 4. Effects of treatment with PMA, okadaic acid, or calphostin C on TF-1 cells. TF-1 cells were deprived of GM-CSF overnight, then are loaded into sensor chambers. A: One chamber was exposed to a 6 min bolus of 100 ng/ml PMA (closed circles), and a control chamber was exposed to 0.1% DMSO vehicle (open circles). B: One chamber was exposed to a bolus of 1 μg/ml okadaic acid (closed circles) and the other with 1% dimethylformamide vehicle (open circles). C: Cells were pre-treated with 12.5 nM calphostin C (closed circles) under fluorescent light for 60 min, or underwent a sham pre-treatment with 0.1% DMSO vehicle (open circles) under fluorescent light for 60 min. Once in the microphysiometer, the cells were exposed to a 6 min pulse of 5 ng/ml GM-CSF at time zero. Rates were normalized to basal rates prior to sample injection. The data presented here are from single experiments, representative of several separate runs.

TABLE 1. Inhibition of GM-CSF stimulation of TF-1 cells

Stimulus[1]	Herb. A (3.4 μM) (%)	Calphos. C (12.5 nM) (%)	Genistein (166 μM) (%)
GM-CSF 5 ng/ml	−45	−66	−47
PMA 250 ng/ml	−40	−68	−35

[1]Serum starved TF-1 cells were stimulated with a 6 min bolus of 5 ng/ml GM-CSF or 100 ng/ml PMA in the presence or absence of kinase inhibitor. Data are representative of pairs of chambers taken from several experiments.

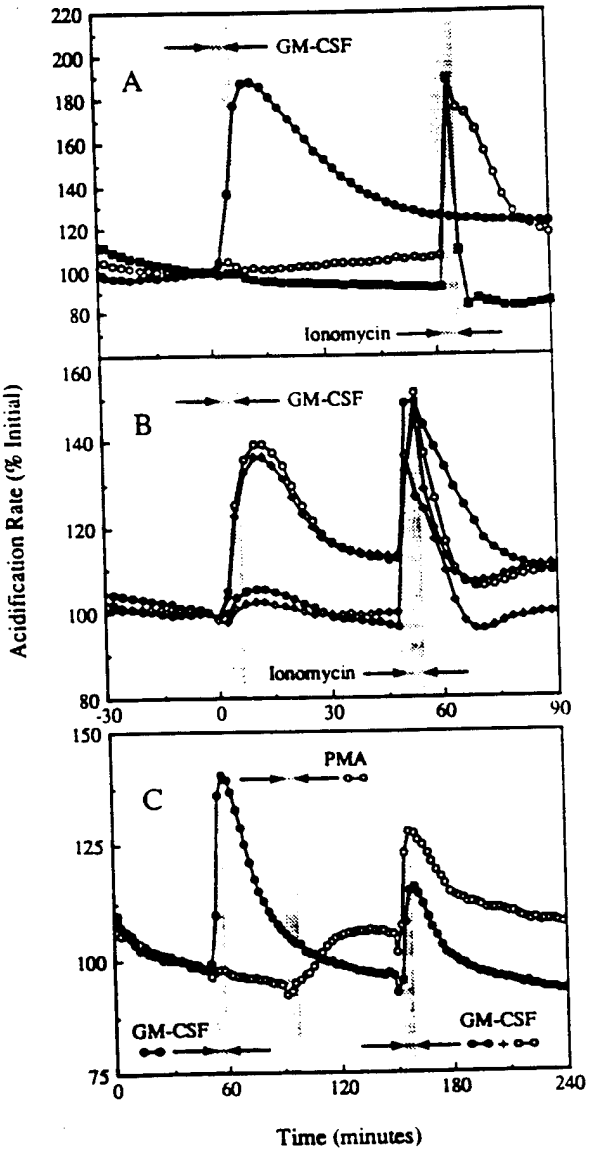

Fig. 5. Effects of PMA depletion of protein kinase C on GM-CSF stimulation of acidification rate. TF-1 cells were treated with PMA in three different protocols and tested for stimulation of acidification rate by GM-CSF. A: TF-1 cells were treated with 16 μM PMA overnight in RPMI containing 10% FBS. Control cells were treated with the 0.1% DMSO solvent vehicle. The PMA treated cells became adherent to the plastic flask and were removed by incubation with 5 mM EDTA in PBS for 5 min at 37°C. The cells were pelleted, washed once in RPMI without bicarbonate or serum with 10 mM HEPES, and then loaded into sensor chambers. At time zero, a 7 min bolus of 5 ng/ml GM-CSF was injected into chambers containing PMA treated cells (closed squares) and control cells (closed circles). A third chamber containing control cells was not exposed to GM-CSF (open circles). After monitoring the acidification rates for 1 h, a second injection, containing 1 μg/ml ionomycin, was made into the chambers containing cells treated with PMA (closed squares) and the chamber containing control cells that had not been exposed to GM-CSF (open circles). Rates were normalized to the initial rates prior to GM-CSF injection. B: TF-1 cells were treated with 1 nM PMA for 1 and 2 h in RPMI containing 10% FBS. Cells were also treated with 1 nM 4-α-PMA or mock treated with 0.1% DMSO vehicle. The PMA treated cells became adherent to the plastic flask even after a 1 h treatment and were removed by incubation with 5 mM EDTA in PBS for 5 min at 37°C. The cells were pelleted, washed once in RPMI without bicarbonate or serum with 10 mM HEPEs, and then loaded into sensor chambers. At time zero, a 7 min bolus of 5 ng/ml GM-CSF was injected into chambers containing mock treated control cells (open circles), cells treated with 1 nM PMA for 1 h (closed circles) or 2 h (open diamonds), and cells treated for 2 h with 1 nM 4-α-PMA (closed diamonds). After monitoring acidification rates for 50 min, a second injection, containing 1 μg/ml ionomycin, was made into all of the chambers. Rates were normalized to the initial rates prior to the GM-CSF injection. C: TF-1 cells were loaded into two chambers. One chamber was exposed to a bolus of 5 ng/ml GM-CSF (closed circles) at 52 min, and the other was exposed to a bolus of 100 ng/ml PMA (open circles) at 93 min. At about 153 min, both chambers were exposed to a second bolus of GM-CSF. Rates were normalized to basal rates prior to the first GM-CSF injection, and the presented data are representative of three separate runs.

PMA or 2 h with 1 nM 4-α-PMA (an analogue of PMA which does not activate PKC). After pre-treatment the cells were washed and loaded into cell capsules, then tested for acidification response to GM-CSF. The cells treated with PMA had diminished ability to respond to GM-CSF exposure. As shown in Figure 5B, the 2 h treatment was more effective than the 1 h treatment in blocking the GM-CSF response. Cells pre-treated with 4-α-PMA or given a mock pre-treatment with culture medium entirely retained their responsiveness to GM-CSF. Subsequent exposure to ionomycin caused a strong acidification response in all cases, as had been observed using cells pre-treated with PMA for 18 h, indicating that these short-term PMA-treated cells retain the ability to respond to a different second messenger stimulus. As shown in Figure 5C, a brief 6 min exposure to PMA did not block the GM-CSF acidification response, but did diminish its amplitude. A similar reduction in amplitude is observed in cells previously exposed to a bolus of GM-CSF.

To further explore the mechanism by which PMA pre-treatment abrogates the GM-CSF response, cells were incubated with various concentrations of PMA for 18 h prior to use in the microphysiometer. As shown in Figure 6A, the GM-CSF response, expressed as integrated peak area, decreases with increasing PMA concentration, and the ionomycin response, also expressed as integrated peak area, gradually rises. The increases in acidification rate due to ionomycin exposure provide a control for cell viability and cellular ability to respond to a second messenger activating stimulus. The concentration of PMA required to block the GM-CSF response was determined by utilizing the ratio of the integrated GM-CSF response to the integrated ionomycin response (Ratio GM/Iono). A monotonic decrease in Ratio GM/Iono vs. PMA concentration is shown in Figure 6B. Interpolation of the data gives a value of 0.8 nM for the concentration of PMA required to decrease the GM-CSF stimulated metabolic response by 50%.

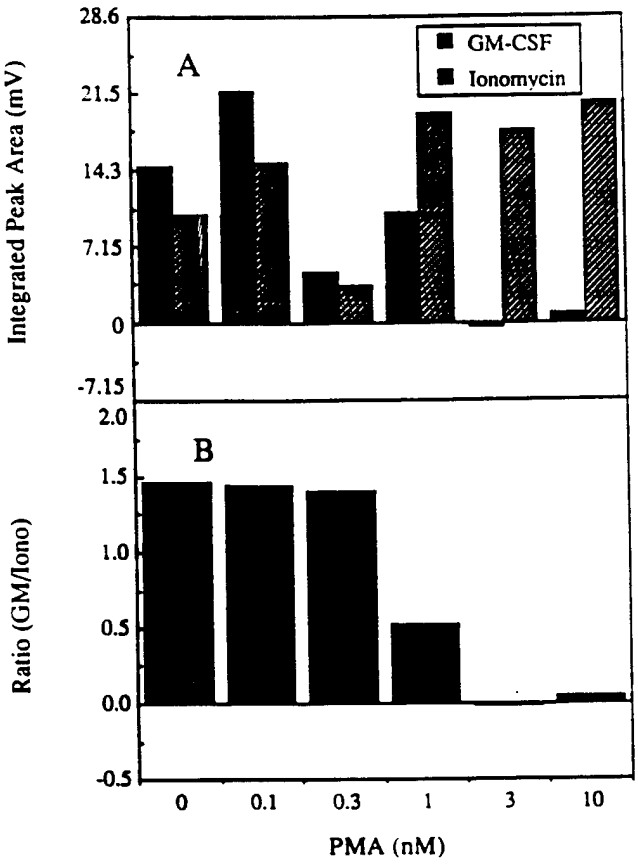

Fig. 6. Titration of the inhibition of GM-CSF metabolic burst by chronic PMA treatment. TF-1 cells were treated for 18 h as described in Fig. 5A with concentrations of PMA from 0–10^{-8} M and (A) the cells were tested for acidification response to 5 ng/ml GM-CSF as described in Fig. 5A. A secondary exposure to a bolus of 1 μg/ml ionomycin was also performed as before. The values displayed in the bar graph are the integrated peaks of GM-CSF and ionomycin acidification responses. The ratio of the integrated peak values for GM-CSF response vs. the ionomycin response is displayed (B) for the various concentrations of PMA used to pre-treat the cells. These data are from a single experiment and are representative of several separate runs.

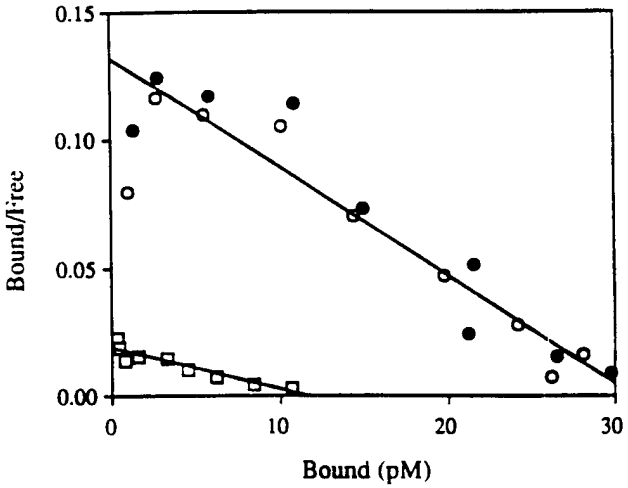

Fig. 7. Effect of chronic PMA treatment on GM-CSF high-affinity receptors. TF-1 cells (3×10^5) were cultured in a T75 flask for 17 h in culture medium containing 1 nM PMA and no GM-CSF (open squares). At the same time, two other flasks of TF-1 cells were also deprived of GM-CSF overnight. After 15 h, 1 nM PMA was added to one of these flasks, and no addition was made to the remaining flask. Cells were harvested at 17 h, using 5 mM EDTA when necessary to remove cells adhering to the plastic flask. The cells were washed once with culture medium without GM-CSF and stored on ice until they were assayed for GM-CSF receptors using radiolabeled GM-CSF. Binding data from cells treated with PMA for 2 h (open circles), 17 h (open squares), and untreated cells (closed circles) are displayed as Scatchard plots. Linear regression was used to determine dissociation constants reported in the text.

Down-regulation of GM-CSF receptors by long-term PMA treatment

Previous observations by Kitamura et al. (1989) indicated that TF-1 cells differentiate in response to extended PMA treatment, resulting in macrophage-like cells. Loss of the GM-CSF activated metabolic burst in cells treated for 18 h with PMA occurred at similar concentrations to those reported to cause cellular differentiation, 0.3–3 nM. For this reason, the effect of PMA on the TF-1 high-affinity GM-CSF receptor was investigated. Scatchard analysis of ^{125}I-labeled GM-CSF binding data (Fig. 7) shows that the density of GM-CSF receptors decreased from 3,800 sites/cell to 1,370/cell in response to treatment of the cells with 1.0 nM PMA for 17 h. Furthermore, the binding affinity for GM-CSF at the remaining sites was also decreased from 200 pM to 600 pM (Kd). In contrast to 17 h PMA treatment, TF-1 cells treated with 1 nM PMA for only 2 h were unchanged with respect to both high-affinity GM-CSF receptor density and affinity.

PMA effects on GM-CSF stimulated TF-1 cell proliferation

The effects of PMA treatment on GM-CSF stimulated proliferation was assayed using the MTT reduction method (Mossman, 1983). Twin groups of cells were incubated for 18 h in a range of PMA concentrations. After incubation with the PMA, 4 ng/ml GM-CSF was added to one set of cells and a sham addition was made to the second set of cells. An interesting relationship between the GM-CSF and PMA driven proliferaiton of TF-1 cells was revealed in this experiment. As shown in Figure 8A, PMA has no apparent affect on GM-CSF driven proliferation of TF-1 cells until the concentration of PMA reaches 4 nM, at which point cell growth begins to decrease. When GM-CSF is not added to the PMA treated cells, the PMA treatment alone is found to stimulate TF-1 cell proliferation, resulting in optimum growth rate at 4 nM PMA. At higher PMA concentrations, TF-1 growth rate is progressively decreased. If the GM-CSF activated component of proliferation (the difference in the rates of cell growth in PMA treated cells with GM-CSF or without GM-CSF) is calculated and plotted as displayed in Figure 8B, its contribution to TF-1 proliferation is shown to be negligible at 4 nM PMA. At this concentration of PMA, the growth rate in the presence of GM-CSF and PMA was equivalent to PMA alone. The concentration of PMA at which the GM-CSF activated component of proliferation is reduced by 50% was 1 nM. This value correlates well with

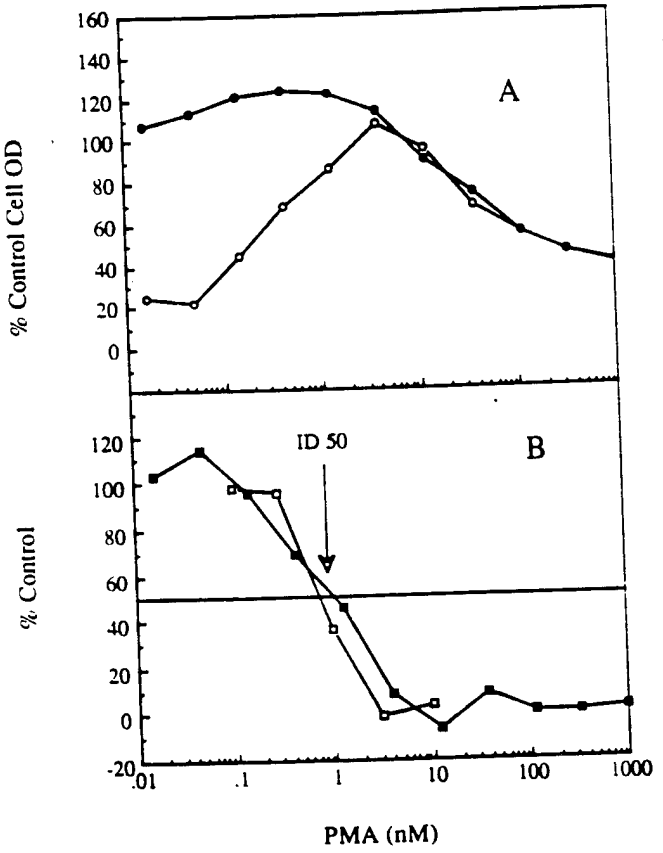

Fig. 8. Effect of chronic PMA treatment on GM-CSF driven cell proliferation. The MTT method was used to quantitate proliferation of TF-1 cells in the presence of various concentrations of PMA with or without GM-CSF. A: TF-1 cells were exposed to various concentrations of PMA for 18 h, after which 4 ng/ml GM-CSF was added to one set of cells (closed circles) and no addition was made to the other set (open circles). The results are displayed as the percent of control cell optical density (not treated with PMA) after MTT staining as described in Materials and Methods. B: The difference between values obtained in A with and without GM-CSF (closed squares) is displayed vs. the concentration of PMA used to treat the cells. The magnitude of the GM-CSF activated acidification burst (data from Fig. 6B) vs. PMA concentration is displayed (open squares) as percent control for comparison.

the concentration of PMA (0.8 nM) at which the GM-CSF activated metabolic burst was reduced by 50% (Fig. 8B).

DISCUSSION

Earlier work demonstrated that extracellular acidification rate can be used as a probe to detect receptor specific activation of TF-1 cells by the GM-CSF (De Vries et al., 1991). Here we have investigated the mechanism by which GM-CSF activation of cells causes rapid increases in acidification. Activation of the sodium/proton antiporter was shown to cause a low amplitude, short-lived acidification burst when GM-CSF was administered in a 6 min bolus. Antiporter activation has been reported to occur in response to GM-CSF stimulation of several hemopoetic/myeloid stem cell lines (Caracciolo et al., 1990; Vallance et al., 1990). The major component of the acidification response was larger in amplitude, longer lived, and glucose dependent. This component of extracellular acidification is most likely due to glycolytic energy metabolism. According to Owicki and Parce (1992) and Parce et al. (1989), lactic and carbonic acid produced during energy-generating carbohydrate metabolism are the primary causes of extracellular acidification. The observation that glucose uptake is increased by GM-CSF cell activation (Hamilton et al., 1988) is also consistent with increased glycolysis being the source of the GM-CSF triggered acidification increase.

Both the kinetics and amplitude of the acidification response to GM-CSF stimulation are dependent on a variety of factors, including the concentration of cytokine added, the pre-treatment of the cells with respect to various inhibitors and activators of metabolic processes, and the pre-treatment of the cells with respect to the degree of deprivation of cytokine. Cells are deprived of cytokine (starvation) in two ways. During culture, cells are split into fresh medium containing cytokine. During culture the cells consume the cytokine, reducing its concentration with time. The longer the cells are maintained in culture between splittings, the lower the concentration of cytokine in the medium. This is a form of starvation if the cytokine concentration becomes low enough. This component of starvation is difficult to control as it depends on cell density, and probably the "health" of the cells at the time of splitting. The second component of starvation is achieved by removing the cells from culture and incubating them in medium containing no cytokine for a well-defined period of time. Because both of these components have doubtless contributed to the results presented in the present work, we see considerable variation in both the basal acidification rates and the GM-CSF response from one experiment to the next. This variation, however, does not affect the conclusions drawn in this report because control cells from the same flask of cells are typically run in parallel with the experimental cells. A detailed study of the quantitative aspects of cytokine starvation will be reported elsewhere.

Activation and translocation of PKC in response to GM-CSF, IL-3, and CSF-1 receptor ligation has been reported (Cook et al., 1989; Farrar et al., 1985; Evans et al., 1987; Imamura et al., 1991). We have shown that PKC activation by PMA (Castagna et al., 1982) or inhibition of serine phosphatase by okadaic acid (Haystead et al., 1989) in TF-1 cells will cause an increase in acidification rate. Evidence for PKC involvement in GM-CSF signalling was provided by calphostin C inhibition of the GM-CSF triggered acidification response. Calphostin C is reported to be a specific inhibitor of PKC which blocks the PKC diacylglycerol binding site (Bruns et al., 1991).

Long-term treatment of TF-1 cells with PMA is known to deplete cellular PKC (Blackshear, 1988), and was shown to block the GM-CSF acidification response. Receptor binding measurements demonstrated that chronic PMA exposure caused loss of the high-affinity GM-CSF receptor from the surface of the cells. Short-term PMA exposure also inhibited the GM-CSF acidification response, but this occurred without the loss of the high-affinity receptor. The observed rapid desensitization of the GM-CSF receptor by PMA is similar to

that reported for PMA inhibition of GM-CSF dependent activation of tyrosine phosphorylation in MO7 cells (Kanakura et al., 1991). It is also possible that PMA activation of PKC desensitizes the signalling pathway by overstimulating and depleting available internal messengers, such as protein kinase substrates or PKC itself. The ionomycin control demonstrated that the cells were still capable of the acidification response after short-term (1–2 h) PMA treatment, if they were excited through the calcium signalling pathway.

Recently it has been shown that diacylglycerol is released in response to GM-CSF, IL-3, and CSF-1 in murine bone marrow macrophages without release of inositol trisphosphate (Veris and Hamilton, 1991). Our data is consistent with activation of the diacylglycerol second messenger signalling pathway in response to a bolus of GM-CSF, resulting in an extracellular acidification burst via PKC activation. Intracellular calcium does not appear to play a role in GM-CSF signal transduction (Vario and Hamilton, 1991). This is consistent with the fact that desensitization of the GM-CSF response by prior exposure to GM-CSF or PMA does not result in desensitization of the ionomycin triggered acidification response. Ionomycin may be acting through calmodulin activated kinases (Exton, 1988) independent of the PKC pathway.

The tyrosine kinase inhibitors genistein and herbimycin A reduced the metabolic response to GM-CSF receptor activation. They also inhibited the PMA stimulation of acidification rate to a similar degree, suggesting that tyrosine kinases subsequent to PKC activation are being inhibited or that the inhibitors are not specific under these conditions.

Measurement of GM-CSF stimulated proliferation of TF-1 cells treated for 18 h with various levels of PMA revealed a complex effect of PMA. At 1 nM PMA presumably down-regulated GM-CSF driven proliferation by down-regulating high-affinity GM-CSF receptors, but at the same time 1 nM PMA also caused an increase in proliferation. The combination of these effects resulted in no net decrease in cell proliferation. This observation held true up to a concentration of 4 nM PMA, at which point the cell proliferation began to decrease, most likely due to PKC depletion. PKC depletion has been shown to inhibit proliferation stimulated by various CSFs (Vario and Hamilton, 1991). By calculating the difference in proliferation rate between TF-1 cells exposed to PMA, then treated with or without GM-CSF, a GM-CSF dependent component of TF-1 cell proliferation was identified. Although the effect of PMA on TF-1 cell proliferation is a complex model which must consider the differentiation of TF-1 cells and the interaction of PMA and GM-CSF signalling, it is interesting to note that a correlation exists between the GM-CSF activated metabolic burst and GM-CSF dependent component of TF-1 proliferation.

This study of GM-CSF enhanced acidification rate in TF-1 cells illustrates how non-specific extracellular acidification rate signals can be used to investigate signal transduction pathways. Coupled with specific enzyme inhibitors, enzyme activators, and cells transfected with receptors or other putative signal transducing proteins, extracellular acidification measurement using the silicon microphysiometer should provide a valuable tool for further investigations of transmembrane and intracellular signal transduction.

ACKNOWLEDGMENTS

The authors thank Katherine Fok, Lisa Alajoki, Karen De Moor, and Greg Baxter for their technical assistance, Drs. R. Kastelein and A. Shanafelt for providing rhGM-CSF, Don Miller and Jeffrey Libby for valuable technical discussions, Gill Humphries and Jack Owicki for reviewing the manuscript, and the CytoSensor™ Product Development Team for providing the microphysiometer and supplies. DNAX Research Institute is supported by Schering-Plough Corporation. This work was supported in part at Molecular Devices Corporation by the Defense Advanced Research Projects Agency, contract MDA972-92-C-0005.

LITERATURE CITED

Blackshear, P.J. (1988) Approaches to the study of protein kinase C involvement in signal transduction. Am. J. Med. Sci., *296*:231–240.

Bolton, A.E., and Hunter, W.M. (1973) The labeling of proteins to high specific activities by conjugating to a 125-I containing acylating agent: Application to radioimmunoassay. Biochem. J., *133*:529–539.

Bruns, R., Miller, F.D., Merriman, R.L., Howbert, J.J., Heath, W.F., Kobayashi, E., Takahashi, I., Tamaoki, T., and Nakano, H. (1991) Inhibition of protein kinase C is light-dependent. Biochem. Biophys. Res. Commun., *176*:288–293.

Caracciolo, D., Pannocchia, A., Treves, S., Ghigo, D., Gallo, E., Tarella, C., Bussolins, F., Turrini, F., Tamponi, G., and Bosia, A. (1990) Role of Na+/H+ exchange in the granulocyte-macrophage colony-stimulation factor-dependent growth of a leukemic cell line. J. Cell. Physiol., *143*:133–139.

Castagna, M., Takai, Y., Kaibuchi, K., Sano, K., Kikkawa, U., and Nishizuka, Y. (1982) Direct activation of calcium-activated, phospholipid-dependent protein kinase by tumor-promoting phorbol esters. J. Biol. Chem., *257*:7847–7851.

Cook, N., Dexter, T.M., Lord, B.I., Cragoe, E.J., and Whetton, A.D. (1989) Identification of a common signal associated with cellular proliferation stimulated by four haemopoietic growth factors in a highly enriched population of granulocyte/macrophage colony-forming cells. EMBO J., *8*:2967–2974.

DeVries, J., Indelicato, S.R., Meyer, L., and Wada, H.G. (1991) Real time assessment of cellular metabolism from GM-CSF mediated stimulation of TF-1 cells as measured by a microphysiometer (Molecular Devices Corp). (Abstract) Third Intl. Workshop on Cytokines, Stresa, Italy.

Evans, S.W., Rennick, D., and Farrar, W.L. (1987) Identification of a signal-transduction pathway shared by haematopoietic growth factors with diverse biological specificity. Biochem., J., *244*:683–691.

Evans, J.P.M., Mire-Sluis, A.R., Hoffbrand, A.V., and Wickremasinghe, R.G. (1990) Binding of G-CSF, GM-CSF, tumor necrosis factor-α, and γ-interferon to cell surface receptors on human myeloid leukemia cells triggers rapid tyrosine and serine phosphorylation of a 75-Kd protein. Blood, *75*:88–95.

Exton, J.H. (1988) Mechanisms of action of calcium-mobilizing agonists: Some variations on a young theme. FASEB J., *2*:2670–2676.

Farrar, W.L., and Linnekin, D. (1990) Regulation of protein kinases and gene expression by immunocytokines. Ann. N.Y. Acad. Sci., *594*:240–252.

Farrar, W.L., Thomas, T.P., and Anderson, W.B. (1985) Altered cytosol/membrane enzyme redistribution on interleukin-3 activation of protein kinase C. Nature, *315*:235–237.

Gasson, J.C. (1991) Molecular physiology of granulocyte-macrophage colony-stimulating factor. Blood, *77*:1131–1145.

Gearing, D.P., King, J.A., Gough, N.M., and Nicola, N.A. (1989) Expression cloning of a receptor for human granulocyte-macrophage colony-stimulating factor. EMBO J., *8*:3667–3676.

Hamilton, J.A., Vario, G., and Lingelback, S.R. (1988) Activation and proliferation signals in murine macrophages: Stimulation of glucose uptake by hemopoietic growth factors and other agents. J. Cell. Physiol., *134*:405–415.

Hayashida, K., Kitamura, T., Gorman, D.M., Arai, K.-I., Yokota, T., and Miyajima, A. (1990) Molecular cloning of a second subunit of the receptor for human granulocyte-macrophage colony-stimulating

factor (GM-CSF): Reconstitution of a high-affinity GM-CSF receptor. Proc. Natl. Acad. Sci. U.S.A., *87*:9655–9659.

Haystead, T.A.J., Sim, A.T.R., Carling, D., Honnor, R.C., Tsukitani, Y., Cohen, P., and Hardie, D.G. (1989) Effects of the tumour promoter okadaic acid on intracellular protein phosphorylation and metabolism. Nature, *337*:78–81.

Imamura, K., Dianoux, A., Nakamura, T., and Kufe, D. (1991) Colony-stimulating factor 1 activates protein kinase C in human monocytes. EMBO J., *9*:2423–2428.

Isfort, R.J., and Ihle, J.N. (1990) Multiple hematopoietic growth factors signal through tyrosine phosphorylation. Growth Factors, *2*:213–220.

June, C.H., Fletcher, M.C., Ledbetter, J.A., Schieven, G.L., Siegel, J.N., Phillips, A.F., and Samuelson, L.E. (1990) Inhibition of tyrosine phosphorylation prevents T-cell receptor-mediated signal transduction. Proc. Natl. Acad. Sci. U.S.A., *87*:7722–7726.

Kanakura, Y., Druker, B., DiCarlo, J., Cannistra, S.A., and Griffin, J.D. (1991) Phorbol 12-myristate 13-acetate inhibits granulocyte-macrophage colony stimulating factor-induced protein tyrosine phosphorylation in a human factor-dependent hematopoietic cell line. J. Biol. Chem., *266*:490–495.

Kitamura, T., Tange, T., Terasawa, T., Chiba, S., Kuwaki, T., Miyagawa, K., Piao, Y.-F., Miyazono, K., Urabe, A., and Takaku, F. (1989) Establishment and characterization of a unique human cell line that proliferates dependently on GM-CSF, IL-3, or Erythropoietin. J. Cell. Physiol., *140*:323–334.

Kitamura, T., Takaku, F., and Miyajima, A. (1991a) IL-1 up-regulates the expression of cytokine receptors on a factor-dependent human hemopoietic cell line, TF-1. Int. Immunol., *3*:571–577.

Kitamura, T., Sato, N., Arai, K., and Miyajima, A. (1991b) Expression cloning of the human IL-3 receptor c-DNA reveals a shared beta subunit for the human IL-3 and GM-CSF receptors. Cell, *66*:1165–1174.

Kobayashi, E., Nakano, H., Morimoto, M., and Tamaoki, T. (1989) Calphostin C (UNC-1028C), a novel microbial compound, is a highly potent and specific inhibitor of protein kinase C. Biochem. Biophys. Res. Commun., *159*:548–553.

McConnell, H.M., Rice, P., Wada, H.G., Owicki, J.C., and Parce, J.W. (1991) The microphysiometer biosensor. Curr. Opin. Struc. Biol., *1*:647–652.

McConnell, H.M., Owicki, J.C., Parce, J.W., Miller, D.L., Baxter, G.T., Wada, H.G., and Pitchford, S. (1992) The cytosensor microphysiometer: biological applications of silicon technology. Science, *257*:1906–1912.

Miller, D.L., Owicki, J.C., and Parce, J.W. (1991) Real-time detection of agonist-induced acetylcholine receptor (AChr) activation in TE671 cells with a silicon-based biosensor. JASEB J., *5*:A1600.

Miyajima, A., Kitamura, T., Harada, N., Yokota, T., and Arai, K. (1992) Cytokine receptors and signal transduction. Annu. Rev. Immunol., *10*:295–331.

Mossman, T. (1983) Rapid colorimetric assay for cellular growth and survival: Application to proliferation and cytotoxicity assay. J. Immunol. Methods, *65*:55–63.

Nag, B., Wada, H.G., Fok, K.S., Green, D.J., Sharma, S.D., Clark, B.R., Parce, W.J., and McConnell, H.M. (1992) Antigen-specific stimulation of T cell extracellular acidification by MHC class II-peptide complexes. J. Immunol., *148*:2040–2044.

Owicki, J.C., and Parce, J.W. (1992) Biosensors based on the energy metabolism of living cells: The physical chemistry and cell biology of extracellular acidification. Biosens. Bioelectron., *12*:255–272.

Owicki, J.C., Parce, J.W., Kercso, K.M., Sigal, G.B., Muir, V.C., Venter, J.C., Fraser, C.M., and McConnell, H.M. (1990) Continuous monitoring of receptor-mediated changes in the metabolic rates of living cells. Proc. Natl. Acad. Sci. U.S.A., *87*:4007–4011.

Parce, J.W., Owicki, J.C., Kercso, K.M., Sigal, G.B., Wada, H.G., Muir, V.C., Bousse, L.J., Ross, K.L., Sikic, B.I., and McConnell, H.M. (1989) Detection of cell-affecting agents with a silicon biosensor. Science, *246*:243–247.

Paris, S., and Pouyssegur, J. (1983) Biochemical characterization of the amiloride-sensitive Na+/H+ antiporter in Chinese hamster lung fibroblasts. J. Biol. Chem., *258*:3503–3508.

Raley-Susman, K.M., Kercso, K.M., Parce, J.W., Owicki, J.C., and Sapolsky, R.M. (1992) Direct measurement of neurotransmitter activation of cellular metabolism in cultured hippocampal neurons. J. Neurosci., *12*:773–780.

Tada, H., Shiho, O., Kuroshima, K., Koyama, M., and Tsukamoto, K. (1986) An improved colorimetric assay for interleukin-2. J. Immunol. Methods, *93*:157–165.

Tetsu, A., Ishida, J., Nakagawa, S., Ogawara, H., Watanabe, S., Itoh, N., Shibuya, M., and Fukami, Y. (1987) Genistein, a specific inhibitor of tyrosine-specific protein kinases. J. Biol. Chem., *262*:5592.

Uehara, Y., Murakami, Y., Sugimoto, Y., and Mizuno, S. (1989) Mechanism of reversion of Rous sarcoma virus transformation by herbimycin A: Reduction of total phosphotyrosine levels due to reduced kinase activity and increased turnover of p60v-src1. Cancer Res., *49*:780–785.

Vallance, S.J., Downes, C.P., Cragoe, E.J., and Whetton, A.D. (1990) Granulocyte-macrophage colony-stimulating factor can stimulate macrophage proliferation via persistent activation of Na+/H+ antiport. Biochem. J., *265*:359–364.

Vario, G., and Hamilton, J.A. (1991) Signalling through CSF receptors. Immunol. Today, *12*:362–369.

Veris, N., and Hamilton, J.A. (1991) GM-CSF and IL-3 stimulate diacylglycerol generation in murine bone marrow-derived macrophages. Biochem. Biophys. Res. Commun. *179*:586–591.

Wada, H.G., Owicki, J.C., and Parce, J.W. (1991) Cells on silicon: bioassays with a microphysiometer. Clin. Chem., *37*:600–601.

Whetton, A.D., Monk, P.N., Consalvey, S.D., Huang, S.J., Dexter, T.M., and Downes, C.P. (1988) Interleukin-3 stimulates proliferation via protein kinase C activation without increasing inositol lipid turnover. Proc. Natl. Acad. Sci. U.S.A., *85*:3284–3288.

JOURNAL OF CELLULAR PHYSIOLOGY 161:597–605 (1994)

Activation of TNF-R1 Receptor in the Presence of Copper Kills TNF Resistant CEM Leukemic T Cells

H. GARRETT WADA*, KATHERINE S. FOK, BRIAN M. FENDLY, NANCY Y. CHIANG, AND HOWARD H. SUSSMAN

Molecular Devices Corporation, Sunnyvale, California 94089 (H.G.W., K.S.F.), Genentech Inc., South San Francisco, California 94080 (B.M.F., N.Y.C.), and Stanford University School of Medicine, Stanford, California 94305 (H.H.S.)

The cytotoxic effects of TNF on malignant cells are known to be mediated through high affinity surface receptors. The precise mechanism by which transformed cells are selectively killed by the activation of these receptors is yet unknown, but several intracellular signaling pathways are known to be involved. Phospholipase A2 activation by TNF-α has been shown to be important in the transduction of signals leading to cell death. We have used monitoring of extracellular acidification rate as a measure of cellular metabolism to follow the early time course of TNF effects on a human leukemic T cell line (CEM-SS cells). CEM-SS cells were relatively resistant to TNF cell killing but TNF caused an early stimulation of metabolism within 2–4 hr, followed by a suppression of metabolic activity occurring over 20 hr. In contrast, a TNF sensitive subclone of CEM cells (C1Ca) showed a rapid and dramatic decrease in metabolic activity corresponding to cytotoxicity within 18 hr. It was discovered that cupric o-phenanthroline markedly potentiated the effects of TNF on the resistant CEM-SS cells leading to cell death. This observation was specific for copper because ferric o-phenanthroline was without effect at the same concentration. The copper cytotoxic effect was shown to be mediated through the TNF-R1 receptor and independent of phospholipase A2 signaling.

TNF-α is a cytokine produced by activated macrophages, T cells, mast cells and some epithelial tumor cells which can induce a wide variety of cellular responses including hemorrhagic necrosis of transplanted tumors, cell proliferation, cytotoxicity, inflammation, and anti-viral responses (Fiers, 1991; Matthews and Neale, 1987). The mechanisms by which a single cytokine can have such varied effects on different cells has been the object of much investigation. There are two TNF receptors, the TNF-R1 (p55) and the TNF-R2 (p70 or p75), through which TNF exerts its effects on cells (Fiers, 1991; Tartaglia and Goeddel, 1992). When considering the selective killing of transformed cells by TNF, the work of Tartaglia and Goeddel indicates that TNF-R1 is the receptor responsible for activating signals leading to direct cytotoxicity (Tartaglia et al., 1993). Heller et al. (1992) have provided evidence using TNF-R2 transfected HeLa cells that TNF-R2 was also required in addition to TNF-R1 to deliver the signals resulting in cell death. Consequently, there is some controversy over the receptor requirements for TNF-mediated cytotoxicity.

The precise mechanism by which TNF receptor activation causes cytotoxicity is not known; however, two modes of cell killing have been observed: lysis (Espevik and Missen-Meyer, 1986) and apoptosis (Schmid et al., 1986). There is evidence that the cytotoxic effects of TNF do not require transcription or translation because inhibitors of these processes do not block TNF action. On the contrary, TNF sensitivity of cells is often enhanced by actinomycin D or cycloheximide (Kull and Cuatrecasas, 1981). This suggests that TNF cytotoxicity is a process originating in the cytoplasm and is inhibited by protective proteins. More recent studies have indicated that reactive oxygen species (ROS) generated in the mitochondria are a source of TNF activated toxicity (Scholze-Osthoff et al., 1992). This is particularly relevant to the mechanism of TNF-activated apoptosis because it has been determined that an antioxidant inhibitor of apoptosis, Bcl-2, is localized in the mitochondrial membranes, as well as nuclear membranes (Hockenbery et al., 1993).

In the present study, we have investigated the TNF cytotoxic response of a human leukemic T cell line, CEM-SS (Nara et al., 1987), which expresses only TNF-R1. Using the technique of microphysiometry to monitor cellular metabolic activity, it was possible to follow the early time course of TNF cytotoxicity. This technique measures the rate of cellular acidic metabolite

Received January 24, 1994; accepted May 26, 1994.

*Address reprint requests/correspondence to H. Garrett Wada, Molecular Devices Corp., 4700 Bohannon Dr., Menlo Park CA 94025.

production and secretion into the extracellular medium (acidification rate), which has been shown by Parce et al. (1989) and McConnell et al. (1992) to be a parameter by which cytotoxic events or cellular activation events can be monitored. Using microphysiometry, it was possible to show changes in the metabolic activity of CEM-SS cells, which are relatively resistant to TNF, within 1–2 hr of TNF exposure, but no cell killing within a 24 hr period. A TNF-sensitive subclone of CEM cells (C1Ca), stably transfected with the neomycin resistance marker and cultured in G418, exhibited a rapid TNF cytotoxic response. Both cell lines were used to study TNF cytotoxicity. Because copper is a transition metal ion that can catalyze the production of highly toxic hydroxyl free-radicals from ROS via the Haber-Weisse reaction (McCord and Day, 1978), the effects of copper in combination with TNF were investigated. It was found that activation of the TNF-R1 receptor either by TNF-α or by anti-receptor antibody followed by second antibody results in cytotoxicity when the o-phenanthroline chelate of cupric ion is present.

MATERIALS AND METHODS

Cells and reageants

CEM-SS (4) and CEM-C1Ca cells were obtained from Chris Simonson (GeneLabs Inc., Redwood City, CA) and cultured in RPMI 1640 with L-glutamine (Gibco, Grand Island, NY) supplemented with penicillin/streptomycin (Gibco) and 10% fetal bovine serum (Sigma, St. Louis, MO). The cells were split 1:10 every third day. The CEM C1Ca cells were tranfected with a neomycin resistance marker and cultured with 50 μg/ml G418. Unless otherwise specified, all chemicals and reagents were from Sigma Chemical Co. TNF-α, anti-hTNF-α antisera, and anti-hIL-2 antisera were from Genzyme (Cambridge, MA), and cupric chloride and o-phenanthroline were from Aldrich (Milwaukee, WI). Anti-human TNF-R1 receptor monoclonal antibody, #4E4, anti-human TNF-R2 receptor monoclonal antibody, #1H9, anti-human GP120 monoclonal antibody, #5B6, were from Genentech Inc. (S. San Francisco, CA).

Measurement of extracellular acidification using the Cytosensor® microphysiometer

The cells were harvested on the third day after passage by centrifugation, and the cell pellets were resuspended into loading medium at 0.6 to 1×10^6 cells/ml. Loading medium is low buffering RPMI (Molecular Devices Corp., Menlo Park, CA) supplemented with penicillin/streptomycin and 10 mM HEPES. One ml of cell suspension was loaded into sterile cell capsule cups (Molecular Devices Corp.), as previously described using a fibrin clot to immobilize the cells (Wada et al., 1993). The assembled capsule cups were loaded into Cytosensor® microphysiometer chambers, and running medium, low buffering RPMI supplemented with penicillin/streptomycin and 1 mg/ml HSA (endotoxin-free human serum albumin, Miles Labs., Elkhart, IN), was pumped through each chamber. TNF-α and the test materials were added to 30 ml of running medium and applied to the cells approximately half an hour after the chambers were loaded on the microphysiometer. When necessary, DMSO was used as a vehicle for dissolving test materials and diluted to less than 0.1% in running medium. The basal cellular acidification rate (metabolic rate) measured by the instrument (Parce et al., 1989) was normalized to 100% of basal rate prior to the addition of TNF or other test materials.

FACS analysis

CEM-SS and C1Ca cells were analyzed for TNF-R1 and TNF-R2 using cell surface monoclonal antibody staining and FACS analysis. A single cell suspension was prepared for each line by washing twice in phosphate-buffered saline (PBS)/1% fetal bovine serum. Cells were adjusted to 10^7 cells/ml in PBS/1% fetal bovine serum. An 100 μl aliquot from each cell line was incubated with 1 μg of either monoclonal anti-TNF-R1 (4E4), anti-TNF-R2 (1H9), or an irrelevant antibody (anti-GP120, 5B6) for 30 minutes on ice. The cells were washed 3× in PBS/1% fetal bovine serum and incubated with fluorescein-conjugated sheep (Fab')2 fragment to mouse IgG (Cappel, West Chester, PA) for 30 minutes on ice. The cells were washed 3× in PBS/1% fetal bovine serum and analyzed on a FACScan (Becton Dickinson, San Jose, CA).

RESULTS

The effects of TNF-α on CEM cells were detectable as alterations in acidification rate

The microphysiometer measures the rate of extracellular acidification, a function of the cell's metabolism. Over time, cells in the microphysiometer tend to show an early period of equilibration during which their acidification rates either rise or fall to a new steady state, depending upon the particular cell line. The present studies were conducted with CEM-SS cells which are resistant to TNF-α-induced cytotoxicity, and with a subclone, CEM-C1Ca, transfected with the neomycin resistance marker and grown in G418 (50 μg/ml). The untreated CEM-SS cells showed an initial steep decrease in rate lasting less than 30 min which was followed by an increase over the initial 2–4 hr to 125% of the initial base line, and then showed a steady rise to 175% by 18 hr (Fig. 1A). In contrast, when CEM-SS cells in the microphysiometer were treated with 1 ng/ml recombinant h-TNF-α, the acidification rate was mildly stimulated above the controls values for 1–2 hr, but after 4 hr there was a steady reduction in rate of acidification (Fig. 1A). After 18 hr of TNF exposure, the acidification rate had fallen from a peak value of 160% of the initial value to 120%. The untreated cells continued to have an increased acidification which was 175% of the initial rate at 18 hr. The C1Ca subclone of the CEM-SS cell line was shown to be very sensitive to TNF cytotoxicity. Exposure to TNF at 1 ng/ml resulted in a drop in the acidification to 12% of the initial rate within 18 hr, and a concentration as low as 0.01 ng/ml resulted in a drop to a value 60% of the initial rate at 18 hr (Fig. 1B). In order to examine the specificity of decrease in acidification rate as being a measure of TNF cytotoxicity, the effects of anti-TNF-α neutralizing antibody were tested. Using the C1Ca cells, the neutraliz-

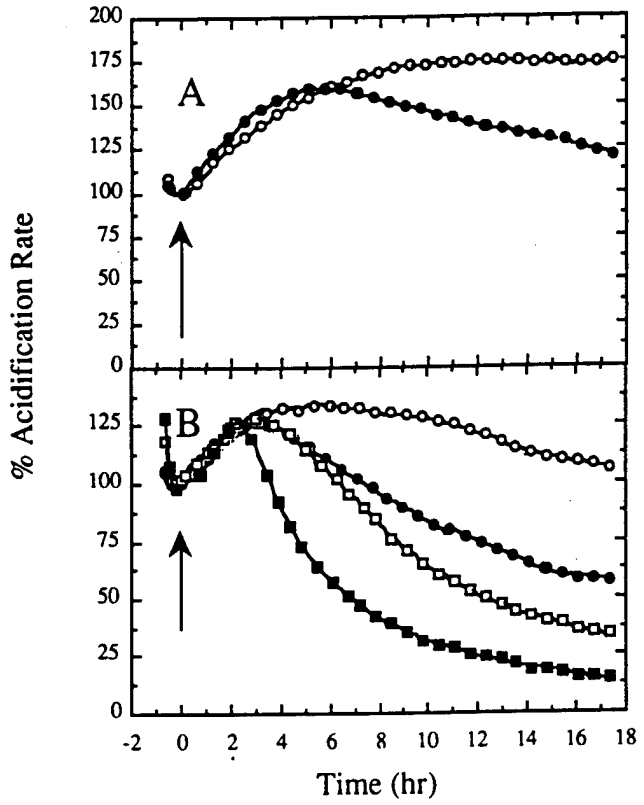

Fig. 1. Acidification response of CEM cells to TNF-α. **A:** CEM-SS cells were loaded into Cytosensor chambers as described in Materials and Methods and exposed, starting at 0 time, continuously to 1 ng/ml TNF-α (closed circles) or to media alone (open circles). Acidification rates were monitored for approximately 18 hr. **B:** CEM-C1Ca cells were loaded and exposed to 0 (open circles), 0.01 ng/ml (closed circles), 0.1 ng/ml (open squares), and 1 ng/ml TNF (closed squares) for approximately 18 hr. The arrows indicate when cells were exposed to TNF.

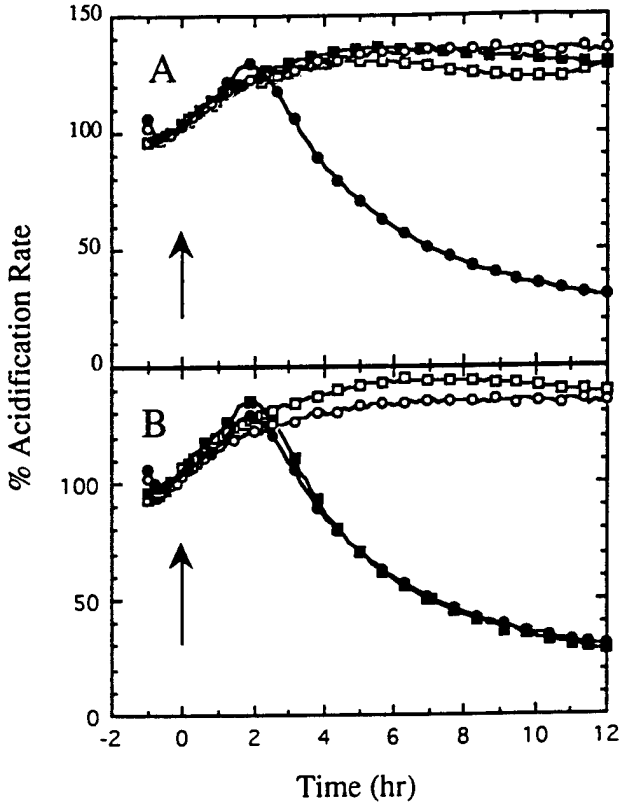

Fig. 2. Anti-TNF-α blockade of cytotoxic response. The effect of anti-TNF-α antibody on the acidification response was tested using CEM-C1Ca cells. **A:** Cells were exposed in the microphysiometer chamber to 1 ng/ml TNF (closed circles), media alone (open circles), 1 ng/ml TNF plus anti-TNF antisera (closed squares), and anti-TNF antisera alone (open squares). **B:** Cells were treated with TNF plus anti-IL-2 antisera (closed squares) as a control, with anti-IL-2 antisera (open squares), media alone (open circles), and TNF (closed circles). The arrows indicate when cells were exposed to TNF.

ing rabbit antiserum was shown to block the TNF-mediated decrease in acidification rate (Fig. 2A). A control antiserum, rabbit anti-hIL-2, had no effect on the acidification rate decrease (Fig. 2B).

Anti-TNF-R1 receptor antibody blocks the cytotoxic response of CEM cells to TNF-α

In order to determine whether the TNF-activated metabolic changes in CEM cells were mediated through TNF receptor interactions, the CEM-SS and the C1Ca subclone were incubated with monoclonal anti-TNF receptor antibodies, anti-human TNF-R1 (p55) and anti-TNF-R2 (p70; Pennica et al., 1991; Marsters et al., 1992) and analyzed by flow cytometry. Both of these cell lines were found to express only the TNF-R1 receptor on their surface (Fig. 3). Pretreatment of the C1Ca cells with anti-TNF-R1 antibody, 4E4, 15 minutes prior to and during exposure to TNF-α, substantially blocked the cytotoxic response to TNF (Fig. 4A), but an isotype-matched control antibody (anti-GP120) did not. Anti-TNF-R2 antibody also did not block the cytotoxic response to TNF (data not shown). The metabolic changes in CEM-SS cells in response to TNF were also substantially blocked by anti-TNF-R1 antibody (Fig. 4B).

The effect of reducing and oxidizing agents on TNF-mediated cytotoxicity

Because the presence of reducing agents such as N-acetylcysteine (NAC) has been reported to inhibit the activating effects of TNF-α on HIV-1 replication in T cells (Roederer et al., 1990) and NFkB transcriptional activation factor (Schreck et al., 1991), we tested the effects of reducing agents and oxidizing agents on TNF cytotoxicity using CEM-SS cells and its subclone C1Ca cells. The addition of 10 mM β-mercaptoethanol caused a small decrease in the cytotoxic effect of TNF-α on C1Ca cells (Fig. 5A). The addition of 10 mM NAC did not produce a significant reduction in the cytotoxic effect of TNF-α (Fig. 5B). Each reducing agent increased the basal acidification rates of both C1Ca and CEM-SS cells. Oxidizing agents, cupric o-phenanthroline or hydrogen peroxide also increased the basal acidification rates of C1Ca and CEM-SS cells and also enhanced the TNF cytotoxicity. In particular, cupric o-phenanthroline at 1 μM, a subtoxic concentration, significantly enhanced cell killing by TNF in the TNF-resistant CEM-SS cells (Fig. 6). When 1 μM ferric 0-phenanthroline was tested, no synergy with TNF cytotoxicity was

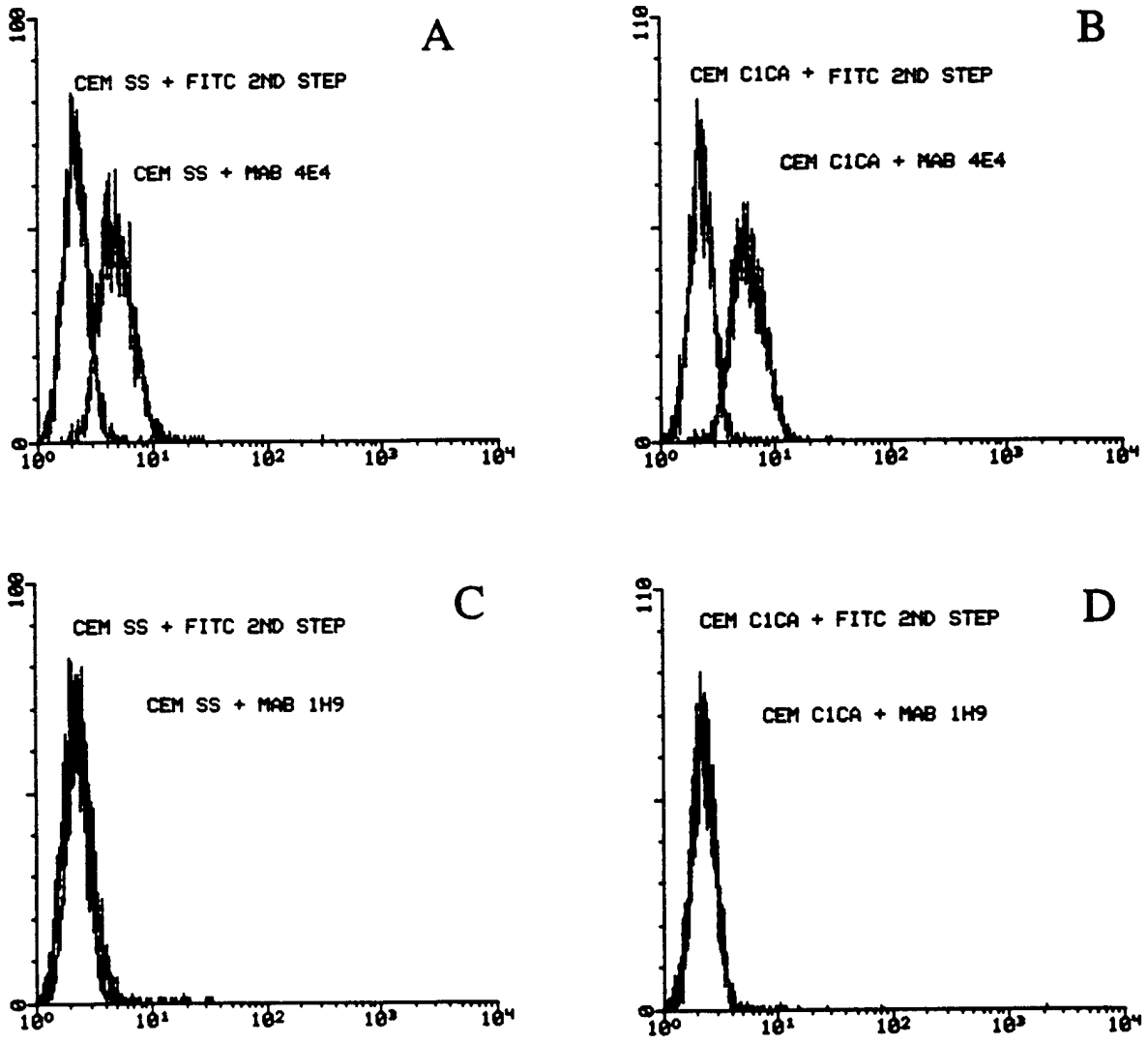

Fig. 3. FACS data showing TNFR1 expression CEM-SS and C1Ca cells. CEM-SS and CEM-C1Ca cells were preincubated with anti-TNFR1 (4E4) or with anti-TNFR2 (1H9) then stained with FITC anti-mouse IgG. Background staining was determined by staining cells with FITC anti-mouse IgG only. **A:** Histogram overlay of TNFR1 expression on the cell surface of CEM-SS cells. **B:** Histogram overlay of TNFR1 expression of the surface of CEM-C1Ca cells. **C** and **D:** Histogram overlays showing no staining of CEM-SS or CEM-C1Ca cells by anti-TNFR2 antibody.

observed. The anti-oxidant, butylated hydroxyanisole (BHA), did not inhibit nor did it accelerate the copper-enhanced TNF cytotoxicity (Table 1). Dramatic inhibition of the copper-enhanced cell killing was achieved by the addition of the strong copper chelator, diethyldithiocarbamic acid (DCTA), demonstrating the importance of free or weakly chelated copper. Relevant to the mechanism of copper toxicity, it was observed that the combination of 1 μM copper and reducing agent, 10 mM NAC, was cytotoxic to the CEM-SS cells. In separate experiments, a color change from blue to red confirmed the reduction of Cu(II) to Cu(I) in the presence of 10 mM NAC and 10 μM cupric o-phenanthroline. The color change was reversible, changing back after about 30 minutes due to air oxidation of the copper. As shown in Table 2, either agent alone was not cytotoxic. BHA at 25 μM also did not inhibit copper/reducing agent cytotoxicity. It was also observed that the combination of 1 μM cupric o-phenanthroline and 2 mM hydrogen peroxide was highly cytotoxic to the cells (Table 2), and that this cytotoxicity was blocked by DCTA.

The copper-potentiated TNF cytotoxicity is inhibited by TNF-R1 antibody and TNF-R1 aggregation triggers TNF independent copper cytotoxicity

The copper-potentiated TNF cytotoxicity was inhibited by an anti-TNF-R1 antibody known to be a TNF-α antagonist (Pennica et al., 1991; Marsters et al., 1992). As shown in Figure 7A, when CEM-SS cells were pretreated for 15 minutes with the anti-R1 antibody, the copper-potentiated killing was reduced approximately 50%. It was also noted that when cells were treated with anti-R1 and copper alone, the cells exhibited a

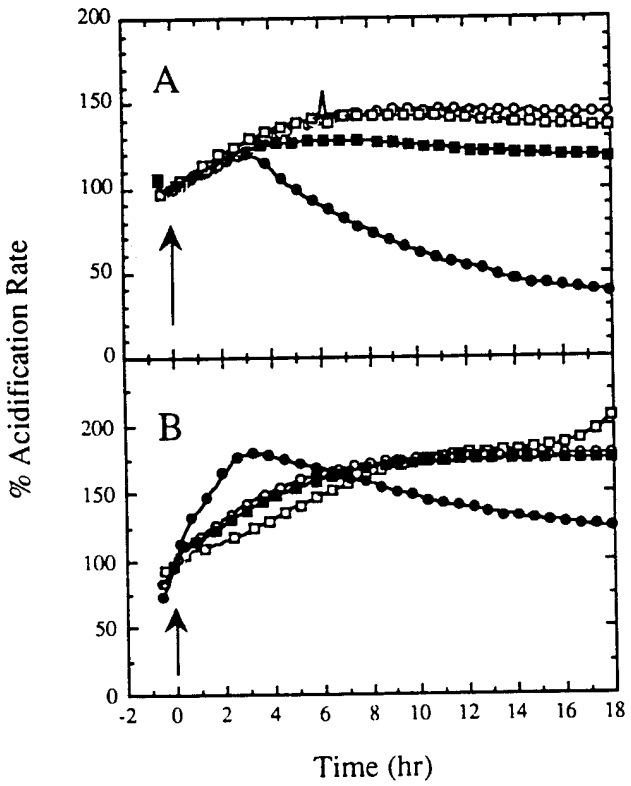

Fig. 4. Anti-TNFR1 monoclonal antibody blocks the TNF activated decrease in acidification rate. The effect of monoclonal anti-TNFR1 antibody (4E4) was tested in the microphysiometer. **A:** C1Ca cells were loaded in four microphysiometer chambers and two chambers were pretreated with 1 μg/ml anti-TNFR1 for 15 min. The cells were then treated continuously with the same antibody plus 1 ng/ml TNF-α (closed squares) or plus media (open squares). The other two chambers were pretreated with an isotype matched, IgG_{1k}, anti-GP120 antibody as a control at 1 μg/ml. The cells were then treated continuously with the same antibody plus 1 ng/ml TNF-α (closed circles) or media (open circles). **B:** CEM-SS cells were loaded in microphysiometer chambers and pretreated with either anti-TNFR1 antibody or control antibody under the same conditions as described in A. The arrows indicate when cells were exposed to TNF.

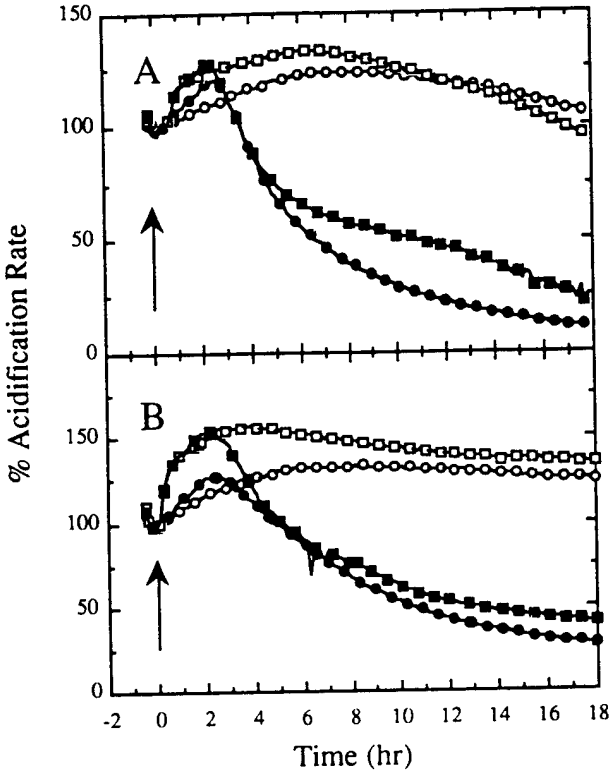

Fig. 5. Treatment with β-mercaptoethanol or N-acetylcysteine does not block TNF effects on CEM-C1Ca cells. C1Ca cells were loaded into microphysiometer chambers and pretreated with reducing agents prior to exposure to TNF-α. **A:** After pretreatment for 15 min with 10 mM β-mercaptoethanol (β-ME), the cells were continuously exposed to 1 ng/ml TNF plus β-ME (closed squares) or media plus β-ME (open squares). Untreated cells were exposed to 1 ng/ml TNF (closed circles) or media alone (open circles) as controls. **B:** After pretreatment for 15 min with 10 mM N-acetylcysteine (NAC), the cells were continuously exposed to 1 ng/ml TNF plus NAC (closed squares) or media plus NAC (open squares). Untreated cells were exposed to 1 ng/ml TNF (closed circles) or media alone (open circles) as controls. The arrows indicate when cells were exposed to reducing agents.

slowly developing decrease in metabolic activity which suggested that low level activation of the receptor may be occurring. In order to determine whether antibody-mediated aggregation of TNF-R1 could also trigger the copper-potentiated cytotoxic response, anti-mouse IgG antibody was used following anti-R1 to cause receptor capping. The second antibody treatment triggered the copper-potentiated cytoxic response in the absence of TNF to the same extent as 1 ng/ml TNF (Fig. 7B).

Quinacrine inhibits the TNF-activated metabolic changes in CEM cells, but not the copper-potentiated cell killing

When CEM-SS cells were pretreated for 30 minutes with 10 μM quinacrine, a phospholipase A2 inhibitor, and then exposed to a moderate level (0.1 ng/ml) of TNF, the expected metabolic alterations which are observed with control cells were inhibited (Fig. 8A). When this same experiment is done in the presence of 1 μM cupric o-phenanthroline, we observed no significant inhibition of the copper-potentiated TNF cytotoxicity (Fig. 8B).

DISCUSSION

In the present study, the early effects of TNF-α on cell metabolism and cell death in a T cell leukemia-derived line, CEM, were evaluated using extracellular acidification as a probe. Both TNF-α resistant and sensitive cell lines were used in these experiments. These studies have shown that: (1) early effects of TNF-α on cellular metabolism are mediated through TNF-R1; (2) copper at nontoxic concentrations potentiates TNF effects in a TNF-α resistant cell line, leading to cell death by a mechanism that requires activation of TNF-R1, and (3) the mechanism by which nontoxic concentrations of copper causes cell death requires activation and internalization of TNF-R1 and can proceed in the absence of TNF-α if the receptor is activated by other means, such as antibodies to the receptor and a second antibody.

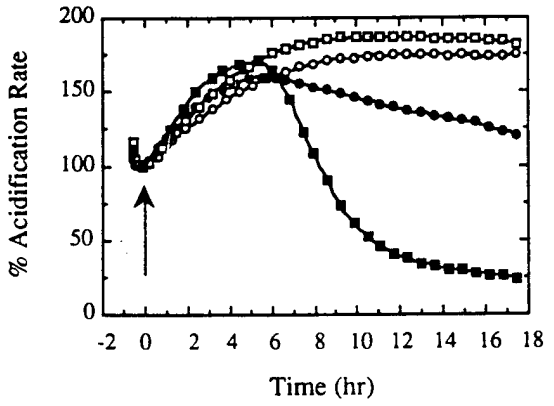

Fig. 6. Cupric o-phenanthroline potentiates TNF cytotoxicity. The effects of an oxidizing agent, cupric o-phenanthroline (COP), on TNF cytotoxicity was tested using CEM-SS cells. CEM-SS cells were loaded into microphysiometer chambers and monitored for acidification rate changes during their treatment with TNF in the presence and absence of COP. Cells were exposed to 1 ng/ml TNF (closed circles), media alone (open circles), 1 μM COP (open squares), and 1 ng/ml TNF plus 1 μM COP (closed squares). The arrows indicate when cells were exposed to effector agents.

TABLE 1. Effects of transition metals on CEM-SS cells in combination with TNF-α

Test substances	Concentration	Acidification rate (% control)[1]
TNF-α	1 ng/ml	84
TNF-α + Cu++/o-ph.(COP)	1 ng/ml, 1 μM	29
TNF-α + Fe+++/o-ph.	1 ng/ml, 1 μM	94
TNF-α + COP + DCTA	1 ng/ml, 1 μM, 1 mM	90
TNF-α + COP + BHA	1 ng/ml, 1 μM, 25 μM	27

[1]Acidification rate after 10 hr of treatment with 1 ng/ml TNF-α + test substance relative to treatment with test substance alone (100%).

TABLE 2. Effects of copper plus NAC or H_2O_2 on CEM-SS cells

Test substances	Concentration	Acidification rate (% control)[1] 2 hr	5 hr	10 hr
Control	0	100	100	100
Cu++/o-ph.(COP)	1 μM	107	110	109
NAC	10 mM	161	118	109
DDCA	1 mM	127	109	77
COP + NAC	1 μM, 10 mM	120	65	20
COP + NAC + DTCA	1 μM, 10 mM, 1 mM	106	92	73
COP + NAC + BHA	1 μM, 1 mM, 25 μM	54	24	12
COP + H202	1 μM, 2 mM	94	54	16
COP + H202 + DTCA	1 μM, 2 mM, 1 mM	117	135	131

[1]Acidification rate at the specified time after continuous exposure to the various treatments was normalized to % of control, no treatment (100%).

CEM-SS cells which are resistant to TNF exhibit an extracellular acidification response to TNF-α treatment which is characterized by a mild stimulation in acid production followed by a gradual decrease in acidification rate. A subclone of CEM-SS cells, C1Ca, is particularly sensitive to TNF, characterized by a rapid drop in acidification rate, proceeding to cell death. These early changes in acid production by the CEM cells reflect changes in cellular metabolism which are probably due to alterations in glucose utilization. Earlier studies have shown that activation of several growth factor receptor systems results in glucose-dependent increases in extracellular acidification and sodium/H+ antiporter activation (Parce et al., 1989; McConnell et al., 1992; Wada et al., 1993). TNF has been shown to activate growth factor mitotic metabolic pathways (Manchester et al., 1993). This would explain the early rise in acidification rate in cells after TNF-α treatment. The later drop in acidification rate correlates with the cytotoxic events that are activated by TNF, as shown by the observation that 1–10 ng/ml TNF cause CEM-C1Ca cells to undergo cell lysis after an overnight exposure. The increased sensitivity of C1Ca cells may be due to the lack of protective proteins, because these cells were selected and cultured in the presence of G418, a compound which inhibits protein synthesis (Tartaglia et al., 1993), similar to what has been described in the presence of cycloheximide (Kull and

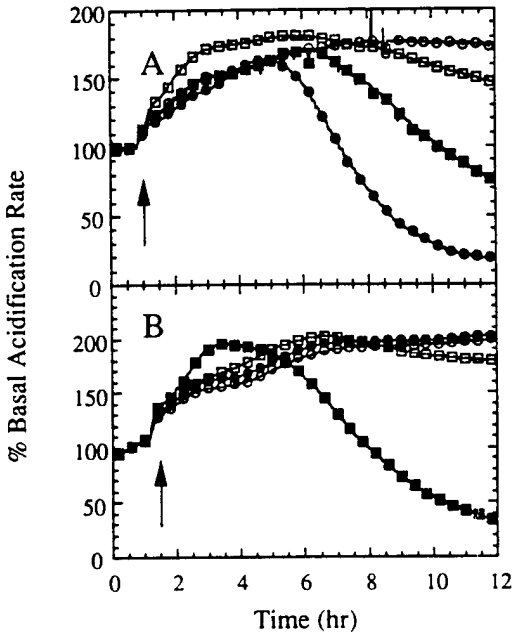

Fig. 7. Anti-TNFR1 antibody inhibits the cupric o-phenanthroline-potentiated TNF cytotoxicity, and TNFR1 capping with anti-TNFR1 plus anti-IgG antibody activates TNFR1 without the addition of TNF. The effects of anti-TNFR1 antibody on cupric o-phenanthroline-potentiated TNF cytotoxicity was tested using microphysiometry. **A:** CEM-SS cells were loaded into Cytosensor chambers and pretreated with 1 μg/ml anti-TNFR1 antibody for 30 min prior to exposure to a combination of 1 μM cupric o-phenanthroline (COP) and 1 ng/ml TNF-α plus anti-TNFR1 (closed squares) or 1 μM COP plus anti-TNFR1 (open squares). Cells were exposed to control isotype matched antibody (anti-GP120) for 30 min prior to exposure to 1 μM COP and 1 ng/ml TNF-α plus anti-GP120 (closed circles) or 1 μM COP plus anti-GP120 (open circles) as controls. **B:** CEM-SS cells were tested for their response to capping of the TNFR1 receptors in the presence of COP. After pretreatment for 15 min with 1 μg/ml anti-TNFR1, cells were exposed to anti-mouse IgG for 15 min and then continuously exposed to 1 μM COP alone (closed squares). Control treatments were run which consisted of pretreatment with anti-TNFR1 antibody, no anti-IgG treatment, and continuously exposed to COP (open squares); no pretreatment with anti-TNFR1 antibody, pretreatment with anti-IgG and continuously exposed to COP (closed circles), and no pretreatment and continuously exposed to COP (open circles). The arrows indicate time of anti-IgG exposure.

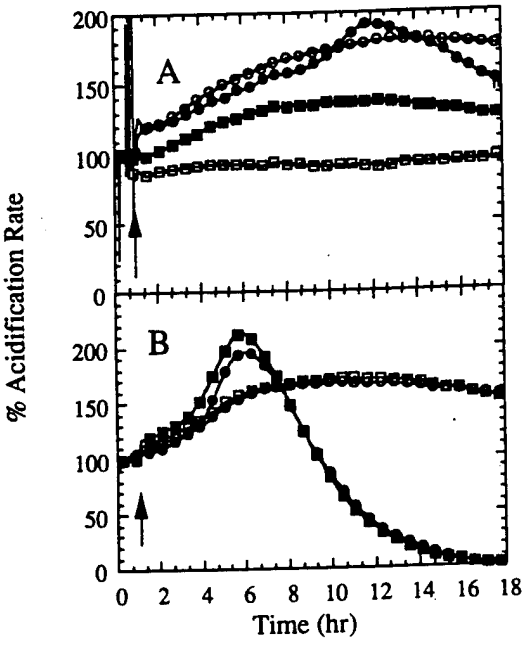

Fig. 8. Quinacrine inhibits the metabolic effects of TNF on CEM-SS cells, but does not block the copper-potentiated TNF cytotoxicity. Quinacrine was tested for its effect on TNF cytotoxicity. A: CEM-SS cells were loaded in chambers and pretreated for 30 min with 10 μM quinacrine and then exposed to 0.1 ng/ml TNF-α plus quinacrine for 18 hr (closed squares) or media plus quinacrine (open squares). Control cells were mock pretreated with media alone and exposed to 0.1 ng/ml TNF-α for 18 hr (closed circles) or media (open circles). B: CEM-SS cells were treated as in A with the addition of 1 μM COP to the media at the time of TNF exposure. Cells were pretreated for 30 min with 10 μM quinacrine and then exposed to 0.1 ng/ml TNF-α and 1 μM COP plus quinacrine for 18 hr (closed squares) or media plus 1 μM COP and quinacrine (open squares). Control cells were mock pretreated with media alone and exposed to 0.1 ng/ml TNF-α and 1 μM COP for 18 hr (closed circles) or media plus 1 μM COP (open circles). The arrow indicates time of exposure to TNF.

Cuatrecasas, 1981). Possible candidates for the protective proteins are manganous superoxide dismutase (Wong et al., 1989) and the more recently proposed anti-oxidant inhibitor of apoptosis, Bcl-2 (Hockenbery, 1993). Preliminary measurements show a 30–50% decrease in Bcl-2 levels by Western blot analysis, which may be significant. A 10% decrease in superoxide dismutase levels in the CEM-C1Ca cells by enzymatic assay suggests that it is not a factor here.

The TNF-activated acidification response was shown to be mediated through the TNF-R1 receptor by the blocking of the response in cells continuously treated with monoclonal anti-TNF-R1 antibody during exposure to TNF-α. The present study showing the importance of TNF-R1 in TNF cytotoxicity is in agreement with the recent experiments which showed TNF-R1 knock-out mice are resistant to endotoxic shock (Pfeffer et al., 1993; Rothe et al., 1993) and the earlier in vitro work showing induction of cytotoxicity by anti-TNF-R1 agonist antibodies (Tartaglia et al., 1993). Our results indicate that the TNF-R2 receptor is not required for the TNF cytotoxic signaling in CEM cells, because the CEM cell line does not have TNF-R2 receptors on their surface. This result is in contrast with the proposal that TNF-R2 is required for TNF cytotoxicity which was based on a study using TNF-R2 transfected HeLa cells (Heller et al., 1992). An earlier study of the effects of anti-TNF-R1 and R2 antibody on the cytotoxicity of TNF in U239 cells by Shalaby et al. (1990), suggested that both TNF receptors are independently involved in cytotoxic signaling in these cells. These results together underscore the variable requirement for cytotoxic signaling by TNF-R1 or TNF-R2 receptors in different cell lines.

A most striking effect observed during this study was that cupric o-phenanthroline markedly potentiated the TNF effects in the CEM-SS cells. These cells are resistant to TNF cytotoxicity, only showing metabolic changes as measured by a slight decrease in the rate of acidification over time. However, when cupric o-phenanthroline was included with TNF-α, cytotoxicity leading to cell death occurred. Two factors were involved: (1) this effect was specific for copper o-phenanthroline; it was not seen with ferric o-phenanthroline; (2) activation of TNF-R1 was required. The activity of the copper appears to be dependent upon the presence of unbound or weakly chelated copper ion, as indicated by the observation that DCTA, a strong copper chelator, blocks the copper activation of TNF cytotoxicity. The chelator can be operating in two different modes to inhibit cytotoxicity. Firstly, DCTA can interfere with the interaction of copper ions with critical cell components. We observed that copper bound to ceruloplasmin or serum albumin was not active in potentiating TNF-activated cytotoxicity (unpublished observation). Secondly, the DCTA can act by blocking the cellular reduction of the cupric ion to the cuprous form. This study shows that N-acetylcysteine and β-mercaptoethanol activate the cytotoxicity of copper and that this activation correlates with the chemical reduction of the copper. The data suggest that reduction of the metal ion to the cuprous, Cu(I), form may be an important step in the initiation of copper-potentiated TNF cytotoxic effects. It has been observed that copper-catalyzed oxidative damage of DNA bases in vitro requires the presence of a reducing agent such as ascorbate or mercaptoethanol to maintain the copper in the Cu(I) form that appears to damage DNA through a hydrogen peroxide intermediate (Dizdarogh et al., 1990). Cuprous and ferrous ions react rapidly with hydrogen peroxide in a manner similar to the Fenton reaction (Halliwell and Gutteridge, 1984) or with hydrogen peroxide and superoxide, in the Haber-Weiss reaction (McCord and Day, 1978). Both reactions result in the production of highly toxic hydroxyl free-radicals causing damage to nucleic acid, membrane lipids, and other critical cell components. In the CEM cells, some level of specificity for the copper ions exists because iron did not substitute for copper potentiation of TNF cytotoxicity. This may be a function of the specific intracellular trafficking of the copper ion verses iron, resulting in the concentration of the copper into critical subcellular localizations with ROS-generating systems such as endocytic vesciles or mitochondrial membranes. Our findings that BHA did not inhibit the TNF activation of copper cytotoxicity in CEM-SS cells suggest that if ROS is involved, it is sequestered in intracellular compartments protected from exogenous free-radical trapping

agents, which is consistent with an intracellular rather than an extracellular, plasma membrane, site of action.

These present studies showed that activation and internalization of TNF-R1 are required for the cytolytic effects of copper. The involvement of TNF-R1 for copper-induced cytolysis was demonstrated in experiments which showed that pretreatment of cells with anti-TNF-R1 antibody, which competes with TNF for binding to the receptor, inhibited copper-potentiated cytotoxicity in proportion to its competition for binding. Incubation of the anti-TNF-R1 antibody with CEM-SS cells in the presence of copper was not cytotoxic; however, when a second antibody was added to cause receptor capping, the copper-induced cytotoxicity was observed. These experiments suggest that activation and internalization of the receptor are required for the cytotoxic effects of copper. In the experimental system containing nontoxic amounts of copper o-phenanthroline and TNF-α, the binding of TNF to the receptor serves to activate the receptor and initiate internalization of the receptor. These results indicate that the copper is being bound to the receptor, probably exerting its effects internally during subsequent receptor processing.

It is tempting to speculate that the endocytosis of the TNF receptor complex, which has been reported to be necessary for the TNF cytotoxic effects (Fiers, 1991), may be a vehicle by which copper is internalized and subsequently released in the acidic environment of the endocytic vesicles to exert cell killing effects. The cytotoxicity resulting from exposure of cells to copper o-phenanthroline and a reducing agent is probably a similar effect with the formation of Cu(I) which can bind to the cysteine-rich regions of nonligand bound membrane receptors that are known to slowly cycle through intracellular pools, as is the case for transferrin receptors (Stein and Sussman, 1986) and LDL receptors (Basu et al., 1981). Another possibility is that the interaction between copper and TNF-R1 is indirect, mediated through a signaling pathway such as the phospholipase A2 pathway which has been implicated in TNF-α cytotoxicity (Suffys et al., 1987, Neale et al., 1988; Hayakawa et al., 1993). However, the results of experiments conducted in the presence of a phospholipase A2 inhibitor, quinacrine, showed that quinacrine inhibited the TNF-induced acidification rate response, but did not block the copper-potentiated cytotoxic response. These results suggest that copper-potentiated cytotoxicity is independent of the phospholipase A2 pathway.

In summary, it is clear that copper ions exert cytotoxic effects in TNF-resistant CEM cells and that this is a TNF-R1-mediated process. Further studies will be required to determine the mechanisms leading to copper-potentiated TNF cytotoxicity; however, it is plausible that the TNF-α activated copper cytotoxicity is related to the catalysis of reactions generating highly toxic ROSs in situ.

ACKNOWLEDGMENTS

The authors thank Wally Parce for a critical reading of the manuscript, Chris Simonsen for providing the CEM cell lines, Liisa Alioki for her expert cell culture assistance, Peter Panfili for performing SOD assays, and Brent Rupnow and Susan Knox for performing Western analyses for Bcl-2. This work was supported in part by Defense Advanced Research Projects Agency, Contract MDA972-92-C-0005.

LITERATURE CITED

Basu, S.K., Goldstein, J.L., Anderson, R.G.W., Brown, M.S. (1981) Monensin interrupts the recycling of low density lipoprotein receptors in human fibroblasts. Cell, *24:*493–502.

Dizdaroglu, M., Auroma, O.I., and Halliwell, B. (1990) Modification of bases in DNA by copper ion- 1,10-phenanthroline complexes. Biochemistry, *29:*8447–8451.

Espevik, T., and Nissen-Meyer, J. (1986) A highly sensitive cell line WEHI 164 clone 13, for measuring cytotoxic factor/tumor necrosis factor from human monocytes. J. Immunol. Methods *95:*99–105.

Fiers, W. (1991) Review. Tumor necrosis factor. Characterization at the molecular, cellular and *in vivo* level. FEBS Lett. *285:*199–212.

Halliwell, B., and Gutteridge, J.M.C. (1984) Oxygen toxicity, oxygen radicals, transition metals and disease. Biochem. J., *219:*1–14.

Hayakawa, M., Ishida, N., Takeuchi, K., Shibamoto, S., Hori, T., Oku, N., Ito, F., and Tsujimoto, M. (1993) Arachidonic acid-selective cytosolic phospholipase A2 is crucial in the cytotoxic action of tumor necrosis factor. J. Biol. Chem., *268:*11290–11295.

Heller, R.A., Song, K., Fan, N., and Chang, D.J. (1992) The p70 tumor necrosis factor receptor mediates cytotoxicity. Cell, *70:*47–56.

Hockenbery, D.M., Oltvai, Z.N., Yin, X.-M., Milliman, C.L., and Korsmeyer, S.J. (1993) Bcl-2 functions in an antioxidant pathway to prevent apoptosis. Cell, *75:*241–251.

Kull, F.C., Jr., and Cuatrecasas, P. (1981) Possible requirement of internalization in the mechanism of *in vitro* cytotoxicity in tumor necrosis serum. Cancer Res., *41:*4885–4890.

Manchester, K.M., Heston, W.D., and Donner, D.B. (1993) Tumour necrosis factor-induced cytotoxicity is accompanied by intracellular mitogenic signals in ME-180 human cervical carcinoma cells. Biochem. J., *290:*185–190.

Marsters, S.A., Frutkin, A.D., Simpson, N.J., Fendly, B.M., and Ashkenazi, A. (1992) Identification of cysteine-rich domains of the type 1 tumor necrosis factor receptor involved in ligand binding. J. Biol. Chem., *267:*5747–5750.

Matthews, N., and Neale, M.L. (1987) Studies on the mode of action of tumor necrosis factor on tumor cells *in vitro*. Lymphokines, *14:*223–252.

McConnell, H.M., Owicki, J.C., Parce, J.W., Miller, D.L., Baxter, G.T., Wada, H.G., and Pitchford, S. (1992) The Cytosensor microphysiometer: Biological applications of silicon technology. Science, *257:* 1906–1912.

McCord, J.M.A., and Day, E.D. (1978) Superoxide-dependent production of hydroxyl radical catalyzed by an iron-EDTA complex. FEBS Lett., *86:*139–142.

Nara, P.L., Hatch, W.C., Dunlop, N.M., Robey, W.G., Arthur, L.O., Gonda, M.A., and Fischinger, P.J. (1987) Simple, rapid, quantitative, syncytium-forming microassay for the detection of human immunodeficiency virus neutralizing antibody. AIDS Res. Hum. Retroviruses, *3:*283–302.

Neale, M.L., Fiera, R.A., and Matthews, N. (1988) Involvement of phospholipase A2 activation in tumour cell killing by tumour necrosis factor. Immunology, *64:*81–85.

Parce, J.W., Owicki, J.C., Kercso, K.M., Sigal, G.B., Wada, H.G., Muir, V.C., Bousse, L.J., Ross, K.L., Sikic, B.I., and McConnell, H.M. (1989) Detection of cell-affecting agents with a Silicon biosensor. Science, *246:*243–247.

Pennica, D., Kohr, W.J., Fendly, B.M., Shire, S.J., Raab, H.E., Borshardt, P.E., Lewis, M., Goeddel, D.V. (1991) Characterization of a recombinant extracellular domain of the type 1 tumor necrosis factor receptor: Evidence for TNF-α induced receptor-aggregation. Biochemistry, *31:*1134–1141.

Pfeffer, K., Matsuyama, T., Kundig, T.M., Wakeham, A., Kishihara, K., Shahinian, A., Wiegmann, K., Ohashi, P.S., Kronke, M., and Mak, T.W. (1993) Mice deficient for the 55 kd tumor necrosis factor receptor are resistant to endotoxic shock, yet succumb to *L. monocytogenes* infection. Cell, *73:*457–467.

Roederer, M., Staal, F.J.T., Raju, P.A., Ela, S.W., Herzenberg, L.A., and Herzenberg, L.A. (1990). Cytokine-stimulated human immunodeficiency virus replication is inhibited by N-acetyl-L-cysteine. Proc. Natl. Acad. Sci. USA, *87:*4884–4888.

Rothe, J., Werner, L., Lotscher, H., Lang, Y., Koebel, P., Kontgen, F., Althage, A., Zinkernagel, R., Steinmetz, M., and Bluethmann, H. (1993) Mice lacking the tumour necrosis factor receptor-1 are resis-

tant to TNF-mediated toxicity but highly susceptible to infection by *Listeria monocytogenes*. Nature, *364*:798–802.

Schmid, D.S., Tite, J.P., and Ruddle, N.H. (1986) DNA fragmentation: Manifestation of target cell destruction mediated by cytotoxic T-cells, lymphotoxin-secretory helper T-cell clones, and cell-free lymphotoxin-containing supernatant. Proc. Natl. Acad. Sci. USA, *83*:1881–1885.

Schreck, R., Rieber, P. and Baeuerle, P.A. (1991) Reactive oxygen intermediates as apparently widely used messengers in the activation of the NF-κB transcription factor and HIV-1. EMBO J., *10*: 2247–2258.

Schulze-Osthoff, K., Bakker, A.C., Vanhaesebroeck, B., Beyaert, R., Jacob, W.A., and Fiers, W. (1992) Cytotoxic activity of tumor necrosis factor is mediated by early damage of mitochondrial functions. J. Biol. Chem., *267*:5317–5323.

Shalaby, M.R., Sundan, A., Loetscher, H., Brockhaus, M., Lesslauer, W., and Espevik, T. (1990) Binding and regulation of cellular functions by monoclonal antibodies against human tumor necrosis factor receptors. J. Exp. Med., *172*:1517–1520.

Stein, B.S., and Sussman, H.H. (1986) Demonstration of two distinct transferrin receptor recycling pathways and transferrin-independent receptor internalization in K-562 cells. J. Biol. Chem. *261*: 10319–10331.

Suffys, P., Beyaert, R., Roy, F.V., and Fiers, W. (1987) Reduced tumour necrosis factor-induced cytotoxicity by inhibitors of the arachidonic acid metabolism. Biochem. Biophys. Res. Commun., *149*:735–743.

Tartaglia, L.A., and Goeddel, D.V. (1992) Two TNF receptors. Immunol. Today, *13*:151–153.

Tartaglia, L.A., Roth, M., Hu, Y.F., and Goeddel, D.V. (1993) Tumor necrosis factor's cytotoxic activity is signaled by the p55 TNF receptor. Cell, *73*:213–216.

Wada, H.G., Indelicato, S.R., Meyer, L., Kitamura, T., Miyajima, A., Kirk, G., Muir, V.C., and Parce, J.W. (1993) GM-CSF triggers a rapid, glucose dependent extracellular acidification by TF-1 cells: Evidence for sodium/proton antiporter and PKC mediated activation of acid production. J. Cell. Physiol., *154*:129–138.